LBNL-45044

ERNEST ORLANDO LAWRENCE
BERKELEY NATIONAL LABORATORY

Ozone-Surface Interactions: Investigations of Mechanisms, Kinetics, Mass Transport, and Implications for Indoor Air Quality

Glenn C. Morrison

Environmental Energy Technologies Division

December 1999

Ph.D. Thesis

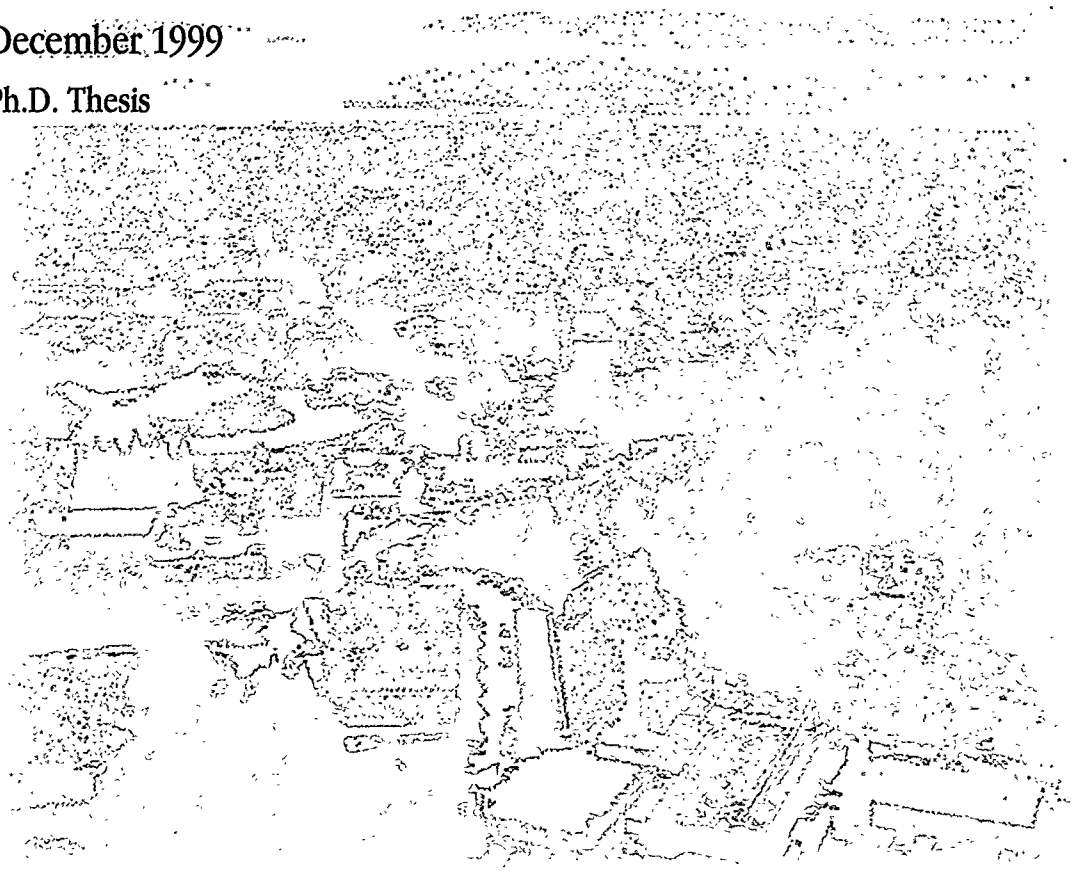

DISCLAIMER

Portions of this document may be illegible in electronic image products. Images are produced from the best available original document.

ABSTRACT

In this dissertation, I present the results of laboratory investigations and mathematical modeling efforts designed to better understand the interactions of ozone with surfaces. In the laboratory, I exposed carpet and duct materials to ozone and measured ozone uptake kinetics and the ozone induced emissions of volatile organic compounds. To understand the results of my experiments, I developed mathematical models to describe dynamic indoor aldehyde concentrations, mass transport of reactive species to smooth surfaces, the equivalent reaction probability of whole carpet due to the surface reactivity of fibers and carpet backing, and ozone aging of surfaces.

Carpets, separated carpet fibers, and separated carpet backing all tended to release aldehydes when exposed to ozone. Secondary emissions were mostly n-nonanal and several other smaller aldehydes. The pattern of emissions suggested that vegetable oils may be precursors for these oxidized emissions. I discuss several possible precursors and experiments in which linseed and tung oils were tested for their secondary emission potential. Dynamic emission rates of 2-nonenal from a residential carpet may indicate that intermediate species in the oxidation of conjugated olefins can significantly delay aldehyde emissions and act as reservoir for these compounds. The ozone induced emission rate of 2-nonenal, a very odorous compound, can result in odorous indoor concentrations for several years.

Surface ozone reactivity, is a key parameter in determining the flux of ozone to a surface, is parameterized by the reaction probability, which is simply the probability that an ozone molecule will be irreversibly consumed when it strikes a surface. In laboratory studies of two residential and two commercial carpets, I determined the ozone reaction

probability for carpet fibers, carpet backing and the equivalent reaction probability for whole carpet. Typically reaction probability values for these materials were 10^{-7}, 10^{-5}, and 10^{-5} respectively.

To understand how internal surface area influences the equivalent reaction probability of whole carpet, I developed a model of ozone diffusion into and reaction with internal carpet components. This was then be used to predict "apparent" reaction probabilities for carpet. I combine this with a modified model of turbulent mass transfer developed by Liu, et al. to predict deposition rates and indoor ozone concentrations. The model predicts that carpet should have an equivalent reaction probability of about 10^{-5}, matching laboratory measurements of the reaction probability.

For both carpet and duct materials, surfaces become progressively quenched ("aging"), losing the ability to react or otherwise take up ozone. I evaluated the functional form of aging and find that the reaction probability follows a power function with respect to the cumulative uptake of ozone. To understand ozone aging of surfaces, I developed several mathematical descriptions of aging based on two different mechanisms. The observed functional form of aging is mimicked by a model which describes ozone diffusion with internal reaction in a solid. I show that the fleecy nature of carpet materials in combination with the model of ozone diffusion below a fiber surface and internal reaction may explain the functional form and the magnitude of power function parameters observed due to ozone interactions with carpet.

The ozone induced aldehyde emissions, measured from duct materials, were combined with an indoor air quality model to show that concentrations of aldehydes indoors may approach odorous levels. I show that ducts are unlikely to be a significant

sink for ozone due to the low reaction probability in combination with the short residence time of air in ducts.

LBNL-45044

Ozone-Surface Interactions: Investigations of Mechanisms, Kinetics, Mass Transport, and Implications for Indoor Air Quality

Glenn Charles Morrison
(Ph.D. Thesis)

Department of Engineering
University of California, Berkeley

and

Environmental Energy Technologies Division
Ernest Orlando Lawrence Berkeley National Laboratory
University of California
Berkeley, California 94720

December 1999

This work was supported by the Assistant Secretary for Energy Efficiency and Renewable Energy of the U.S. Department of Energy under Contract No. DE-AC03-76SF00098, and the U.S. Environmental Protection Agency STAR Fellowship Program.

TABLE OF CONTENTS

LIST OF FIGURES

LIST OF TABLES

ACKNOWLEDGEMENTS

This work is a product of many hours working in the lab, writing at my desk, and thinking on BART. These alone were not enough to allow me to accomplish my task. The quality of my thesis is a reflection of Priscilla's encouragement, understanding, and honest criticism. Bill Nazaroff has challenged me to be a better writer, researcher, and communicator. If I have absorbed even a portion what he has to teach me, then I can succeed at any task. I must thank Al Hodgson for allowing me to take up space in his lab. Al, thank you for teaching me to question my results and then question again. Much thanks to Joan Daisey for her advice and ideas during the year that Bill was in Israel. I may never meet a better scientist. My work was advanced tremendously by the electronics advice of my brother Steve and my best friend Joe. I thank my parents, Betty and Dave, for encouraging independence and critical thinking. Thanks to Professors Robert Harley and Cathy Koshland for taking the time to carefully review and improve this document. This research was funded through a grant from the U.S. Environmental Protection Agency STAR Fellowship Program and by the Office of Energy Efficiency and Renewable Energy, U.S. Department of Energy, under contract No. DE-AC03-76SF00098.

CHAPTER 1

Introduction to Ozone and Its Influence on Indoor Air Quality

1.1 Background

Ozone (O_3) is a major component of photochemical smog. While some regions, such as the Los Angeles basin, have had success in reducing ozone concentrations, ozone and photochemical smog continue be a problem not only in Los Angeles, but throughout the United States, and indeed, throughout much of the urbanized world. In the western United States, high ozone concentrations are generally associated with densely populated urban areas, although tropospheric ozone can form at low levels in pristine areas. In the eastern United States, moderately high ozone levels are observed to occur over broad regions. Other countries experience high ozone concentrations, e.g., Mexico and Greece.

Ozone is a strongly oxidizing, gas-phase compound formed as a secondary pollutant species through the interaction of sunlight, nitrogen oxides, and organic compounds. Nitrogen oxides are primarily released into urban air from fuel combustion for electricity generation and in automobile internal combustion engines. Organic compounds can be released from both anthropogenic sources (e.g., solvent emissions from house painting) and natural sources (e.g., terpene emissions from forest canopies). The energy of sunlight powers the chemical transformation of these primary emissions into the familiar orange-brown haze over urban areas, known as photochemical smog (Seinfeld, 1986).

The dominant route of ozone exposure for humans is through inhalation. As much as 90% of inhaled ozone reacts in the pulmonary system in healthy nonsmoking adults

(Gerrity et al., 1988). In acute exposure studies, the chief effects of ozone inhalation are reduced lung function and inflammatory responses of both upper and lower airways. With increasing ozone concentration, inhalation exposure causes both the vital capacity (total volume) and the forced expiratory flow rate to decrease. Ozone reduces the ability of endurance athletes to complete specific exercises in laboratory settings. However, symptoms tend to diminish in subjects who have been repeatedly exposed. In addition, there is a wide variability in individual sensitivity to ozone (Bylin, 1996). Epidemiological studies of exposure at high ambient concentrations (> 240 $\mu g\ m^{-3}$) show correlations with cough, sore throat, lower and upper respiratory symptoms, shortness of breath, and eye irritation. Symptoms may be found at lower concentrations in exercising adults while athletic performance can be hindered at high concentrations. A positive correlation has been observed between daily ozone concentration and hospital admissions, especially for respiratory-related diseases (Nyberg and Pershagen, 1996).

Assessment of exposure requires quantification of both the breathing zone concentration of a pollutant and the time of exposure. Therefore, details of time spent in specific locations along with pollutant levels in those locations are critical in evaluating risk for individuals and populations. Several studies of human activity have shown that people spend about 90 % of their time indoors (Szalai, 1972; Jenkins et al., 1992). Yet monitoring of airborne pollutants takes place outdoors. Were the indoor and outdoor concentrations equal at all times, outdoor monitoring would suffice to quantify exposure. However, indoor concentrations differ from those outdoors for VOCs (Brown et al., 1984) and many other pollutants. Concentrations of ozone are usually much lower in buildings than outside. Even so, it has been estimated that indoor ozone exposure

dominates total exposure for the general population (Weschler et al., 1989). Thus, the use of outdoor measures of pollution is not sufficient to address unique features of indoor pollutant exposure.

Field studies of ozone concentrations in and around buildings have shown that the indoor to outdoor concentration ratio (I/O) ranges from about 0.1 to 0.8 (Weschler et al., 1989). The value of I/O is strongly dependent on ventilation rate, where a higher ventilation rate leads to a higher I/O. Ozone concentrations indoors are reduced due to both heterogeneous reactions with indoor surfaces and gas-phase homogeneous reactions (e.g., reaction with nitric oxide to form nitrogen dioxide). On the other hand, some office equipment, such as photocopiers can act as an indoor ozone source, potentially increasing indoor ozone concentrations. In recent years, "ozone generators" have become a popular indoor appliance used for air and surface cleaning. These devices have the potential to significantly increase indoor ozone concentrations (Kissel, 1993; Boeniger, 1995).

Indoor environments represent a special challenge to engineers and health researchers. Not only are concentrations of pollutants strongly influenced by unique indoor processes, but also this is where people spend the majority of their time. For these reasons, it is valuable to build an understanding of processes that influence indoor air quality.

The task of measuring or predicting human exposure to pollutants in indoor environments is complicated by the many variables that affect concentrations. Ventilation and infiltration rates may be unsteady, interior air movement may be a mixture of laminar and turbulent flows, and these flows can be dynamically influenced by heat sources (convection), wind (pressure gradients across building shell), forced flow (fans or

mechanical ventilation) and the movement of occupants. Emission sources themselves can be complicated by being located at a single point (e.g., a cigarette), being spread out over a large area (e.g., painted walls), and having time-varying emission rates. Air exchange between rooms of a building may be difficult to predict without detailed information about interior pressures and leakage between zones.

Some simplifications have eased the analysis burden. The rate of air mixing in an average sized room with some air exchange is usually high enough for complete mixing to occur over relatively short time scales, e.g. several minutes. While not valid in every situation, material balance models integrating a completely mixed zone (room or entire house) have been successful in predicting indoor concentrations of pollutants, provided the appropriate sources and sinks are incorporated (Weschler et al., 1989).

In a typical deterministic indoor air quality model, a building zone is modeled as a "continuously mixed flow reactor" or CMFR. In a CMFR, pollutants introduced into the zone are instantaneously and uniformly mixed in the volume, V, of the zone. Dynamic changes in concentrations, C, are influenced by sources and sink mechanisms including ventilation, surface adsorption/removal, and chemical reactions. Mathematically, a typical model equation incorporating air exchange rate, λ (volumetric ventilation rate divided by volume), emission rate, E, and surface loss rate is written follows:

$$\frac{dC}{dt} = \lambda C_o + \frac{E}{V} - C\lambda - v_d C\frac{S}{V} \qquad (1.1)$$

The surface loss rate term, $v_d C(S/V)$, incorporates an area averaged mass transfer coefficient (or deposition velocity), v_d, and the surface area to volume ratio, S/V (Shair and Heitner, 1974). The term, C_o, represents the outdoor concentration. Variations on this model will be used extensively in this thesis for predicting indoor concentrations of

ozone and aldehydes based on laboratory measurements of ozone interactions with carpets and other indoor materials.

The deposition velocity captures all of the dynamics of pollutant transfer and uptake on surfaces and averages them over the entire building zone. Predicting the value of v_d for specific conditions at a specific site can be complex. To separate the problem into simpler, more manageable pieces, Cano-Ruiz et al. (1993) suggested that mass transfer to a surface could be tackled separately from the uptake on the surface. The surface uptake could be parameterized by the reaction probability, γ, which is the rate at which a pollutant reacts on a surface divided by the rate at which that species strikes the surface. The reaction probability is independent of fluid flow conditions in the room, and can be measured independently, in a laboratory setting. Cano-Ruiz et al. then used simplified descriptions of a variety of fluid flow regimes (turbulent, convective, laminar, etc.) to predict the rate of mass transfer to a surface, given information about fluid flow or energy, and pollutant diffusivity. By combining the simplified mass-transfer relationships with the surface reaction probability (as measured by various researchers for a variety of materials), they created models to describe the deposition velocity which reasonably matched observations in the field. In a more recent development, Lai and Nazaroff (2000) showed that mass transport through a turbulent boundary layer can be treated in a mathematically tractable way, by creating correlations based on the results of direct numerical simulations of near surface flow.

Ozone reactions with surfaces can improve air quality by lowering indoor ozone concentrations. However, reaction products formed in these interactions may contribute to degradation of air quality. Weschler et al. (1992) found that several aliphatic aldehydes

were released when carpets were exposed to ozone in laboratory chambers. They suggested that a vegetable oil coating, introduced during manufacture of carpet, may be the source of these aldehydes. The secondary emission of aldehydes from carpet is an important finding for several reasons: carpet is a common installed flooring material, carpet has a high intrinsic surface area, and the odor threshold is very low for compounds produced by the surface reactions of ozone on carpet.

Carpets are found in most homes and businesses and constitute about 70% of the market in newly installed floor coverings (Carpet and Rug Institute, 1998). Approximately 11 m^2 of carpet were sold per household ($\sim 10^8$ households) in 1997. Wall-to-wall carpet is manufactured with synthetic fibers imbedded in a stiff backing. Bundles of fibers are typically looped through the backing, creating a ~0.2 - 1 cm thick mat of fibers that are sometimes trimmed to create a "cut pile" style. The diameter of a typical fiber ranges from 50 to 100 μm and there are typically several million exposed fibers per square meter of carpet. Installation of carpet can add a significant amount of surface area to a room, providing many locations for ozone to react and form secondary emission products. Presently, synthetic fibers (nylon, olefin, and polyester) constitute approximately 99% of the entire U.S. market for carpet fibers. Wool is the most common natural fiber used in carpet but constitutes less than 1% of the fiber market (Carpet and Rug Institute, 1998).

The aldehydes released as ozone reaction products from carpet and other indoor materials such as paint (Reiss et al., 1995) have low odor thresholds and may contribute to poor air quality when the reaction products desorb from surfaces. As molecular weight increases, odor and irritation thresholds decrease (Cometto-Muniz et al., 1998). In my

studies with carpet, the emission rate of aldehydes tends to *increase* with carbon chain-length, up to C_9. The opposite trends of these two phenomena amplify the odorous nature of secondary carpet emissions and show that compound-specific measurements (as opposed to total VOC determinations) are very important. Wide variability in individual sensitivity is also an important factor. For example, individual odor threshold detection of octanal can range from 1 to 100 ppb.

The secondary effect of ozone reacting with surfaces to form volatile compounds may contribute to health problems associated with time spent in buildings. In recent years, much attention has been given to a phenomenon known as "sick building syndrome." Building inhabitants complain of a variety of symptoms commonly including eye and mucous membrane irritation, lethargy, and headaches (Hedge, 1989). These symptoms usually cannot be strongly correlated with measured physical and chemical parameters. Investigators have ascribed the effects to multiple factors, including psychosocial aspects of the work environment, inadequate ventilation, airborne microbial contaminants, or the presence of VOCs (Molhave, 1989; Stolwijk, 1991; Mendell, 1993; Ten Brinke et al., 1998). VOCs are plausible contributors because some, such as aldehydes and organic acids, are known to be irritating at relatively low concentrations (Cometto-Muniz, et al. 1998). Wolkoff et al. (1999), recently showed that organic radical species may be very irritating to lab mice, leading to speculation that ozone reactions with airborne olefinic species may contribute to discomfort of building occupants. Hydroxyl radicals have been shown to form in indoor spaces by the reaction of ozone with compounds associated with cleaning products (Weschler and Shields, 1997). The production of low-volatility ozone reaction products has been shown to lead to the

formation of airborne particles (Weschler and Shields, 1999), which may also be a health hazard.

Ozone reactions with surfaces result in a reduction in indoor ozone concentrations. However, oxidation of surfaces can also lead to irreversible damage. It has long been known that ozone reacts with products made of natural rubber, eventually making these products unusable. Works of art are also subject to degradation by pollutants. Grosjean et al. (1993) showed that several colorants used in paintings can fade in the presence of ozone.

The indoor interactions of ozone result in a tricky public health and welfare trade-off. On one hand, ozone reactions reduce exposures by reducing indoor ozone concentrations. On the other hand, these reactions can lead to several secondary problems: odorous compound emissions from surfaces, formation of radicals and particles, and damage to surfaces. Control of ozone entry into indoor spaces is an obvious way to reduce all of these problems. However, ozone will continue to be an indoor problem until outdoor ozone formation is controlled, or there is widespread use of indoor ozone control measures in buildings. Modifications to the manufacture of carpets and other indoor surfaces may help reduce oxidized product emissions and limiting the release of volatile olefins indoors may help control particulate formation. Until significant progress has been made on any of these fronts, there will continue to be a trade-off between the problems associated with ozone and those associated with its secondary effects. To address this issue, I endeavored to build an understanding of the processes that influence ozone uptake at surfaces and the formation of secondary emission products.

1.2 Goals

There remain many unanswered questions regarding ozone interactions with surfaces in buildings. We know that ozone is removed at surfaces, reducing indoor concentrations. We do not yet understand the mechanisms that result in observed uptake rates at building surfaces. The observation of reaction product emissions is strong evidence of specific reaction mechanisms. One important example is the observation that aldehydes may form when ozone reacts with carpet (Weschler et al., 1992). However, no comparison has been made between reaction product formation rates on carpets and ozone uptake rates. Formation rate quantification of carbonyl species emitted from painted surfaces indicated that a significant fraction of the ozone might have been involved in reactions with carbon-carbon double bonds (Reiss et al., 1995).

In this thesis, I studied ozone reactions with carpet with several goals in mind. First, I wanted to quantify the absolute and relative emissions of aldehydes from several carpet types. Using this information, I would suggest the general class of surface precursors and perhaps specific reactive species that are present on carpets. I also hoped to quantify the amount of deposited ozone that is responsible for oxidized emission products. Average emission rates and cumulative emissions of reaction products would allow me to predict the indoor concentrations of compounds such as odorous aldehydes and also for how long these emissions might occur.

The high surface area to volume ratio indoors serves to strongly influence indoor pollutant dynamics. Carpet is a good example of a commonly installed high surface area material. Installing carpet in a home can increase the total surface area by an order of magnitude. While this increased surface area may provide more locations for ozone to be

consumed, it may also be responsible for more secondary oxidized emissions. It is important to understand how ozone is transported to the carpet face and into the carpet fiber mat. A successful mathematical model of this system should be able to answer several questions: How much intrinsic surface area is available for reaction? Under what conditions does ozone penetrate to the carpet backing? How can the whole carpet reaction probability be calculated from information about the reactivity of carpet fibers and backing?

Thus, a second general goal was to better characterize reactive gas uptake on topographically complex surfaces and attempt to answer the questions posed above. Carpet serves as a good model material for several reasons: it is present in most homes and businesses, it has the potential to add significant amounts of surface area to indoor spaces, and ozone reaction rates are readily measured on the whole carpet, and on its constituent parts (fibers, carpet backing) using simple laboratory reactors. I approached this topic by comparing laboratory measurements of the reaction probability on carpet with mathematical models of ozone transfer to and into the carpet mat.

There is one finding that is common to most studies of ozone uptake on indoor material surfaces: as a material is continuously exposed to ozone, the ozone reaction probability on that surface becomes progressively smaller. This is also known as ozone aging of surfaces. It is not yet clear why this occurs and how the aging of a particular material may be predicted or interpreted. A mechanistic understanding of the dynamics of surface aging may provide a means to more reliably predict the time dependence of indoor ozone concentrations. Mechanisms that describe surface aging may also help explain how some surfaces are damaged by ozone. For these reasons, I hoped to develop

several possible mechanisms to explain surface aging, then eliminate mechanisms that do not match experimental observations of ozone aging of carpet and other surfaces.

In their examination of literature values of the reaction probability on surfaces, Cano-Ruiz et al. (1993) noted that no information was available on ozone uptake on materials that line ducts. Ventilation ducts are found in most commercial buildings and serve as the main conduits through which outdoor air is delivered to indoor spaces. Ozone reactions with these surfaces again have the potential to reduce indoor ozone concentrations but also increase the concentration of reaction products. For this thesis, I aimed to measure the reaction probability of several surfaces typically found in ventilation ducts, while quantifying any secondary reaction products emitted from these surfaces. These results could then be used to predict the impact ozone-duct material interactions have on indoor air quality.

1.3 Outline of dissertation

This section provides an introduction to the general organization of the thesis. There are six chapters following this introductory chapter. Chapters 2 through 6 present specific research topics. Chapters 2 and 3 describe laboratory studies and results of ozone interactions with carpet. Chapter 4 and 5 discuss the development of mathematical models of ozone deposition on carpet and the mechanisms that govern ozone aging of surfaces. Chapter 6 combines laboratory measurements and mathematical analysis to predict ozone penetration through ducts and the influence of duct surfaces on organic compound concentrations in indoor spaces. Chapter 7 is a summary of the work and contains suggestions for future research. The dissertation concludes with five appendices

that provide additional details on selected aspects of the studies presented in the body of the work.

In Chapter 2, I describe the laboratory investigation of ozone interactions with carpet surfaces and the secondary emission of oxidized reaction products. In this study, I exposed carpet, and carpet backing to ozone in small chambers and quantified the secondary release of aldehydes. Carpet fibers were similarly tested in a Teflon tubular reactor. I examined the difference between carpets that had been stored in a sealed bag for greater than a year, and carpets that had been stored in a ventilated chamber for the same period. I suggest reaction mechanisms and chemical precursors for the reaction products based on average and dynamic emission rates and aldehyde emission patterns. I also use the emissions data to predict indoor air quality impacts of ozone-carpet chemistry for a typical home.

In Chapter 3, I present the results of laboratory measurements of ozone uptake rate and reaction probability on carpets. The ozone reaction probability on whole carpet, carpet fibers and carpet backing can all be extracted from the experiments described in Chapter 2. The dynamic reaction probability data are analyzed and a simple empirical correlation is suggested to describe ozone aging of these surfaces.

I develop mathematical models of ozone uptake by carpet in Chapter 4. First, I modify an existing turbulent deposition model to incorporate the surface reaction probability. This model describes transport of ozone from bulk room air to the tips of carpet fibers. A diffusion model is developed to simulate reaction and mass transport in the region below the carpet fiber tips. This diffusion model uses information about carpet geometry and the reaction probability of the fibers and carpet backing to generate an

equivalent flat surface reaction probability located at the fiber tips. I then compare the predictions of the models to the deposition results in Chapter 3.

In Chapter 5, I suggest several mechanisms for ozone aging of surfaces. I analyze these mechanisms and derive mathematical relationships that can be compared to observed aging phenomena. The most promising aging mechanism is combined with the carpet model discussed in Chapter 4 to simulate ozone aging of carpets for comparison with dynamic reaction probability measurements presented in Chapter 3.

Ducts and the materials that line ducts are examined in Chapter 6. I allow ozone to react with duct materials in experiments that are similar to those used to examine ozone-carpet interactions. I measure dynamic ozone reaction probabilities on these surfaces and the oxidized reaction products that are emitted. I connect surface aging results to an ozone penetration model to simulate dynamic ozone penetration through typical duct configurations. I also predict the indoor concentration of oxidized reaction products in a building based on experimental results.

1.4 References

Boeniger, M.F. *American Industrial Hygiene Association Journal.* **1995**, *56*, 590-598.

Brown, S.K.; Sim, M.R.; Abramson, M.J.; Gray, C.N. *Indoor Air.* **1994**, *4*, 123-134.

Bylin, G. *Scandinavian Journal of Working Environment Health.* **1996**, *22:supp.3*, 52-71.

Cano-Ruiz, J.A.; Kong, D.; Balas, R.B.; Nazaroff, W.W. *Atmospheric Environment.* **1993**, *27A*, 2039-2050.

Carpet and Rug Institute. *Carpet and Rug Institute Industry Review.* 1998.

Cometto-Muniz, J.E.; Cain, W.S.; Abraham, M.H. *Experimental Brain Research.* **1998**, *118*, 180-188.

Gerrity, T.R.; Weaver, R.A.; Berntsen, J.; House, D.E.; O'Neil, J.J. *Journal of Applied Physiology.* **1988**, *65*, 393-400.

Grosjean, D.; Grosjean E.; Williams E.L. *Atmospheric Environment Part A-General Topics.* **1993**, *27,* 765-772.

Hedge, A. *Environment International.* **1989,** *15*, 143-158.

Jenkins, P.L.; Phillips, T.J.; Mulberg, E.J.; Hui, S.P. *Atmospheric Environment.* **1992,** *26A*, 2141-2148.

Kissel, J.C. *Journal of Exposure Analysis and Environmental Epidemiology.* **1993**, *3,* 155-164.

Lai, A.C.K.; Nazaroff, W.W. *Journal of Aerosol Science.* **2000**, *31*, in press.

Mendell, M.J. *Indoor Air.* **1993**, *3*, 227-236.

Molhave, L. *Environment International.* **1989**, *15*, 65-74.

Nyberg, F.; Pershagen, G. *Scandinavian Journal of Work Environment and Health.* **1996**, *22: supp. 3*, 72-95.

Reiss, R.; Ryan, P.B.; Koutrakis, P.; Tibbets, S.J. *Environmental Science and Technology.* **1995**, *29*, 1906-1912.

Seinfeld, J.H. *Atmospheric Chemistry and Physics of Air Pollution.* John Wiley & Sons, New York. 1986.

Shair, F.H.; Heitner, K.L. *Environmental Science and Technology.* **1974**, *8*, 444-451.

Stolwijk, J.A. *Environmental Health Perspectives.* **1991**, *95*, 99-100.

Szalai, A., Ed. *The Use of Time: Daily Activities of Urban and Suburban Populations in Twelve Countries.* The Hague. 1972.

Ten Brinke, J.; Selvin, S.; Hodgson, A.T.; Fisk, W.J.; Mendell, M.J.; Koshland, C.P.; Daisey, J.M. *Indoor Air.* **1998**, *8*, 140-152.

Weschler, C.J.; Shields, H.C.; Naik, D.V. *JAPCA: Journal of the Air and Waste Management Association.* **1989**, *39*, 1562-1568.

Weschler, C.J.; Hodgson, A.T.; Wooley, J.D. *Environmental Science and Technology.* **1992**, *26*, 2371-2377.

Weschler, C.J.; Shields, H.C. *Environmental Science and Technology.* **1997**, *31*, 3719-3722.

Weschler, C.J.; Shields, H.C. *Atmospheric Environment.* **1999**, *33*, 2301-2312.

Wolkoff, P; Clausen, P.A.; Wilkins, C.K.; Hougaard, K.S.; Nielsen, G.D. *Atmospheric Environment*. **1999**, *33*, 693-698.

CHAPTER 2

Ozone Interactions with Carpet: Release of Primary and Secondary Volatile Organic Compounds

2.1 Background

Indoor emission sources contribute significantly to indoor air pollutant concentrations. Volatile organic compounds can be released into the indoor space as a primary emission product from furnishings, or as the byproduct of chemical reactions at surfaces or in the gas phase. For example, ozone can react at surfaces forming reaction products on the surface. Volatile reaction products can then be released, degrading indoor air quality (Weschler, et al., 1992; Reiss et al., 1995a).

In this chapter, I report on investigations of ozone interactions with carpeting to better understand the sources of oxidized products and the impact on indoor environments. I placed four different carpets in separate ventilated chambers for 15 to 20 months to reduce the primary emissions of volatile compounds. These carpets, along with stored (unventilated) samples, were then subjected to a controlled atmosphere containing ozone. I measured the release rates, and time-integrated releases of the oxidized products of ozone reactions with these surfaces. From this information, along with assumptions about the geometry and ventilation conditions of typical homes, I predicted how these ozone-surface interactions would influence indoor concentrations of odorous compounds. The dynamic pattern of emissions also reveals information about the form of the precursor surface species, and reaction mechanisms.

The following section reviews recent research suggesting that ozone interactions

with indoor surfaces can degrade air quality by forming volatile oxidized compounds. I also outline accepted reaction mechanisms of ozone with olefins, the probable precursor for aldehydes observed in ozone-surface exposure studies.

The "Methods" section of this chapter covers, in detail, the laboratory methods used to prepare and expose carpet samples, and to quantify aldehyde emissions. The general laboratory methods also extend to experiments performed to measure ozone deposition rates, as described in Chapter 3. I separate the "Results" section into descriptions of primary emissions, and of cumulative and dynamic oxidized emissions for each carpet. I also describe the results of emission studies for several natural oils. I analyze these results in the "Discussion" section. I first examine the pattern of emissions as these may suggest precursor compounds, and compare them to results from natural oil exposed to ozone. These oils were chosen based on their chemical structure and previously reported oxidized compound emissions. The dynamic and cumulative emissions are examined for a residential carpet that was found to be a strong emitter of 2-nonenal, a very odorous compound. Simulations of average and dynamic indoor air concentrations were performed to determine the extent to which secondary emissions from carpets contribute to odors.

2.1.1 Ozone reactive chemistry in indoor environments

2.1.1.1 Ozone and carpet

In 1992, Weschler et al. reported that organic compounds associated with carpet can react with ozone to form several volatile, aliphatic aldehydes. Ozone gas-phase reactions reduced the concentration of some volatile species such as 4-phenylcyclohexene

(a species associated with the smell of new carpet), 4-vinylcyclohexene, and styrene; however, these reactions should not result in the emissions of the homologous series of n-aldehydes detected. Indeed, the total mass concentration of VOCs increased due to the jump in emissions of C1 through C10 n-aldehydes. They surmised that these compounds were formed as ozone reacted with low-volatility surface species, and were most strongly associated with carpet fibers rather than carpet backing. They suggested that these species were either unsaturated vegetable-based oils or the products of incomplete polymerization of carpet fibers.

The concentration of individual aldehydes in the room-sized test chamber was typically in the range of 0.1 to 5 ppb when carpet was exposed to 30-50 ppb O_3. These ozone levels represent typical daytime indoor mole fractions in polluted areas. Aldehydes have very low odor thresholds, in the range of 1 to 50 ppb. This observation showed that carpets can act as a "reservoir" for precursor species that, when exposed to ozone, release odorous levels of aldehydes. Although the concentrations measured do not reach the threshold of irritation for individual aldehydes (Cometto-Muñiz et al., 1998), the combined emissions of aldehydes under severely polluted conditions may create an odorous indoor environment. The intensity of pungency (irritancy) may be hyperadditive, additive or hypoadditive, depending on the component mixtures (Cometto-Muñiz and Hernández, 1990). It is not yet clear if odor thresholds can be exceeded with mixtures of species with individual concentrations below their respective thresholds (Berglund and Lindvall, 1992; Patterson et al., 1993).

2.1.1.2 Ozone and latex paint

Reiss et al. (1995a) studied the influence of ozone on the formation of volatile product species from painted surfaces. They exposed latex paint to ozone in glass tubular reactors and measured the ozone removal rate and emissions of several volatile organic compounds. They detected no increase in formic or acetic acids upon exposing the paint to ozone, and in fact, measured small decreases, which they suggested was due to timing of sampling (generally, VOC emissions from materials decrease with time as they are depleted from the material). They found that methanal, ethanal and acetone emissions increased from some paints with ozone exposure. In some cases the emission rate correlated with ozone uptake, but this was not a consistent trend.

2.1.1.3 Building studies

If ozone can initiate increased emissions of carbonyl compounds from indoor surfaces, then studies of VOCs in residences may reveal this phenomena under field conditions. During the winter and summer of 1993, Reiss et al. (1995b) measured several carbonyl compounds in four residences in the greater Boston, Massachusetts area. They found that the "mean effective" emission rate of formic acid, acetic acid, acetone, butanone, and C_1,C_2, C_4-C_6 n-aldehydes were higher during the summer period where the indoor ozone concentration was higher. However, statistical analysis of correlations between emissions and the environmental variables ozone, humidity, and temperature could not conclusively demonstrate that ozone-surface reactions were causal.

In a similar study, Zhang and Lioy (1994) monitored indoor and outdoor concentrations of several aldehydes and ozone from six residences in central New Jersey.

They found that indoor ozone concentrations correlated with ethanal, n-pentanal, the sum of n-pentanal and iso-pentanal, and formic acid. Correlations were significant but not strong, with Spearman correlation coefficients (r) ranging from 0.35 to 0.48.

2.1.2 The gas-phase chemistry of ozone and alkenes

Ozone reacts rapidly with organic compounds that contain double bonds. Figure 2.1 illustrates the likely pathways for gas-phase reactions of ozone with alkenes (Atkinson et al., 1995). Reactions of ozone with pure hydrocarbon alkenes produces a *molozonide* (also known as a primary ozonide, initial ozonide, or *primärozonide*) that rapidly decomposes to produce two carbonyls and two Criegee-biradical products. The carbonyl formed depends on the substituents R_i. Where either substituent is hydrogen, the carbonyl compound formed is an aldehyde. Otherwise, ketones are formed. The biradical can be stabilized by colliding with another gas-phase molecule (M), typically nitrogen. Atkinson and others have shown that the hydroperoxide channel is very important. Ozone reactions with alkenes commonly produce near stoichiometric yields of OH radicals (Atkinson et al., 1995). Due to the significant concentration of terpenes (e.g. due to emissions from wood and cleaning products) in indoor air, the production of OH radicals may strongly influence indoor oxidation chemistry (Nazaroff and Cass, 1986; Weschler and Shields 1996) and may also lead to the formation of secondary particulate matter (Weschler and Shields, 1997).

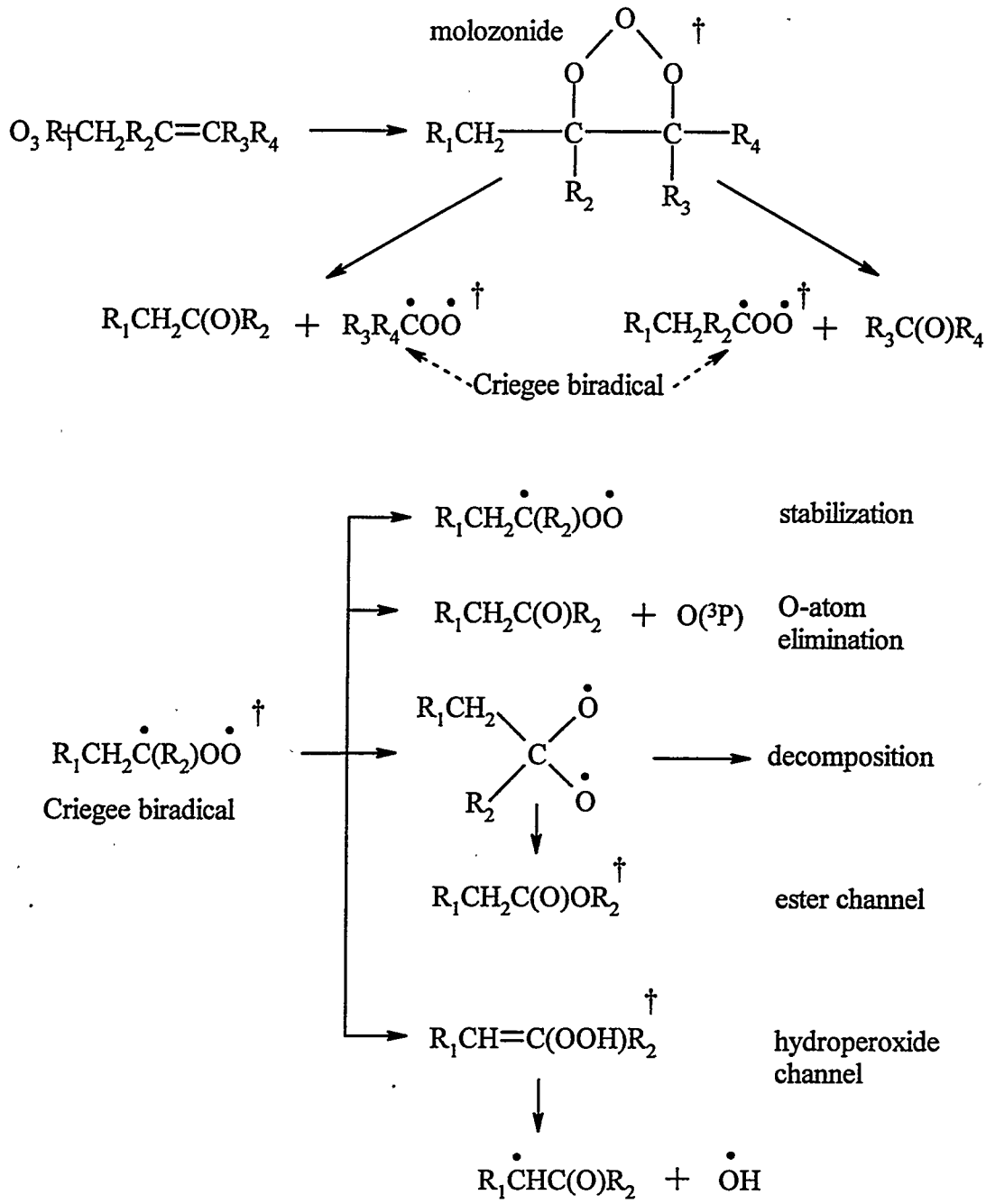

Figure 2.1. Generalized reaction sequence for gas-phase ozone reactions with alkenes (based on equations 1, and 2a-2d, from Atkinson et al.,1995). Energetic (unstable) species are denoted with †.

2.1.3 Solution-phase chemistry of ozone and alkenes

Much of the ozone loss by reaction in this study occurs at the surface of the tested material. Weschler et. al. (1992) suggested that the aldehydes produced (in their study of carpets exposed to ozone) are the result of ozone reacting with vegetable based fatty acid/ triglycerides (i.e. vegetable oils) that may have been used in the manufacture of carpet. Carpet fibers may be woven using machines that require the fibers to be lubricated, and Weschler suspects this coating may be the source of the reactive surface (personal communication). Fibers are also treated in several processing steps that include washing with sulfonated vegetable oils (Wingate, 1979). Residue from washing may also be a significant source of aldehyde precursors.

While little is known about the kinetics of ozone reactions with unsaturated fatty acids at interfaces, much work has been done in solution chemistry with lipids. Ozonation of lipids has long been used to determine the position of double bonds by identifying the reaction products (Molinari, 1903; Hilditch, 1956; Gunstone et al., 1994).

In liquid solution, ozone reaction mechanisms and products are similar to those in the gas phase. As an example, the ozone reaction mechanism with oleic acid (a fatty acid) is shown in Figure 2.2. Oleic acid (or its ester) is a common constituent of vegetable and animal based oils and has been used to waterproof textiles (Windholz and Budavari, 1983). Initially, ozone attaches across a double bond to form a molozonide. At low temperatures (~ -100 °C), the molozonide can be isolated, but it tends to cleave at room temperature to form products that are strongly dependent on the properties of the solution (Gunstone, 1994). Typically, an ozonide is formed from the rearrangement of the molozonide. Many ozonides are stable at room temperature, but can be decomposed

rapidly to form aldehydes and carboxylic acids upon heating.

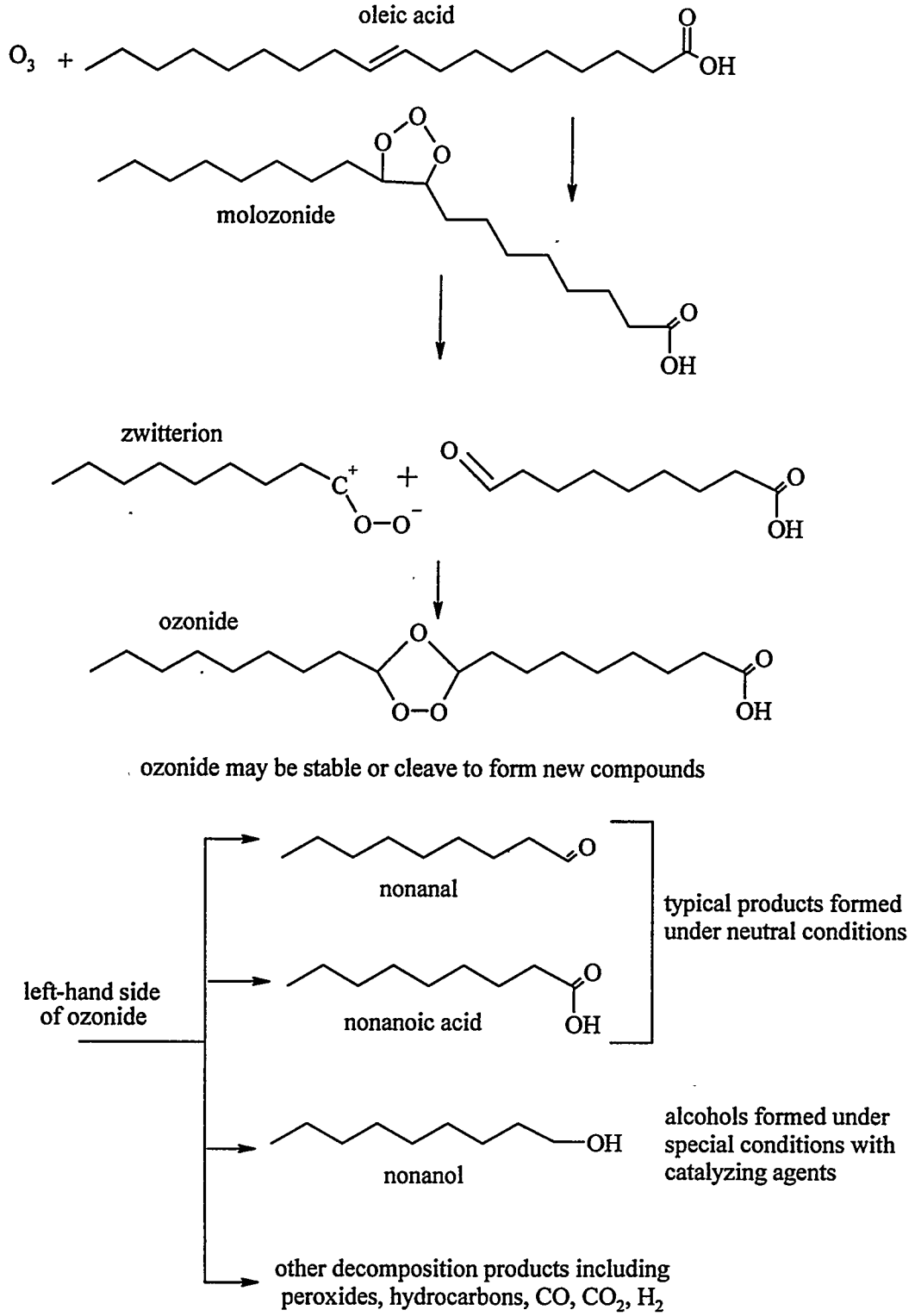

Figure 2.2. Ozone oxidation of oleic acid. Ozone attacks a double bond, creating a semi-stable ozonide which may decompose to aldehydes, acids and other compounds.

Yields of acids increase with increasing pH, or under oxidative conditions. Reducing conditions favor aldehyde formation. Choice of solvents is very important; under certain conditions, alcohols (instead of aldehydes and acids) may be generated. Other products of the decomposition may include H_2, CO, CO_2, and hydrocarbons. Note that solution chemistry may not be relevant to chemistry at the interface where no liquid film is present.

2.2 Methods

2.2.1 Materials

Four carpets were chosen for this study. Carpets CP1 and CP3 are residential, nylon fiber, cut pile carpets; CP2 and CP4 are commercial, olefin fiber, loop carpets. Carpet characteristics, such as fiber composition and stain-resist treatments are shown in Table 2.1. These carpets were chosen to represent commonly installed carpets in California. The fibers of residential carpets CP1 and CP3 had applied treatments of stain resistant coatings. CP4 had no applied treatment but consisted of stain resistant fibers. No treatment information was available for CP2, but commercial carpets do not usually have applied treatments. Styrene-butadiene rubber (SBR) was used as the adhesive in all carpet backing samples.

The carpets were prepared by cutting squares (232 cm^2) from newly manufactured rolls. Half of the samples were enclosed in air-tight aluminum foil pouches and are referred to in the text as "stored." The rest of the samples were placed in 19 L chambers. Filtered air (using activated carbon as a filtration media to remove ozone and VOCs) was used to ventilate the chambers at a constant rate of 10 L min^{-1} for greater than 12 months.

This allowed most of the volatile compounds to be released from the carpet samples, thus simulating carpet materials long after installation, but without soiling. These ventilated samples are referred to in the text as "aired." I chose several pieces of the aired samples (representing each of carpets CP1 through CP4) for use in experiments designed to target interactions at carpet fibers and on the backing of carpet. Using a scalpel, I trimmed the fibers off of some samples, to a level flush with the carpet backing. Fibers were separated from one another using wool-carders. After fiber removal from the face of the carpet backing, fibers remained imbedded in the backing matrix, extending above the backing by less than 0.5 mm. No carpet padding materials were tested in conjunction with these carpet samples.

Table 2.1. Carpet sample characteristics.

sample designation	installation location	style	fiber composition	fiber treatment
CP1	residential	cut pile	nylon	3M Scotchgard Stain Release™
CP2	commercial	loop	olefin, stain resistant	unknown
CP3	residential	cut pile	nylon	Monsanto Wear-Dated™
CP4	commercial	loop	olefin, stain resistant	no treatment

2.2.2 Overview of experimental apparatus

The apparatus used for whole carpet and carpet backing experiments is shown in Figure 2.3. A 10.5-L electropolished stainless steel reaction chamber was placed inside a temperature-controlled cabinet. The sample material (either whole carpet or carpet backing sample) was placed in a Teflon frame so that only the upper surface was exposed to air and this assemblage was placed on a Teflon shelf inside the reaction chamber.

Ozone was generated in the reactor inlet stream using ultraviolet (UV) light. An in-line water sparger was placed in the temperature controlled cabinet for humidifying the reactor supply air. A portion of the vented exhaust was sampled by an ultraviolet photometric ozone analyzer (Dasibi, Model 1003 AH). An electromechanical 3-way valve was used to direct the air stream from the inlet to the ozone analyzer so that either supply air or chamber air ozone concentrations could be measured. The chamber was maintained at 296 ± 0.5 K and 50 ± 5% relative humidity based on an initial calibration using a Vaisala temperature and humidity probe. During these experiments, the chamber was continuously ventilated with a total of 1.2 ± 0.05 L min^{-1} air. A feedback control program (described in detail in Appendix A.1) was used to control the level of ozone in the chamber so that it remained at about 100 ppbv throughout the entire experiment, unless otherwise indicated. Prior to each experiment, the chamber, Teflon frame, and shelf were washed in methanol and dried in an oven at 65 °C. The Teflon parts were then sealed in the reactor. Subsequently, the chamber was ventilated for 4 h with air containing a high ozone level, >4000 ppb. This procedure quenched the reactor walls so that the baseline removal of ozone in the reactor was less than 1% under standard experimental conditions.

An alternative configuration was used to isolate gas phase reactions of ozone with carpet emissions (see Figure 2.4). Two identical electropolished chambers were used. The first chamber, containing the carpet sample, was ventilated with 1.1 L min^{-1} air (no ozone) and the exhaust directed to the second chamber. At the inlet of the second chamber, 0.1 L min^{-1} air with ozone is mixed with the stream from the first chamber. The second chamber acts to isolate gas phase ozone reactions, leaving the carpet surface unexposed to ozone.

2.2.3 Ozone generation

An ultraviolet (UV) lamp was used to directly control the rate of formation of ozone in a portion of the air supply flowing at 0.1 L min^{-1}. This feed stream is later mixed with the main stream of supply air and directed to the inlet of the reactor. A diagram of the ozone generator is shown as Figure A.1.2 in Appendix A.1. This unit is designed such that sliding the shielding tube to expose or cover more of the lamp can vary the flux of UV light to the quartz tube.

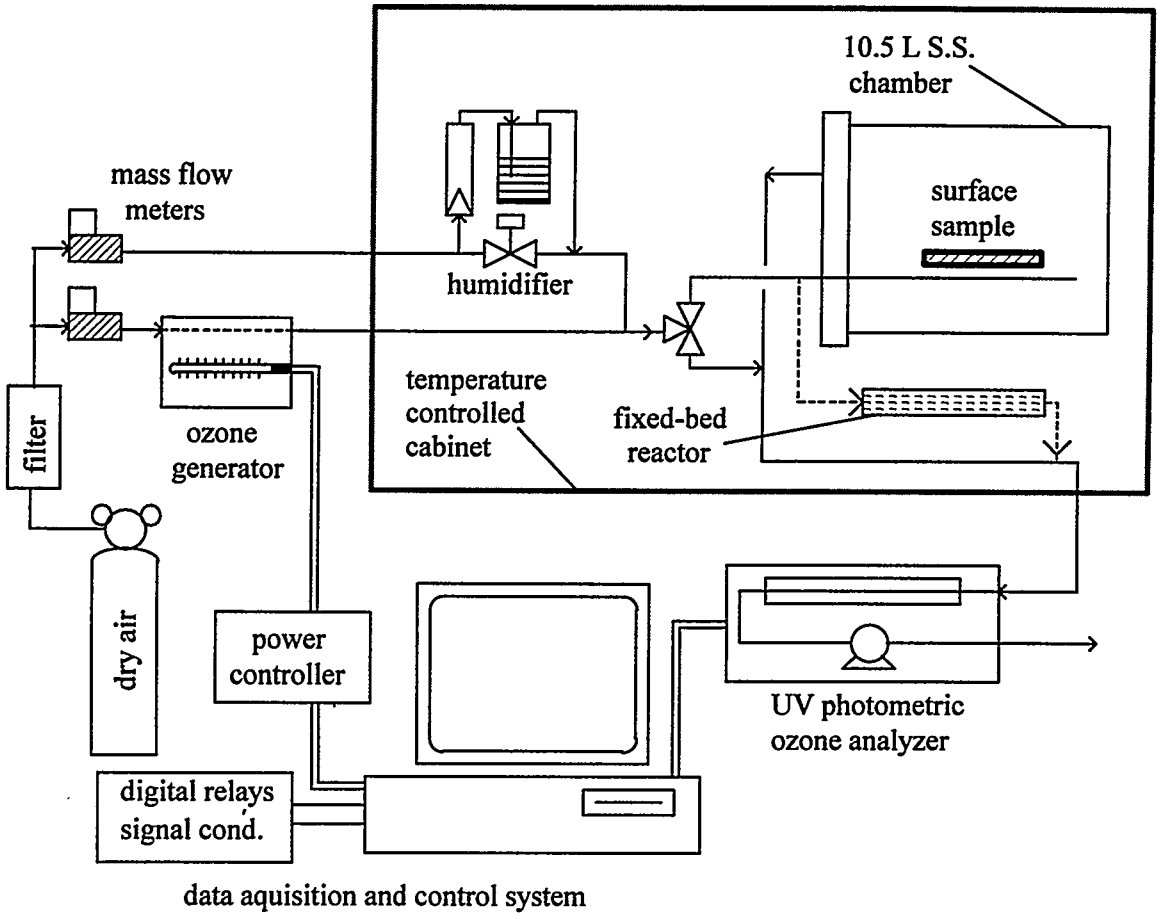

Figure 2.3. Diagram of typical experimental apparatus. Dry air is metered, humidified and mixed with ozonated air, then directed to the reaction chamber. Ozone and VOC concentrations are measured at the reactor exhaust. Ozone level is controlled using a computer controlled feedback system.

Ultraviolet light with a narrow wavelength band surrounding 254 nm illuminates

air flowing through the quartz tube. Quartz is used because it is nearly transparent to UV light at this wavelength. The formation of ozone in the quartz tube follows this mechanism:

$$O_2 \xrightarrow{h\nu} 2O\bullet$$
$$O_2 + O\bullet \xrightarrow{M} O_3$$

where h is Planck's constant, ν is the frequency and $h\nu$ represents the energy required to photolyze di-oxygen to its free radical form, O•. An inert species, M, stabilizes O_3 by removing excess energy of the O_2 + O• reaction.

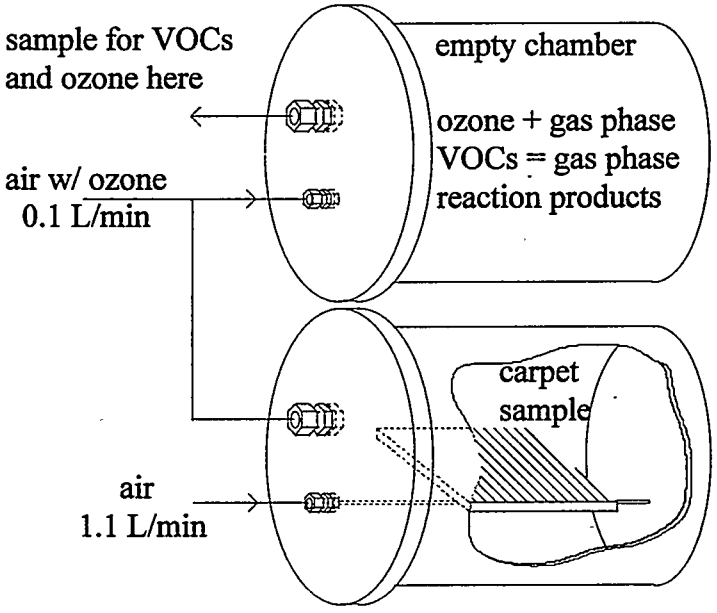

Figure 2.4. Experimental apparatus for examining gas-phase chemistry separate from surface chemistry.

The ultraviolet lamp requires a sufficiently high voltage source to operate and requires a "ballast" to provide the current. The ballast can operate at a variety of input voltages, as long as the lamp electrode voltage is high enough to create a continuous current through the mercury vapor in the lamp. In my case, I used a power supply that

operates by supplying voltage to the lamp from a 24 volt DC source. As the voltage varies, so does the power output of the lamp. Formation of ozone in the quartz exposure tube rises or falls proportionally. Thus, the ozone formation rate in the quartz tube can be crudely controlled manually using the sliding light shield shown in Figure A.1.2. It can be more finely controlled by adjusting the ballast output of the lamp voltage. To vary the ultraviolet lamp radiant output, I varied the DC source voltage to the power supply. A diagram of the circuit built for this purpose is shown in Figure A.1.2 in Appendix A.1. In this circuit, a range of 0-5 V DC from an analog output computer board is transformed into approximately 18-24 V DC for the UV lamp power supply. A calibration is shown in Figure 2.5.

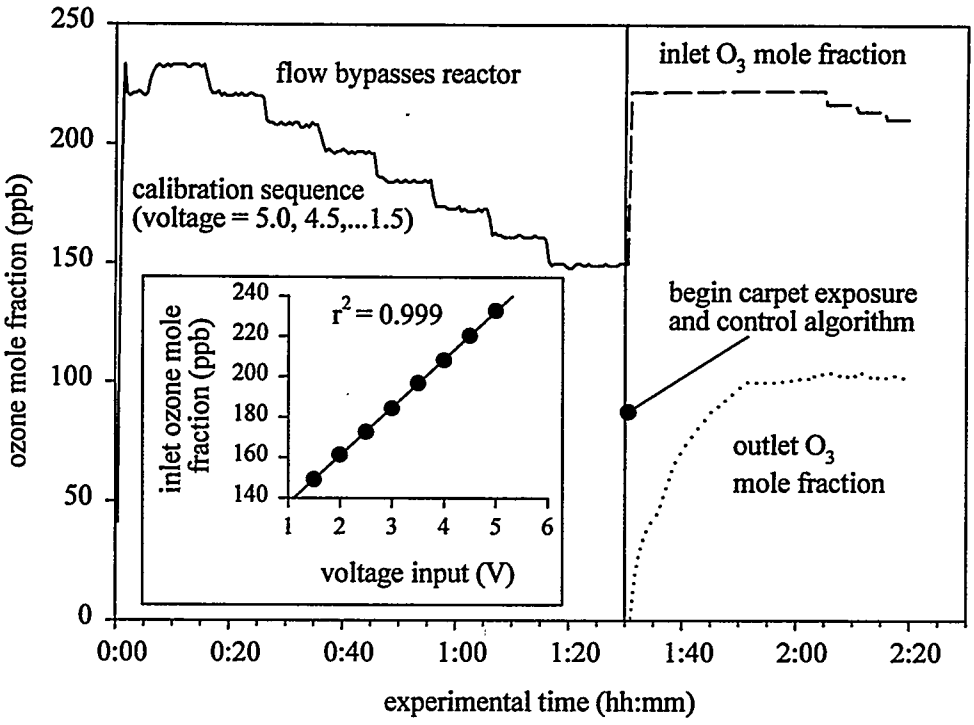

Figure 2.5. Typical calibration sequence for ozone generation and control system. Voltage to the UV lamp is incrementally decreased, decreasing the ozone generation rate and subsequently decreasing ozone concentration at the chamber inlet. Inset: linear relationship between input voltage to control circuit and inlet ozone concentration.

2.2.4 Ozone feedback control and valve operation

A continuously running program, written in the Microsoft Visual Basic 3.0 language, was used to operate the ozone concentration control system and valves. This program also collected raw digital data (including temperature, ozone concentration, and volumetric flowrate of supply air) from the analog-digital board (PC Boards Inc.), converted this data to engineering units and wrote the columnar data in a text file. The control system relies on the initial calibration of the UV lamp output shown in Figure 2.5 to control the downstream ozone concentration. An outline of the control procedure and the program code can be found in Appendix A.1.

2.2.5 Fixed-bed reactor: carpet fiber experiments

A small, tubular reactor was used to measure ozone uptake on carpet fibers separated from the backing. Carpet fibers were weighed and packed into a 15-cm long Teflon tube whose inner diameter was 1.75 cm. The typical mass of fibers placed in the reactor was two grams. For these fixed-bed experiments, the flowrate was 1.2 L min^{-1}. The upstream ozone mole fraction was maintained at about 100 ppbv. The downstream mole-fraction was continuously measured to determine ozone uptake on the fibers.

Once per hour, during the fixed-bed experiment, the inlet stream was directed away from the reactor to the ozone analyzer to verify the inlet mole-fraction. I found that the inlet mole-fraction varied slightly, becoming slightly elevated when "pressurized" (due to flow resistance across a bed of fibers) relative to "not pressurized" (when the inlet stream bypasses the reactor, and flows directly to the ozone analyzer). In early experiments with small diameter reactors, this difference was as much as 10% of the nominal inlet concentration. For experiments using the 1.75 cm × 15 cm reactor, the

difference between the elevated concentration and the nominal inlet concentration was less than the precision of the ozone analyzer (about 1 ppb in this range); thus no corrective measures were taken.

2.2.6 Vegetable oils

One of the goals of this project was to identify the precursor compounds that form volatile aldehyde species. The primary analytical tool for identification (in this study) is the reaction of the surface precursors with ozone itself. The structure of aldehydes produced by the reaction is a direct measure of the location of double bonds on the precursor molecules. If known vegetable oil samples are exposed to ozone and the pattern of aldehyde emissions matches that of the carpet emissions, then a probable precursor has been found.

Salthammer et al. (1999) showed that the compounds 2-octenal, 2-nonenal, and 2,4-nonadienal were formed as oxidation products of linoleic acid, a component of linseed oil. As will be shown later, these compounds were found to be released from carpets CP1 and CP3. Air oxidation was the primary mechanism studied by Salthammer et al.; it is not clear if ozone was ever used in their experiments.

With this evidence, I chose several types of linseed oil to expose to ozone: Bortz products "boiled" linseed oil; Winsor and Newton "drying", "cold pressed", and "refined" linseed oils . In addition, the location of double-bonds in the constituents of tung oil (derived from the seeds of the tung tree) suggest that it may form 2,4-nonadienal when exposed to ozone (Gunstone et al. 1994). Therefore, I also exposed a readily available form of tung oil (McCloskey brand, used as a wood sealant) to ozone.

To determine what compounds are released from ozone exposed oils, I used the same fixed bed reactor described in Section 2.2.5. I coated one side of a rectangular (5.5 × 15 cm) piece of heavy duty aluminum foil with a thin layer of the sample oil. The mass of oil was measured and the foil was immediately rolled up to just fit inside the reactor, oil side in. For tung oil, I allowed the mineral spirits to evaporate for four hours before inserting the foil into the reactor. Since the relative emission rate of aldehydes was key, I was not concerned with a small amount of gas that could have bypassed between the foil and the reactor wall. An initial VOC sample (Tenax cartridge) was taken at the reactor outlet with 1.2 L min^{-1} nitrogen flowing through the reactor. Then the inlet concentration was set to approximately 100 ppb O_3 with an air flowrate of 1.2 L min^{-1}. The downstream concentration of ozone was noted and Tenax samples were drawn during a period between 20 and 40 minutes after initiation of ozone. The ozone concentration did not change during the sampling period.

2.2.7 Analytical

2.2.7.1 Ozone measurement

The ozone analyzer was a Dasibi Photometric U.V. Ozone Analyzer model 1003 AH. It operates on the principle of absorption of ultraviolet light by ozone to measure the concentration in a continuous flow tubular cell. The ultraviolet lamp generates light at a wavelength of (primarily) 254 nm. Ozone readily absorbs light at this wavelength. The instrument flushes the detection cell with ozone-free air approximately every 45 seconds as a measure of zero ozone. The zero-ozone photomultiplier value is compared with the sample value and the ozone concentration is calculated based on this difference and Beer's law.

A test to confirm the performance of the ozone analyzer was conducted using a difference method and a chemiluminescent NO/NO_2 (NO_x) analyzer. Ozone reacts with nitric oxide to form nitrogen dioxide (NO_2). A stream containing ozone was mixed with a nitric oxide calibration standard. The NO concentration was greatly in excess of the ozone concentration. The calibration ozone concentration was simply the difference between the NO value before and after mixing. This method works well because pre-calibrated bottles of NO can be purchased as primary calibration standards for the NO_x analyzer. Ozone cannot be stored easily, making the use of bottled ozone standards impossible. Other methods for testing the performance of the analyzer were not available.

2.2.7.2 Measurement and identification of volatile organic compounds

2.2.7.2.1 Sample collection

Gas samples for the analyses of individual volatile organic compounds (VOCs) were collected from the reactor (fixed bed or CMFR) exhaust stream. A sampling time-line is shown in Figure A.2.1, Appendix A.2. For aired samples, a "zero" hour sample was collected 0.5 h after installing the sample in the reactor with ventilation but no ozone. After initiation of ozone, samples were collected at average elapsed times of 24 and 48 hours. Intermediate samples were also obtained at various times as necessary, especially during the first 6 hours of ozone exposure. Stored samples were ventilated in the reactor for 24 h before the initial, "zero" sample was collected.

Samples for most VOCs were collected on Tenax-TA sorbent tubes and were analyzed by thermal desorption gas chromatography/mass spectrometry (GC/MS). This technique closely follows work previously reported (Hodgson and Girman, 1989). Samples were collected by drawing 2 L (typical volume) of reactor exhaust gas at 100

cm^3 s^{-1} through the Tenax cartridges. The sample flow was controlled using a mass flow meter attached to a sample pump. Because the presence of water can interfere with analyses on a GC/MS system, the sorbent was "dried" by allowing 1 L dry nitrogen to purge each sample tube before thermal desorption.

2.2.7.2.2 Internal standard generation

Each sample tube was spiked with an internal standard for analysis on the GCMS system. The standard, bromofluorobenzene (BFB), was chosen because the compound has several useful properties. Ion fragments unique to BFB are not common as fragments from most VOCs measured as emissions from the materials studied. BFB is inert; it will not interact with the surfaces of tubing or samplers. BFB has a moderate vapor pressure, typical of the average vapor pressure of compounds of interest for this study. With the temperature program used, the retention time coincides with decane, which may be problematic in a system that cannot distinguish ion fragments. However, decane was not commonly found in my samples.

A constant concentration of BFB was generated in a continuous gas stream by flowing the gas through an oven containing a diffusion vial filled with BFB. At the oven temperature of 34 °C, BFB was emitted at a constant rate of 240 ng/min from a diffusion vial (as determined by periodic measurements of mass lost). A sample of 5 cm^3 was drawn from this standard gas stream (glass syringe with Teflon plunger) and injected into the Tenax sampler with a concurrent helium flow of 100 cm^3 min^{-1}. The resulting BFB mass on the sampler was 120 ng.

2.2.7.2.3 GC/MS analysis

The VOC sampler, after being loaded with the internal standard, was placed into a Chrompack Thermal Cryogenic desorption unit. This device heats the sampler to 225 °C, desorbing the VOCs from the Tenax. The desorbed compounds immediately enter a liquid-nitrogen cooled (-100 °C) capillary column where they condense on the inner surface or packing. The small total mass of the Chrompack capillary column allows it to be rapidly heated, approximating an instantaneous injection of VOCs into the capillary column of a gas chromatograph (Hewlett Packard model HP6890). The gas chromatograph uses helium as a carrier gas to separate the VOCs for analysis in the mass selective detector (Hewlett Packard model HP5973). Details of operation for the desorption unit, gas chromatograph, and mass spectrometer are shown in Table 2.2

Table 2.2. Operational parameters for cryogenic injection system, gas chromatograph, and mass selective detector, for VOC measurements.

Cryogenic injection system: Chrompack CP-4020TCT				
	tube oven	capillary trap	elapsed time	mode
desorption	250 °C	-100 °C	5 min	bypass GC
injection	250 °C	250 °C	1 min	no split
Gas chromatograph: Hewlett Packard model HP6890				
column	J & W DB1701	30 m × 0.25mm	1 μm film thickness, 14% cyanopropyl-phenyl methylpolysiloxane	
column pressure	120 kPa			
temperature program	40 °C, 5 min	40 °C-90 °C, 3.5 degrees min^{-1}	90 °C-250 °C, 5.0 degrees min^{-1}	total time= 51.3 min
Quadrapole mass spectrometer: Hewlett Packard model HP5973				
pressure	10^{-6} torr	mass range	30-300	3-17 min
temperature	280 °C	(m/z)	35-350	17-51.3 min

Individual VOCs were quantified using pure standards; most were obtained from Sigma-Aldrich. A known volume, or mass, of each compound was dissolved in methanol, making up a specified concentration. Typically, about 30 μl of a liquid pure compound was dissolved into 5 ml of methanol and allowed to mix thoroughly in an ultrasonic bath. Then, 100 μl of this solution was dissolved into 10 ml of methanol to make a more dilute solution that could be directly injected onto the Tenax sorption cartridges. Typically, 1 to 5 μl of the final solution was injected onto a clean Tenax sampler with a simultaneous 100 cm^3 min^{-1} N_2 purge gas flow. Twenty minutes of purge gas flow was deemed sufficient to drive methanol off the Tenax, leaving the calibration compounds sorbed to

the Tenax. Ultimately, a calibration curve consisting of 3 to 5 points covering a range of 10 to 100 ng was created to determine a response factor relative to the internal standard.

2.2.7.2.4 Ozone interference in sampling with Tenax sorbent materials

Ozone is known to interact with Tenax-TA, forming several compounds that may interfere with analysis (Clausen and Wolkoff, 1997). Based on chamber blank experiments, where samples were taken in the presence of ozone, these compounds were the most important Tenax-TA decomposition products: nonanal, decanal, phenol, acetophenone, and benzaldehyde. Compound concentration reporting must take into account the formation of these compounds on Tenax-TA. The formation is linearly dependent on the sample time and ozone concentration. Thus the gas phase concentration of an analyte that is also a Tenax byproduct is calculated,

$$C_{an} = \frac{m_{an} - m_{blank} - t_{samp} C_{O3} f_{an}}{V_{samp}} \qquad (2.1)$$

where C_{an} is the calculated concentration of the analyte in the gas stream, m_{an} is the mass of the analyte on the Tenax cartridge, m_{blank} is the average mass of the analyte on a cartridge not exposed to ozone(analytical system blank), t_{samp} is the total sampling time, C_{O3} is the average concentration of ozone during the sampling period, V_{samp} is the sample volume, and f_{an} is a formation factor for the analyte determined by exposing samplers to ozone under different conditions of sample time and ozone concentration.

The most important Tenax/ozone byproducts for this study are nonanal and decanal. The formation factor for nonanal was found to be 0.0015 ng ppb^{-1} min^{-1} and for decanal 0.0023 ng ppb^{-1} min^{-1} with an uncertainty of about 30 %. For most samples, this correction is small relative to the magnitude of the gas phase concentration.

A second form of interference may be due to ozone reactions with analytes on the surface of Tenax. Pellizzari et al. (1984) found that cyclohexene on the surface of Tenax-GC will react with ozone to form cyclohexadiene, benzene, and several isomers of $C_6H_{10}O$. Styrene reacted to form benzaldehyde and benzoic acid. Calogirou et al. (1996) spiked Tenax TA cartridges with terpenes and drew ozonated air through the cartridges for 10 minutes at 100 cm^3min^{-1}. The recovery of some terpenes (e.g. limonene, linalool) was less than 20% when exposed to 120 ppbv O_3. By placing 8 screens coated with MnO_2 upstream of the Tenax cartridge, they were able to bring recoveries to near 100% for most terpenes. However, they also noted that for terpenes that were more polar (e.g. (E)-citral), the recovery was much lower with the scrubber.

I tested several methods of removing ozone without loss of important analytes such as aldehydes. However, any scrubber (such as the denuder used to remove ozone upstream of the DNPH cartridges) removes significant amounts of heavy aldehydes (hexanal and higher). Rather than use a scrubber, I determined the extent to which compounds were degraded by ozone exposure on Tenax-TA under typical sampling conditions.

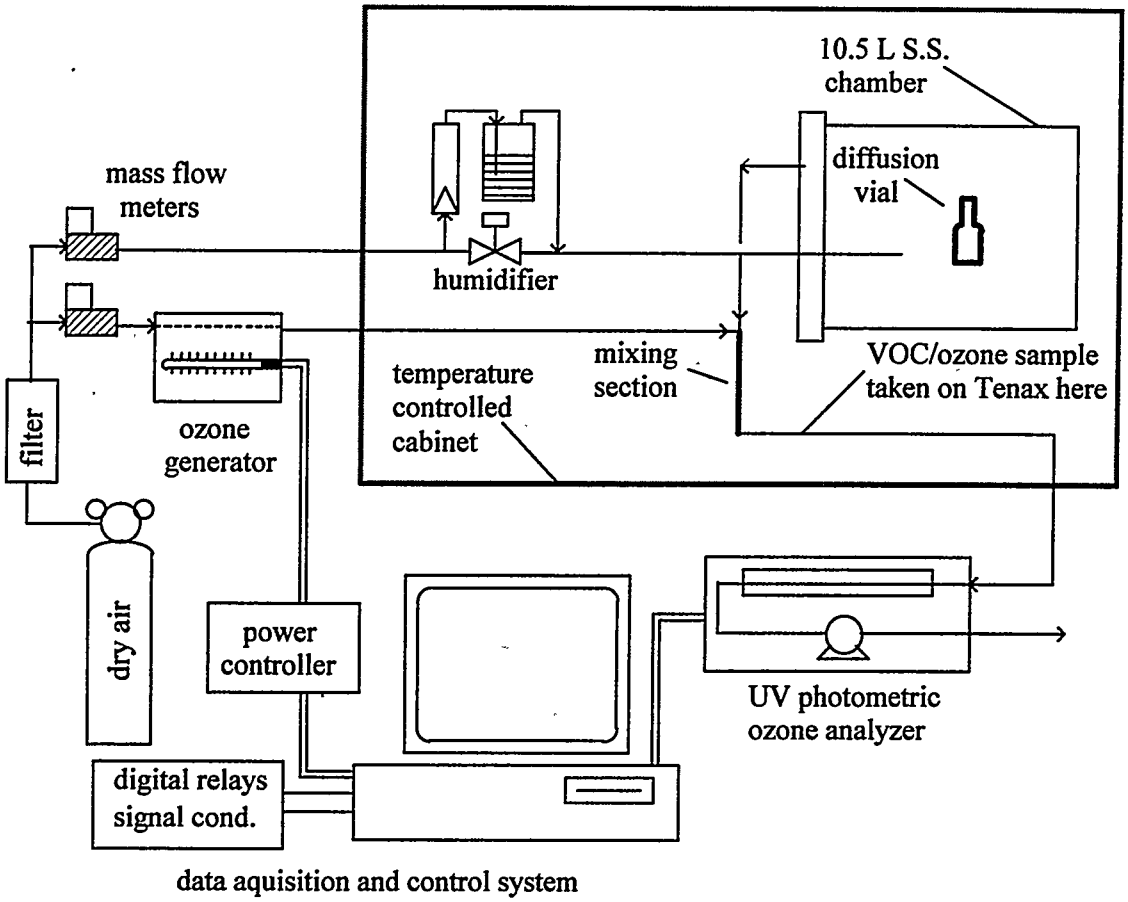

Figure 2.6. Experimental apparatus for measuring ozone degradation of sorbed compounds on Tenax substrate. Note that this apparatus is identical to that shown in Figure 2.3, with the exception that ozone is not mixed into the inlet gas stream. Ozone, instead, is added to the exhaust stream of the chamber containing a diffusion vial of the organic compound to be tested. A short length of tubing is used as a mixing section. Following the mixing section, a sample is drawn on a Tenax filled tube for analysis.

To determine the relative influence of ozone on important analytes such as nonanal and 2-nonenal, I performed the following experiments in the apparatus shown in Figure 2.6. In a 10.5 L stainless steel chamber, I placed diffusion vials containing mixtures of these compounds: undecane, dodecane, tridecane, 2-octanone, 2-dodecanone, 2-octanol, 1-decanol, n-octanal, n-nonanal, n-decananal, 2-octenal, and 2-nonenal. I allowed 1.2 L min^{-1} of air to flow through the reactor for 24 hours to stabilize temperatures and emissions. At the chamber exhaust I introduced ozone with a 0.1 L

min^{-1} flowrate of air. Between the ozone feed and the sampler location, 10 cm of 0.5 cm (inner diameter) Teflon tubing was used as a mixing section. I performed several experiments, varying ozone concentration and sampling time.

The results of that set of experiments demonstrated that ozone degradation of aliphatic aldehydes under normal sampling conditions (100 ppb ozone, 0.1 L min^{-1} sampling flowrate, 20 min sampling time) is negligible. Some degradation of 2-octenal and 2-nonenal was evident, however. For those compounds, total mass detected on the sampler was about 90% of that expected in the absence of ozone. Due to the short residence time of ozone in the exhaust line, it is unlikely that these losses occurred in the gas phase. In the results section, I will quote all emission rate results based on the actual mass detected on the cartridge, recognizing that these results may be slightly lower than the actual values, for unsaturated aldehydes.

2.2.7.3 Measurement of methanal, ethanal and propanal

2.2.7.3.1 Sample collection: DNPH cartridges

Methanal, ethanal and propanal are not easily measured and quantified using the Tenax-TA/GCMS analysis system discussed in Section 2.2.7.3.2 because they do not sorb strongly to Tenax. Instead, these compounds were collected using cartridges filled with silica-gel coated with dinitrophenylhydrazine (DNPH) purchased from Supelco. Most carbonyl compounds react rapidly with DNPH to form hydrazone derivatives. As an example, methanal (also known as formaldehyde) combines with DNPH to form dinitrophenylformazone. These derivatives are easily detected in a liquid sample by absorption of light at a specific wavelength.

Typically, 500 cm^3min^{-1} of sample gas was drawn through the cartridge for one

hour. The method used to measure these light aldehyde species is based on method TO-11A (U.S. Environmental Protection Agency, 1999). The DNPH cartridges were sealed and stored in a freezer at –20 °C then analyzed in batches by high-performance liquid chromatography.

An ozone denuder, constructed of 0.5 m of 0.64 cm diameter copper tubing internally coated with potassium iodide, was used to eliminate interferences due to ozone in the sampling and analysis of methanal, ethanal and propanal (Kleindienst et al., 1998).

2.2.7.3.2 HPLC analysis

The DNPH cartridges (glass tubes) were scored with a Dremel® cut-off saw and snapped into two pieces. The silica-gel granules were then poured into plastic centrifuge cones. Four ml of acetonitrile (ACN) was added using a pipette and the centrifuge cone was sonicated for 5 minutes. The cone was centrifuged for another 5 minutes to separate any small particles from the liquid. About 0.5 ml of this solution was pipetted into a scintillation vial and sealed with a septum cap. The Hewlett-Packard 1090 HPLC uses an autosampler to draw 10 µl samples into a syringe which are then sequentially injected into a Waters Symmetry™ C-18 column. Operating conditions of the HPLC are shown in Table 2.3. The absorbance detector was operated at a wavelength of 360 nm because the dinitrophenyl group attachment readily absorbs radiation at this wavelegnth. Quantification was performed by first creating a calibration curve using pure, derivitized standards from Sigma-Aldrich.

Table 2.3. Operational parameters for analysis of C_1-C_3 aldehydes using high performance liquid chromatography with a light absorption detector.

high perfomance liquid chromatograph: Hewlett Packard 1090 HPLC			
solution A	65% H_2O, 35% ACN	flowrate	0.35 cm^3 min^{-1}
solution B	100% ACN	absorption wavelength	360 nm
temperature	35 °C		

solution mixture profile

time	Solution A
0-2 min	100%
2-11 min	100%-45%
11-16 min	45%

2.3 Results

The carpet samples exhibited a wide range of secondary carbonyl emissions when exposed to ozone. Most of the results are reported in terms of mass emission rates per carpet area ($\mu g\ m^{-2}\ h^{-1}$). The emission rate of an analyte from a material was calculated by the following equation assuming that all environmental variables were constant, the reactor atmosphere was well mixed, and the emission rate was steady:

$$E_{an} = \frac{(C_{an} - C_o)Q}{A} \qquad (2.2)$$

where E_{an} is the emission rate of the analyte per unit area of material (mass per area per time), Q is the volumetric flow rate of the gas stream, C_o is the chamber background concentration of the analyte, and A is the nominal exposed area of the carpet (e.g. the amount of floor area such a carpet sample would cover). For the fixed-bed reactor, the ozone concentration decreases with distance along the reactor and secondary VOC emissions are not likely to be uniform along the length of the reactor. However, equation

2.2 was used to estimate the average emission rate for the whole bed where A is replaced by A_F, the fiber surface area. The average measured fiber diameters, d_f, (by light microscope) and fiber mat height, H_f, can be found in Table 2.4. The identification and quantification of average emission rates for all experiments can be found in Appendix A.2.

The emission rate of total volatile organic compounds (TVOC) is based on the total GC/MS ion current (excluding the internal standard). The TVOC response factor is defined as the average of the individual response factors (on a mass basis) relative to the internal standard, determined for these commonly detected species: octanal, nonanal, decanal, dodecane, dodecanol and dodecene.

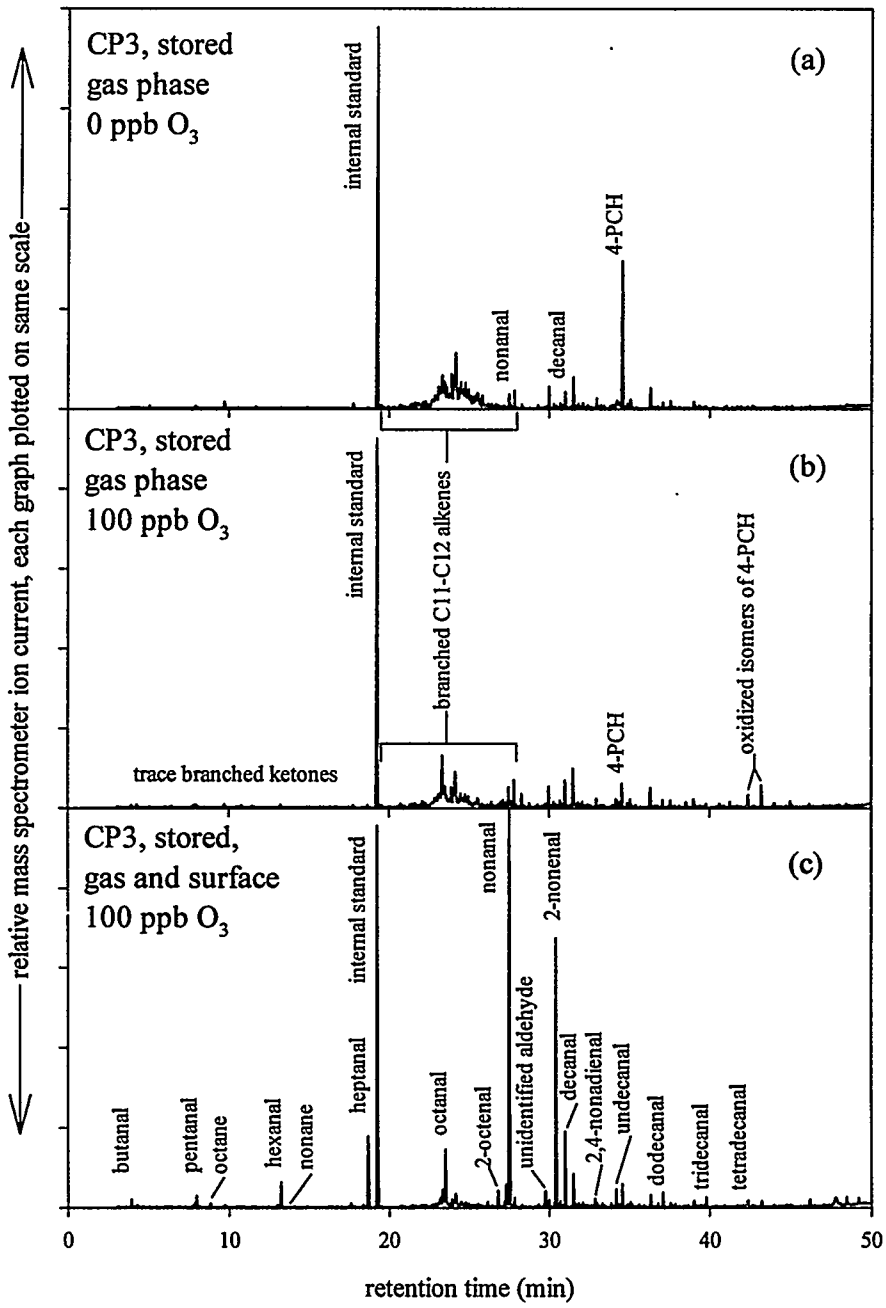

Figure 2.7. GC/MS ioncurrent for stored carpet, CP3: a) aired 24 hours in chamber, no ozone; b) gas-phase reaction products only, O_3 = 100 ppbv; c) surface and gas-phase reaction products, O_3 = 100 ppbv.

2.3.1 Primary emissions

The primary emissions of all "stored" carpets were similar. Fig 2.7(a) shows a GCMS trace of the primary emissions of stored CP3, which is typical of all stored carpet

samples. There are several prominent features, including a broad hump of unresolvable branched C11-C12 alkenes/cycloalkanes near the BFB internal standard. Other compounds common to all stored carpets were 4-phenylcyclohexene (4-PCH), dodecanol, branched alkanes, and several aliphatic aldehydes. Some compounds were specific to a single carpet, e.g. dimethyl-acetamide and benzene from CP1; 2-ethylhexanol, C8-C10 aliphatic acids, and 4-methoxybenzaldehyde from CP2; and dipropyleneglycolmethylether from CP3 and CP4.

The aired carpets released lower levels of primary-emission compounds than stored carpet. Most of the species emitted by the stored carpet were missing. Dodecanol was an exception and was emitted by CP1, CP2 and CP4 at rates 5 to 10% of those from the respective stored carpet. Low levels of some oxidized compounds were evident in these carpets where they were absent in the stored carpets. CP1 released C_4 and C_5 2-ketones, and all aired whole carpet samples released trace levels of aliphatic acids. All of the aired carpets released small amounts of n-aldehydes. Carpet backing tended to release higher levels of primary emission compounds, notably higher levels of aliphatic aldehydes.

The average TVOC emission rate for each experiment is shown in Figure 2.8. The first two bars, for carpet CP1 and CP2, demonstrate how quickly stored carpet emissions can drop while being aired out in the reaction chamber (24-48 h, without ozone). The emissions from carpet CP3 do not drop as dramatically as they do for carpets CP1 and CP2. As expected, carpets that have been aired for over a year ("aired") release fewer compounds than are emitted from the stored carpets.

There are some general trends for changes in TVOC emissions due to ozone

treatment. Usually, the compounds formed by ozone exposure increase overall emissions as demonstrated for stored carpets CP1, CP2 and CP3. TVOC emissions also increase with ozone exposure for all aired carpet exposures. Much of the increased carbonyl compound emissions are offset by reductions in other species such as 4-PCH and isomers of dodecene. Exposure of carpet backing to ozone, in some cases, exhibits a small drop in TVOC emissions (CP2, CP4).

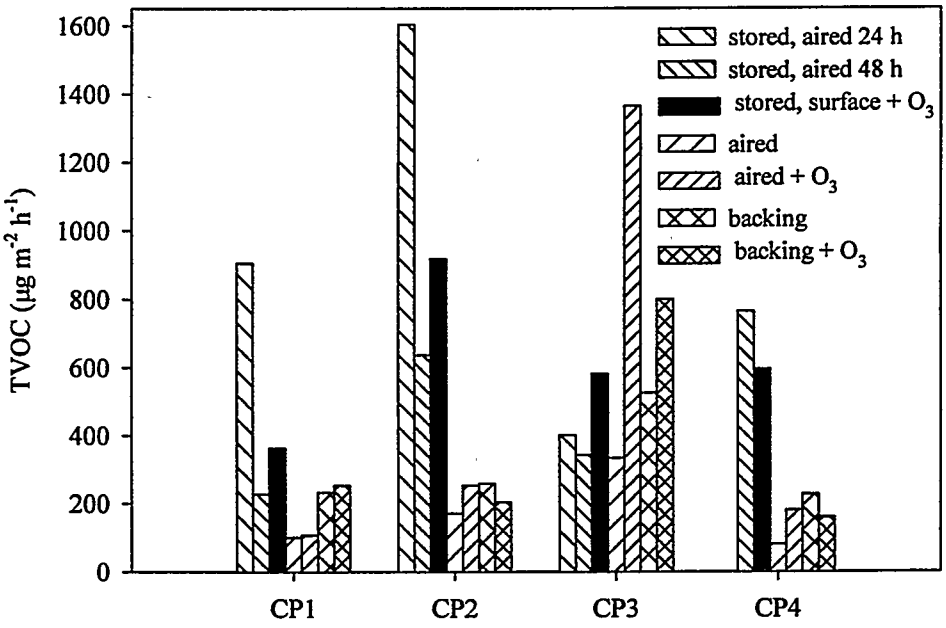

Figure 2.8. Total volatile organic compound emissions (TVOC). TVOC is based on total ion current and calibrated based on average of individual response factors for octanal, nonanal, decanal, dodecane, dodecanol, and dodecene. Note that one data point is missing due to lost sample (CP4, stored, aired 24 h).

2.3.2 Ozone reactive chemistry and secondary emissions

2.3.2.1 Gas-phase chemistry

Gas-phase reactions of ozone with volatile carpet emissions were isolated in the system as described in Section 2.2.2. All of the stored carpets released primary-emission compounds that could react with ozone in the gas phase. Compare GC/MS traces shown

in Figure 2.7(a) and (b). Reactions with ozone drastically reduced the 4-PCH peak and, to a lesser degree, reduced the concentration of branched alkenes.

Each carpet emitted large amounts of C_{11}-C_{12} branched alkenes. I was unable to positively identify these compounds because no primary standards exist. They were tentatively identified based on the ion fragment signature. The signature of branched C_{11}-C_{12} alkenes closely matches that of substituted cyclic, saturated compounds. Thus it is possible that some of these individual compounds have no double-bonds. Ozone reactions appear to reduce the overall concentration of these compounds, implying ozone reactivity. However, hydroxyl radicals formed in the reactions of ozone with alkenes can react with cycloalkanes, potentially reducing the concentration of saturated compounds.

The byproduct of carpet manufacture, 4-PCH, was a prominent primary emission species from all un-aired carpets. Ozone reacts rapidly with 4-PCH, reducing its concentration by about a factor of 10. Two prominent byproducts of this reaction were observed in these gas phase experiments. I isolated these 4-PCH reaction products in an experiment described in Appendix A.3. The attempt to identify the reaction products is also described in Appendix A.3. No conclusive identification was made.

Reactions in the gas phase resulted in trace amounts of ketones and aldehydes. These compounds, listed in Appendix A.2 for each carpet, are expected products of ozone reaction with the C_{11}-C_{12} branched alkenes. For example, branched carbonyls formed in the reaction with CP4 emissions included 3-methyl-2-butanone, 4-methyl-2-pentanone, 3-methyl-pentanal, 3-methyl-2-hexanone, 4-methyl-2-hexanone, and 3-methyl-2-heptanone. Though representative of compounds formed in the ozone reaction with other carpet emissions, the suite of products was distinct for each carpet. There were several other

unidentified, small peaks in the chromatogram that were clearly products of gas-phase ozone reactions.

The ventilation rate in these reactors is relatively high, thus allowing ozone-alkene reactions limited time to react. However, much of the 4-PCH reacted with ozone in the short reaction period. An analysis of reaction rate constants can be found in Appendix A.3.

2.3.2.2 Surface chemistry

The emission results for carpet components in this Section will be discussed for each carpet, i.e. CP1, CP2, etc. The gas-phase concentration of reaction products, from a carpet fully exposed to ozone, is due to gas-phase and surface reactions. The best estimate of surface-only reaction product emission rate is obtained by subtracting the emission rate of the gas-phase-only segment from the emission rate of the combined phenomena. However, the reactive volatile emissions from stored carpet tends to drop rapidly during the experiment; this makes subtraction of emission rate values measured several hours apart less meaningful. Therefore, the total (due to both gas and surface reactions) emission rate of each product will be reported and the difference between gas and surface components will be discussed qualitatively. Gas-phase experiments were not performed with aired whole carpet because the potential for gas-phase reactions was low.

In general, ozone interactions with the surface of the carpets resulted in increased emissions of C_1-C_{12} aliphatic n-aldehydes and, for some carpets, several unsaturated aldehydes. Average, summed aldehyde emissions for each carpet are shown in Figure 2.9. Individual aldehydes released from carpets CP1 – CP4 are shown in Figures 2.10 – 2.13

respectively. Dynamic results for summed aldehyde emissions are shown in Figures 2.14 – 2.21. Also shown in these figures are the dynamic molar ratio of aldehyde emissions and ozone deposition; these results are discussed in Section 2.3.3. The molar ratio described here is identical to the "VOC formation factor" described in Reiss et al. (1995a). The average emission rate of ozone induced carbonyl species (summed over all species) was always higher for stored-whole carpet than for aired whole carpet. The aired backing samples tended to release more of these species than aired whole samples but less than the stored whole samples. Carpet CP3 released significantly more of these compounds than any other carpet, and was a powerful source of 2-nonenal. Other common surface reaction products included cyclopentenone, methoxybenzaldehyde, and trace levels of aliphatic acids. The relative emission rate of reaction products was about the same for stored, aired, backing or fibers for a specific carpet sample, with some exceptions. In all cases (CP1-CP4), the emission rate of aldehydes from fibers drops to undetectable levels during the course of the experiment.

Stored and aired CP1 released similar ozone-induced compounds except that ozone reacted to produce measurable amounts of 2-octenal and 2-nonenal at the surface of stored CP1. The average emission rates of quantified aldehydes is shown in Figure 2.10 for CP1. Nonanal is the strongest emitter. Other important emitters are decanal, hexanal, heptanal, and 2-nonenal.

Aldehyde emissions from the aired whole sample were much lower than for the stored sample. Note that the gas-phase reaction component of n-aldehydes was much stronger for CP1 than for any other carpet. The average emission rate of aldehydes from aired CP1 is generally lower than that of stored or backing samples, and does not

significantly decrease during the experiment.

The emission rates of quantified aldehydes was much higher for the aired backing than for the aired-whole carpet. This is somewhat surprising since Weschler et al. (1992) showed that most of the secondary aliphatic aldehydes derived from fibers. For carpet CP1, there may be more of the aldehyde precursors on the backing than on the fibers.

Dynamic results of summed aldehydes for stored, aired, backing and fiber samples for carpet CP1 are shown in Figures 2.14-2.15. Note that for samples taken at times other than 0, 24, or 48 h (for stored samples, 1, 24, 26, 30, 54 h), no DNPH sample was taken. At these times, the aldehyde summation does not include C_1- C_3 aldehydes. There is a definite downward trend in summed aldehyde emissions rates in the stored and backing experiments that is not as evident from any other carpet samples.

As with all of the carpets, nonanal is the most important secondary reaction product released from CP2 (Figure 2.11), with octanal and decanal somewhat less important. The mean emission rate of summed aldehydes is similar to carpets CP1 and CP4 (Figure 2.9), but there is less of a drop in the secondary emissions from the stored to the aired samples. For some aldehydes, the gas-phase formation of aldehydes in the stored carpet experiment may account for lower emission rate of secondary products from aired carpet. However, for oxidation products such as octanal and nonanal, the difference is much larger. The pattern and release rate of secondary emissions from CP2 backing are very similar to those from the aired carpet.

Dynamic summed aldehyde results for stored, aired, backing, and fiber samples for carpet CP2 are shown in Figures 2.16-2.17. With the exception of the fiber experiment, the summed aldehyde emission rate stays approximately constant through

each experiment. This suggests that there is a large reservoir of precursor molecules on the surface.

Carpet CP3 was the strongest overall emitter of aldehydes and specifically of nonanal and 2-nonenal as shown in Figures 2.9 and 2.12. The next most prominent secondary product was heptanal, with octanal and decanal close behind. Stored CP3 was the only carpet to release detectable amounts of 2,4-nonadienal. The gas phase component of aldehyde formation was negligible compared to the surface component.

A lower rate of secondary emissions was found in the aired sample compared to the stored sample for carpet CP3. This was due mainly to decreases in nonanal and 2-nonenal. The backing demonstrated secondary emission rates even lower than those of the aired carpet. This is in contrast to CP1 where more secondary products came from the backing.

The dynamic summed aldehyde results are shown for carpet CP3 in Figures 2.18-2.19. As with carpet CP2, the dynamic emissions are relatively constant throughout the exposure period for the stored sample. Summed aldehydes rise over a period of about 24 h from the aired carpet sample. This is mainly due to delayed 2-nonenal emissions. This phenomena will be discussed in more detail in Section 2.4.3. A slow rise in summed aldehyde emissions is not as evident from CP3 backing, but delayed 2-nonenal emissions occur nonetheless. The summed emissions from CP3 fibers follow the same general form as those of other carpets: a rapid increase in aldehyde emissions which drop to nearly undetectable levels during the experiment. However, this drop in emissions takes much longer to occur than is observed in other carpet fiber samples.

Nonanal was the strongest ozone reaction product found in CP4 with heptanal,

decanal and octanal of secondary importance (Figure 2.13). The difference between the emissions of aired and stored samples was large, but probably not due to differences in gas-phase formation of aldehydes in stored sample experiments. The backing of CP4 released more aldehydes than the aired sample. The general pattern of product formation was the same for each experiment.

For both the stored and aired sample of CP4, the secondary emissions rise initially, but tend to stabilize in the dynamic results shown in Figures 2.20-2.21. It is not clear if the backing emissions follow the same pattern, since the C_1-C_3 values are included only in the initial samples. As with all other fibers, the secondary emissions of aldehydes drops rapidly over the 24 hour period of exposure.

2.3.3 Ratio of molar emission rate of aldehydes to molar ozone deposition rate

In this section, I compare the molar emission rate of carbonyl species to the loss rate of ozone. This comparison allows me to gather some information about the mechanisms of ozone loss, and to perform a crude material balance on ozone. The dynamic results of each experiment are shown in Figures 2.14 through 2.21. The ratios of the molar emission rate of aldehydes to the molar ozone deposition rate are shown as open circle symbols.

Consider the reaction of ozone with an unsaturated compound. Under neutral conditions, aldehydes and acids are formed in approximately equal amounts: for each ozone molecule consumed, one mole each of an aldehyde and an acid will form. Thus, a molar ratio (with aldehydes) of ~ 1 would be expected where ozone reacted stoichiometrically with a simple olefin. If ozone reacts with fatty acid esters, or fatty

acids, decomposition of the ozonide may form a compound with low volatility, or one that is difficult to detect with my analysis methods. Recall that in Figure 2.2, I showed possible decomposition products of the "left-hand side" of oleic acid. The right hand side may form these low-volatility products: 1,9-nonadioic acid and 8-formyl octanoic acid. Thus only half of the aldehydes formed are volatile enough to be detected by my methods. Decomposition of ozonides formed with fatty acid esters will form even lower volatility compounds that are essentially undetectable. Refined vegetable oils are composed mostly of fatty acid esters but also contain a small fraction of free fatty acids (Gunstone et al., 1994).

Therefore, a better estimate of the expected molar ratio of aldehyde formation would be ~0.5 under neutral conditions and perhaps slightly less, to account for the formation of "other" decomposition products noted in Figure 2.2. The empirical molar ratio, for whole carpet, ranges from 0.8 to less than 0.1, with typical values in the 0.2 to 0.4 range. The high value of 0.8 (from carpet CP3) is unexpected and may be due to conditions on the surface that encourage the formation of aldehydes over acids. Carpet CP3 is also the only carpet to produce large amounts of unsaturated aldehydes. Aldehyde formation may also be favored from the decomposition of conjugated ozonides that form where ozone attacks conjugated double bonds. The molar ratio is typically lower for aired carpet than for stored carpet with the exception of CP3. No further analysis of the reaction mechanisms is possible without quantification of organic acid formation.

The molar ratio for carpets CP2 and CP4 is somewhat lower for fibers than for aired-whole carpet. This means that ozone may be reacting to form compounds other than aldehydes in the fixed bed reactor. It is unclear why this occurs. This may simply be due

to uncertainties in quantifying the molar ratio. After the initial (1 h) sample, the molar ratio uncertainties overwhelm any differences between fibers and aired carpet results.

There is no general trend in the dynamic molar ratio as seen in Figures 2.14 - 2.21. While the molar ratio rises over a 48 h exposure of aired CP1, it drops dramatically for stored CP1. For most samples, the molar ratio is relatively flat, as evidenced by aired CP2, CP3, and CP4. This may be evidence that the chemistry and conditions on the surface remain constant during this exposure period. Note that the uncertainty bars become very large near the end of each fiber experiment. This is due to the increasing uncertainty in the molar ozone uptake value. Near the end of the experiment, the difference between the inlet and outlet ozone concentrations is relatively small, but the uncertainty in the concentration at each location is finite (~1 ppb). The fractional uncertainty in the difference between the concentration at the two locations rises rapidly as the two values approach each other.

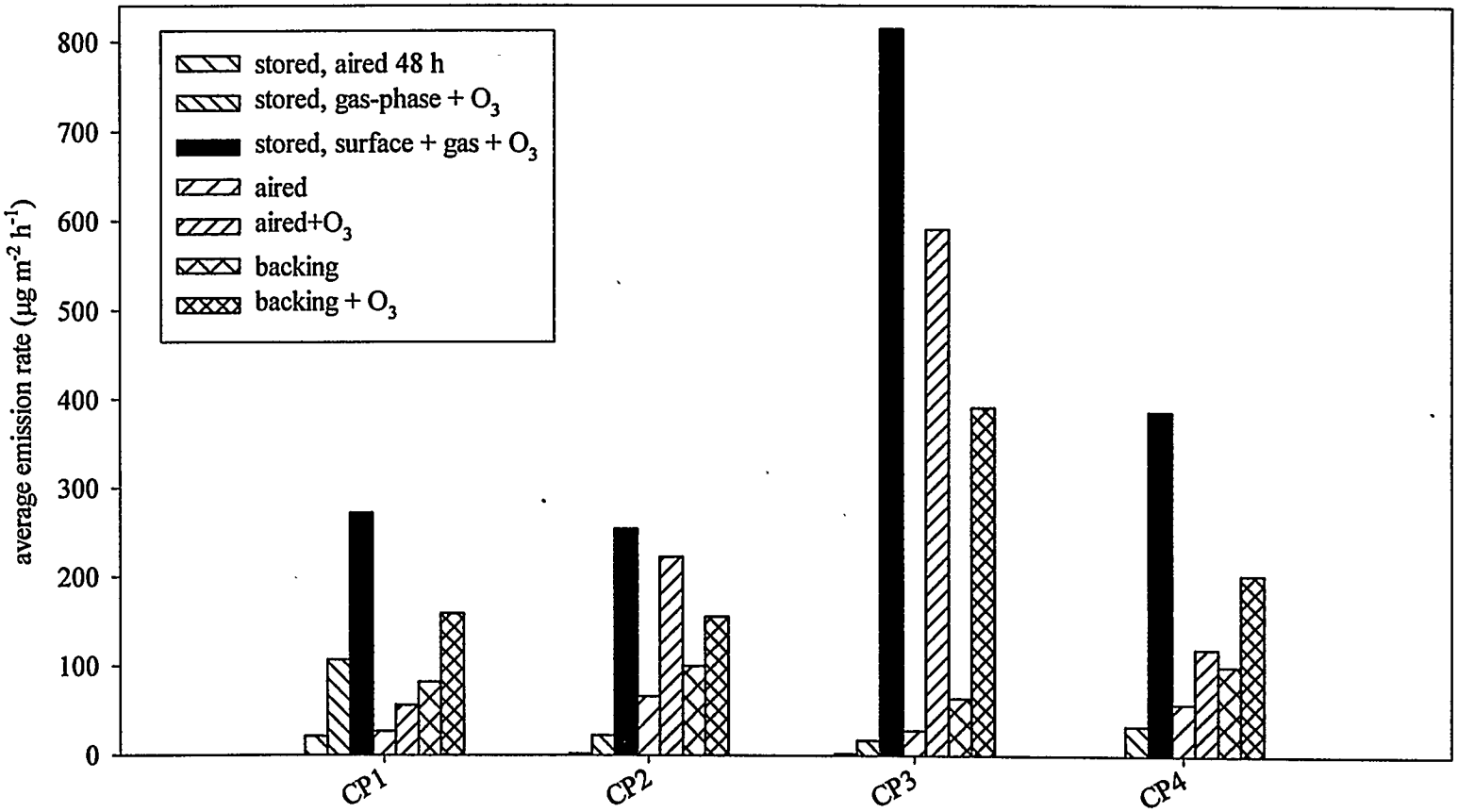

Figure 2.9. Comparison of summed aldehyde carpet emissions with and without ozone exposure. Emissions represent 1) stored, aired for 48 h, no O_3; 2) stored, gas-phase, 100 ppb O_3, 24 h average; 3) stored, surface and gas phase, 100 ppb O_3, 48 h average; 4) aired whole carpet, no O_3; 5) aired-whole carpet, 100 ppb O_3, 48 h average (72 h average for CP3); 6) backing, no O_3; 7) backing, 100 ppb O_3, 48 h average (120 h average for CP3).

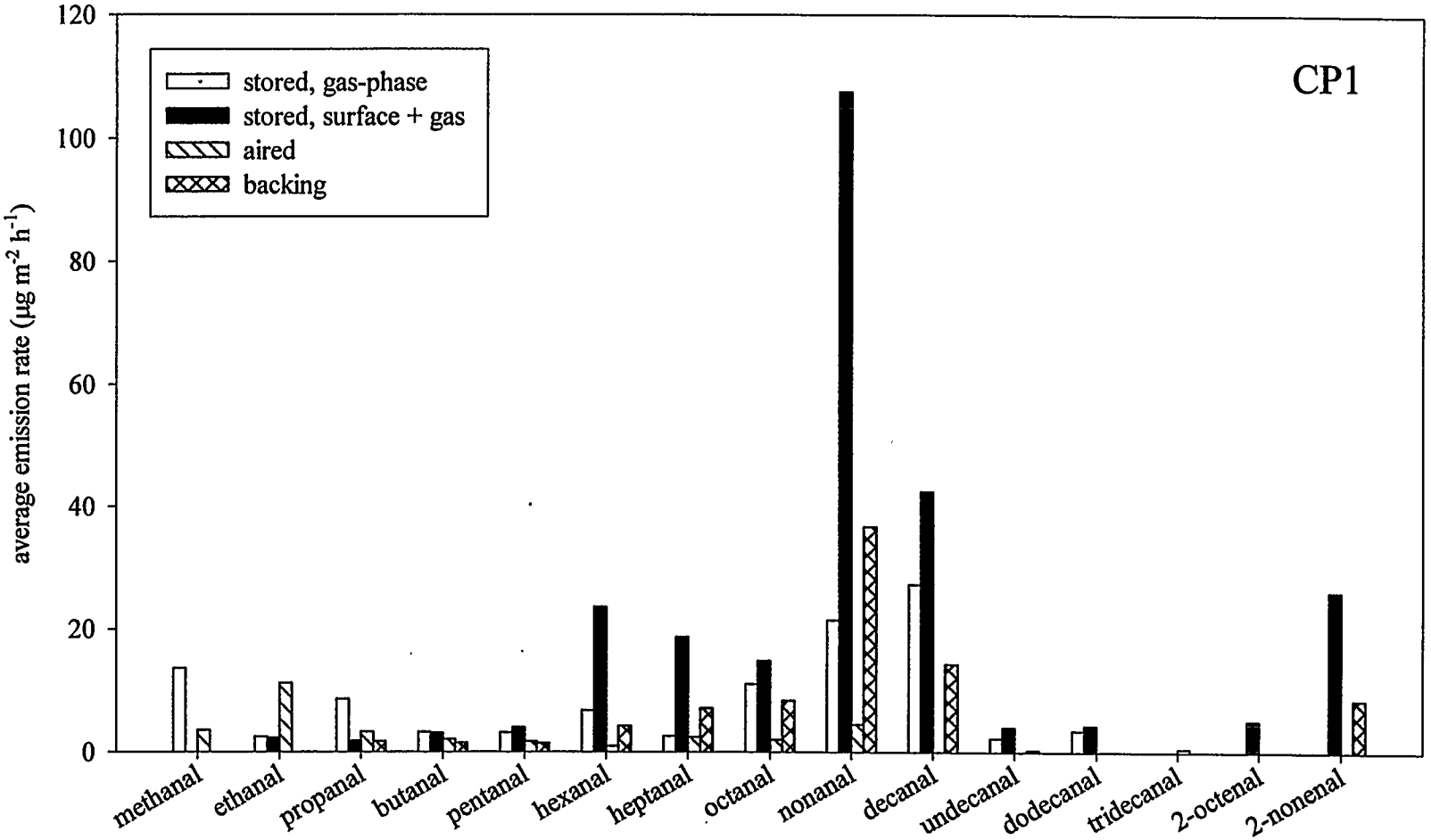

Figure 2.10. Ozone-induced emission rates of individual aldehydes from carpet CP1. Bars represent time-averaged emission rates in the presence of 100 ppb O_3, minus emission rates immediately before O_3 exposure: 1) stored, gas-phase, 24 h average, 2) stored, surface and gas phase, 48 h average, 3) aired-whole carpet, 48 h average; 4) backing, 48 h average. Negative values are not displayed.

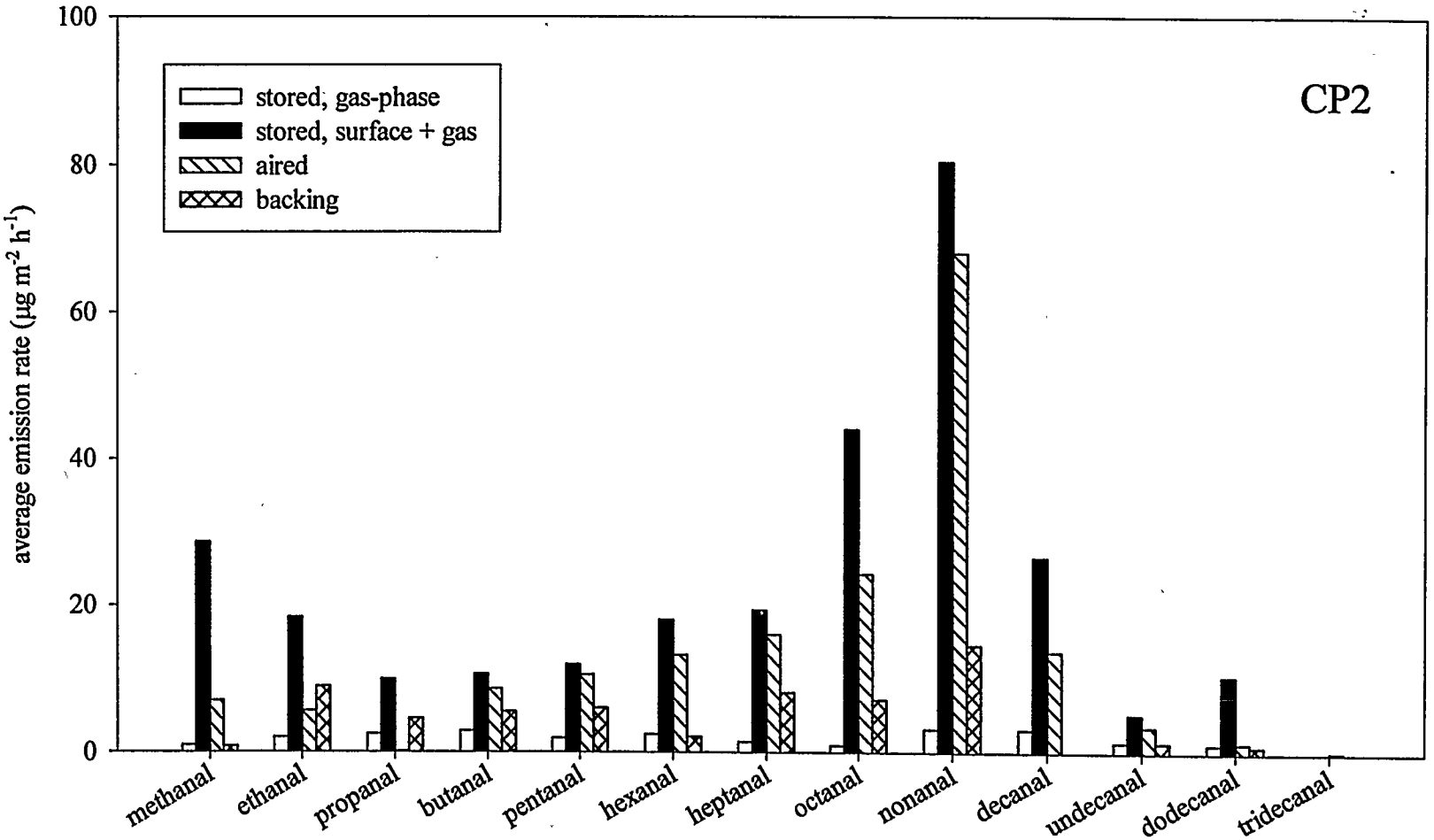

Figure 2.11. Ozone-induced emission rates of individual aldehydes from carpet CP2. Bars represent time-averaged emission rates in the presence of 100 ppb O_3, minus emission rates immediately before O_3 exposure: 1) stored, gas-phase, 24 h average, 2) stored, surface and gas phase, 48 h average, 3) aired-whole carpet, 48 h average; 4) backing, 48 h average. Negative values are not displayed.

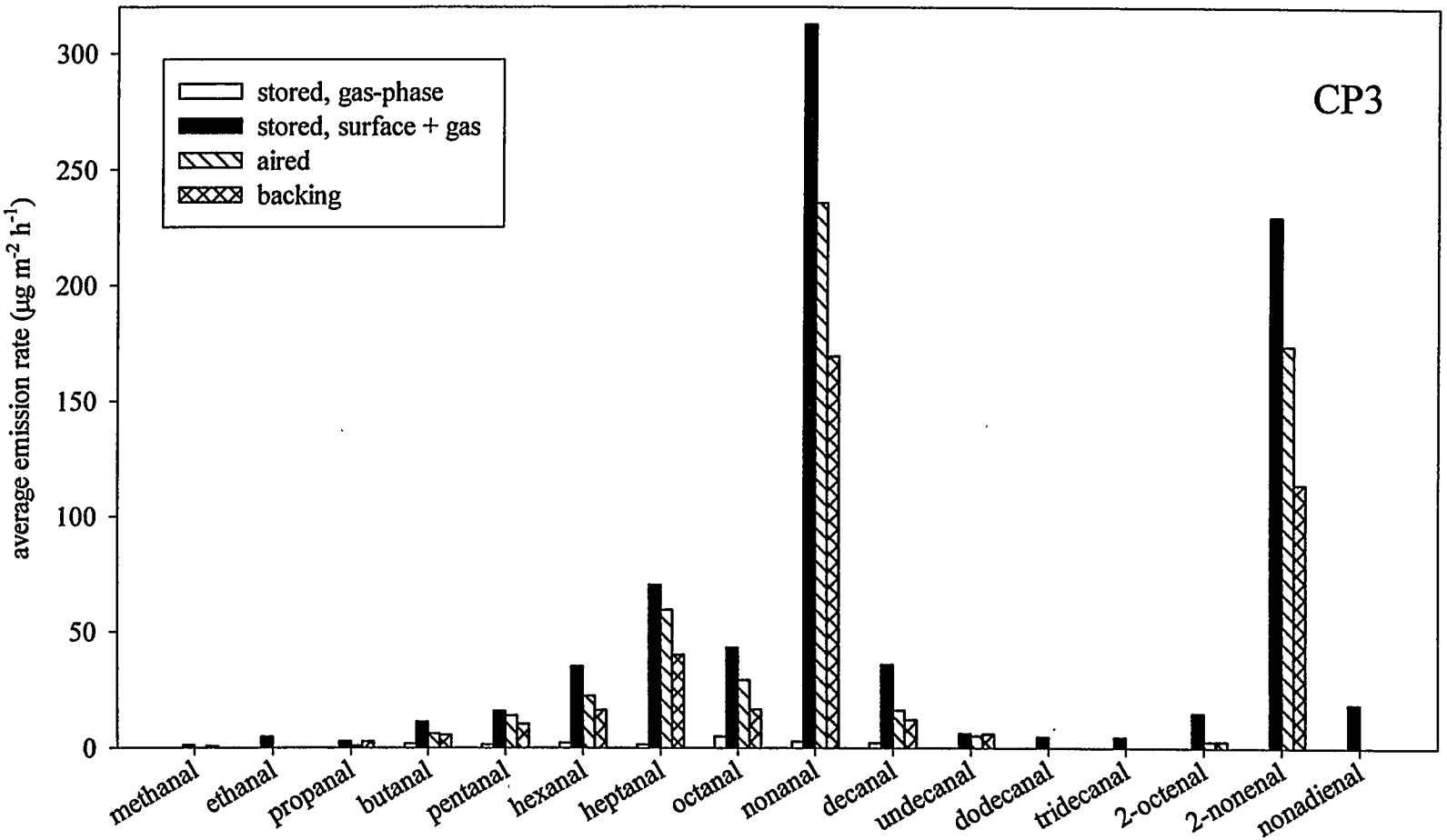

Figure 2.12. Ozone-induced emission rates of individual aldehydes from carpet CP3. Bars represent time-averaged emission rates in the presence of 100 ppb O_3, minus emission rates immediately before O_3 exposure: 1) stored, gas-phase, 24 h average, 2) stored, surface and gas phase, 48 h average, 3) aired-whole carpet, 72 h average; 4) backing, 120 h average. Negative values are not displayed.

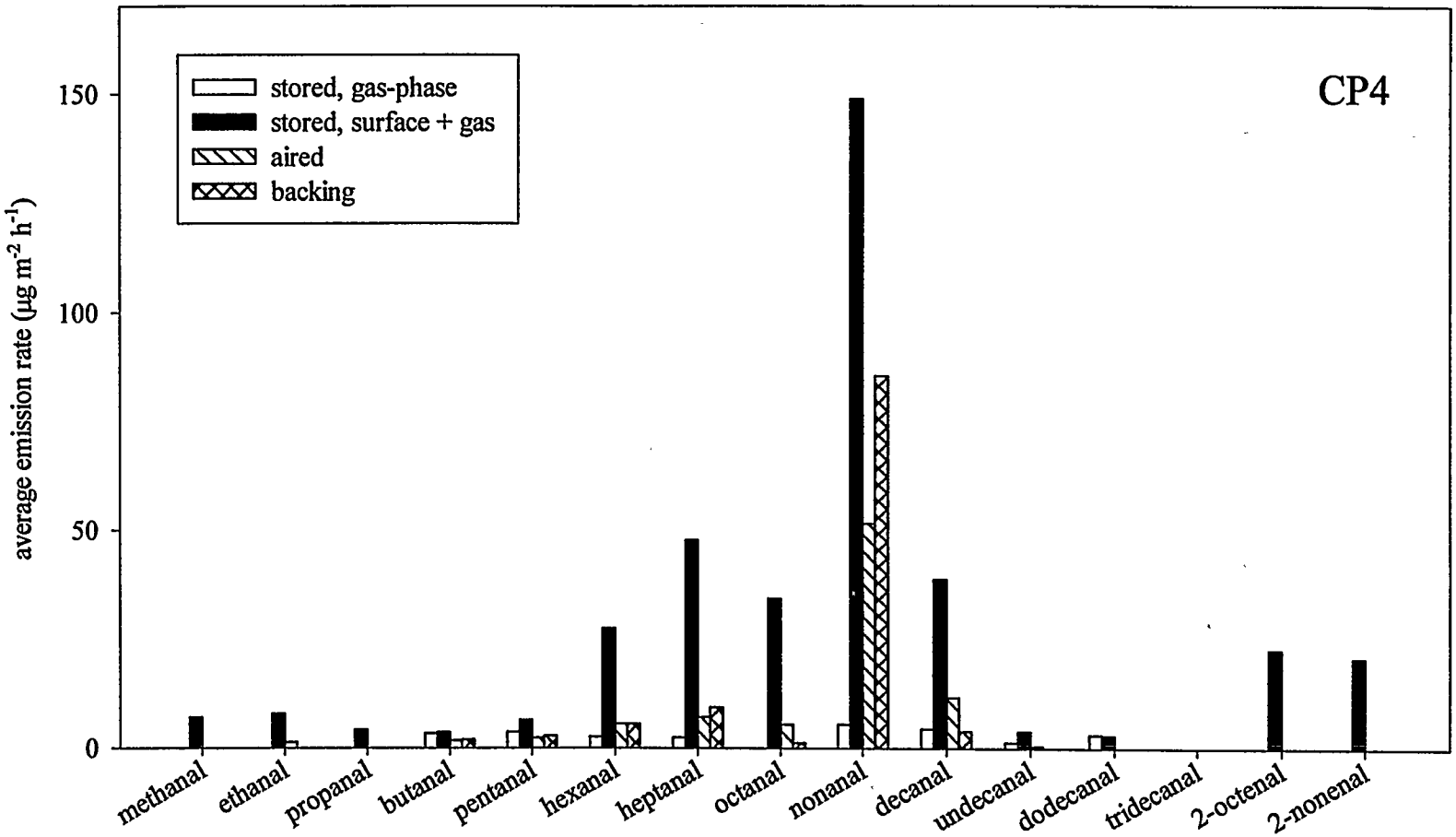

Figure 2.13. Ozone-induced emission rates of individual aldehydes from carpet CP4. Bars represent time-averaged emission rates in the presence of 100 ppb O_3, minus emission rates immediately before O_3 exposure: 1) stored, gas-phase, 24 h average, 2) stored, surface and gas phase, 48 h average, 3) aired-whole carpet, 48 h average; 4) backing, 48 h average. Negative values are not displayed.

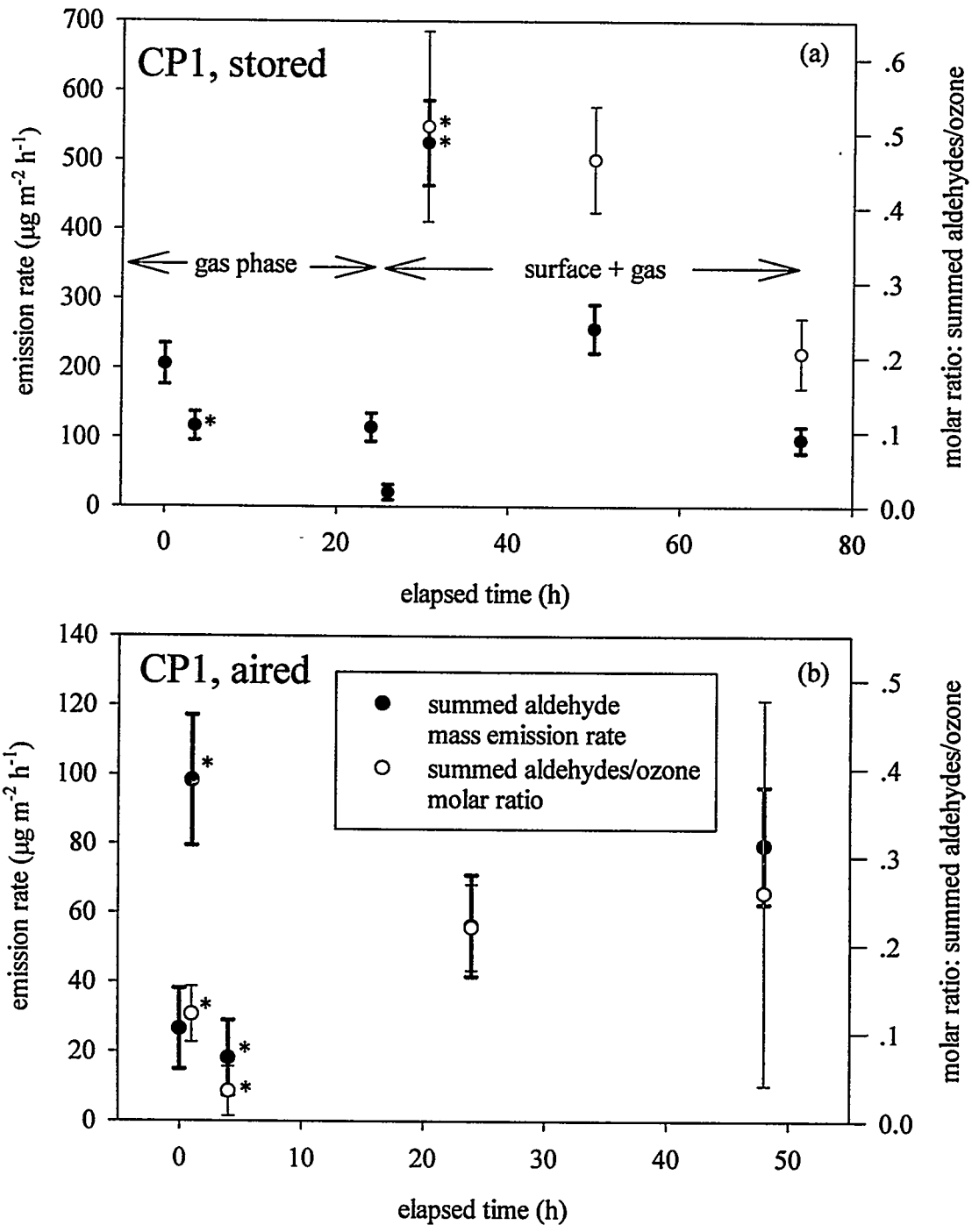

Figure 2.14. Dynamic emissions of summed aldehydes and molar ratios of summed aldehyde emission rates to ozone deposition rates from carpet CP1: (a) stored, (b) aired. * DNPH samples were not take during these sampling periods; C_1-C_3 aldehydes are absent from summation.

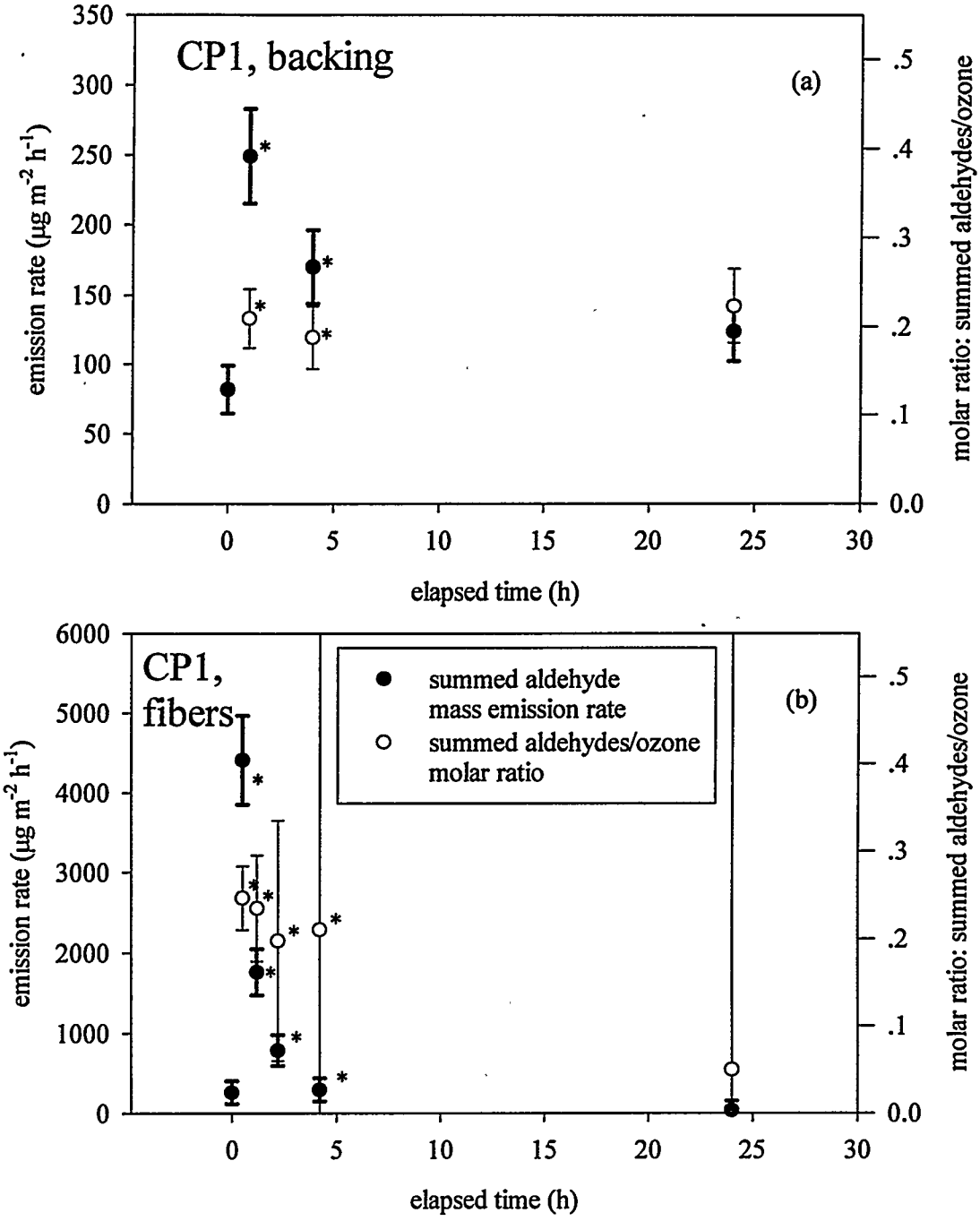

Figure 2.15. Dynamic emissions of summed aldehydes and molar ratios of summed aldehyde emission rates to ozone deposition rates from carpet CP1: (a) backing, (b) fibers. Fiber mass emission rate is normalized to whole carpet area. * DNPH samples were not take during these sampling periods; C_1-C_3 aldehydes are absent from summation.

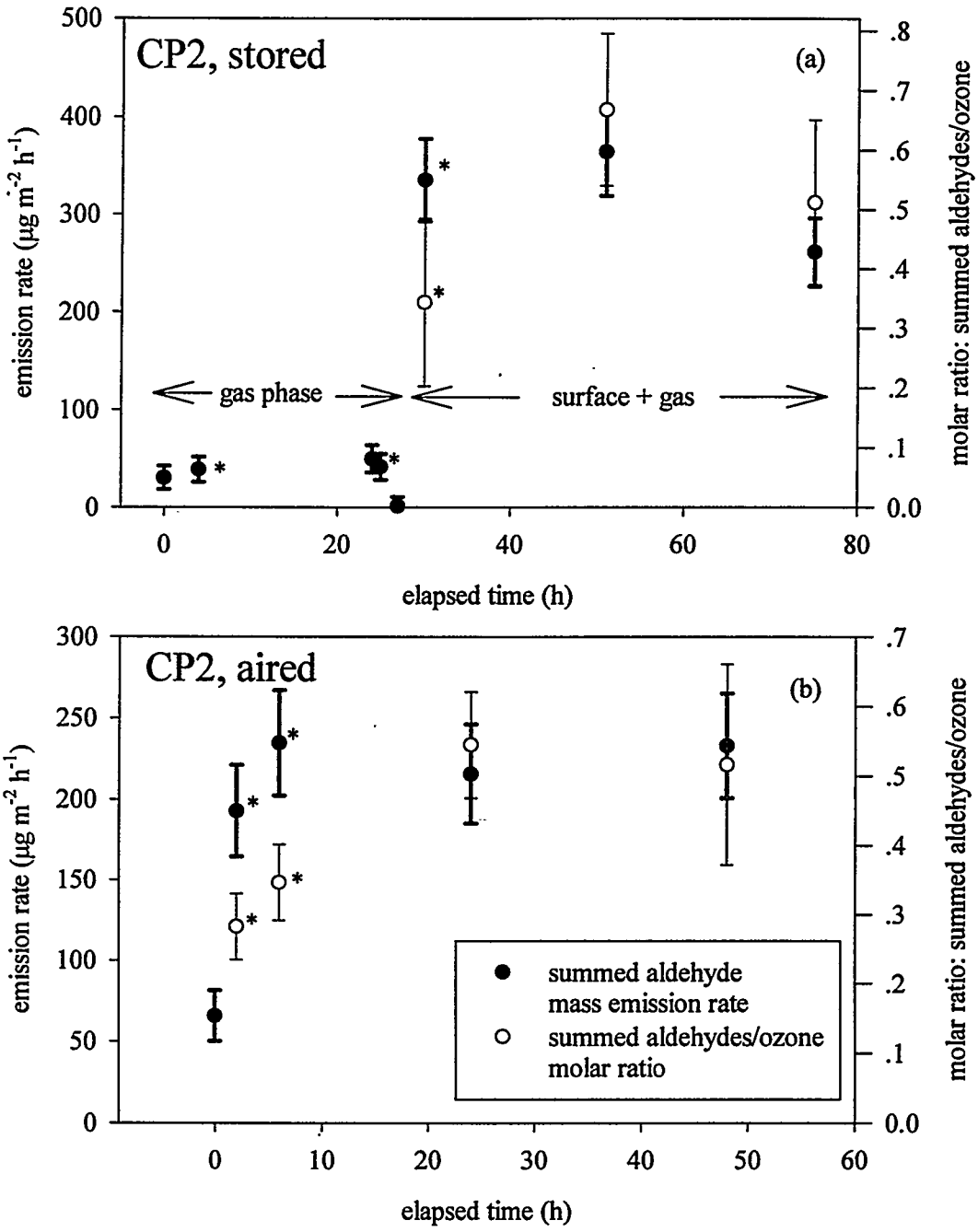

Figure 2.16. Dynamic emissions of summed aldehydes and molar ratios of summed aldehyde emission rates to ozone deposition rates from carpet CP2: (a) stored, (b) aired. * DNPH samples were not take during these sampling periods; C_1-C_3 aldehydes are absent from summation.

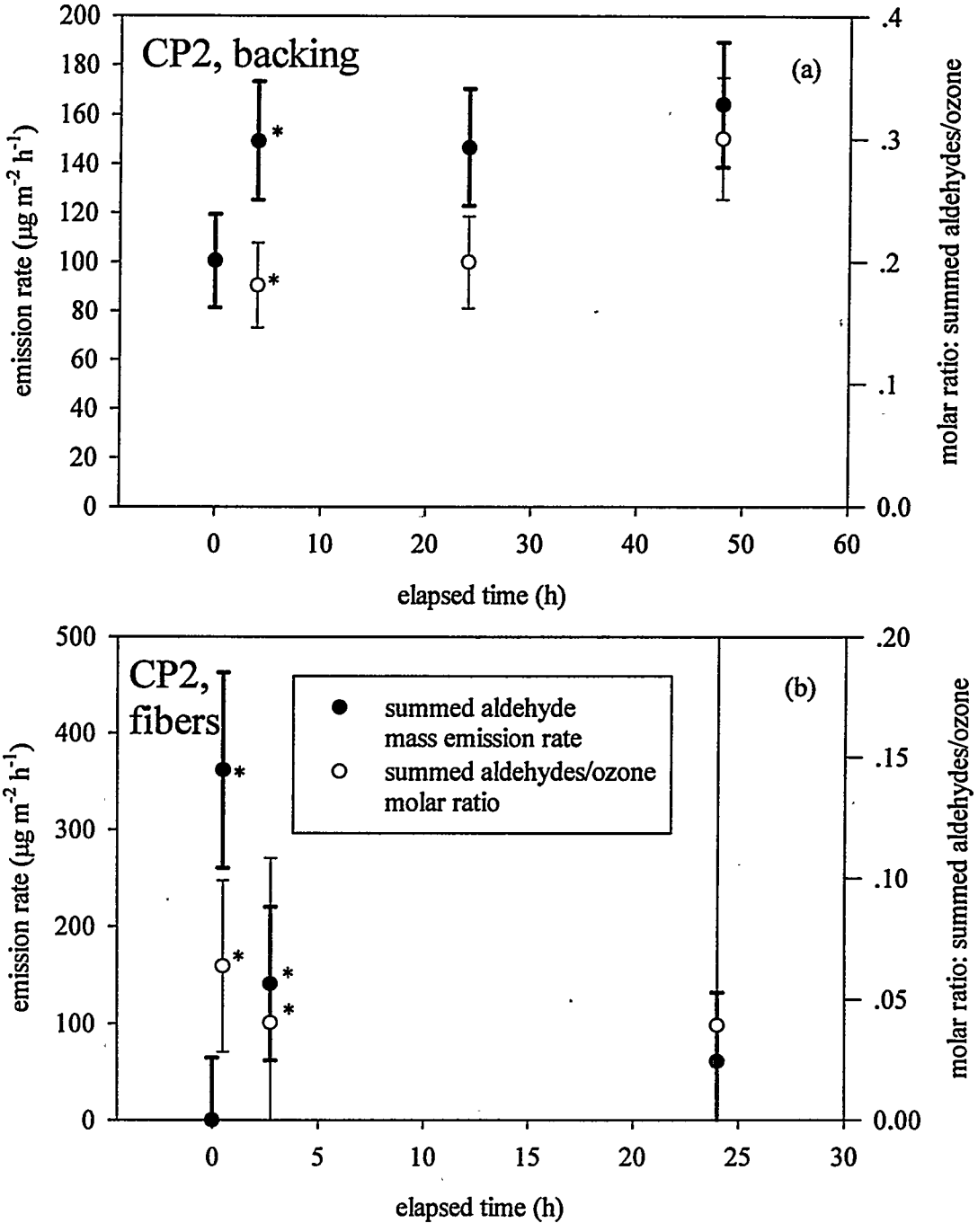

Figure 2.17. Dynamic emissions of summed aldehydes and molar ratios of summed aldehyde emission rates to ozone deposition rates from carpet CP2: (a) backing, (b) fibers. Fiber mass emission rate is normalized to whole carpet area. * DNPH samples were not take during these sampling periods; C_1-C_3 aldehydes are absent from summation.

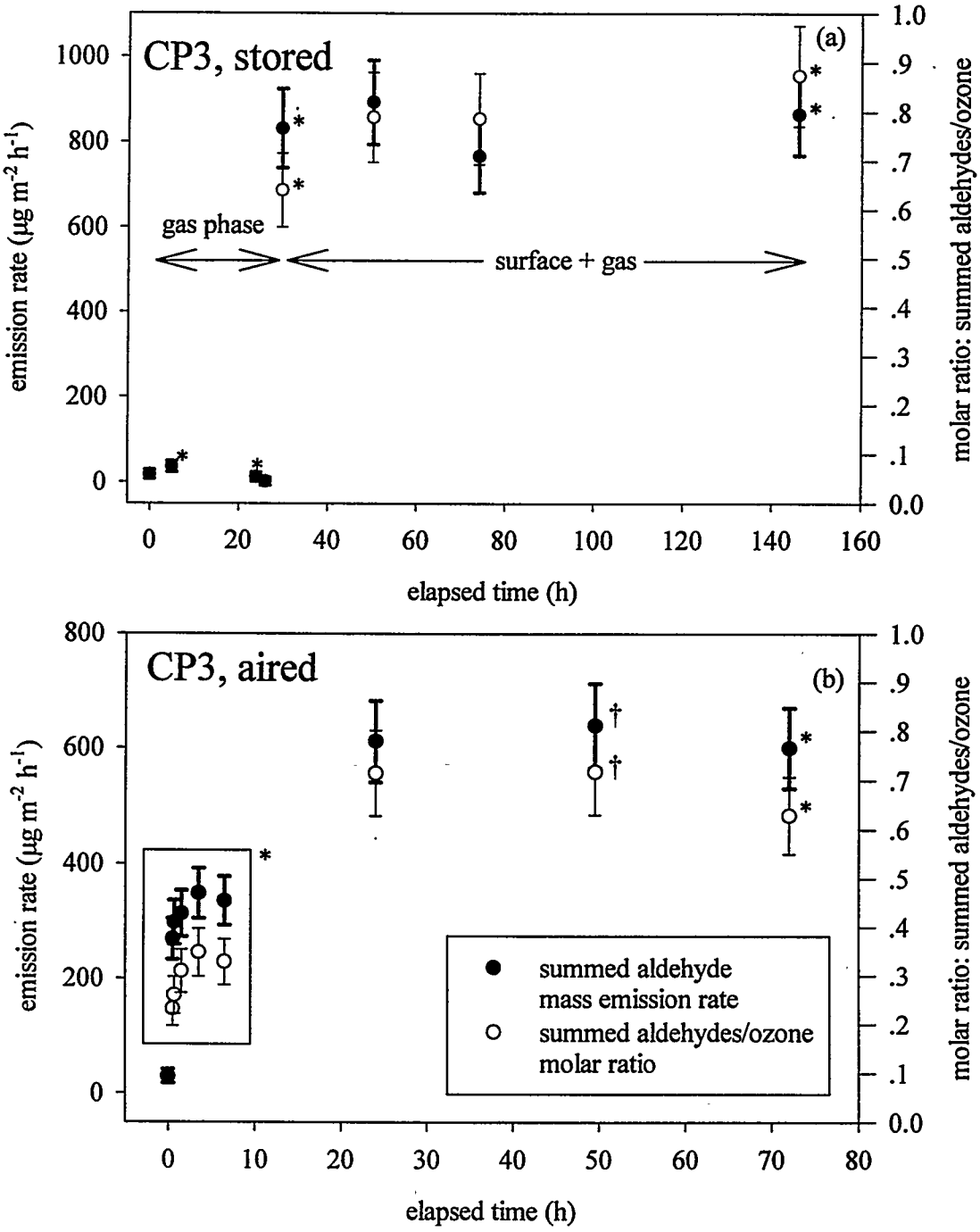

Figure 2.18. Dynamic emissions of summed aldehydes and molar ratios of summed aldehyde emission rates to ozone deposition rates from carpet CP3: (a) stored, (b) aired. * DNPH samples were not take during these sampling periods; C_1-C_3 aldehydes are absent from summation. † 51 h sample is sum of 48 h C_1- C_3 aldehydes and 51 h C_4 and higher aldehydes.

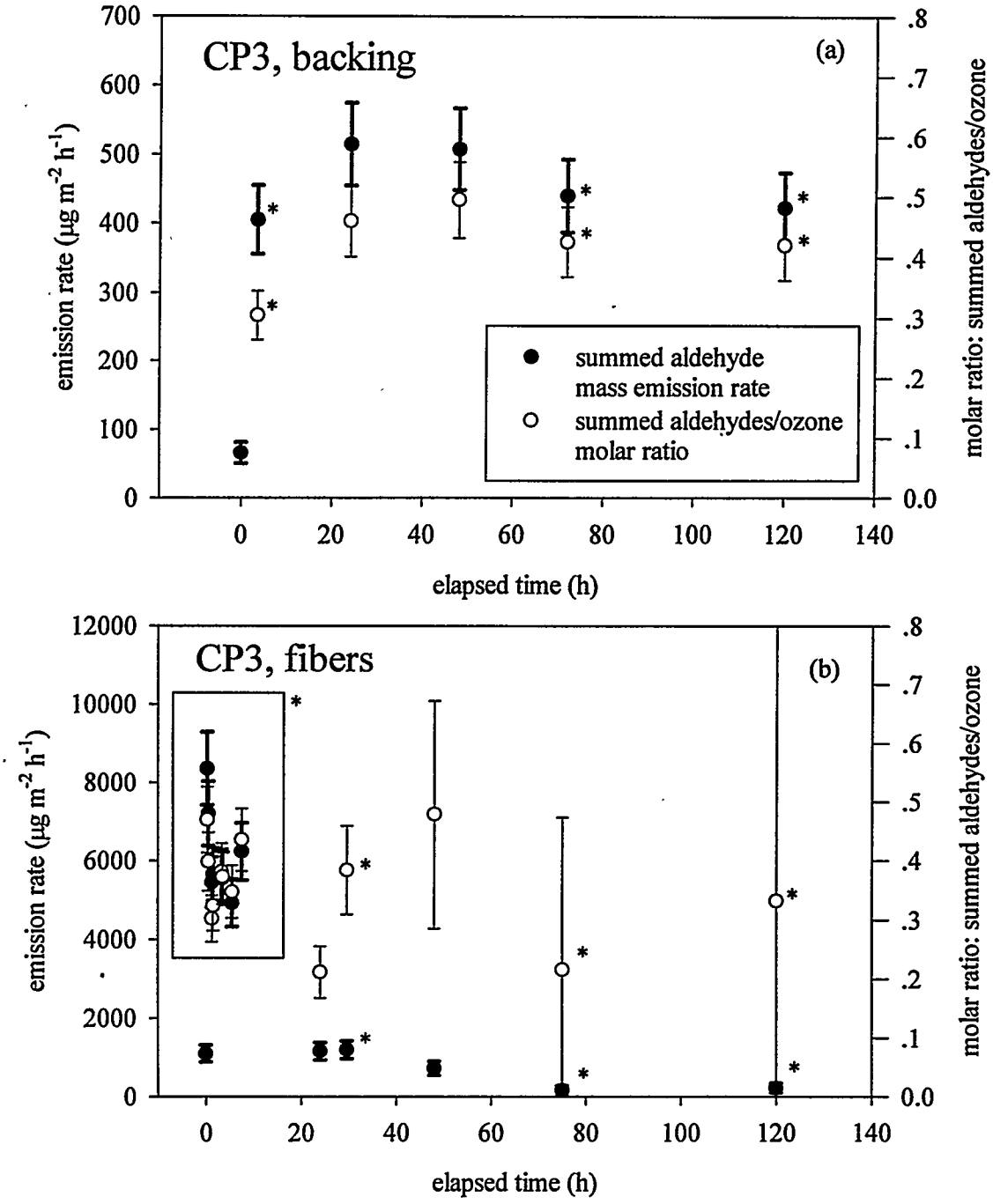

Figure 2.19. Dynamic emissions of summed aldehydes and molar ratios of summed aldehyde emission rates to ozone deposition rates from carpet CP3. (a) backing, (b) fibers. Fiber mass emission rate is normalized to whole carpet area. * DNPH samples were not take during these sampling periods; C_1-C_3 aldehydes are absent from summation.

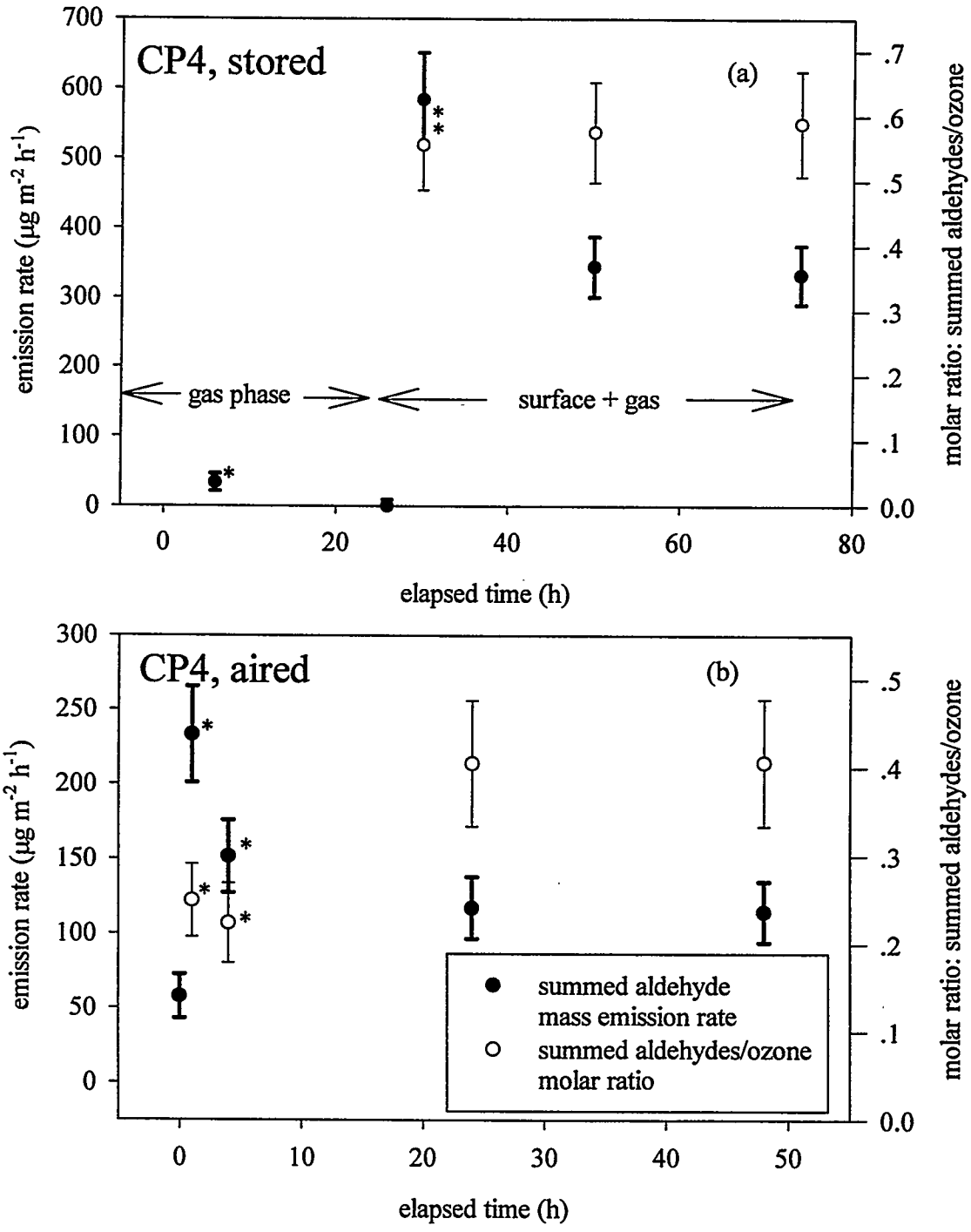

Figure 2.20. Dynamic emissions of summed aldehydes and molar ratios of summed aldehyde emission rates to ozone deposition rates from carpet CP4: (a) stored, b) aired. * DNPH samples were not take during these sampling periods; C_1-C_3 aldehydes are absent from summation.

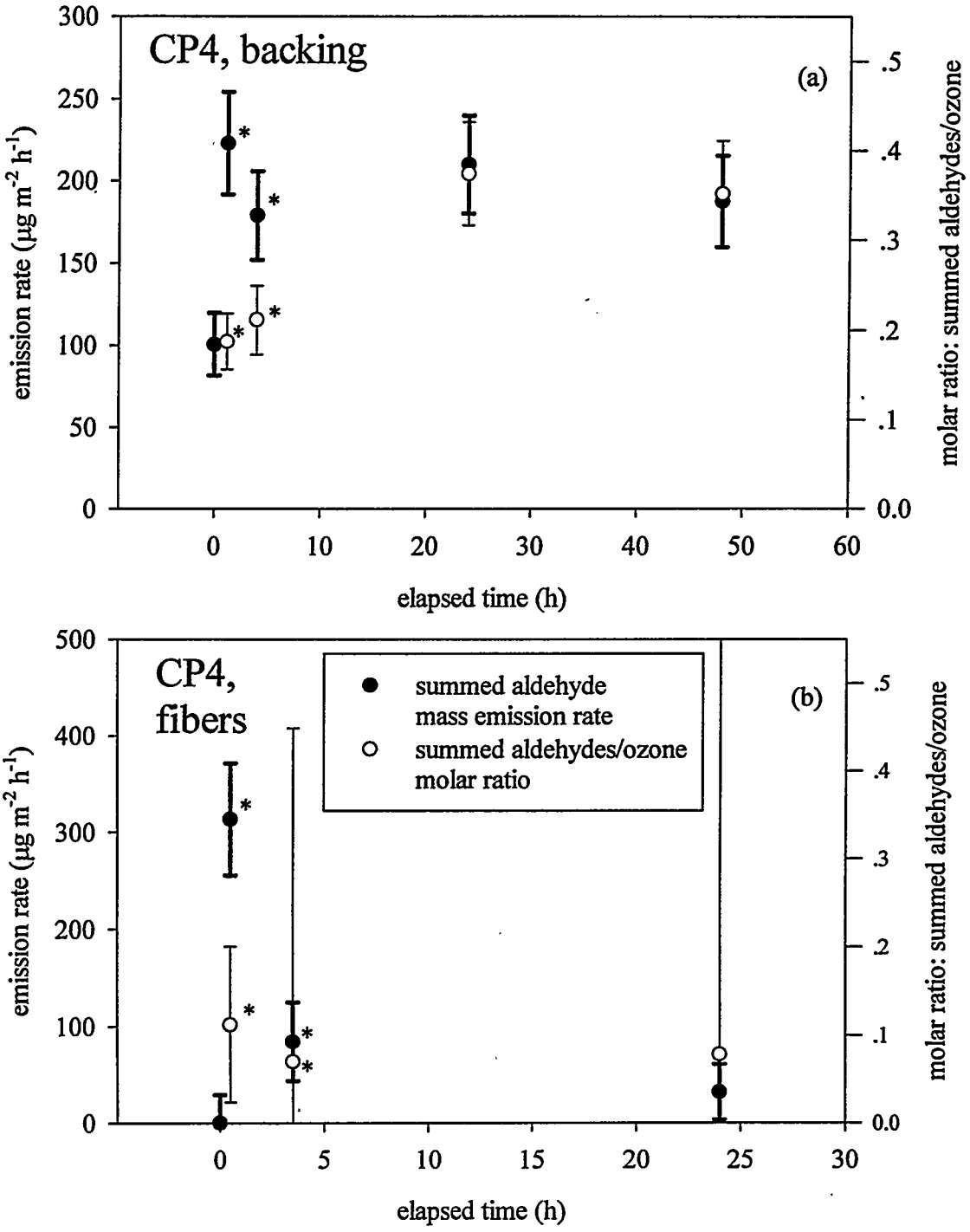

Figure 2.21. Dynamic emissions of summed aldehydes and molar ratios of summed aldehyde emission rates to ozone deposition rates from carpet CP4: (a) backing, (b) fibers. Fiber mass emission rate is normalized to whole carpet area. * DNPH samples were not take during these sampling periods; C_1-C_3 aldehydes are absent from summation.

2.3.4 Cumulative totals

A lower-bound estimate of the potential emissions of an analyte from carpet can be obtained by integrating the dynamic emissions from fibers and backing. In the 48 or 72 h period in which whole carpet samples were exposed, the emissions of secondary compounds do not become exhausted. However, secondary emissions of individual analytes typically drop below detectable levels during fixed bed exposures of fibers. An estimate of the total potential secondary emissions from fibers can be found by time-integrating the emissions from the fixed bed experiment. By summing the time integrated emissions of an analyte from fibers with the time integrated emissions from carpet backing, I can obtain a lower-bound estimate of the potential emissions of secondary compounds from whole carpet (aired) samples.

For example, the dynamic emissions of summed aldehydes from carpet CP3 fibers is shown in Figure 2.19(b). A time-integration of these data results in a cumulative emission rate of 4.6 mg m^{-2}, based on the surface area of the carpet fibers. The contribution of fibers to total carpet emissions (based on horizontally projected area of carpet) can be found by multiplying this value by the normalized fiber area, $R_f = 46$. The contribution to total secondary product emissions from backing is found by time-integrating the results in Figure 2.19(a), with a result of 55.1 mg m^{-2}. This value is a lower bound estimate of the total secondary emissions since emissions of most analytes during the carpet backing experiment are not exhausted during the 120 h exposure period. A lower-bound value for total emissions from CP3 is therefore estimated to be $4.6 \times 46+55.1 = 267$ mg m^{-2}. In this case, the dominant contribution to emissions is from the fibers. The fractional contribution from carpet fibers is estimated to be 0.41, 0.29, 0.79,

and 0.16 for carpets CP1 through CP4. Summed aldehyde results for CP1 through CP4 are shown in Table 2.4. Also shown is an upper bound estimate of the emission rate, E_U, which is E_T normalized by a 24 h exposure period for carpets CP1, 48 h for CP2 and CP4, and 120 h for carpet CP3.

Table 2.4. Carpet characteristics and total emissions of summed aldehydes.[a]

Carpet sample	d_f (μm)	H_f (cm)	R_f	E_T (mg m^{-2})	E_U (μg m^{-2} h^{-1}) {normalization time, h}
CP1	60 ± 5	9.4 ± 0.3	66 ± 7	14	580 {24}
CP2	70 ± 5	5.5 ± 0.6	33 ± 3	11	220 {48}
CP3	80 ± 5	9.9 ± 0.3	46 ± 3	267	2200 {120}
CP4	70 ± 5	3.7 ± 0.6	30 ± 3	12	240 {48}

[a] d_f = fiber diameter; H_f = fiber mat height; R_f = normalized fiber area; E_T = estimated (lower-bound) total potential emissions; E_U = upper-bound emission rate. A video microscope, with a digital scale, was used to determine the average diameter, d_f, of the carpet fibers.

2.3.5 Ozone oxidation of linseed and tung oil

The results of ozone exposure of linseed and tung oils are shown in Figure 2.22. Several important secondary emission compounds were not positively identified in this study. The asterisk (*) denotes species that were tentatively identified as unsaturated aldehydes. The compound denoted nonadienal (*) had a retention time that was identical to 2-nonenal, but produced an ion fragment pattern more closely matched to 2,4-nonadienal. This peak may have obscured a smaller 2-nonenal peak. No 2-nonenal emissions were observed during these experiments. The location of unsaturated carbon-carbon bonds in the species (*) were not identified because pure standards were not available. Based on the structure of linolenic acid, nonadienal (*) may be 3,6-nonadienal, and hexenal (*) may be 3-hexenal.

The patterns of emissions from the various linseed oils are similar to one another. The compounds with the greatest emission rates are, in this order, nonadienal (*), n-

nonanal, hexenal (*), and hexanal. Cold-pressed linseed oil exhibited a somewhat different secondary emission pattern, with relatively higher nonadienal (*) and lower hexenal (*) emission rates. The pattern of emissions from tung oil is quite different from linseed oil, as it was the only oil that exhibited 2,4-nonadienal and 2-heptenal emissions. The emissions were also dominated by nonanal, hexanal and pentanal.

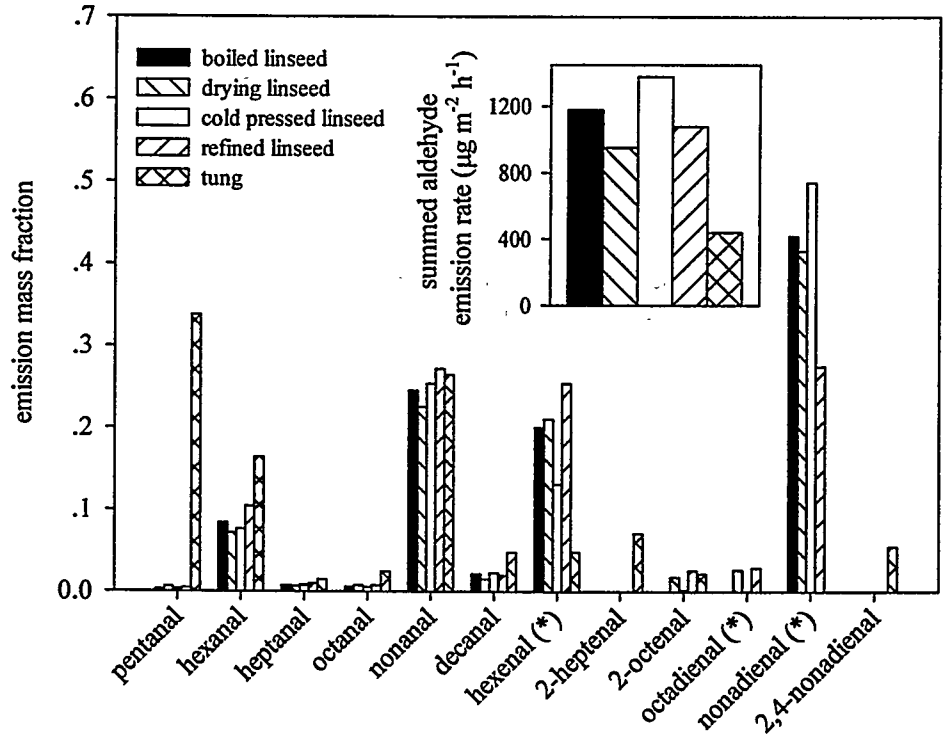

Figure 2.22. Emission mass fractions of aldehydes formed as secondary emission products from ozone exposure of several linseed oil and one tung oil samples. The asterisk (*) denotes species that are tentatively identified, but whose unsaturation location is unknown. Inset plot shows the summed aldehyde emission rate from each oil based on samples taken at an average time of 0.5 h after initiation of ozone exposure, normalized by foil area of 0.0083 m^2.

The inset plot in Figure 2.22 shows the summed aldehyde emission rate for each oil at an average time of 0.5 h after ozone initiation. The emission rate is normalized by the area of the foil (0.0083 m^2). The absolute emission rate of summed aldehydes from the various linseed oils ranged from about 950 to 1300 $\mu g\ m^{-2}\ h^{-1}$, while that from tung

oil was only about 440. To make a comparison of emission rates on an oil mass basis, note that the oil loading on aluminum foil was 7.0, 9.6, 14.6, 11.0, and 7.1 mg for boiled, drying, cold pressed and refined linseed oils and tung oil respectively.

2.4 Discussion

2.4.1 Patterns of emissions

The relative emission rates of secondary compounds may help determine the precursor species responsible for aldehyde emissions. Note that nonanal is the most important emission product in every surface-phase carpet experiment. This result suggests that the precursor species has an unsaturation at the "9" position, counting from a straight-chain hydrocarbon end. Oleic acid, shown in Figure 2.2, is the most common fatty acid found in naturally occurring vegetable oils. Oxidation of oleic acid by ozone will result in emissions of nonanal, suggesting that the precursor may be of vegetable oil origin.

If one assumes that reaction rates of ozone reacting with double bonds located at different locations in the fatty acid backbone are similar (and emission rates are not significantly influenced by other phenomena, such as adsorption), then the pattern of aldehyde emissions reflects the location and relative amount of double bonds in an olefinic precursor. While nonanal is the most common emission product, other aldehydes of similar molecular weight, C_6-C_{10}, are typically released at high rates as well. A good precursor candidate would be a vegetable oil containing double bonds corresponding to the relative emission rates of the aldehydes.

Consider linseed oil as a possible precursor species. Linseed oil is one of the most

commonly used vegetable-based oils in consumer products. It is used in paints as a drying agent and serves as a liquid base for the production of linoleum. It is composed primarily of esters of linolenic, linoleic and oleic acids. Table 2.5 demonstrates the expected aldehyde formation products of these acids based on the location of double bonds. In air oxidation experiments, Salthammer et al. (1999) found that many aldehydes identical to those found in my carpet experiments are released from pure forms of linolenic, linoleic and oleic acids. These species as well as aldehydes formed in the air oxidation of linoleum (Jensen et al., 1995) are also shown in Table 2.5.

Table 2.5. Volatile products of the oxidation of linseed oil constituents.

linseed oil components		
linolenic acid (9,12,15-octadecatrienoic acid)	linoleic acid (9,12-octadecadienoic acid)	oleic acid (12-octadecenoic acid)
aldehydes expected to be formed by ozonolysis		
propanal		
3-hexenal	n-hexanal	
3,6-nonadienal	3-nonenal	n-nonanal
aldehydes formed in air oxidation experiments (Salthammer et al. 1999)		
2-pentenal	hexanal	heptanal
2-hexenal	heptanal	octanal
3-hexenal	2-heptenal	nonanal
2-heptenal	octanal	decanal
2,4-heptedienal	2-octenal	2-decenal
	2-nonenal	
	2-decenal	
	2,4-nonadienal	
	2,4-decadienal	
compounds formed in air oxidation of linoleum (highest emitters in descending order of GC-FID area) (Jensen et al., 1995)		
hexanoic acid, propanoic acid, hexanal, acetic acid, 2-butoxyethanol, pentanoic acid, nonanal, heptanoic acid, butyric acid, octanal, octanoic acid, 2-decenal		

While some of these species were released from carpet, many are not. Unmodified

linseed oil is not directly responsible for these emissions as evidenced by my experiments with oils. Compare the pattern of emissions from the various forms of linseed oil shown in Figure 2.22 and with the pattern of emissions from carpet CP3 (Figure 2.12). Carpet CP3 reacts with ozone to form significantly more nonanal and 2-nonenal than any other aldehyde, yet the ozonolysis of linseed oil forms a large amount of nonanal, and unidentified isomers of hexenal and nonadienal (unidentified, but definitely not 2,4-nonadienal). The pattern of secondary emissions from linseed oil also does not match that of any other carpet sample.

Nonanal and 2,4-nonadienal may be the result of oxidation of oleic acid and 9,11-octadecadienoic acid, or their esters. Few unmodified natural oils contain 9,11-octadecadienoic acid; tung oil is an exception. The pattern of emissions from tung oil is dominated by nonanal, pentanal and hexanal, but also includes some 2,4-nonadienal. The emission pattern does not closely match that of any carpet sample. The fact that 9,11-octadecadienoic acid is identical to linoleic acid, with the exception that one double bond is shifted to an adjacent carbon pair, suggests that the precursor may be the result of the modification of a common oil containing linoleic acid.

There are several processing steps in which vegetable oil based products may come in contact with carpet. Several sulphonated oils (e.g. tallow, tall, castor, olive and cottonseed) are used as cleaning agents and as surfactants in dyeing, wetting out and finishing of textiles. Oil triglycerides are sulphonated by contacting the oil with concentrated sulphuric acid. While none of the primary oils noted above would be a significant source of conjugated dienes (tall oil contains some 9,11-octadienoic acid), processing in a strong acid may result in isomerization. Octa-cis-9-trans-11-dienoic acid

can be formed by alkali isomerization of linoleic acid (Hopkins, 1972). Other processing steps may require fibers or yarn to be lubricated. Lubricated yarns knit more smoothly. They are typically soaked in the lubricant itself or otherwise treated to form a lubricated finish (Wingate, 1979).

Castor oil was listed above as being used by the textile industry, but does not contain conjugated double bonds. However, castor oil can be dehydrated so that conjugated double bonds form, thereby changing the properties of the oil (Gunstone, 1994). Based on the ratio of compounds released, dehydrated castor oil could be a candidate as a precursor species but was not available at the time of my study. For a given unsaturated fatty acid ester, only one volatile aldehyde would be released upon ozone oxidation (not including di-aldehydes). Other products of the ozone/double-bond reaction are likely to be much less volatile and would not be measured in this analysis. Making the assumption that a single aldehyde is derived from a single fatty-acid ester, I estimate that castor oil may present on the carpet at greater than 0.5 g m^{-2}. This leads to an oil thickness of about 10 nm on the fibers. Other possible precursors include isomerized sunflower or linseed oil.

In summary, the pattern of emissions of ozone-induced aldehydes suggests a precursor derived from vegetable oils. The patterns of secondary emissions from several forms of linseed oil and tung oil do not match that derived from carpet experiments. Other possible precursors include dehydrated castor oil and isomerized oils originally containing linoleic acid esters (e.g. linseed oil).

2.4.2 Influence of extended airing on emissions

In Figure 2.9, I show that, when exposed to ozone, the average emission rate of summed of aldehydes from aired carpets is always less than that from stored carpet. For carpets CP1 and CP2, this might be explained, in part, by recognizing that the gas-phase component of aldehyde formation nearly makes up for the difference. Since the aired carpets emit only small amounts of reactants, the gas-phase component of aldehyde formation should be negligible.

The significant reduction in secondary emissions exhibited by aired CP3 and CP4 cannot be attributed to the absence of gas-phase reactants. Only a small fraction of the stored carpet aldehyde production is due to gas-phase reactions for these carpets. I suggest that airing out the carpets (in cleaned, ozone free air) results in a small amount of oxidation of the precursor molecules. Indeed, the initial, no ozone sample of each aired carpet had slightly elevated emissions of several n-aldehydes, in addition to some carboxylic acid species. Jensen et al. (1995) showed that terminal bond oxidation products of the components of linseed oil (Table 2.5) comprised about 50% of VOC emissions. They noted that these form as byproducts of air oxidation "hardening" of linseed oil. Thus air oxidation of vegetable-based oils is likely to reduce the quantity of surface precursors, and also serve as a mechanism for secondary product formation.

Airing out carpets is probably helpful in preventing the introduction of primary emission compounds into indoor environments. It may be somewhat helpful in reducing the emissions of secondary reaction products as well. However, only 20-60% reduction in these emissions was obtained (for CP3 and CP4) after greater than a year of airing. It is unlikely that carpet manufacturers or distributors will be willing to perform such a

lengthy post-manufacturing treatment. It would certainly be more efficient to identify the precursor and replace it with a more benign substitute.

2.4.3 Analysis of dynamic results

In the following section, I will analyze the dynamic emissions of aired carpet CP3. The dynamic emissions can provide insight into the kinetics of surface reactions and provide qualitative information about sorption phenomena. The emissions of carpet CP3 are specifically interesting because of the high 2-nonenal emission rates and the correlations between dynamic emission rates of certain aldehydes.

In Figure 2.23, I show how the emissions of specific aldehydes from CP3 evolve during exposure to ozone. The emissions profile from whole carpet and fibers are presented as stacked area plots (a) and (b), respectively. The area between the curves represents the total emissions of the given compound over the period of the experiment. The label "other aldehydes" refers to the sum of the emissions of all quantified aldehydes other than 2-nonenal, nonanal, octanal and heptanal. Note that for the whole carpet experiment ozone was shut off after an elapsed time of 72 h, for a period of 22 h, then turned on briefly and shut off again. This was done to measure aldehyde decay in the absence of ozone, as well as the short-term increase in aldehyde emissions upon re-exposure to ozone.

Nonanal and 2-nonenal are released in larger amounts than any other compound. Only 0.5 h after initiation of ozone exposure, n-nonanal is emitted at a high rate of 158 $\mu g\ m^{-2}\ h^{-1}$ that increases to a maximum of 306 $\mu g\ m^{-2}\ h^{-1}$ by 48 h. In contrast, 2-nonenal has a barely detectable initial (0.5 h) emission rate of 2 $\mu g\ m^{-2}\ h^{-1}$ that rises more slowly to reach a maximum of 280 $\mu g\ m^{-2}\ h^{-1}$ at 48 h.

In the period between 72 and 94 hours, when the ozone concentration is zero, the aldehyde emissions drop relatively slowly. The emission rate of the summed aldehydes drops by approximately 50% over this period in which about 150 air changes take place. After three air changes in an ideal CMFR reactor, the concentration of an analyte should drop to about 5% of its initial value, once the emission source has been removed. Clearly, the emission rate of each of these aldehydes remains large, long after the ozone has been cleared from the reactor. Two phenomena may explain the continued emissions of aldehydes after ozone exposure: surface adsorption/desorption of aldehydes and delayed decomposition of stable ozonides to aldehydes.

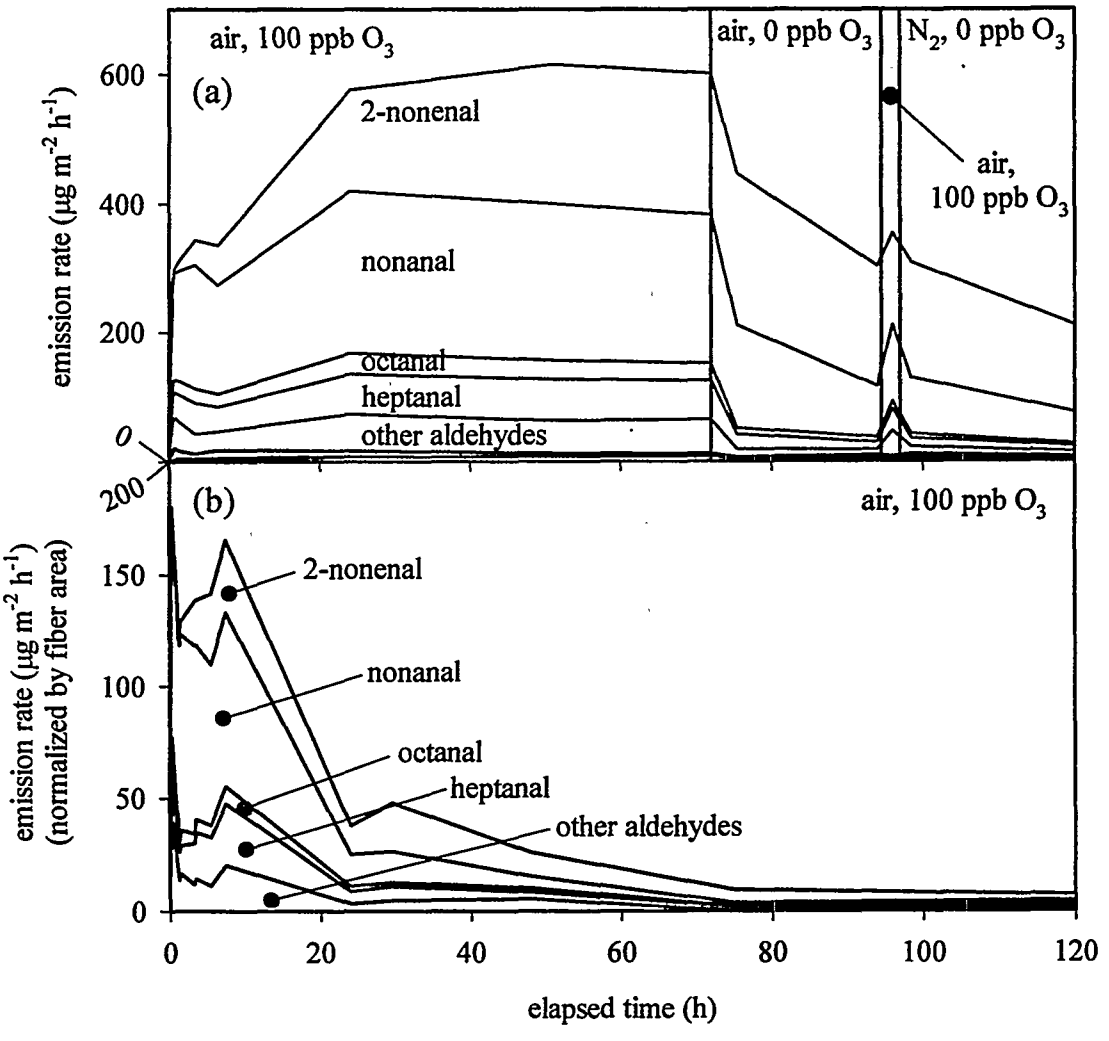

Figure 2.23. Dynamic emission rates from (a) whole carpet CP3 and (b) carpet fibers, during two 5-day exposure experiments. In (a), the ozone generator was turned off at 72 h, and turned on again between 94 and 96 h.

Several researchers have investigated the sorption kinetics of compounds on carpet surfaces. Won et al. (1999) measured sorption/desorption kinetic parameters for several halogenated compounds, toluene, cyclohexane, isopropanol, and methyl-tert-butyl ether several hydrocarbons on different carpet types. Others who have investigated carpet-VOC interactions are An et al. (1999) (ethylbenzene, cyclohexanone, p-dichlorobenzene, benzaldehyde, dodecane), Jørgensen et al. (1999) (toluene, alpha-pinene), Bouhamra and

Elkilani (1999) (toluene), Van Loy et al. (1998) (nicotine, phenanthrene), Colombo et al. (1993) (perchloroethylene, p-dichlorobenzene, alpha-pinene, 1,2,4-trimethylbenzene, 2-butoxyethanol, 2-ethylhexanol, decane, n-dodecane), Sparks et al. (1991) (perchloroethylene, p-dichlorobenzene), and Tichenor et al. (1991) (perchloroethylene, ethylbenzene).

None of these researchers have investigated the sorption kinetics of aliphatic or unsaturated aldehydes on carpet surfaces. However, Weschler et al. (1992) noted that concentrations of aldehydes remained detectable long after ozone was cleared from a chamber containing carpet. They attributed this to strong sorption of the aldehydes to carpet. While it is beyond the scope of this chapter to delve deeply into the subject, some semi-quantitative insights can be gained by analyzing my existing data set and comparing it to measured kinetic parameters for similar compounds. Structurally, compounds that have an aldehyde functional group and an aliphatic carbon chain would be desirable for comparison. Alternatively, other polar functional groups may be comparable, such as ketones and alcohols. It is also important to note that sorption is strongly influenced by vapor pressure of the species. The compounds closest in structure, and vapor pressure (at 23 °C) to C_7-C_{10} n-aldehydes, that have previously been investigated, are benzaldehyde, cyclohexanone, 2-butoxyethanol, and 2-ethylhexanol.

Sorption kinetics are usually parameterized by rate of adsorption,

$$\text{adsorption rate}\left(\mu g\, m^{-2}\, h^{-1}\right) = k_a C_{analyte} \qquad (2.3)$$

and the rate of desorption from a surface,

$$\text{desorption rate}\left(\mu g\, m^{-2}\, h^{-1}\right) = k_d M_{analyte} \qquad (2.4)$$

where $M_{analyte}$ is the surface mass of the analyte per unit area, k_a is the adsorption rate constant, and k_d is the desorption rate constant. At equilibrium, these rates are equal and a sorption equilibrium constant can be deterimined:

$$K_e = \frac{k_a}{k_d} = \frac{M^e_{analye}}{C^e_{analyte}} \tag{2.5}$$

where the superscript e denotes equilibrium values of $M_{analyte}$ and $C_{analyte}$. The reported values of k_a for benzaldehyde, cyclohexanone, 2-butoxyethanol, and 2-ethylhexanol were 0.57, 0.44, 1.26, 0.77 m h^{-1} respectively and of k_d were 0.092, 0.20, 0.24, 0.11 h^{-1} respectively. These correspond to K_e values of 6.2, 2.15, 5.3, and 7.0 m respectively.

My experiments were not designed to measure sorption equilibrium parameters, but an analysis of the system at dynamic steady state can yield a range of sorption equilibrium constant values. The equation describing dynamic species concentration in a CMFR (equation 1.1) can be modified to include the sorption loss term (equation 2.3) and the desorption emission term (equation 2.4). Under dynamic steady-state conditions,

$$\frac{M_{analyte}}{C_{analyte}} = \frac{k_a + Q/A}{k_d} \tag{2.6}$$

where Q is the volumetric flowrate through the reactor (0.072 m^3 h^{-1}), and A is the nominal surface area of carpet (0.023 m^2). As noted before, the emissions of nonanal and other aldehydes continues long after the ozone concentration drops to zero. To obtain a lower-bound estimate of the surface coverage of summed aldehydes, I integrated emissions over the period between 72 and 120 h, with a result of ~15,000 μg m^{-2} based on the nominal surface area of carpet. The maximum concentration in the gas phase of summed aldehydes at 72 h was about 200 μg m^{-3}. In experiments not reported here, I

found minimal aldehyde adsorption to chamber surfaces. Thus, assuming that sorption phenomena on inner reactor surfaces are negligible, an estimate of the carpet sorption equilibrium constant can be found,

$$\frac{M_{analyte}}{C_{analyte}} = 75\,\mathrm{m} \qquad (2.7)$$

This represents an emission weighted average for all aldehydes measured. This ratio is about 40, 60, 110, and 125 m for heptanal, nonanal, decanal and 2-nonenal. These values represent lower-bound estimates of the quotient because only a portion of the potentially released aldehydes were accounted for in the period between 72 and 120 h. Given the range of values of k_a for similar species (An et al., 1999), a range of K_e values can be estimated using equations 2.5 and 2.6 for the emission weighted average aldehyde species: 15 – 20 m. However, because the integration analysis only captures a portion of the potential aldehyde emissions from carpet CP3, I estimate (by an extrapolation to $C_{aldehyde}$ =0) that the actual K_e values are at least a factor of two higher than shown here (30-40 m).

For comparison, an estimate of the equilibrium constant, K_e, for aliphatic aldehydes, can be found using the vapor pressure. An et al. (1999) showed that the sorption equilibrium constant was inversely proportional to the vapor pressure of the species for a given temperature and substrate. Their data-set is particularly relevant to my system because 1) they used a carpet similar to CP3 (nylon fiber pile with SBR adhesive backing), 2) their experimental conditions of temperature and humidity were identical to mine (23 °C, 50%), and 3) among the five compounds they studied, two contained carbonyl groups, one of which was an aldehyde (cyclohexanone and benzaldehyde).

Under these conditions, they found that K_e [m] =6.011/P_o where P_o [mm Hg] is the vapor pressure of the species at 23 °C. The vapor pressures of C_7, C_9 and C_{10} n-aldehydes at 23 °C are 2.77, 0.54, 0.14 mm Hg, based on interpolation between reported vapor-pressure values in Perry et al. (1984). By the correlation of An et al., the predicted K_e for n-heptanal, n-nonanal and n-decanal would be 2.2, 11 and 43 m for nylon pile carpet. The vapor pressure data reported in Perry et al. (1984) for n-octanal was probably in error because they were much lower than that for n-decanal. The species was excluded from this analysis.

Given the coarse nature of the analysis, the weighted-average K_e estimated for aldehydes in my experiments is in the right range, but perhaps somewhat high. Clearly, a more direct measurement of aldehyde sorption kinetics is necessary to discern the extent to which sorption phenomena are responsible for the slow decay in aldehyde emissions from carpet after ozone has been flushed from the chamber. However, the high estimated range of K_e values suggests that the chamber concentration decay may also be influenced by other phenomena, such as delayed ozonide decomposition.

Ozonides, formed by ozone-alkene reactions, may be stable at room temperature. Razumovskii (1966) found that the ozonide of 1-hexene gradually decomposed to acids and aldehydes during storage at 25°C, with a first-order half-life of 1970 hours. Ordinary thermal decomposition of an ozonide is accelerated in the presence of acids and polar solvents (e.g. water) (Razumovskii and Zaikov, 1984). Stable ozonides can serve as temporary storage for aldehydes and may explain some of the delayed release of aldehydes shown in Figure 2.23. The high molar conversion efficiency of ozone reacting to form aldehydes (as shown in Figures 2.14-2.21) suggests that most of aldehydes

formed are eventually released during the experiment. A more compelling case for delayed ozonide decomposition can be made for precursors that form 2-nonenal and heptanal.

Figure 2.24(a) and (b) shows the normalized emission rate (NER) of nonanal, heptanal and 2-nonenal for the same experiments shown in Figure 2.23. The normalized emission rate of an analyte is simply the emission rate divided by the cumulative emissions of that compound during the entire experiment. In Figure 2.24 (a) (whole-aired CP3) and (b) (CP3 fibers) the 2-nonenal NER lags behind that of nonanal and heptanal.

Stability of ozonides may explain the large discrepancy between the dynamic emission rates of nonanal and 2-nonenal. Exposing the carpet to ozone initiates an immediate increase in the emission rate of nonanal. Then the emission rate increases somewhat over the next 72 h. The emission rate of 2-nonenal slowly increases but does not have an initial, rapid increase. I suggest that this effect is primarily due to the formation of an extra-stable ozonide. If the ozonide forms at the "9" location of 9,11-octadecadienoic acid, it will be adjacent to (conjugated with) the double-bond at the "11" location. The proximity of a double-bond may stabilize the ozonide, delaying the decomposition to 2-nonenal and other products. If this were so, then a delay in the emissions of heptanal should also be evident. Heptanal may be formed by the reaction of ozone with singly unsaturated compounds as well as the doubly unsaturated 9,11-octadecadienoic acid. Therefore, the decomposition kinetics of the conjugated ozonide may be masked by decomposition of unconjugated ozonides. In Figure 2.24(a), no lag in the heptanal emissions is evident. However, there is a significant lag in the emissions of heptanal in Figure 2.24(b). In fact, the emission pattern of heptanal appears to lie

somewhere between that of nonanal and 2-nonenal. I suggest that about half of the heptanal forms as the decomposition product of an ozonide of 9,11-octadecadienoic acid and the rest is formed from the decomposition of an unconjugated ozonide.

Nonanal and 2-nonenal are structurally very similar, suggesting that their sorption kinetics should be similar. Large differences in the stability of the precursor ozonides may be a more likely mechanism to explain the large difference in decay rates between emissions of nonanal and 2-nonenal after ozone exposure has ceased. Once again, the ozonide formed may act as a storage medium, releasing 2-nonenal even when ozone is not present.

In Figure 2.24(b), the pattern of the NER of nonanal does not appear to have any significant emissions lag, unlike that of Figure 2.24(a). This may be due to the absence of any backing material in the fixed bed experiment. Won et al. (1999) found that the carpet backing and also carpet pad were much stronger sorption sinks than the fibers for the compounds they tested. While some of the nonanal lag in Figure 2.24(a) may be due to delayed ozonide decomposition, sorption may also significantly influence the dynamic emissions due to the presence of backing.

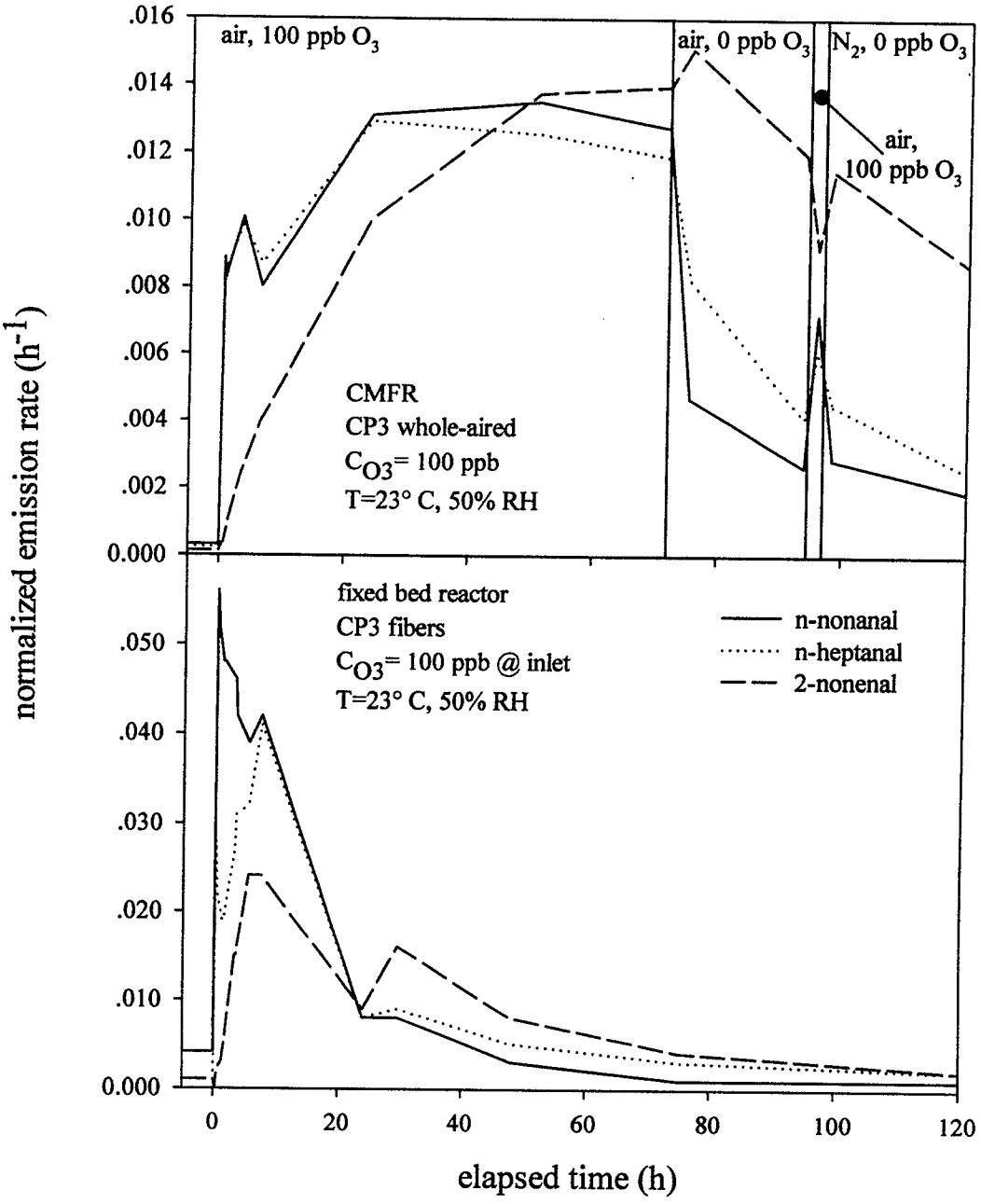

Figure 2.24. Normalized emission rates (NER) of selected aldehydes from carpet CP3: (a) aired carpet, (b) carpet fibers.

In Figure 2.24(a), the NER of 2-nonenal initially increases when the ozone was turned off at 72 h. Again, at an elapsed time of 95 hours, the ozone was briefly turned on, but the 2-nonenal NER drops. It then increases again when the ozone is turned off. This is

a pattern exactly opposite that of any aliphatic aldehyde. Ozone is probably reacting with 2-nonenal somewhere in the reactor or the sampling system. In Section 2.2.7.2.4, I discussed the possibility that aldehydes may react on the Tenax cartridges with ozone, thereby reducing the apparent emission rates of the compounds. While most aldehydes were found to be immune from this effect, 2-nonenal and 2-octenal were degraded somewhat on Tenax during sampling. Due to the complicated influences on 2-nonenal emissions (desorption, ozonide degradation), it is inappropriate to assign all of the 2-nonenal losses to ozone reactions on Tenax. Some losses may occur in the gas phase or as a result of heterogenous reactions with ozone on carpet surfaces. However, it is clear that the actual emission rates are higher than those measured in the presence of ozone.

2.4.4 Implications for indoor air quality

The large quantities of unsaturated surface oils present on carpets could adversely impact indoor air in locations where ozone concentrations are elevated. One can estimate the indoor concentration of a given species based on the emission rate measured under laboratory conditions, extrapolated to conditions in indoor environments. In this estimate, the aldehyde emissions are assumed to be directly proportional to the rate of ozone removal at the surface of the carpet. For example, in the CP3 fiber experiment shown in Figure 2.19(b), the molar ratio of aldehydes emitted per ozone consumed of all quantified aldehydes ranges from 0.22 to 0.47 with an integrated average of 0.39. As an example of a specific compound the molar ratio of 2-nonenal released to ozone reacted is about 0.11. Using the value derived from fiber experiments may represent a lower bound. The molar ratio value for 2-nonenal from CP3 aired carpet is 0.19 and from stored carpet CP3 is

0.17.

The flux, F, of ozone to a flat indoor surface can be parameterized by the deposition velocity, v_d,

$$F = v_d C_{ozone} \tag{2.8}$$

where, C_{ozone} is the spatial average concentration of ozone indoors (usually measured at the center of a room). The deposition velocity of ozone to carpet indoors is discussed in more detail in Chapters 3 and 4. The concentration of ozone indoors can be estimated from a completely mixed flow reactor (CMFR) at steady-state (Weschler et al., 1989) ,

$$C_{ozone} = \frac{\lambda C^{o}_{ozone}}{\lambda + \overline{v}_d \frac{S_T}{V}} \tag{2.9}$$

where C^{o}_{ozone} is the outdoor concentration of ozone, λ is the air exchange rate, $\overline{v}_d$ is the area-averaged deposition velocity, S_T is the total indoor surface area, and V is the indoor volume.

Under average conditions in Los Angeles, the annual average outdoor ozone mole fraction ranges from 20 to 54 ppb (Cass et al., 1991). I use a middle value of 37 ppb, and combine this with an estimated surface area to volume ratio of 3 m^{-1}, an air exchange rate of 1 h^{-1} and a mean deposition velocity of 1.4 m h^{-1} (0.04 cm s^{-1}). The resulting time-averaged indoor ozone mole fraction is 7.1 ppb.

Using these values, I can estimate the flux of ozone to carpet and multiply this by the aldehyde emission ratio to obtain an estimated emission rate, E_i (moles per carpet area per time), for compound *i*. The steady-state concentration of compound *i* indoors is then calculated using a similar CMFR analysis as above,

$$C_i = \frac{E_i S_C MW_i}{\lambda V} \qquad (2.10)$$

where S_C is the horizontally-projected area of the carpet and MW_i is the molecular weight of compound i. This equation computes the increment in concentration of species I from secondary carpet emissions and neglects removal processes other than ventilation. The indoor concentrations were estimated assuming $S_C/V = 0.4\ m^{-1}$ (appropriate for wall-to-wall carpet) and $\lambda = 1\ h^{-1}$. The indoor concentrations for 2-nonenal and nonanal from carpet CP3, the two compounds with the highest emissions, are 2.5 and 3.6 $\mu g\ m^{-3}$. Odor thresholds for 2-nonenal and nonanal are 0.8 $\mu g\ m^{-3}$ and 13 $\mu g\ m^{-3}$ (Devos et al., 1990).

In Figure 2.25 I demonstrate that the odor threshold for several compounds produced by ozone-carpet interactions may be approached or exceeded in indoor air. The black bars (Case 1) represent calculated aldehyde concentrations for selected compounds based on the above analysis and assumptions. For "average" conditions, only the concentration of 2-nonenal exceeds the odor threshold. The second set of bars (Case 2) in the figure represents a more extreme case. For Case 2 I assume that the stored-carpet is representative of a new carpet installation. I also allow the outdoor ozone concentration to rise to 120 ppb, an unhealthy, but not uncommon value occurring midday during the summer in many urban areas. Under these conditions, three compounds exceed the odor threshold: nonanal, 2-nonenal and 2,4-nonadienal. The doubly unsaturated 2,4-nonadienal was only found to be emitted from stored CP3, but the emissions were high enough that odor thresholds are easily surpassed. Other compounds such as octanal and decanal approach their respective odor thresholds.

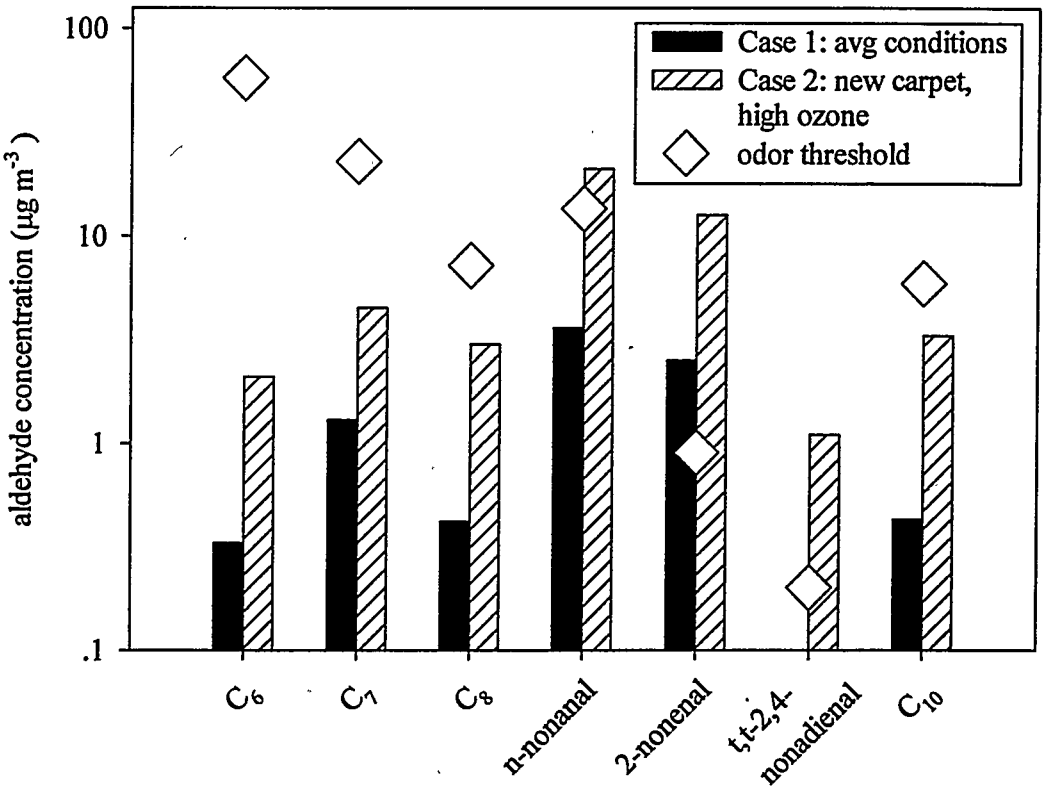

Figure 2.25. Model estimates of indoor aldehyde concentrations under two conditions for house containing carpet CP3. Case 1: indoor ozone concentration 7.1 ppb, well aired carpet using aldehyde molar ratios from fiber experiments with carpet CP3. Case 2: indoor ozone concentration 23 ppb, newly installed carpet using molar ratios from stored whole carpet CP3 experiments. Odor threshold values taken from Devos et al. (1990).

The aired-carpet concentrations calculated for average conditions could be maintained for more than a year if the emission rate is constant. This is easily calculated based on the total emissions, E_T (for summed aldehydes this is shown in Table 2.4). Using the same approach, carpet CP3 was estimated to release at least 74 mg m^{-2} of 2-nonenal over its lifetime. Under conditions where the average indoor ozone concentration is somewhat lower (2.3 ppb), the concentration of 2-nonenal could be maintained at the odor threshold for nearly four years. This result is based on a lower bound estimate of cumulative emissions. For carpet CP3 backing, the emission rate of 2-nonenal was still very strong, even after 120 h of exposure to ozone at 100 ppb. Thus, only a fraction of the

potential emissions is included.

The previous analysis assumed a constant ozone concentration to obtain an estimate of average aldehyde concentrations indoors. Now consider the more realistic scenario in which the indoor ozone concentration follows a diurnal cycle. Returning to the CMFR to calculate indoor air quality, one can develop a model of indoor aldehyde concentration which includes 1) reaction of ozone with surfaces to produce ozonides, 2) delayed decomposition of these ozonides, and 3) sorption kinetics.

For this analysis, I will assume that ozone/alkene reactions are instantaneous, but rates are limited by the flux of ozone to the surface of carpet. I will also only consider the formation of 2-nonenal as an example product species. The following set of equations describe the time-dependent concentration of 2-nonenal in indoor air ($C_{nonenal}$) and on the surface ($M_{nonenal}$), and the ozonide on the surface ($M_{ozonide}$),

$$V\frac{dC_{nonenal}}{dt} = \left(k_d M_{nonenal} A_s - k_a C_{nonenal} A_s\right) + QC^o_{nonenal} - QC_{nonenal} \qquad (2.11)$$

$$\frac{dM_{nonenal}}{dt} = k_a C_{nonenal} + k_1 M_{ozonide} - k_d M_{nonenal} \qquad (2.12)$$

$$\frac{dM_{ozonide}}{dt} = fv_d C_{ozone} - k_1 M_{ozonide} \qquad (2.13)$$

This set of equations assumes first-order decomposition of the ozonide to 2-nonenal with a rate constant k_1. It also assumes that the supply of alkene surface reactant is not consumed in the simulated time period. In equation 2.11, the term in parentheses contains the sorption/desorption kinetic terms where k_d and k_a are the desorption and adsorption rate constants for a linear isotherm. The second equation describes the time-dependent surface concentration of 2-nonenal influenced by sorption kinetics and the decomposition

of the ozonide. The last equation describes the time dependent surface concentration of the ozonide, formed at a rate limited by the deposition velocity, v_d, and the formation factor, f.

By examining the above equations, we can see that there are several parameters necessary to perform a simulation. Sorption parameters may be taken from literature values for the adsorption of organic compounds to carpet. Colombo et al. (1993) reported values of k_a and k_d for several organic compounds sorbed to carpet. For the purposes of this exercise, I will use the values quoted for a n-dodecane sorbed to carpet, as this system provided the largest sorption equilibrium coefficient in the Colombo et al. data set. (Sparks et al. (1991) measured very strong sorption of p-dichlorobenzene, but the kinetic parameters measured for the same compound by Colombo, et al. were much higher, making both values suspect. The sorption equilibrium values for the semi-volatile compounds tested by Van Loy et al. (1998) are also not relevant because they are much higher than the highest estimated values for aldehydes on carpet.) The kinetic sorption values were, $k_a = 1.86$ m h^{-1} and $k_d = 0.13$ h^{-1} for n-dodecane. The formation factor, f, can be taken directly from experimental observations, assuming that all ozonides decomposed and all 2-nonenal desorbed from the carpet surface: 0.11 mol 1-nonenal (mol ozone deposited)$^{-1}$. The decomposition rate constant for the ozonide cannot be precisely evaluated from my experiments, since they were not designed for that purpose. However, an estimate may be made based on decay rate time constant arguments.

Referring to Figure 2.23, during the period between 72 and 94 h, the ozone concentration is zero, and the 2-nonenal concentration is decaying. First, I will assume that the decay follows a typical exponential decay pattern, where,

$$C(t = 94h) = C(t = 72h)e^{-22h/\tau} \quad (2.14)$$

where τ is the characteristic decay time. While the equations 2.11 through 2.13 demonstrate that the form of the decay may be more complicated than first order exponential decay, the limited data set precludes a more detailed analysis. In this case, C(t=94h)=60.6 $\mu g\ m^{-3}$ and C(t=72h)=76.5 $\mu g\ m^{-3}$ of 2-nonenal. This results in a decay rate time-constant of about 95 h.

This decay is influenced by several processes, each associated with a characteristic time constant. Production of the surface aldehyde is slowed at a rate related to the inverse of the ozonide decomposition rate constant, k_1, because production of the ozonide has ceased. Release of the aldehyde from the surface has a time constant, k_d^{-1}, associated with it. Ventilation itself has a tendency to remove gas phase 2-nonenal with a characteristic time of VQ^{-1}. The ventilation time constant for this system is about 0.15 h and the characteristic time associated with desorption is k_d^{-1} = 7.6 h for n-dodecane. Neither of these characteristic time values come close to explaining the slow decay of 2-nonenal. Thus, I will ascribe the bulk of the delayed decay to ozonide decomposition. This allows me to estimate the decomposition constant $k_1=(95\ h)^{-1}=0.01\ h^{-1}$. If the adsorption of aldehydes is much stronger than the upper bound based on the Colombo, et al. data set, the ozonide decomposition rate will be higher. For the following simulation exercise, $k_1 = 0.01\ h^{-1}$ can be considered a lower bound.

To simulate the diurnal influence of ozone on indoor aldehyde concentrations, I made several assumptions. For simplicity, ozone concentrations indoors follow a sinusoidal form where C_{O3}=0 at 6:00 am and 6:00 pm and reaches a maximum at 12:00

noon. The indoor maximum concentration is 40 $\mu g\ m^{-3}$ (20 ppb). The simulation takes place in a 25 m^3 room, with 10 m^2 carpet and a ventilation rate of 25 $m^3\ h^{-1}$. The deposition velocity of ozone is 1.4 m h^{-1} on all surfaces, and the formation factor of the ozonide is 0.1 mol 2-nonenal per mol ozone deposited on carpet. In Figure 2.26, 2-nonenal results for three simulations are shown: 1) no influence of sorption or ozonide decomposition kinetics; 2) influence of adsorption only, where $k_a = 1.86$ m h^{-1} and $k_d = 0.13\ h^{-1}$; 3) influence of adsorption and ozonide kinetics where $k_1 = 0.01\ h^{-1}$.

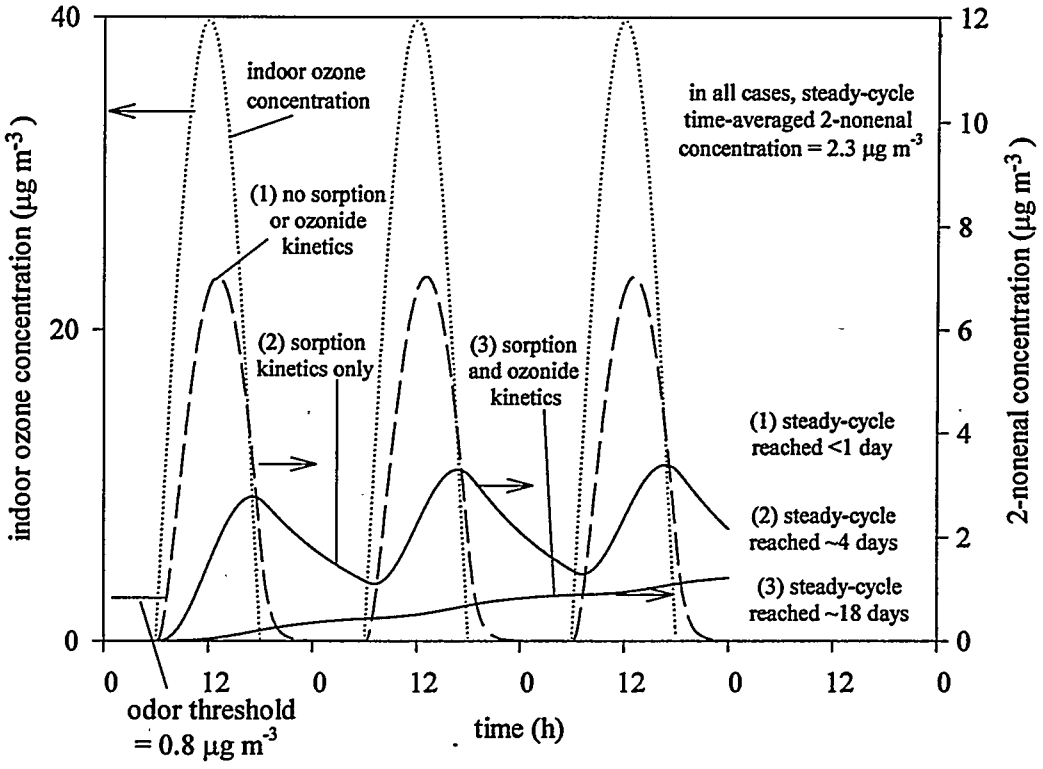

Figure 2.26. Three-day simulation of 2-nonenal concentrations in residence based on (1) no sorption or ozonide kinetics; (2) sorption kinetics only; (3) sorption and ozonide kinetics.

With no significant sorption or delay due to ozonide decomposition, the 2-nonenal concentration resembles the shape of the ozone concentration curve, with peak concentrations occurring near noon. Delays in peak concentration are due only to the

CMFR residence time. The highest rate of aldehyde exposure occurs near noon, but if sorption kinetics are taken into account, the peak concentration occurs nearly 6 h later. The addition of ozonide kinetics flattens out the 2-nonenal time profile so much that the concentration has not peaked, even after three days. In this case, steady-cycle conditions do not occur until 18 days have passed. The slow decomposition of ozonides could significantly influence the day to day aldehyde exposure people may experience indoors.

2.4.5 Ozone uptake and secondary emissions from styrene-butadiene adhesive backing

The ozone-induced secondary emission rate of aldehydes from carpet backing was of the same magnitude as that measured from aired carpet samples (See Figure 2.9; Secondary emission rates were somewhat larger from the backing of CP1 and CP4 than from aired samples of the same carpet). The pattern of secondary aldehyde emissions was approximately the same for both whole-aired carpet and carpet backing. These findings suggest that the volatile products derive from the same or similar species in each case. However, the molar ratio of aldehyde emission rate to ozone uptake rate for backing, in all cases, is smaller than that for aired-whole carpet samples. A smaller molar ratio means that more ozone reacted with the material for a given amount of secondary aldehyde emissions. The structure of the backing may explain this result. In all cases, the backing is made of two polypropylene mesh sheets. Fibers are woven through one sheet, and an adhesive is applied to secure the carpet fibers in place with the second sheet. The adhesive, in all cases is a styrene-butadiene co-polymer. The typical polymeric subunit for a 25% styrene, 75% butadiene SBR co-polymer is (Hart, 1983)

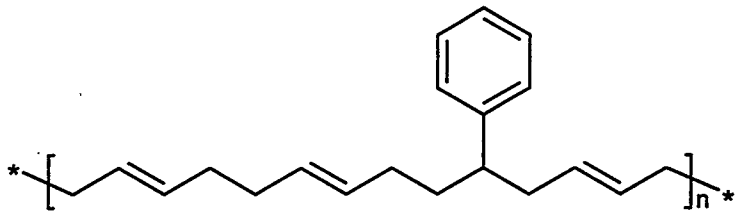

Note the presence of double bonds. A polymer made of these subunits may react with ozone to form low-volatility oxidized species because the double bonds are a part of the polymer backbone. Reactions on backing that include reactions on the SBR adhesive could explain lower values of the molar ratio of secondary aldehyde emission rate to ozone uptake rate. It is also possible that some polymer subunits are derived from the polymerization of butadiene with a second butadiene monomer. Two subunits are possible from this polymerization:

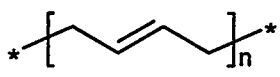

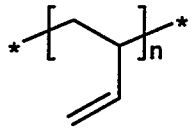

The first structure is similar to the backbone of the typical SBR subunit: double-bonds form part of the polymer backbone. The second subunit contains a double bond as part of a branched structure. Ozone reaction at this branched double bond would result in the formation of methanal. However, there was no striking difference in methanal emissions from carpet backing relative to whole-carpet samples of the same carpet type.

2.4.6 Some additional interesting chemistry

In Tables A.2.2-A.2.9 of Appendix A.2, I show that small amounts of octane and nonane were formed when carpets were exposed to ozone. Formation of octane and

nonane may be due to ozonide degradation followed by decarbonolation (Pryde and Cowan, 1971). Greiner and Muller (1962) ascribe hydrocarbon formation due to decarbonylation of aldehydes in the presence of peroxide:

$$RCH_2CH_2CHO \rightarrow RCH_2CH_2\overset{\bullet}{C}=O \xrightarrow{-CO} RCH_2\overset{\bullet}{C}H_2 \rightarrow RCH_2CH3 + RCH=CH_2 + RCH_2CH_2CH_2CH_2R$$

Razumovskii and Yur'ev (1967) suggested that the zwitterion decomposes directly, $RCH_2\overset{+}{C}HO\overset{-}{O} \rightarrow RCH_3 + CO_2$. Gaseous CO, CO_2, H_2, O_2 were also detected from this decomposition. Story et al. (1968) favor radical mechanisms of hydrocarbon formation. Common to these mechanisms is that the chain length is reduced by one carbon when forming the hydrocarbon. While the low emission rates of these two alkanes will probably not significantly influence indoor air quality, the formation of these compounds helps verify that these aldehydes are formed as products of ozonide degradation.

It should be noted that there are two compounds missing from the primary emissions from stored carpet. Weschler et al. (1992) noted that both styrene and 4-ethenylcyclohexene were present in the reaction chamber after 168 h of airing for those carpets with styrene-butadiene rubber (SBR) adhesive in the carpet backing. Ozone reactions reduced the concentration of these compounds but products of the reactions were not specifically identified. In my studies, neither styrene nor ethenylcyclohexene were detected in the primary emissions from any stored carpet (carpets CP1-CP4 contained SBR in the backing). It seems that either carpet makers have modified the manufacture of SBR so that emission rates of these compounds are reduced, or that long term, air-tight, storage has the effect of reducing the emission rates of these compounds to

undetectable levels.

2.5 Conclusions

The furnishings we place in our homes can affect the quality of indoor air. Furnishings can release into indoor air unhealthy volatile compounds that remain from manufacturing processes. In addition, reactive gases, such as ozone, can interact with their surfaces to create new, more irritating and odorous, volatile compounds. In this study, I allowed ozone to react in the gas phase and at the surface of carpets to better understand how and to what extent these interactions form odorous aldehydes and other species.

Ozone reactions with carpet surfaces form C_1 through C_{13} aliphatic and unsaturated aldehydes, many of which have very low odor thresholds. These carpets can act as "reservoirs" for these odorous compounds, with the emission rates regulated by the indoor concentration of ozone. Carpet CP3, a commonly installed, residential, olefin-fiber, cut-pile carpet had an especially large reservoir of precursors of n-nonanal and 2-nonenal. The compound 2-nonenal has an extremely low odor threshold of 0.8 $\mu g\ m^{-3}$. In a residence where carpet CP3 is installed, concentrations of 2-nonenal are likely to exceed the odor threshold, even under conditions where the indoor ozone concentration is very low. Based on a conservative integration of the total emissions of 2-nonenal, use of this carpet could result in odorous levels of aldehydes for several years.

The dynamic emissions of aldehydes from carpet CP3 indicate that several physical and chemical processes delay emissions of aldehydes. Weschler et al. (1992) suggested that strong adsorption of aldehydes to carpet surfaces may have accounted for

the observed elevated concentrations of aldehydes after the elimination of ozone from the reaction chamber. While adsorption may strongly influence the dynamic emissions of aldehydes from my carpet samples, I suggest that delayed decomposition of an intermediate ozonide may also be important. The emission rate of the unsaturated aldehyde, 2-nonenal, is significantly delayed relative to aliphatic aldehydes. This may be due to differences in the rates of decomposition of two types of ozonides: 1) an ozonide formed at a double bond with no other nearby double bonds; 2) the intermediate formed from ozone attack at a conjugated double bond site, resulting in a conjugated, and more stable ozonide.

Some carpets in this study were aired for greater than a year to reduce the emissions of volatile primary compounds. A comparison of the secondary, ozone-induced emissions from stored and aired carpets shows that airing has the effect of lowering the emission rate of aldehydes, but not markedly. The surfaces of carpets are probably oxidized or otherwise modified by exposure to clean air, thus reducing potential ozone reaction sites. Airing out carpets results in only a moderate overall decrease in odorous secondary emissions and would not be an efficient method of pre-treating carpets prior to installation. A more effective method of reducing these emissions would be to eliminate or modify the coating that contains the unsaturated precursors.

The manner in which ozone reacts with surfaces to produce odorous compounds results in competing public health concerns. The high surface area inherent in fleecy materials, such as carpet, can potentially be an important sink for ozone, improving indoor air quality by reducing ozone concentrations. However, these experiments show that the decrease in ozone concentration may result in a corresponding increase in

odorous compound concentrations. It is not yet clear how strongly odors influence the feeling of well-being, whereas the toxicity of ozone is well proven. Before modifications are made in carpet manufacture, the competing processes should be considered in the broader context of public health.

2.6 References

An, Y.; Zhang, J.S.; Shaw, C.Y. *HVAC & R Research.* **1999**, *5*, 297-316.

Atkinson, R.; Tuazon, E.C.; Aschmann, S.M. *Environmental Science and Technology.* **1995**, *29*, 1860-1866.

Berglund, B.; Lindvall, T. *Annals of the New York Academy of Science.* **1992**, *641*, 277-293.

Bouhamra, W.; Elkilani, A. *Environmental Science & Technology.* **1999**, *33*, 2100-2105.

Calogirou, A.; Larson, B.R.; Brussol, C.; Duane, M.; Kotzias, D. *Analytical Chemistry.* **1996**, *68*, 1499-1506.

Cass G.R.; Nazaroff W.W.; Tiller C.; Whitmore P.M. *Atmospheric Environment.* **1991**, *25A*, 441-451.

Clausen, P.A.; Wolkoff, P. *Atmospheric Environment.* **1997**, *31*, 715-725.

Colombo, A.; DeBortoli, M.; Knöppel, H.; Pecchio, E.; Vissers, H. *Indoor Air.* **1993**, *3*, 276-282.

Cometto-Muñiz, J.E.; Hernández, S.M. *Perception & Psychophysics.* **1990**, *47*, 391-399.

Cometto-Muñiz, J.E.; Cain, W.S.; Abraham, M.H. *Experimental Brain Research.* **1998**, *118*, 180-188.

Devos M.; Patte F.; Rouault J.; Laffort P.; Van Gemert L.J.; Eds. *Standardized Human Olfactory Thresholds.* Oxford University Press: Oxford, 1990.

Greiner A.; Muller, U. *Journal für Praktische Chemie.* **1962**, *15*, 313.

Gunstone, F.D.; Harwood, J.L.; Fred B. Padley, F.B.; Eds. *The Lipid Handbook.* 2nd edition. Chapman & Hall, London, New York, 1994.

Hart, H. *Organic Chemistry: A short course.* Houghton Mifflin Company, Boston, 1983.

Hilditch, T.P. *The Chemical Constitution of Natural Fats.* 3rd edition. John Wiley & Sons, New York, 1956.

Hopkins, C.Y. In *Topics in Lipid Chemistry.* Gunstone, F.D. ed. John Wiley and Sons, New York. vol. 3. 1972 .

Hodgson, A.T.; Girman, J.R. *Design and Protocol for Monitoring Indoor Air Quality,* ASTM STP 1002, Nagda, N.L.; Harper, J.P.; Eds. American Society for Testing and Materials, Philadelphia, 1989, 244-256.

Jensen, B.; Wolkoff, P.; Wilkins, C.K.; Clausen, P.A. *Indoor Air.* **1995**, *5*, 38-43.

Jørgensen, R.B.; Bjørseth, O.; Malvik, B. *Indoor Air.* **1999**, *9*, 2-9.

Kleindienst T.E.; Corse E.W.; Blanchard F.T.; Lonneman W.A. *Environmental Science and Technology.* **1998**, *32*, 124-130.

Molinari, E. *Annuario della Society Chimica di Milano.* **1903**, *9*, 507.

Nazaroff, W.W.; Cass, G.R. *Environmental Science and Technology.* **1986**, *20*, 924-934.

Patterson, M.Q.; Stevens, J.C.; Cain, W.S.; Cometto-Muñiz, J.E. *Chemical Senses.* **1993**, *18*, 723-734.

Pellizzari, E.; Demian, B.; Krost, K. *Analytical Chemistry.* **1984**, *56*, 793-798.

Perry, R.G.; Green D.; Maloney, J.O. *Perry's Chemical Engineering Handbook.* McGraw Hill, Inc. New York, 1984.

Pryde, E.H.; Cowan, J.C. *Ozonolysis* in *Topics in Lipid Chemistry.* Vol. 2. Gunstone, F.D.; Ed. John Wiley & Sons, Inc., New York, 1971.

Razumovskii, S.D. *Journal of Organic Chemistry, USSR.* **1966**, *2*, 1910.

Razumovskii, S.D.; Zaikov, G.E. *Studies in Organic Chemistry 15: Ozone and Its Reactions With Organic Compounds.* Elsevier Science Publishers B.V. Amsterdam, The Netherlands, 1984.

Razumovskii, S.D.; Yur'ev, Y.N. *Journal of Organic Chemistry, USSR.* **1967**, *3*, 251.

Reiss, R.; Ryan, P.B.; Koutrakis, P.; Tibbetts, S.J. *Environmental Science and Technology.* **1995a**, *29*, 1906-1912.

Reiss, R.; Ryan, P.B.; Tibbetts, S.J.; Koutrakis, P. *Journal of the Air and Waste Management Association.* **1995b** *45*, 811-822.

Salthammer, T.; Schwarz, A.; Fuhrmann, F. *Atmospheric Environment.* **1999**, *33*, 75-84.

Sparks, L.E.; Tichenor, B.A.; White, J.B.; Jackson, M.D. *Indoor Air.* **1991**, *1*, 577-592.

Story, P.R.; Hall, T.K.; Morrison, W.H.; Farine, J.C. *Tetrahedron Letters.* **1968**, *5*, 397.

Tichenor, B.A.; Guo, Z.;, Dunn, J.E.; Sparks, L.E.; Mason, M.A. *Indoor Air.* **1991**, *1*, 23-35.

U.S. Environmental Protection Agency. *Compendium of Methods for the Determination of Toxic Organic Compounds in Ambient Air.* EPA/625/R-96/010b. Office of Research and Development, Center for Environmental Research Information. 1999.

Van Loy, M.D.; Nazaroff, W.W.; Daisey, J.M. *Journal of the Air & Waste Management Association.* **1998**, *48*, 959-968.

Weschler, C.J.; Shields, H.C.; Naik, D.V. *JAPCA: Journal of the Air & Waste Management Association.* **1989**, *39*, 1562-1568.

Weschler, C.J.; Hodgson, A.T.; Wooley, J.D. *Environmental Science and Technology.* **1992** *26*, 2371-2377.

Weschler, C.J.; Shields, H.C. *Environmental Science and Technology.* **1996**, *30*, 3250-3258.

Weschler, C.J.; Shields, H.C. *Environmental Science and Technology.* **1997**, *31*, 3719-3722.

Wingate, I.B. *Fairchild's Dictionary of Textiles.* 6th edition, Fairchild Publications. New York, 1979.

Windholz, M.; Budavari, S.; Eds. *The Merck Index.* 10th edition, Merck & Co., Inc. Rahway, New Jersey, 1983.

Won, D.; Corsi, R.L.; Rynes, M. *Proceedings of the 92nd Annual Meeting of the Air and Waste Management Association.* **1999**. Paper number 99-165.

Zhang, J.; Lioy, P.J. *Indoor Air.* **1994**, *28*, 95-105.

CHAPTER 3

The Rate of Ozone Uptake on Carpets: Experimental Studies

3.1 Background

Indoor air pollutant concentrations are often influenced by the large amount of surface area associated with building materials and furnishings. Ozone is a strong oxidant which can react with many surfaces, making indoor ozone concentrations particularly sensitive to the high surface area to volume ratio (S/V) present indoors. Because of this, indoor concentrations of ozone are typically lower than outdoor concentrations, when there are no indoor ozone sources (Weschler et al., 1989). Carpet is commonly present in buildings and can potentially be one of the most significant ozone sinks due to its high intrinsic surface area. With about 10 million fibers per square meter woven tightly into a textile backing, the presence of carpet can increase the indoor surface to volume ratio by more than an order of magnitude compared with hard-surface floors.

The extent to which carpet may be responsible for lowering indoor ozone concentrations is not yet known. Field monitoring yields conflicting results regarding the importance of carpet in residences in reducing indoor ozone concentrations. Lee et al. (1999) measured ozone decay rates in 43 California residences and compared these rates with characteristics such as the presence of carpet, number of bedrooms, and house type. They found that indoor ozone decay rates were statistically higher in homes with floor space that was 100% carpeted, compared to homes with less than 100% carpet. Avol et al. (1998) measured indoor and outdoor ozone concentrations at 126 southern California

homes in 1994. Those factors most strongly correlating with the indoor concentration were the outdoor concentration and the pattern of window opening. They found no correlation with the presence of carpet.

To understand how carpet and other surfaces influence indoor air concentrations of ozone, it is instructive to examine indoor air quality models. The importance of surface area, S, becomes apparent when the CMFR model, introduced in Chapter 1 (equation 1.1), is applied to a building space,

$$\frac{C}{C_o} = \frac{\lambda}{\left(\lambda + v_d \frac{S}{V}\right)} \tag{3.1}$$

To obtain this steady-state form of the equation describing species concentration in a CMFR, it was assumed that there were no ozone emission sources or gas-phase loss mechanisms. Recall that λ is the air exchange rate and v_d is the area averaged, ozone deposition velocity. The indoor to outdoor concentration ratio, C/C_o, is reduced as the surface area to volume ratio, S/V, becomes larger, but increases as λ increases. A key parameter influencing the relative importance of surface loss in determining C/C_o is the deposition velocity, v_d.

By modeling air movement in indoor environments, Cano-Ruiz et al. (1993) showed that the deposition velocity can be determined by separately considering the surface reactivity and mass transport to surfaces. Materials with higher surface reactivity may serve to increase the ozone deposition velocity, independently from mass transport induced by fluid motion and diffusion. Their model uses the idea that a pollutant, such as ozone, must overcome transport resistance before reacting irreversibly on a surface. If the surface reaction probability is represented as a resistance, the sum of the mass-transport

and reaction resistances represents the overall mass-transfer resistance, R_o, so, $R_o = R_g + R_s$ where R_g is the resistance through the entire gas phase, and R_s is the resistance to irreversible uptake on a surface. The gas-phase resistance may be separated further to more accurately describe transport through different regions in the gas phase. The surface resistance may be considered to be independent of fluid flow conditions and, once known, can be used to predict pollutant flux to a surface under a variety of fluid flow conditions. The independent nature of the surface resistance makes it a valuable data point where environmental conditions (indoors, for example) are highly variable.

The surface resistance, R_s, can, in turn, be parameterized by the reaction probability, γ. This parameter is also known as the uptake coefficient, or the (mass) accommodation coefficient. In the present case, the reaction probability is the rate at which ozone molecules are irreversibly consumed at a specified boundary, divided by the rate at which ozone strikes that boundary. For a flat, non-porous, material the boundary coincides with the interface between air and surface. For other surfaces, the boundary must be defined more carefully.

Cano-Ruiz et al. (1993) showed that the reaction probability could be used, in conjunction with mass-transport models to predict indoor ozone deposition rates. They derived mass-transfer relationships for both laminar and turbulent indoor air conditions. Using typical values of turbulence intensity along with laboratory measured values of reaction probabilities, they predicted ozone loss rates indoors which roughly match those measured in field observations. Their model assumed that indoor surfaces are flat but recognized that higher surface-area materials (sometimes referred to as "fleecy") may influence deposition rates by providing extra surface area and modifying fluid flow across

the surface. In Chapter 4, I describe a more recent model of turbulent mass transfer in an enclosure (Lai and Nazaroff, 2000) and extend that model to incorporate reactive gas uptake on smooth surfaces.

Cano-Ruiz et al. (1993) also reported values of reaction probability for several materials where previously only the deposition velocity had been reported. In Table 3.1, I have reproduced data from their Tables 1-3, and added more recently published results. Ozone deposition velocities have been reported for individual materials commonly used indoors, and for entire rooms (Nazaroff et al., 1993; Cano-Ruiz, et al., 1993). Sabersky et al. (1973) noted that the deposition velocity decreased with time as a material such as plywood was exposed to ozone. This "aging" effect was reversible for plywood but not for some other materials. Other researchers have also noted this aging effect (Mueller et al., 1973; Reiss et al., 1994). Some evidence suggests a seasonal difference in room-averaged ozone deposition velocity, possibly due to surface aging or regeneration (Weschler et al., 1992).

Recognizing that the ozone reaction probability on carpet surfaces may strongly influence indoor ozone concentrations, I studied ozone uptake characteristics on common carpet types by exposing them to ozone in environmentally controlled chambers. I also separated the fibers from the backing, and measured the ozone uptake on these surfaces separately. These measurements allow me to validate deposition and aging models of ozone uptake on carpet developed in Chapters 4 and 5. In addition, I will use these results to compare the relative importance of fleecy materials versus flat surfaces in reducing indoor concentrations of ozone.

Table 3.1: Ozone reaction probability measured on various surfaces. [a]

Ozone reaction probabilities from chamber experiments		
reference	material	reaction probability, γ [b]
Simmons and Colbeck, 1990	FEP Teflon	5.5×10^{-7}
	dirty glass	2.9×10^{-6}
	clean glass	5.5×10^{-6}
	gray tiles (new)	3.8×10^{-5}
	red tiles (new)	4.5×10^{-5}
	gravel	4.8×10^{-5}
	concrete slab	7.9×10^{-5}
	outdoor concrete	4.4×10^{-5}
	bricks (new)	2.2×10^{-4}
	bricks (old)	2.2×10^{-4}
Sutton et al., 1976	polyethylene sheet	
	8% rel. humidity	7×10^{-7}
	70% rel. humidity	1.4×10^{-6}
Sabersky et al., 1973	cotton muslin	$>2 \times 10^{-4} - 1.9 \times 10^{-6}$
	lamb's wool	$>2 \times 10^{-4} - 4.6 \times 10^{-7}$
	neoprene	$>2 \times 10^{-4} - 1.9 \times 10^{-6}$
	plywood	$4.7 \times 10^{-6} - 5.8 \times 10^{-7}$
	nylon	$5.1 \times 10^{-6} - 5.5 \times 10^{-8}$
	polyethylene sheet	$3.5 \times 10^{-6} - 1.2 \times 10^{-6}$
	linen	$1.1 \times 10^{-6} - 6.3 \times 10^{-7}$
	Lucite	$7.0 \times 10^{-7} - 5.5 \times 10^{-8}$
	aluminum	$1.1 \times 10^{-7} - 5.5 \times 10^{-8}$
	plate glass	$1.1 \times 10^{-7} - 5.5 \times 10^{-8}$
Mueller et al., 1973	aluminum	
	5% rel. humidity	4.9×10^{-8}
	40-50% rel. humidity	$7.0 \times 10^{-7} - 1.3 \times 10^{-7}$
	87% rel. humidity	2.4×10^{-6}
	stainless steel	$1.7 \times 10^{-6} - 9 \times 10^{-7}$
Cox and Penkett, 1972	aluminum	
	32% rel humidity	7.7×10^{-8}
	83% rel humidity	2.3×10^{-7}
Morrison et al., 1998	galvanized sheet steel	1.1×10^{-6}
	new duct liners	$(0.8 - 3.2) \times 10^{-5}$
	used duct liner	4.8×10^{-5}

Table 3.1: Ozone reaction probability on various surfaces. (continued)

reference	material	reaction probability, γ
Ozone reaction probabilities from tube penetration experiments		
Altschuler and Wartburg, 1961	Teflon	2×10^{-8}
	glass	$2 \times 10^{-7} - <1 \times 10^{-8}$
	stainless steel (304)	$>3 \times 10^{-6} - <2 \times 10^{-8}$
	stainless steel (316)	$8 \times 10^{-6} - 1 \times 10^{-7}$
	aluminum	$>1.3 \times 10^{-6} - <1.3 \times 10^{-7}$
	polyethylene	$1.7 \times 10^{-6} - 8 \times 10^{-7}$
	PVC (Nalgon)	$5 \times 10^{-6} - 8 \times 10^{-7}$
	PVC (Tygon)	$(2\text{-}5) \times 10^{-6}$
Cohen et al., 1968	glass	$<1.6 \times 10^{-7}$
	silicon rubber	1×10^{-5}
	polyethylene	3×10^{-6}
	nylon	1.7×10^{-7}
	PVC	$3 \times 10^{-6} - 1.2 \times 10^{-6}$
Reiss et al., 1994	glass	$<1 \times 10^{-6}$
	latex paint	
	9% rel humidity	3×10^{-6}
	56% rel humidity	$1.7 \times 10^{-5} - 4 \times 10^{-7}$
	91 % rel humidity	8×10^{-5}
	vinyl wallpaper	5×10^{-6}
	paper wallpaper	1×10^{-6}
Ozone reaction probabilities from low pressure experiments		
Stephens, et al., 1986	ground charcoal	$2.0 \times 10^{-3} - 4.0 \times 10^{-5}$
Tkalich et al., 1984	quartz	7.0×10^{-11}
	stainless steel	$3.5 \times 10^{-5} - 4.0 \times 10^{-9}$
de Gouw and Lovejoy, 1998	organic liquids in a rotating wetted-wall reactor	
	methacrolein (-75 °C)	1.5×10^{-2}
	α-pinene (-70 – -30 °C)	$2\text{-}3 \times 10^{-3}$
	toluene (-70 °C)	6×10^{-4}
	1-tridecene (-20 – 0 °C)	7×10^{-4}
	canola oil (-10 – 20 °C)	$(5\text{-}8) \times 10^{-4}$
	tridecane (-5 °C)	3×10^{-5}
	2-tridecanone (25 – 55 °C)	$(0.9 - 1.2) \times 10^{-4}$
	tridecanal (40 – 60 °C)	1×10^{-4}
	1-tridecanol (30 – 50 °C)	2×10^{-5}
	tridecanoic acid (65 °C)	4×10^{-5}

[a] Updated from Cano Ruiz et al. (1993). [b] For an entry with two values, the first is the initial or unexposed reaction probability, while the second is the final experimental value.

3.2 Methods

3.2.1 Experimental

The four carpets chosen for this study are the same ones used in Chapter 2. These included two residential and two commercial carpets (see Table 2.1) that were either stored in sealed foil containers ("stored") or stored in 19 L ventilated chambers ("aired"). Using a scalpel, fibers were trimmed from several aired samples to make an exposed carpet backing sample ("backing"). Fibers obtained from this operation were separated from each other using wool carders.

The experimental configuration and operation are also identical to those described in Chapter 2. Briefly, whole carpet (stored or aired) or backing samples were placed in a 10.5 L stainless steel chamber, in a Teflon frame (see Figure 2.3), and exposed to a controlled atmosphere containing 100 ppb O_3 and humidified to 50% relative humidity. A typical experiment operated for 48 h with some exceptions. Carpet fibers were exposed to ozone in a Teflon tubular reactor (see Figure 3.1), where the inlet ozone mole fraction was initially set to ~100 ppb. The inlet and outlet ozone concentrations for both reactor configuration were monitored and archived for analysis.

3.2.2 Determining the reaction probability, γ

The surfaces I studied are generally porous and are not flat. Thus, the boundary upon which the reaction probability is defined may not coincide with the gas/solid interface. At the tips of carpet fibers, pollutants exchange between a region of free-moving air above the fibers and a more stagnant region of inter-fiber air. For this research I defined the whole carpet reaction probability, γ_o, based on mass transfer to a flat

horizontal plane at the tips of the carpet; the area of this plane will be known as the "horizontally projected area" or "superficial area." The reaction probability of the carpet backing, γ_b, is similarly defined at a flat plane on the upper surface of the backing. Carpet fibers are approximately cylindrical, but are not smooth. For this study, I defined the fiber reaction probability, γ_f, on the surface of a cylinder with a diameter equal to the average carpet fiber diameter, as measured using a light microscope. To parameterize the relationship between superficial area and the additional surface area arising from fibers, I define the normalized carpet area, R_f=1+(fiber surface area)(superficial area)$^{-1}$. For a value of R_f of 50, there is about 50 times more potential area for reaction than the superficial area of the carpet. Note that this does not take into account surface area provided by porosity of the fiber itself.

3.2.2.1 Determining the reaction probability on whole carpet and carpet backing

The reaction probability can be difficult to measure directly. Cano-Ruiz et al. (1993) showed that the pollutant-specific reaction probability can be determined for a material by comparing two easily measured loss rate terms in a continuously mixed flow reactor (CMFR): the surface deposition velocity, v_d, and the mass transport limited deposition, v_t,

$$\gamma = \left[\frac{\langle v \rangle}{4} \left(\frac{1}{v_d} - \frac{1}{v_t} \right) \right]^{-1} \qquad (3.2)$$

where <v> is the Boltzmann velocity for the pollutant (e.g. <v> for ozone is 3.62×10^4 cm s^{-1} at 296 K). Equation 3.2 was used to calculate both the reaction probability of whole carpet, γ_o, and of carpet backing, γ_b.

The deposition velocity, v_d, is a common measure of the loss rate of pollutants indoors and represents a mass-transfer coefficient in a specific setting. The flux, F, of a pollutant to an indoor surface is given by,

$$F = v_d C \tag{3.3}$$

where C is the pollutant concentration at an arbitrary, but consistent location (usually the center of a room). The deposition velocity may differ significantly for a pollutant that is exposed to the same material in different fluid dynamic systems such as different rooms in a home, different air-exchange rates, etc. If the area-averaged deposition velocity is known for a room or building, then the concentration of a pollutant may be estimated using existing indoor air quality models (Weschler et al., 1989).

For carpets in a laboratory reactor, treated as a CMFR at steady state, the ratio of the outlet concentration to inlet concentration is given by,

$$\frac{C}{C_o} = \frac{\lambda}{\lambda + (S_c/V)v_{dc} + (S_r/V)v_{dr}} \tag{3.4}$$

where λ is the air-exchange rate for the reactor, C_o is the inlet pollutant concentration, C is the outlet (and internal) concentration of the pollutant, S_c is the superficial surface area of the carpet, S_r is the area of all other accessible surfaces in the reactor, V is the volume of the chamber, v_{dc} is the deposition velocity of the pollutant to carpet, and v_{dr} is the area averaged deposition velocity of the pollutant to all other inner reactor surfaces. The term, $(S_r/V)v_{dr}$, can be determined independently by operating the reactor without the carpet sample installed. Thus, experiments can be conducted in which v_{dc} is the only unknown term. The mass-transport-limited deposition velocity, v_t, in equation 3.2 was determined by coating the carpet with potassium iodide (considered a perfect sink for ozone) (Parmar

and Grosjean, 1990), and performing a typical experiment with this modified material. There is no resistance to ozone removal at the potassium iodide coated carpet surface, thus the carpet deposition velocity, v_{dc}, in equation 3.4 represents the mass transport limited value, v_t, for that experiment.

3.2.2.2 Determining the reaction probability on carpet fibers

The fixed bed reactor described in Chapter 2 allowed me to measure the reaction probability at the surface of carpet fibers. To facilitate the analysis of this system, I designed the reactor to operate in plug-flow fashion. For plug-flow assumptions to be valid, the Bodenstein number (compare to Peclet number) should be greater than 100 (Schlatter, 1987), where

$$N_{Bo} = \frac{U_e L}{D} \tag{3.5}$$

Here, L is the total length of the packed section of the reactor, D is the diffusivity of the pollutant, and U_e is the effective gas velocity given by the volumetric flowrate divided by the product of the cross-sectional area of the reactor and the bed porosity. For a typical carpet fiber experiment in this dissertation, the Bodenstein number, N_{Bo} is approximately 800.

Assuming this system acts as a perfect plug flow reactor (see Figure 3.1), the concentration in a thin, cross-sectional slice of the reactor is constant. One can show by performing a material balance through this segment of the reactor that the rate of change of ozone in the segment is balanced by the flux of ozone in and out of the slice and the ozone loss by reaction at the surface of the fibers. Note that, in an ideal plug flow reactor, flux is due entirely to advection; diffusion in the direction of flow is considered

negligible.

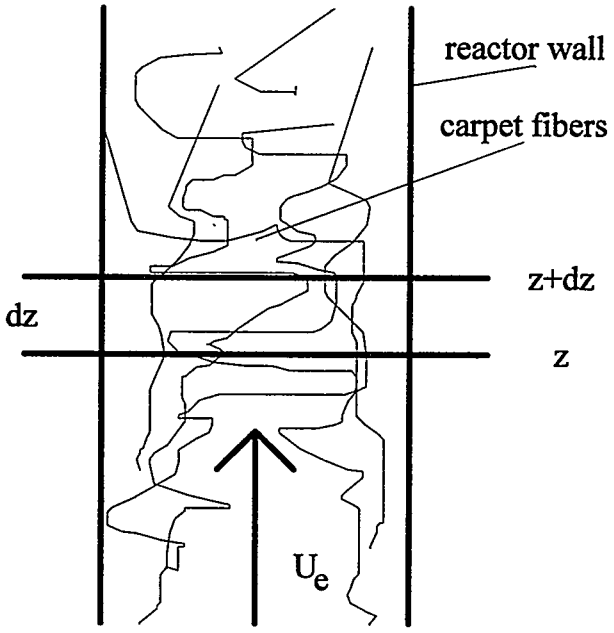

Figure 3.1. Tubular reactor containing carpet fibers. Ozone is transported through the reactor at the effective gas velocity, U_e, and removed at fiber surfaces. The derivation of the fiber reaction probability invokes a material balance over a thin cross-sectional slice of thickness dz that moves along the reactor at a velocity U_e.

However, a plug flow reactor can be more easily analyzed by noting that a thin slice moving at the same rate and direction as the superficial velocity acts as a batch reactor. Assuming that surface reactions are first order in the reactant ozone, the rate of change of ozone with distance along the reactor axis can be shown to be

$$U_e \frac{dC}{dz} = -kC \qquad (3.6)$$

where k is a first-order rate constant dependent on reactor bed variables such as fiber surface area and fiber surface reaction probability. Once again, consider the thin cross-sectional slice of the reactor. In this volume, the total amount of surface area for reaction can be shown to be

$$A = \frac{4m_f}{d_f \rho_f} \tag{3.7}$$

where m_f is the mass of fibers contained in the slice, d_f is the fiber diameter, and ρ_f is the fiber density. The loss rate of ozone to the surface is equal to the ozone surface flux times the surface area:

$$r_s = \frac{C_s(z)\gamma\langle v\rangle m_f}{d_f \rho_f} \tag{3.8}$$

where $C_s(z)$ is the concentration of ozone adjacent to the fiber surface, at a distance z along the reactor. Initially, I assume that ozone loss is dominated by surface kinetics; the resistance associated with mass transport of ozone to the fiber surface is negligible making $C_s(z)$ approximately equal to the bulk concentration of gas-phase ozone at position z , C(z). Thus, by comparison of equations 3.6 and 3.8, the rate constant, k, in equation 3.6 can be shown to be

$$k = \frac{\gamma\langle v\rangle m_f}{d_f \rho_f V_s} \tag{3.9}$$

where V_s is the volume of the reactor slice. For a uniformly packed reactor, the ratio m_f/V_f is constant and is equal to the solidity (1-p, where p is the bed porosity) times the fiber density ρ_f. Thus,

$$k = \frac{\gamma\langle v\rangle(1-p)}{d_f} \tag{3.10}$$

and so, equation 3.6 can be rewritten

$$\frac{dC}{dz} = -\frac{\gamma\langle v\rangle(1-p)}{U_e d_f} C \tag{3.11}$$

Solving equation 3.11, the effective reaction probability at a cylindrical fiber surface, γ_f,

is given by,

$$\bar{\gamma}_f = \frac{1}{L}\int_0^L \gamma dz = -\frac{d_f Q}{< v > p(1-p)V} \cdot \ln\left(\frac{C_L}{C_o}\right) \qquad (3.12)$$

where C_o is the ozone concentration at the reactor inlet, C_L is the ozone concentration at the end of the reactor (z=L), d_f is the fiber diameter, p is the porosity, and Q is the volumetric flowrate of gas through the reactor, and V is the total reactor volume. For this equation to be valid, the ozone concentration can only vary axially, and the surface resistance to ozone deposition must dominate over mass-transfer resistance.

To verify that equation 3.12 is valid under experimental conditions, I found the approximate reaction probability at which the mass transfer and surface resistances are equal. The mass-transfer resistance can be approximated by the reciprocal of the Sherwood number for a cylinder in cross flow (Churchill and Bernstein, 1977),

$$Sh_g = 0.3 + \frac{0.62 Re_d^{0.5} Sc^{0.33}}{\left[1+(0.4/Sc)^{0.66}\right]^{0.25}}\left[1+\left(\frac{Re_d}{28200}\right)^{0.625}\right]^{0.8}, \; Re_d Sc > 0.2 \qquad (3.13)$$

where the Reynolds number is $Re_d=(U_e d_f)\nu^{-1}$, the Schmidt number is $Sc=\nu D^{-1}$, and ν is the kinematic viscosity. The surface resistance can be represented by the reciprocal of the surface Sherwood number, Sh_s:

$$Sh_s = \gamma \frac{\langle v \rangle d_f}{4D} \qquad (3.14)$$

Typical experimental values were $U_e = 9$ cm s^{-1} and $d_f = 7 \times 10^{-3}$ cm. At a temperature of 296 K, other parameters are $\nu=0.15$ cm^2 s^{-1}, $D=0.167$ cm^2 s^{-1}, and Sc=0.93 . The Reynolds number was Re_d=0.63. Setting equations 3.13 and 3.14 equal, a limiting value of $\gamma \cong 0.002$ was obtained. Therefore, equation 3.12 is valid for a reaction probability

significantly lower than 0.002. Due to limitations in the precision of ozone measurements, the highest measurable fiber surface reaction probability is about 10^{-5}. Thus equation 3.12 is valid for these experiments.

3.3 Results and discussion

There are two phenomena that are generally applicable to every material tested, whether whole carpet, backing or fiber. (1) Every sample reacts with ozone to remove some of it from the reaction chamber. (2) The ability of the material to react with ozone decreases with exposure. An example of the time profile of the inlet and outlet ozone concentration for a CMFR experiment testing whole carpet (CP2) is shown in Figure 3.2(a). The feedback control program modifies the inlet concentration to keep the outlet concentration constant at 100 ppb. As the exposure progresses, the upstream concentration must be decreased, to make up for a decreasing ozone flux to the surface of the carpet. This "quenching" of surfaces, also known as aging, is interpreted in terms of a decrease in the reaction probability for each surface. Brief deviations from the ozone set-point, seen as spikes in the figure, are typically due to electronic noise that gives occasional false readings. In some CMFR experiments, the ozone concentration drifted slightly above the set-point because the lower limit of ozone generation had been reached. A time profile for a fixed bed experiment for CP2 fibers is shown in Figure 3.2(b). No control routine is used to maintain a fixed outlet ozone concentration in the fiber experiments. The inlet mole fraction is set (but not controlled) at the required level and the outlet mole fraction is allowed to increase as the fiber surfaces become quenched.

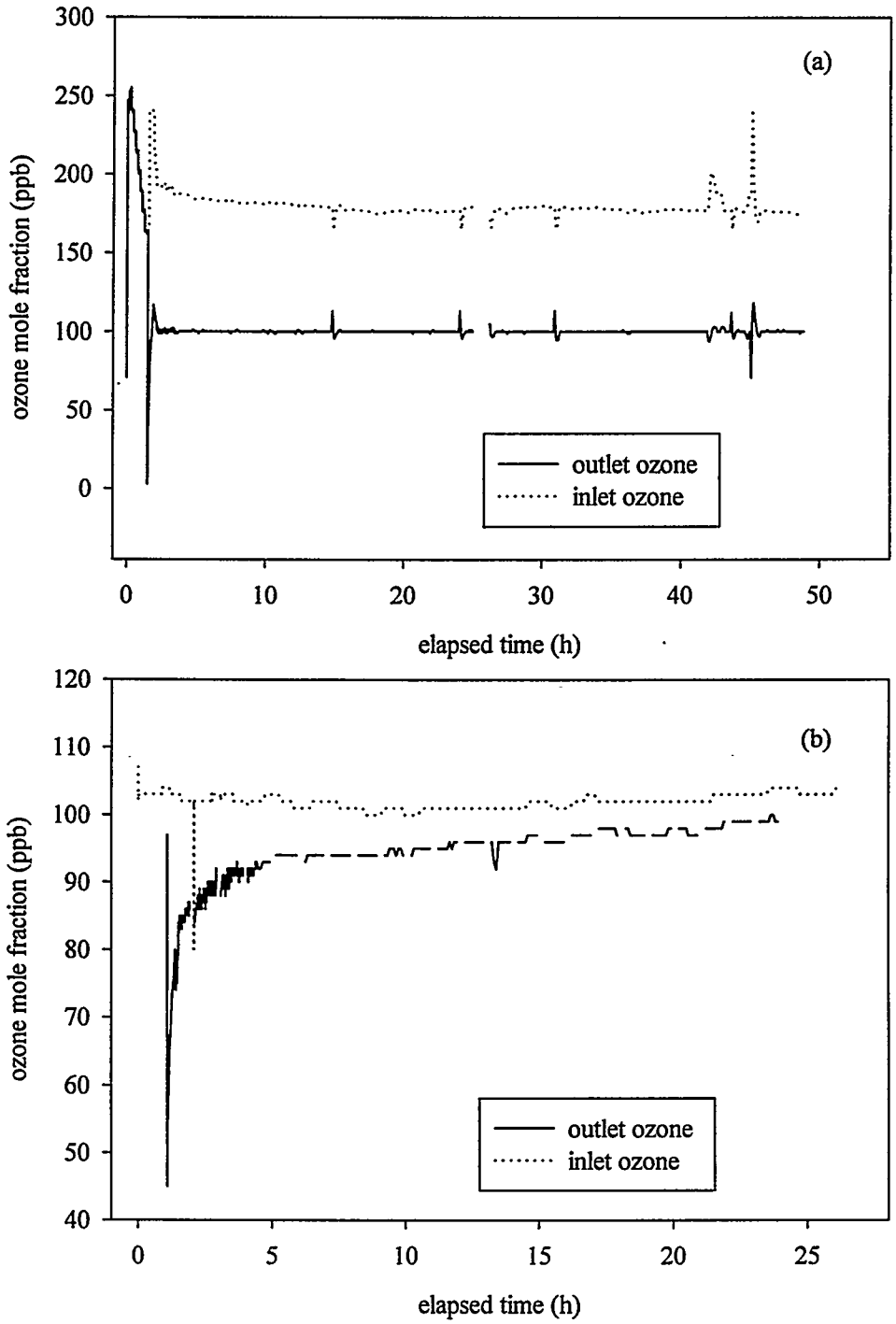

Figure 3.2. Time profile of inlet and outlet ozone mole fraction: (a) in a CMFR experiment testing aired carpet CP2; (b) in a fixed bed experiment testing carpet CP2 fibers.

Plots of the reaction probability as a function of elapsed time for whole carpet, γ_o, backing, γ_b, and fibers, $\bar{\gamma}_f$, are shown for carpets CP1 through CP4 in part (a) of Figures 3.3 through 3.6, respectively. The whole carpet reaction probability, γ_o, initially decreases quickly, but tends to flatten out with exposure. This trend holds for all whole carpet and backing experiments. However, the fiber reaction probability, $\bar{\gamma}_f$, tends to drop more strongly throughout the 48-h experiment for all fibers. This is, in part, due to the fact that ozone exposures are greater per total surface area in the fixed bed experiments. Consider CP3 as an example. The cumulative uptake on the whole carpet, U_o, is 18 $\mu g\ cm^{-2}$, based on the superficial area of the carpet. Taking into account internal area, parameterized by R_f, the average uptake on fiber surfaces is about 0.04 $\mu g\ cm^{-2}$, or about 9 times lower than the cumulative uptake in the fiber experiments, U_f.

The ozone reaction probabilities as measured on the whole carpet, γ_o, carpet fibers, $\bar{\gamma}_f$, and backing, γ_b, are shown in Table 3.2-3.4. Recall that γ_o and γ_b are based on the superficial area of carpet while $\bar{\gamma}_f$ is based on the surface area of cylindrical carpet fibers. Each experiment was given an experimental code (exp. code) which reflects the date on which the experiment was started. For example exp. code 90405 designates that this experiment started in 1999 (9) on April 5 (04 and 05). The reaction probabilities are given as initial and final values. The initial value for CMFR experiments, (whole carpet, backing) is taken 15 min after exposure begins. This delay from t=0 is necessary because of large uncertainties in the reaction probability during the rapid changes that occur in the reactor exhaust ozone concentration in the initial moments of exposure. The initial value for PFR (fibers) experiments reflects the first acceptable data point, typically within the

first minute of exposure. The "final" value is that taken at the end of the experiment, where the experimental time is shown in the "time" column in Table 3.2–3.4. Also shown in Tables 3.2–3.4 are the normalized carpet area, R_f, the cumulative uptake of ozone, U, on each surface, and several other values which will be explained in more detail later.

Typically, the initial reaction probability was higher than could be resolved with the experimental setup. An exception to this was an initial reaction probability of ozone with olefin fibers (CP2, CP4) that ranged from 1×10^{-6} to 8×10^{-6}. In all cases, the final (48 h) reaction probability of whole carpet and backing was of the order of 10^{-5}. The fiber surfaces, however, had a much lower reaction probability, $\bar{\gamma}_f$, which averaged about 10^{-7} after 48 h.

The final reaction probability for whole carpet and backing can be compared to that of other materials. With a final γ_o of about 10^{-5}, carpet is comparable in ozone reactivity with some of the more highly reactive materials such as concrete and gravel, and latex paint (see Table 3.1). The accelerated aging experiments of fibers in the fixed bed reactor suggest that $\bar{\gamma}_f$ is similar to value for Lucite, nylon and plate glass. While the final $\bar{\gamma}_f$ is rather low, the initial $\bar{\gamma}_f$ is greater than 10^{-5} for residential carpets CP1 and CP3. The initial $\bar{\gamma}_f$ value for commercial carpets is moderately lower. After aging, there is no clear distinction between commercial and residential carpets with respect to ozone reactivity.

Table 3.2. Initial and final reaction probabilities, cumulative uptake and fitting parameters for whole carpet.[a]

carpet sample	d_f (μm)	R_f	exp. code	γ_o init	γ_o final	U_o (μg cm^{-2})	A* (μg cm^{-2})$^{-B}$	B	r^2	time (h)
CP1	60	66	90405	3×10^{-5}	6.6×10^{-6}	0.9	7×10^{-6}	-0.12	0.93	48
CP2	70	33	90323	6×10^{-5}	1.1×10^{-5}	1.2	1×10^{-5}	-0.07	0.66	48
CP3	80	46	71028	$>10^{-4}$	3.1×10^{-5}	1.7	3×10^{-5}	-0.16	0.72	48
			81130	10^{-4}	1.1×10^{-5}	1.3	2×10^{-5}	-0.1	0.86	38
CP4	70	30	70812	6×10^{-5}	1.2×10^{-5}	1.3	1×10^{-5}	-0.26	0.87	48
			71111	$>10^{-4}$	9.3×10^{-6}	1.1	9×10^{-6}	-0.18	0.91	48
			90412	$>10^{-4}$	6.3×10^{-6}	0.9	6×10^{-6}	-0.29	0.91	48

[a]In this table, d_f is the fiber diameter, R_f is the normalized surface area, γ_o is the reaction probability, U_o is the cumulative uptake and "time" is the total elapsed time of the experimental exposure. A and B are fitting parameters for the relationship shown as equation 3.16, and r^2 is the square of the Pearson product moment correlation coefficient, r.

Table 3.3. Initial and final reaction probabilities, cumulative uptake and fitting parameters for carpet fibers.[a]

carpet sample	d_f (μm)	R_f	exp. code	γ_f init	γ_f final	U_f (μg cm^{-2})	A* (μg cm^{-2})$^{-B}$	B	r^2	time (h)
CP1	60	66	80810	$>10^{-5}$	6.2×10^{-8}	0.07	2×10^{-11}	-2.2	0.95	48
			90427		5.0×10^{-8}	0.022	3×10^{-13}	-3	0	31
CP2	70	33	80727	8×10^{-6}	3.4×10^{-7}	0.149	6×10^{-8}	-0.8	0.95	48
			80817	6×10^{-6}	2.8×10^{-7}	0.153	4×10^{-8}	-0.9	0.98	48
			81116	2×10^{-5}	4.8×10^{-7}	0.055	9×10^{-8}	-0.5	0.99	24
CP3	80	46	80722	$>10^{-5}$	4.0×10^{-7}	0.355	1×10^{-9}	-5.6	0.99	48
			80824	$>10^{-5}$	3.9×10^{-7}	0.335	3×10^{-9}	-4.4	0.95	48
			80824	$>10^{-5}$	2.0×10^{-7}	0.475	1×10^{-8}	-2.9	0.88	168
			81209	$>10^{-5}$	1.4×10^{-7}	0.43	1×10^{-9}	-5.1	0.97	120
CP4	70	30	80820	2×10^{-6}	9.2×10^{-8}	0.042	6×10^{-9}	-0.8	0.98	48
			81118	1×10^{-6}	9×10^{-8}	0.018	4×10^{-9}	-0.8	0.97	24

[a]In this table, d_f is the fiber diameter, R_f is the normalized surface area, γ_f is the reaction probability, U_f is the cumulative uptake and "time" is the total elapsed time of the experimental exposure. A and B are fitting parameters for the relationship shown as equation 3.16, and r^2 is the square of the Pearson product moment correlation coefficient, r.

Table 3.4. Initial and final reaction probabilities, cumulative uptake and fitting parameters for carpet backing.[a]

carpet sample	d_f (μm)	R_f	exp. code	γ_b init	γ_b final	U_b (μg cm^{-2})	A* (μg cm^{-2})$^{-B}$	B	r^2	time (h)
CP1	60	66	80310	$>10^{-4}$	1.2×10^{-5}	1.3	1×10^{-5}	-0.37	0.9	48
			80408	$>10^{-4}$	1.4×10^{-5}	1.3	1×10^{-5}	-0.38	0.88	48
			90423	$>10^{-4}$	1.4×10^{-5}	0.7	1×10^{-5}	-0.31	0.77	24
CP2	70	33	80602	$>10^{-4}$	1.2×10^{-5}	1.2	1×10^{-5}	-0.28	0.76	48
			90414	$>10^{-4}$	1.5×10^{-5}	1.3	1×10^{-5}	-0.12	0.86	48
CP3	80	46	80325	$>10^{-4}$	2.8×10^{-5}	1.7	3×10^{-5}	-0.18	0.85	48
			81215	$>10^{-4}$	2.0×10^{-5}	1.9	4×10^{-5}	-0.47	0.94	48
CP4	70	30	80401	$>10^{-4}$	1.0×10^{-5}	1.3	1×10^{-5}	-0.3	0.92	48
			90419	$>10^{-4}$	1.1×10^{-5}	1.3	1×10^{-5}	-0.28	0.94	48

[a]In this table, d_f is the fiber diameter, R_f is the normalized surface area, γ_b is the reaction probability, U_b is the cumulative uptake and "time" is the total elapsed time of the experimental exposure. A and B are fitting parameters for the relationship shown as equation 3.16, and r^2 is the square of the Pearson product moment correlation coefficient, r.

The cumulative uptake on any tested material can be calculated by a time integration of ozone loss in the reactor,

$$U = \int_{t=0}^{t\_exp} \frac{(C_{in} - C)Q}{A_{(s\,or\,f)}} \qquad (3.15)$$

where t_exp is the total exposure time, Q is the gas flowrate, C_{in} is the inlet ozone concentration, C is the outlet ozone concentration and $A_{(\,)}$ is the area of the material. As a reminder, for whole carpet and backing samples A_s corresponds to the horizontally projected (superficial) area, while A_f, referring to fibers, corresponds to the surface area of a smooth cylinder. For 48-h exposures, the cumulative uptake on whole carpet and backing is remarkably similar across all carpets, with an average of 1.3 μg cm^{-2} and a

range of 0.7 – 1.9 μg cm^{-2}. Whole carpet and backing from CP3 consumed more ozone than any other carpet. This is not surprising, given the high emission rates of oxidized reaction products from CP3 presented in Chapter 2.

Interestingly, the backing tends to take up slightly more ozone over the same period than whole carpet for any given sample. Emission rates of oxidized species are not consistently higher for carpet backing than for whole carpet samples. This may be explained by the presence of styrene-butadiene rubber (SBR) in the backing. Some double bonds may remain after polymerization of SBR, providing sites for ozone reactions. Decomposition of ozonides in the backbone of a polymer are less likely to result in volatile byproducts than decomposition of ozonides of a triglyceride. Thus, a lower volatile product emission rate relative to ozone uptake would be expected if some of the ozone is reacting with SBR.

The cumulative uptake on fibers appears to be much lower than that for whole carpet or backing. Because two reactor configurations were used, a direct comparison cannot be made. However, a rough idea of the degree of "accelerated aging" that takes place in the fixed bed reactor can be found by multiplying the fiber cumulative uptake by the normalized surface area, R_f and dividing this by the whole carpet cumulative uptake. For carpets CP1, CP2, CP3, and CP4 respectively, these values are 5, 4, 9 and 1 (using 48 h experimental values only). The PFR exposed fibers of the first three materials took up significantly more ozone in the same time period than the CMFR fibers. However, there was no significant difference between the cumulative uptake values for CP4.

All of the materials tested were aired out in the chambers as described in Chapter 2, beginning on (8/97). Nevertheless, the experiments took place over a period of about

1.5 y. Some of the materials had been aired for only a few months, while others had been aired for nearly 2 y. However, there appears to be no significant difference in most of the values in Tables 3.2–3.4 due to differences in airing times. There may be a small difference between cumulative uptake for whole carpet CP4 in experiments performed over 1.5 y on several distinct samples. There is steady decrease in U_0 from 8/97 (1.3 mg cm^{-2}), through 11/97 (1.1 mg cm^{-2}) and finally in 4/99 (0.9 mg cm^{-2}). This may be due to non-ozone oxidation of sites while airing as surmised in Chapter 2.

In previously published work (Morrison et. al. 1998), a power-law (log-linear) relationship was observed between the reaction probability and the cumulative uptake of ozone on aging duct surfaces (see Chapter 6). I found this relationship to hold true for carpet and its constituents as well. The relationship is as follows,

$$\gamma = A(U)^B \tag{3.16}$$

where A and B are fitted parameters.

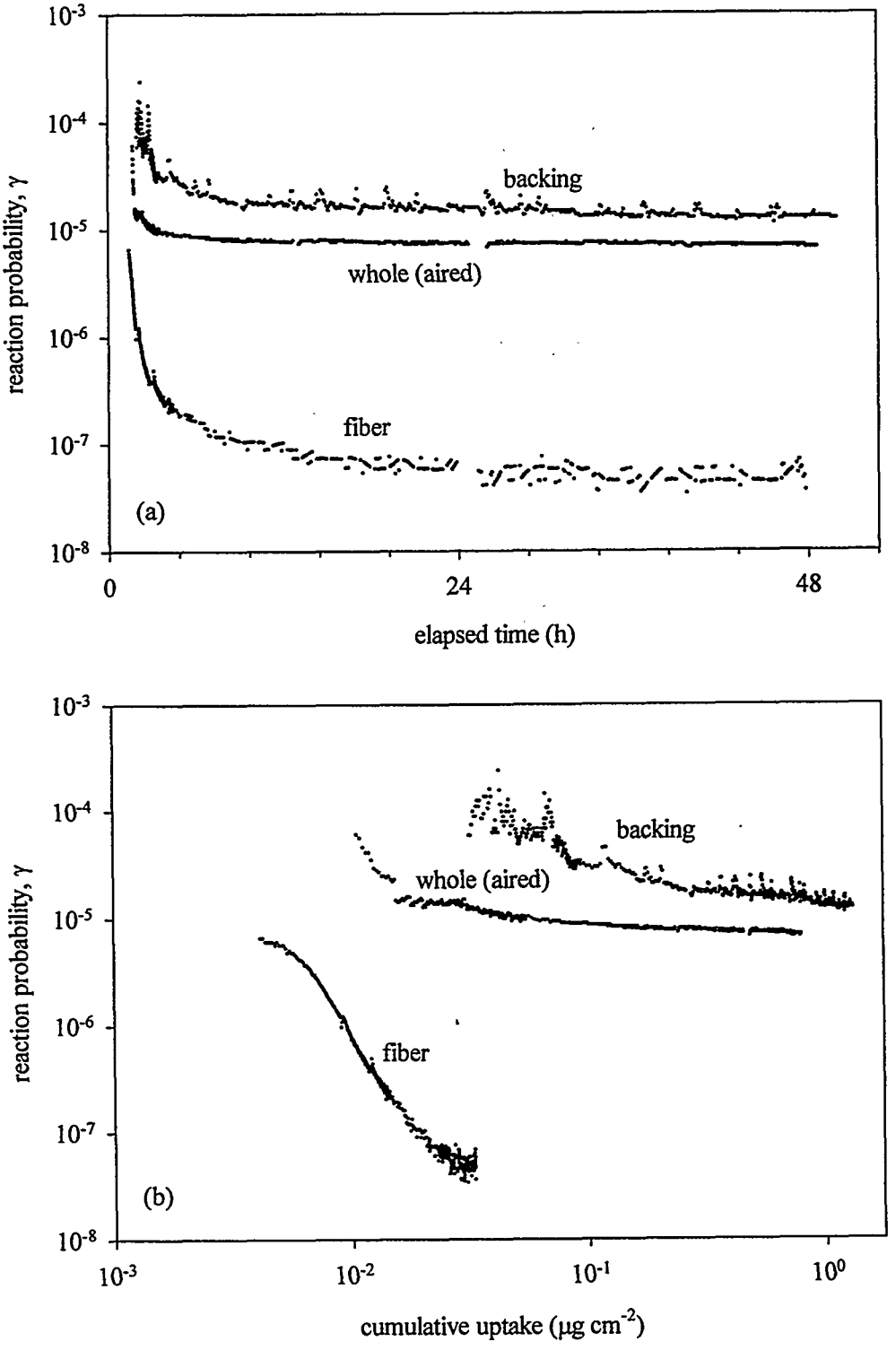

Figure 3.3. Reaction probabilities for whole carpet, CP1 (exp. code 90405), backing (exp. code 80810) and fiber (exp. code 80408). (a) time dependent reaction probability; and (b) reaction probability relative to cumulative uptake of ozone.

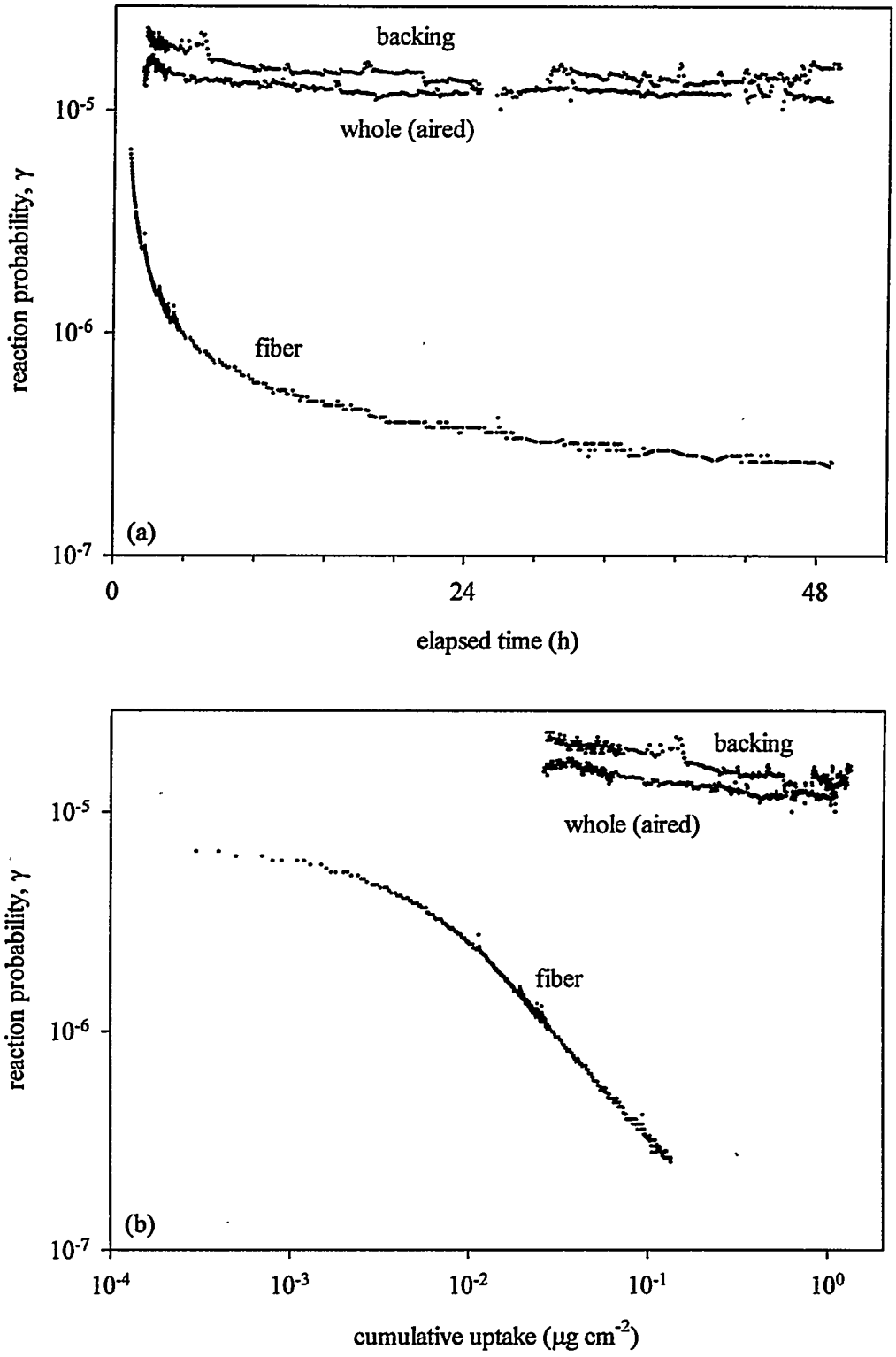

Figure 3.4. Reaction probabilities for whole carpet, CP2 (exp. code 90303), backing (exp. code 80817) and fiber (exp. code 90415). (a) time dependent reaction probability; and (b) reaction probability relative to cumulative uptake of ozone.

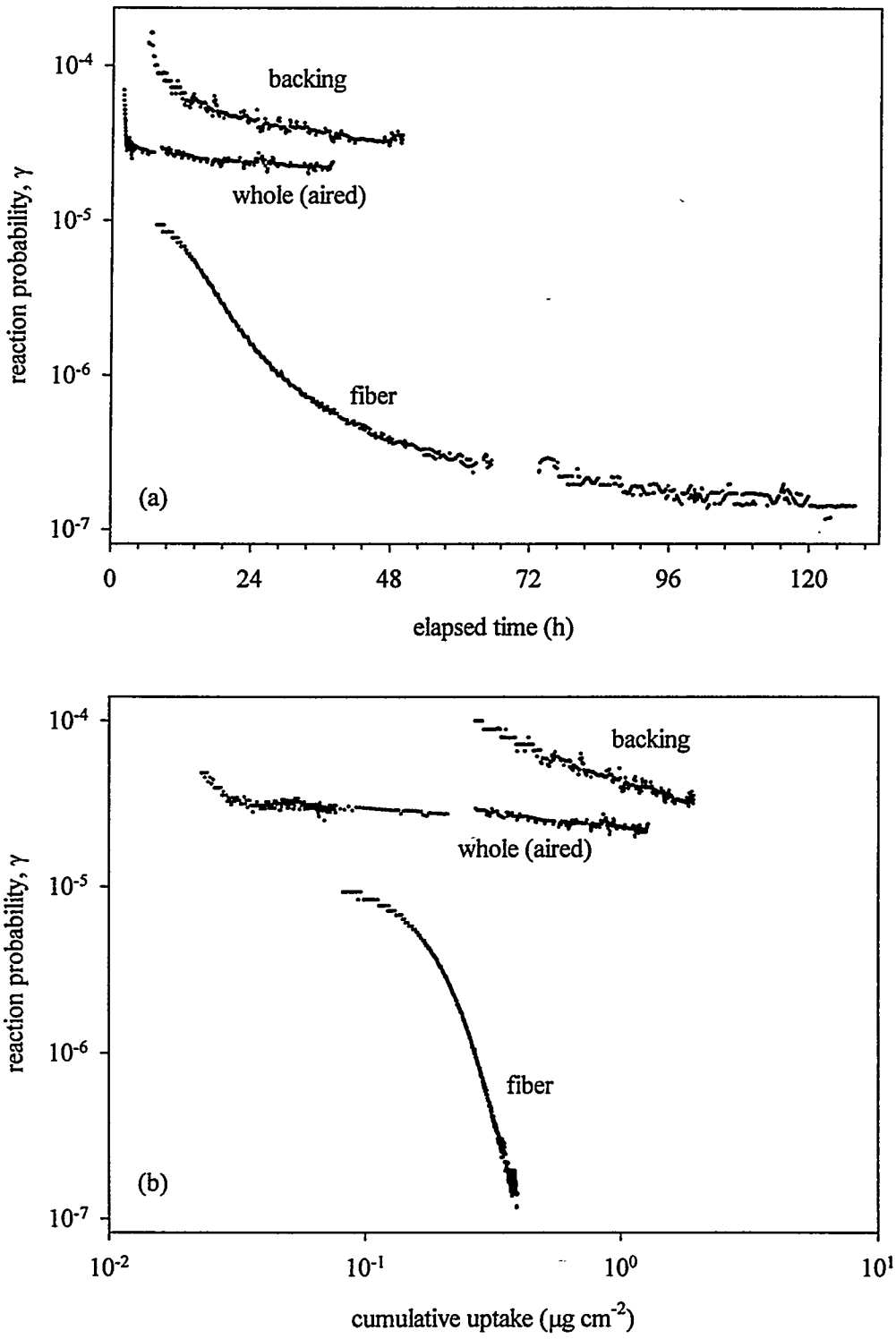

Figure 3.5. Reaction probabilities for whole carpet, CP3 (exp. code 81130), backing (exp. code 81209) and fiber (exp. code 81215). (a) time dependent reaction probability; and (b) reaction probability relative to cumulative uptake of ozone.

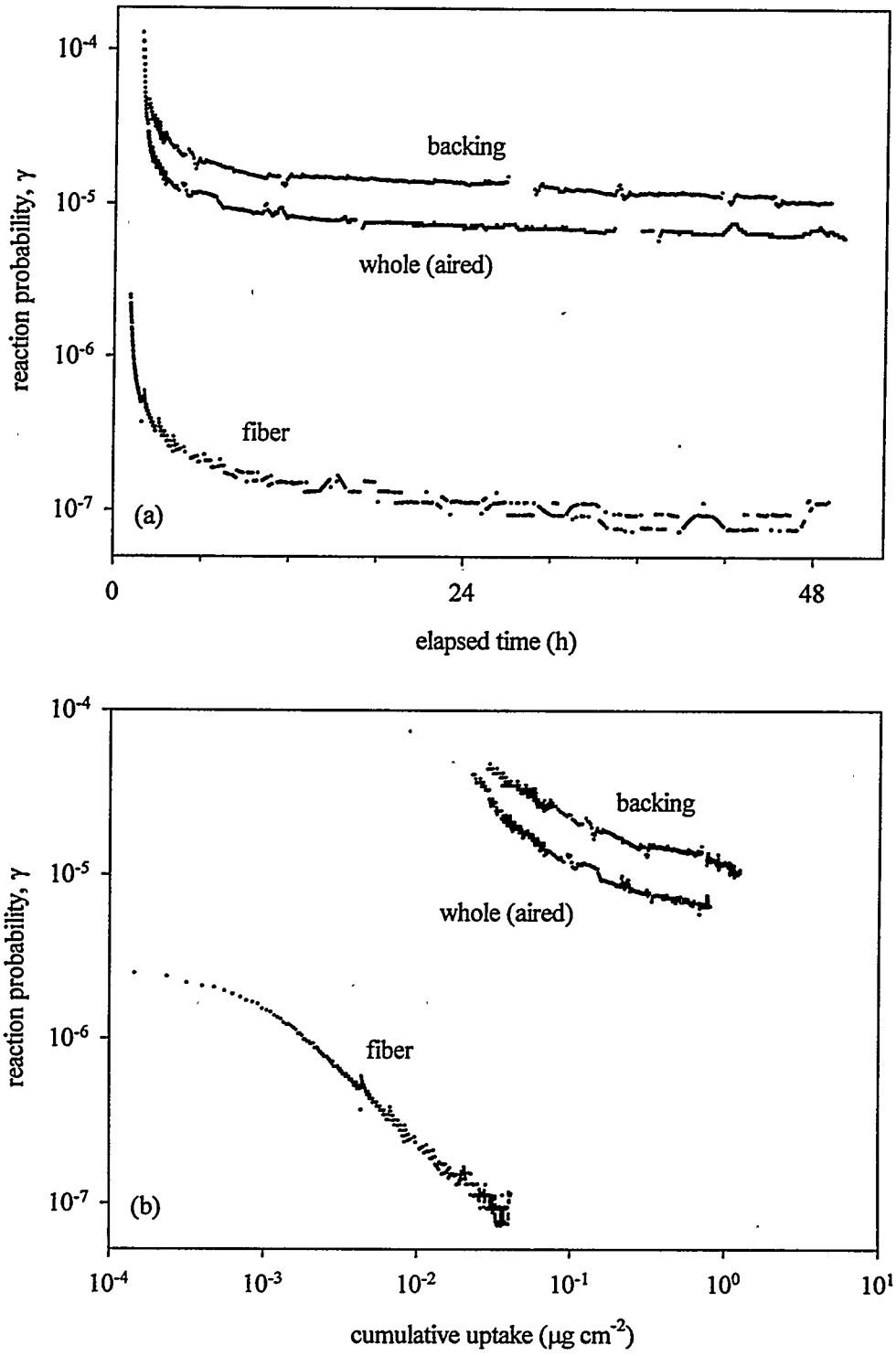

Figure 3.6. Reaction probabilities for whole carpet, CP4 (exp. code 90412), backing (exp. code 80820) and fiber (exp. code 90419). (a) time dependent reaction probability; and (b) reaction probability relative to cumulative uptake of ozone.

Frames (b) in Figures 3.3 through 3.6 demonstrate the relationship between reaction probability and cumulative uptake graphically. Note that the log-linear nature may not endure throughout entire experiments. There is typically more curvature early in an experiment as demonstrated by whole carpet CP1. For CMFR experiments, the initial curvature usually takes place when the reactor ozone concentration is rapidly changing to reach the setpoint concentration. When the concentration has stabilized, the log-linear nature of the γ - U relationship becomes apparent. In Tables 3.2–3.4 I have reported values of A, B and r^2 for all of the CMFR experiments. To obtain these parameters, I used only those experimental data points during which the ozone concentration has stabilized. In a typical experiment, the time to reach 100 ppb O_3 is only about 0.5 h, making the loss of data for this procedure minimal.

The fixed bed (fiber) experiments give a length averaged value of reaction probability, $\overline{\gamma}_f$, rather than any individual fiber reaction probability. The fiber reaction probability, γ_f, can, under certain circumstances, be determined from measurements of $\overline{\gamma}_f$. Initially, the bed of fibers is uniform. Thus at $t = 0$, $\gamma_f = \overline{\gamma}_f$. However, in some cases, the initial outlet concentration, C_L, may be lower than the limit of detection (as was true for CP3). The reaction probability is so high that all of the ozone is being removed in the front of the bed. As the surfaces age, the reaction probability decreases, and more ozone is allowed to pass deeper into the bed. This means that the spatial variation in γ_f may be large. After long exposure, C_L, approaches C_o, and all of the fibers are exposed to nearly the same concentration. If the integrated exposure of all fiber surfaces is nearly the same, then I may assume that γ_f is also nearly the same throughout, or $\gamma_f \cong \overline{\gamma}_f$.

Therefore, measurements near the completion of a fixed-bed reactor experiment better reflect the aging phenomena of individual fibers. For consistency in calculating the fitting parameters A and B, I chose data points that lay between two points: 1) the point at which the ozone concentration at the exhaust reached 70% that of the inlet ozone concentration. 2) the last data point of the experiment. This range of values was evaluated using the above expression, and the parameter values are shown in Tables 3.2–3.4.

Parameter values of A and B were very among similar carpets.. The parameter A is typically around 1×10^{-5} $(\mu g\ cm^{-2})^{-B}$ while the range of B is broader, -0.07 to -0.29. The absolue values of B for carpet backing trended higher with results ranging from –0.12 to -0.47. The relationship between reaction probability and cumulative uptake for fibers was remarkably log-linear, with most r^2 values of 0.95 and greater. There was a distinct difference between values of parameter B for olefin and nylon fibers. The nylon fibers of CP1 and CP3 had large negative values of B ranging from –2.2 to –5.6. The olefin fibers of carpets CP2 and CP4 had a tighter range of B values, typically –0.8. The physical or chemical phenomena that cause these differences is unknown at this time.

3.4 Conclusions

Prediction of ozone loss rates in indoor settings is critically dependent on the accurate measurements of kinetics of ozone decomposition on surfaces. In this study, I measured the reaction probability of ozone on whole carpet. The kinetics of ozone loss on carpet fibers and backing were also measured, as well as the phenomenon known as ozone surface aging. I found that the final experimental value of the reaction probability of whole-carpet and backing was typically around 10^{-5}, comparable to more highly

reactive materials such as concrete and latex paint. Carpet fibers were comparable to Lucite and nylon in ozone reactivity, with a final experimental value of the reaction probability of about 10^{-7}.

All materials tested lost the ability to consume ozone with increasing exposure (ozone aging). This aging pattern was similar to that found in experiments with duct materials (Morrison et al., 1998, and Chapter 6) in that the reaction probability was related to the cumulative uptake of ozone by a power-law function (equation 3.16). The value of the power-law exponent ranged between –0.1 and –0.5 with a typical value around –0.3, for whole carpet and carpet backing, which is similar to that found in the duct material study. The power-law exponent for nylon fibers was between –2 and -5 and for olefin fibers was typically about -0.8. It is unclear at this time why there is such a large difference between fiber types.

In Chapter 4, I will combine the aged values of the reaction probability of carpet components with a model of ozone deposition to carpet surfaces. This will demonstrate how carpets can be an important sink for ozone, even though the superficial area of painted walls may be much higher. In the Chapter 5, I will discuss the importance of the value of the power law exponent, B, as it relates to a model of ozone aging of surfaces. This analysis may help illuminate the origin of differences in these fitted parameters.

3.5 References

Altschuler, A.P.; Wartburg, A.F. *International Journal of Air and Water Pollution.* **1961**, *4*, 70-78.

Avol, E.L.; Navidi W.C.; Colome S.D. *Environmental Science and Technology.* **1998**, *32*, 463-468.

Cano-Ruiz, J.A.; Kong, D.; Balas, R.B.; Nazaroff W.W. *Atmospheric Environment.* **1993,** *27A,* 2039-2050.

Churchill, S.W.; Bernstein, M. *Journal of Heat Transfer.* **1977,** *99,* 300 .

Cohen I.C.; Smith A.F.; Wood, R. *Analyst.* **1968,** *93,* 507-517.

Cox, R.A.; Penkett, S.A. *Atmospheric Environment.* **1972,** *6,* 365-368.

de Gouw, J.A.; Lovejoy, E.R. *Geophysical Research Letters.* **1998,** *25,* 931-934.

Lai, A.C.K.; Nazaroff, W.W. *Journal of Aerosol Science.* **2000,** *31,* in press.

Lee, K.; Valarino, J.; Dumyahn, T.; Ozkaynak, H.; Spengler, J.D. *Journal of the Air and Waste Management Association.* **1999,** *49,* 1238-1244.

Morrison, G.C.; Nazaroff, W.W; Cano-Ruiz, J.A.; Hodgson, A.T.; Modera, M.P. *Journal of the Air and Waste Management Association.* **1998,** *48,* 941-952.

Mueller, F.X.; Loeb, L.; Mapes, W.H. *Environmental Science and Technology.* **1973,** *7,* 342-346.

Nazaroff, W.W.; Gadgil, A.J.;Weschler, C.J. In *Modeling of Indoor Air Quality and Exposure*; Nagda, N.L., Ed.; ASTM STP 1205; American Society for Testing and Materials: Philadelphia, PA, 1993; 81-104.

Parmar, S.S.; Grosjean, D. *Atmospheric Environment.* **1990,** *24A,* 2695-2698.

Reiss, R.; Ryan, P.B.; Koutrakis, P. *Environmental Science and Technology.* **1994,** *28,* 504-513.

Sabersky, R.H.; Sinema, D.A.; Shair, F.H. *Environmental Science and Technology.* **1973,** *7,* 347-353.

Schlatter, J.C. *A Practical Guide to Catalyst Testing.* Catalytica, Inc. Mt. View, California, 1987.

Simmons, A.; Colbeck, I. *Environmental Technology.* **1990,** *11,* 973-978.

Stephens S.; Rossi, M.J.; Golden, D.M. *International Journal of Chemical Kinetics.* **1986,** *18,* 1133-1149.

Sutton, D.J.; Nodolf, K.M.; Makino, K.K. *ASHRAE Journal,* **1976,** *18,* 21-26.

Tkalich, F.S.; Klimovskii, A.O.; Lisachenko A.A. *Kinet. Catal.* **1984,** *25,* 942-948.

Weschler, C.J.; Shields, H.C.; Naik, D.V. *JAPCA: The Journal of the Air and Waste Management Association.* **1989,** *39,* 1562-1568.

Weschler, C.J.; Shields, H.C.; Naik, D.V. In *Tropospheric Ozone and the Environment II: Effects, Modeling and Control.* Berglund, R. Ed; Air & Waste Management Association: Pittsburgh, PA, 1992; 681-702.

CHAPTER 4

The Rate of Ozone Uptake on Carpet: Mathematical Modeling

4.1 Background

Ozone concentrations are lower indoors because, in part, ozone molecules migrate through fluid-mechanical boundary layers to react irreversibly with surfaces. Several authors have investigated the nature of indoor mass transport of pollutant species and developed models to combine mass transport with species loss by removal at surfaces (Crump and Seinfeld, 1981; Nazaroff et al., 1993; Cano-Ruiz et al., 1993; Lai and Nazaroff, 2000). These models do not directly address the influence of surface roughness on uptake of gaseous pollutants. This limitation may be especially important for the characterization of species deposition to carpet. Carpet presents a rough, complex surface to the bulk gas. The high surface area inherent in carpet might strongly influence indoor ozone concentrations. Yet, existing mathematical models are not equipped to understand how roughness and surface area influence deposition. A fundamental understanding of how reactive species deposition comes about can help determine how selection of carpet can impact indoor air quality, e.g. how does fiber diameter and density relate to its intrinsic ability to react with ozone.

The objective of this chapter is to develop models of mass transport and uptake on carpet surfaces to generate predictions of ozone loss rates in indoor settings. One model should be able to characterize reactive gas deposition to surfaces with characteristic roughness scales typical of carpet. A second model should generate an overall carpet

reaction probability (see Chapter 3) based on the reaction probability of inner surfaces. The combination of these two models would provide a complete description of species deposition to carpet.

To accomplish these objectives, I first extend a recently developed model (Lai and Nazaroff, 2000) of turbulent transfer of pollutant species to smooth surfaces by incorporating resistance associated with the surface reaction probability. While the model is strictly valid only for smooth surfaces it may work well for carpet as well. This is because the scale of roughness on carpet is generally much smaller than the concentration boundary layer predicted by the model.

Next, I connect the flux of the species at the top of the carpet fibers to the concentration gradient inside the fiber mat. The reaction probability has been defined as the rate at which a species is irreversibly consumed at an interface divided by the rate at which the species strikes the interface. For a flat surface, such as a painted wall, the interface is trivially coincident with the wall surface. In the case of fleecy materials, the definition of the boundary becomes less certain. In Chapter 3, I defined the reaction probability at three separate boundaries: whole carpet, fiber, and backing. In this chapter, I will use these same descriptions of the fiber and backing reaction probability to derive the whole carpet reaction probability based on a mathematical model of diffusion and reaction in a geometric system that represents carpet. I will also show that the whole carpet reaction probability may be reasonably defined at the tips of carpet fibers, despite the complicated geometry, and the presence of fluid motion above the fiber tips. A numerical evaluation of ozone flux at the surface of carpet will allow the reaction probability of fiber and backing surfaces to be connected to a reaction probability defined

at the interface between the tips of the carpet fibers and the gas above. This "whole carpet" reaction probability can then be compared to that of other indoor sinks, such as painted walls. The results of the analyses of mass transport to carpet, in the porous carpet mat, and surface uptake are combined to derive an overall model of ozone deposition to carpet. Finally I use these findings of these mathematical treatments to compare the relative uptake of ozone on painted walls and carpet to show that carpet can be a significant sink for ozone in a typical residence.

4.2 Analysis and extension of turbulent mass-transfer model to systems with finite surface resistance

4.2.1 Description of model

Reactive gas species can be removed from indoor air by transfer of that species from bulk air to a surface. Species transport is influenced primarily by advection and diffusion as described by the advective-diffusion equation (Bird et al., 1965),

$$\frac{\partial C}{\partial t} = \bar{\nabla} \cdot \left(D\bar{\nabla}C - C\bar{U} \right) \tag{4.1}$$

Equation 4.1 assumes that no homogeneous reaction or formation of species C takes place; D represents the molecular diffusivity of gaseous species C and $\bar{U}$ is the velocity vector. The term $C\bar{U}$ is the advective flux of species C and $D\bar{\nabla}C$ is the diffusive flux.

Indoor air motion can be laminar or turbulent (Nazaroff et al., 1990; Cano-Ruiz et al., 1993). The connection between laminar flow conditions and surface resistance has been described by Cano-Ruiz et al. (1993). They also described deposition under turbulent conditions using models developed by Crump and Seinfeld (1981).

Near a surface, the species flux, J, can be described by a modification of Fick's law,

$$J = -(\varepsilon + D)\frac{\partial C}{\partial y} \tag{4.2}$$

where ε is the turbulent eddy diffusivity. The eddy diffusivity increases with distance from the surface, y, because turbulent eddy size increases. The functional form of the eddy diffusivity has been the subject many studies. Chief among these for indoor air applications are Corner and Pendlebury (1951), Crump and Seinfeld (1981), and most recently Lai and Nazaroff (2000).

Lai and Nazaroff analyzed the direct numerical simulation (DNS) results of turbulence by Kim et al. (1987). They noted that the normalized turbulent viscosity, ν_t/ν, could be described using power-law fits to the DNS results applied to three successive layers adjacent to the surface. They also argued that the turbulent viscosity is well-approximated by the eddy diffusivity for submicron particles. Gaseous species are far smaller than particles, and so the same approximation should hold. An outline of the key elements of the Lai-Nazaroff (LN) model follows.

Deposition velocity, v_d, is a species mass transfer coefficient defined here as,

$$v_d = \frac{|J(y=0)|}{C_\infty} \tag{4.3}$$

where C_∞ is the species concentration outside the concentration boundary layer. Lai and Nazaroff define three dimensionless parameters for convenience in model development: the dimensionless species concentration (C^+), distance from the wall (y^+), and deposition velocity (v_d^+).

$$C^+ = \frac{C}{C_\infty} \tag{4.4}$$

$$y^+ = \frac{yu^*}{\nu} \tag{4.5}$$

$$v_d^+ = \frac{v_d}{u^*} \tag{4.6}$$

Here, u* is the friction velocity, defined by,

$$u^* = \sqrt{\frac{\tau_w}{\rho_a}} \tag{4.7}$$

where τ_w is the shear stress at the wall and ρ_a is the fluid density.

The friction velocity is a central parameter in the LN model. In an indoor setting, the friction velocity can be determined by measuring the velocity profile perpendicular to the wall and incorporating this data into a plot of the "law of the wall" (Bejan, 1995),

$$\frac{U}{U_\infty} = \frac{2.5u^*}{U_\infty} \ln\left(\frac{yU_\infty}{\nu}\right) + D \tag{4.8}$$

where U_∞ is the free-stream velocity. The friction velocity is then obtained from the slope of a line representing U/U_∞ vs. $\ln(yU_\infty/\nu)$ (Brunn, 1995). Lai and Nazaroff report a representative range of u* values in rooms to be 0.3 to 3 cm s^{-1}.

The LN model assumes that flux is constant in the concentration boundary layer, allowing equation 4.2 to be combined with equations 4.3-4.6 to achieve

$$v_d^+ = \left(\frac{\varepsilon + D}{\nu}\right)\frac{\partial C^+}{\partial y^+} \tag{4.9}$$

4.2.2 Extension of three-layer model to surfaces with finite resistance to reactive gas uptake

At this point, my analysis deviates from the LN model. In their model, Lai and Nazaroff assume that particles deposit irreversibly on a surface. The concentration of airborne particles is set equal to zero where the particles comes to within a distance of $d_p/2$ from the wall. Thus, they define a boundary condition at $y^+=(d_p/2)u^*/\nu$ where $C^+=0$ and d_p is the particle diameter.

For my system, the definition of the boundary location and the concentration boundary condition change. A gaseous species like ozone may either be irreversibly taken up by the surface or bounce off the surface, unchanged. This condition is parameterized by the reaction probability, γ, of the surface for uptake of the reactive species. The inner boundary at which ozone is reflected or irreversibly taken up is defined at a position 2/3 λ_{mfp} away from the surface, where λ_{mfp} is the mean free path of ozone. For ozone at 298 K, and atmospheric pressure, the mean free path is about 7×10^{-8} m which is much less than the typical concentration boundary layer thickness (Cano-Ruiz et al., 1993). Thus, I set the boundary condition at $y^+ = 0$ to be $C^+ = C_w^+$, where C_w^+ is the dimensionless concentration of ozone at the wall as defined below. The second boundary condition is set by assuming that $C^+ = 1$ at the outer edge of the fluid-mechanical boundary layer, where $y^+=30$ (Bejan, 1995).

Equation 4.9 can be rearranged, integrated and evaluated as follows, subject to the boundary conditions set above,

$$\int_{C_w^+}^{1} \frac{dC^+}{v_d^+} = \int_0^{30} \left(\frac{\nu}{\varepsilon_p + D} \right) dy^+ = \Gamma \tag{4.10}$$

The left hand side can be solved directly, noting that at the wall ($y^+=0$), the flux to the wall is dependent on the reaction probability, and equal to the overall transport flux,

$$J(y=0) = C_w \frac{\gamma \langle v \rangle}{4} = v_d C_\infty \tag{4.11}$$

thus,

$$C_w^+ = \frac{C_w}{C_\infty} = \frac{4v_d}{\gamma \langle v \rangle} = \frac{4v_d^+ u^*}{\gamma \langle v \rangle} \tag{4.12}$$

Solving the left hand side of equation 4.10 and retaining the notation, Γ, to denote middle term of equation 4.10, one obtains

$$\frac{1 - \frac{4v_d^+ u^*}{\gamma \langle v \rangle}}{v_d^+} = \Gamma \tag{4.13}$$

Rearranging, the dimensionless deposition velocity is then

$$v_d^+ = \left(\Gamma + \frac{4u^*}{\gamma \langle v \rangle} \right)^{-1} \tag{4.14}$$

To evaluate the term, Γ, in equations 4.10 and 4.14, an expression for the functional dependence of the eddy diffusivity is required. Lai and Nazaroff show that, these expressions appropriately describe the gradient in the eddy diffusivity,

$$\varepsilon = 7.669 \times 10^{-4} \nu \left(y^+ \right)^3 \qquad 0 \le y^+ \le 4.3 \tag{4.15}$$

$$\varepsilon = 1.00 \times 10^{-3} \nu \left(y^+ \right)^{2.8214} \qquad 4.3 \le y^+ \le 12.5 \tag{4.16}$$

$$\varepsilon = 1.07 \times 10^{-2} \nu \left(y^+ \right)^{1.8895} \qquad 12.5 \le y^+ \le 30 \tag{4.17}$$

with the caveat that the DNS results of Kim et al. may only approximately apply to enclosure flow as typified by indoor air. Note that the term Γ is dependent only on the kinematic viscosity and the species diffusivity. For air at 1 atm and 296 K, the kinematic viscosity (ν) is 0.15 $cm^2\ s^{-1}$ and the ozone diffusivity (D) is 0.167 $cm^2\ s^{-1}$ (Massman, 1998). For these parameters, the middle term of equation 4.10 can be numerically integrated with the result, $\Gamma = 13.31$.

The concentration boundary layer of gaseous pollutants is significantly larger than those of particles because molecular diffusivity is much larger than the Brownian diffusivity of non-molecular sized particles. As noted by Lai and Nazaroff, the concentration boundary layer thickness, δ^+, can be estimated for a smooth surface by a simple power-law dependence on the Schmidt number ($Sc=\nu/D$):

$$\delta^+ = 24.7 Sc^{-1/3} \tag{4.18}$$

For gases, the Schmidt number is of the order 1, so that the concentration boundary layer thickness is approximately $\delta^+ = 25$. With an outer boundary at $y^+ = 30$ this model adequately encompasses the concentration boundary layer for reactive gas deposition.

Figure 4.1 shows the results of this analysis. Values of u* were chosen to coincide with the range of typical indoor values reported by Lai and Nazaroff. The Boltzmann velocity of ozone at 298K is 3.6×10^4 cm s^{-1}. Where the reaction probability is very low, surface resistance dominates, and the deposition velocity is approximated by

$$v_d = \frac{\gamma \langle v \rangle}{4} \tag{4.19}$$

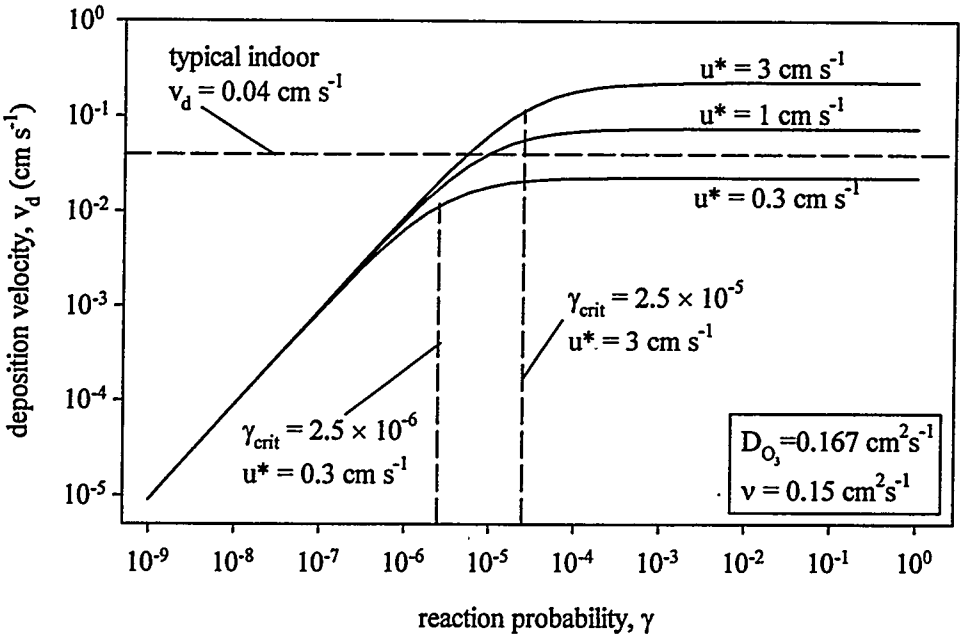

Figure 4.1. Deposition velocity (v_d) as a function of the smooth-surface reaction probability, based on extension of Lai-Nazaroff model to reactive gas deposition. Also shown are values of the critical reaction probability, γ_{crit}, for u* values of 0.3 and 3 cm s^{-1}, and the typical indoor ozone deposition velocity.

This result implies that there is a negligible concentration gradient adjacent to the surface such that $C_w \cong C_\infty$, as expected. Where the reaction probability is high, and surface resistance is negligible, the deposition velocity is approximated by,

$$v_d = \frac{u^*}{\Gamma} \tag{4.20}$$

The reaction probability drops out of the equation and the deposition velocity is directly proportional to the friction velocity. Cano-Ruiz et al. (1993) conceived of a "critical reaction probability" that distinguishes the zone of surface resistance dominance ($\gamma << \gamma_{crit}$) from the zone of mass transport resistance dominance ($\gamma >> \gamma_{crit}$). This critical parameter value is obtained by setting the two terms on the right hand side of equation 4.14 equal:

$$\gamma_{crit} = \frac{4u^*}{\Gamma\langle v \rangle} \tag{4.21}$$

For ozone, the value of γ_{crit} ranges from 2.5×10^{-6} for $u^* = 0.3$ cm s^{-1}, to 2.5×10^{-5} for $u^* = 3$ cm s^{-1}.

It is instructive to compare model predictions to direct measurements of the ozone deposition velocity. In a review of indoor pollutant deposition, Nazaroff et al. (1993) reported that ozone deposition velocity values ranged from about 0.015 to 0.075 cm s^{-1}, but tended to cluster around 0.04 cm s^{-1}. A recent survey of homes in California reported an average ozone deposition velocity of 0.049 ± 0.017 cm s^{-1}. The deposition velocity to carpet measured in my experimental chamber was about 0.06 cm s^{-1} for a whole carpet reaction probability, γ_o, of 10^{-5}. This corresponds to a friction velocity of about 1 cm s^{-1}, demonstrating that the fluid mechanical conditions in my experimental chamber are similar to that of typical indoor spaces. It is intriguing that the intersection of the "typical" indoor u* of 1 cm s^{-1} and the "typical" indoor deposition velocity of 0.04 cm s^{-1} corresponds to an area averaged reaction probability of 10^{-5}, which is the typical of the reaction probability of aged whole carpet.

Development of a model for reactive gas deposition to rough surfaces is the next logical extension of the LN model. However, the roughness scale of some carpets may be small enough that it will not significantly modify the concentration boundary layer for gases. Consider the definition of the dimensionless boundary layer where $C^+ = 0.9$ (Lai and Nazaroff, 2000),

$$\delta^+ = \frac{\delta u^*}{\nu} \tag{4.22}$$

where δ is the concentration boundary layer thickness. As noted earlier, a typical range of indoor u^* values is 0.3 – 3 cm s^{-1}, δ^+ for gases was estimated to be 25 and ν for air is 0.15 cm^2 s^{-1} at 298 K. Therefore, the concentration boundary layer thickness should lie in the range from 1.25 – 12.5 cm. I estimate that the largest roughness feature on carpets examined in Chapters 2 and 3 is about 0.3 cm. Under many conditions, this is only a small fraction of the scale of the concentration boundary layer. Therefore, the smooth-surface model may be adequate to describe deposition to some carpet types. I surveyed of carpets in residences and buildings and found surface roughness scales as much as 1 cm. For these materials, it may be necessary to develop a deposition model that takes surface roughness into account.

4.3 Development of model of diffusion and reaction into carpet fiber mat

4.3.1 Background

The model of species mass transport presented in Section 4.2 requires that the reaction probability of a surface be specified. This deposition model was developed around the reaction probability of flat surfaces. As discussed earlier, flat (or nearly flat) surfaces commonly occur indoors in the form of glass or painted walls. The model adequately describes deposition to these surfaces but does not encompass irregular surfaces.

Cano-Ruiz et al. (1993) suggested that rough surfaces might be treated as an equivalent flat surface. There is a reaction probability associated with a plane laid flat across the rough surface that encompasses the complications of extra surface area, slight

changes in the flow field, etc. In this section, I develop a model of the equivalent reaction probability associated with a carpet, a topographically complex indoor surface.

A model of the equivalent reaction probability of porous surfaces also has value in describing dynamic changes in surface uptake due to ozone aging of fibers and backing. While the reaction probability of many surfaces has been measured directly, the value invariably changes with exposure. Experimental results from Chapter 3 indicate that very little aging occurred during the weeklong exposure of whole carpet. However, fibers could be rapidly aged in the fixed-bed reactor. To predict the whole carpet reaction probability resulting from long-term ozone exposure, a mathematical model describing mass transport and surface uptake to fibers and carpet backing is needed. The model must account both for the complexities of mass transport and for spatially and temporally varying aging within the carpet.

4.3.2 Link between mass transport above fibers tips and below fiber tips.

A model that combines advective/diffusive transport above the fibers and pure diffusive transport and reaction below the fiber tips requires a mathematical link. The area-averaged flux of ozone to the tips of the fibers must equal the area-averaged flux below the fiber tips under steady-state conditions by continuity. In the reactive gas deposition model, y = 0 at the wall. In this case, I define y=0 at the plane which intersects the tips of the carpet fibers. The flux-matching boundary condition is then written .

$$(D+\varepsilon)\overline{\left.\frac{\partial C}{\partial y}\right|}_{y=0^+} = D\overline{\left.\frac{\partial C}{\partial y}\right|}_{y=0^-} \qquad (4.23)$$

where $\overline{\left.\frac{\partial C}{\partial y}\right|}_{y=0^+}$ represents the area-averaged concentration gradient above the fiber tips,

and $\left.\overline{\frac{\partial C}{\partial y}}\right|_{y=0^-}$ is the area averaged concentration gradient below the fiber tips. As given by equation 4.11, the flux to a the plane at the fiber tips (left side of equation 4.11) is proportional to the equivalent reaction probability, γ_o. Thus combining equation 4.11 with equation 4.23, yields,

$$\gamma_o = \frac{4D}{C_w \langle v \rangle} \left.\overline{\frac{\partial C}{\partial y}}\right|_{y=0^-} \tag{4.24}$$

To evaluate the expression $\left.\overline{\frac{\partial C}{\partial y}}\right|_{y=0^-}$, a model that can evaluate the concentration profile below the fiber tips is required.

4.3.3 One-dimensional model incorporating diffusion into carpet mat and reaction at fiber and backing surfaces

The basic elements of carpet are the fiber mat and the backing. Conceptually, the fiber mat is a porous structure with internal surface area provided by fiber and backing surfaces. In reality, carpet geometry can be quite complex. Fibers are usually not perfect cylinders, often taking the shape of the die used in manufacturing the fiber (e.g. with trilobal or pentalobal cross-sections; Jerde, 1992). Light microscope images of the fibers used in the experiments described in Chapters 2 and 3 revealed an irregular, corrugated cross-section. Fibers are not strictly independent, but are usually formed into bundles that may be twisted. The bundle itself is not uniform. The diameter of a fiber bundle usually narrows at the point of attachment to the carpet backing. Carpet fiber mats can be formed from cut fibers, or looped back though the carpet so that no fiber tips are exposed. Nevertheless, the analysis of pollutant deposition to carpet can be made tractable by

introducing geometric simplifications that capture key attributes such as surface area and depth.

Transport and reaction of ozone with the internal surfaces sets up complicated concentration gradients. I propose that the gradients in all directions other than normal to the carpet (y-axis) are unimportant in determining the whole carpet reaction probability in most cases. In a later section, I develop a two-dimensional model that takes radial concentration gradients around fibers into account and show that for typical carpet parameters (geometry, reaction probability of fiber and backing surfaces), a one dimensional model is sufficient.

For one-dimensional diffusion with first-order loss (reaction with fiber surfaces), the governing equation under steady state conditions is,

$$D\frac{d^2C}{dy^2} = k_s C \tag{4.25}$$

where k_s is a reaction rate term for the loss of ozone on fiber surfaces. Assuming that reaction on fiber surfaces is rate limiting, the rate constant is related to the readily measured fiber-mat parameters,

$$k_s = \frac{\gamma_f \langle v \rangle}{4}\left(\frac{A_f}{V_{fm}}\right) \tag{4.26}$$

The term, A_f/V_{fm}, is the fiber area (A_f) per unit volume of fiber-mat (V_{fm}) and can be found by measuring the fiber-mat porosity (p) and the fiber diameter (d_f):

$$\left(\frac{A_f}{V_{fm}}\right) = \frac{4(1-p)}{d_f p} \tag{4.27}$$

The differential equation 4.25 requires two boundary conditions to solve, one at the top of

the fiber-mat, and one at the carpet backing. The top boundary occurs in the vicinity of the tips of the fibers, defined here as y=h. Note that the origin of the y-axis is shifted in this model with respect to the discussion in Sections 4.2 and 4.3.2. Under steady-state conditions, the concentration at any point in the carpet mat is constant in time, so I set the concentration at y=h to C_o, the bulk concentration in room air,

$$C = C_o \qquad y = h \qquad (4.28)$$

Note that the a flux-matching conditions was also introduced at the interface between the fiber tips and the bulk room air. Both of these conditions (flux matching and a constant concentration at y = h) hold under steady-state conditions. At the bottom of the fiber-mat, the carpet backing acts (in this model) as a barrier to diffusion, but also as a sink for ozone. For a known backing reaction probability (γ_b), the flux of ozone to the backing is given by

$$D\frac{dC}{dy}\bigg|_{y=0} = \frac{\gamma_b \langle v \rangle}{4} C(0) \qquad y = 0 \qquad (4.29)$$

It is useful to cast the governing equation and boundary conditions in dimensionless units by defining

$$C' = \frac{C}{C_o} \qquad (4.30)$$

$$y' = \frac{y}{h} \qquad (4.31)$$

Thus, the dimensionless governing equation under steady state conditions is

$$\frac{d^2C'}{dy'^2} = A_1^2 C' \qquad (4.32)$$

where

$$A_1 = \sqrt{\frac{\gamma_f \langle v \rangle h^2 (1-p)}{d_f D}} \tag{4.33}$$

with boundary conditions

$$\frac{dC'}{dy'} = k_y C' \qquad y' = 0 \tag{4.34}$$

$$C' = 1 \qquad y' = 1 \tag{4.35}$$

where

$$k_y = \frac{\gamma_b \langle v \rangle h}{4D} \tag{4.36}$$

An analytical solution for this problem was derived:

$$C' = \frac{(A_1 - k_y)e^{-A_1 y'} + (A_1 + k_y)e^{A_1 y'}}{(A_1 - k_y)e^{-A_1} + (A_1 + k_y)e^{A_1}} \tag{4.37}$$

In Figure 4.2, the dimensionless concentration profile (horizontal axis) is plotted against y′ for typical carpet parameters. The concentration, C′, as assumed, is unity at y′=1 for all cases. As ozone penetrates the fiber mat, it reacts with fiber surfaces and the concentration drops. For a fiber reaction probability (γ_f) as high as 10^{-3}, ozone penetrates only a short distance into the mat. Even for γ_f as low as 10^{-5}, only about 5% of the ozone reaches the backing. Below this reaction probability, more ozone reaches and reacts with the backing. When the fiber reaction probability is less than 10^{-8}, the concentration profile is linear. The linearity indicates that the fibers have very little influence on concentration because the differential equation 4.32 can be approximated by,

$$\frac{d^2 C'}{dy'^2} = 0 \tag{4.38}$$

because A_l^2 is very small. The solution to equation 4.38 is linear:

$$C' = a + by' \tag{4.39}$$

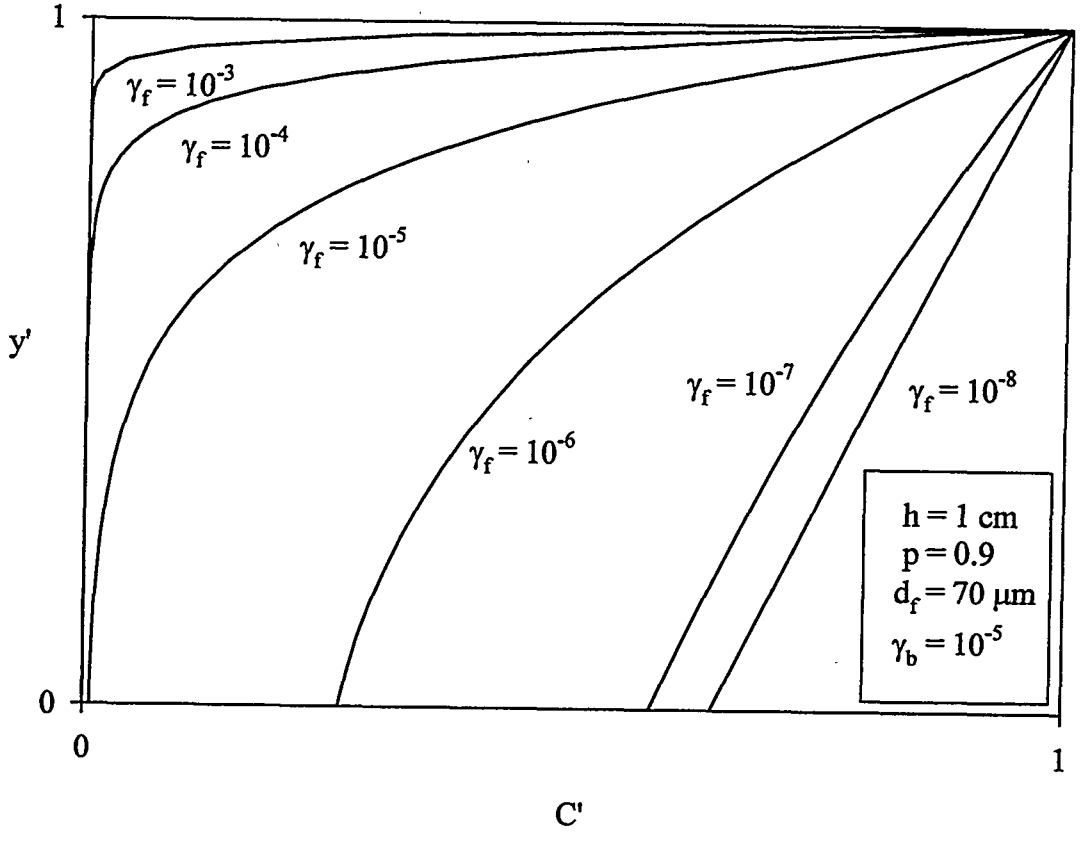

Figure 4.2. Dimensionless concentration profile in carpet mat where h=1 cm, p = 0.9, d_f = 70 μm, and $\gamma_b = 10^{-5}$.

Because there is no horizontal concentration gradient in this model, the mean vertical concentration gradient, $\left.\overline{\frac{\partial C}{\partial y}}\right|_{y=0^-}$ in equation 4.24 (note the shifted y-origin) is approximately equal to $\left.\frac{dC}{dy}\right|_{y=h}$ for low fiber reaction probabilities. For higher values of γ_f, a significant portion of the flux to the top of the carpet mat is due to uptake at the tip of the fiber. With a porosity of 0.9, 10% of the horizontally projected area of the carpet is associated with carpet tips. The whole carpet reaction probability can be evaluated

directly (returning to dimensionless units),

$$\gamma_o = \frac{4pDA_1}{h\langle v\rangle}\left[\frac{(k_y - A_1)e^{-A_1} + (A_1 + k_y)e^{A_1}}{(A_1 - k_y)e^{-A_1} + (A_1 + k_y)e^{A_1}}\right] + (1-p)^2\gamma_f \qquad (4.40)$$

I evaluated γ_o for a typical carpet configuration, varying the fiber and backing reaction probability. The results are shown in Figure 4.3. Recall that the normalized fiber area, R_f, is a measure of the relative increase in surface area (above the nominal carpet area) due to fibers. The normalized fiber area is related to geometric parameters used here:

$$R_f = \frac{4(1-p)h}{d_f} \qquad (4.41)$$

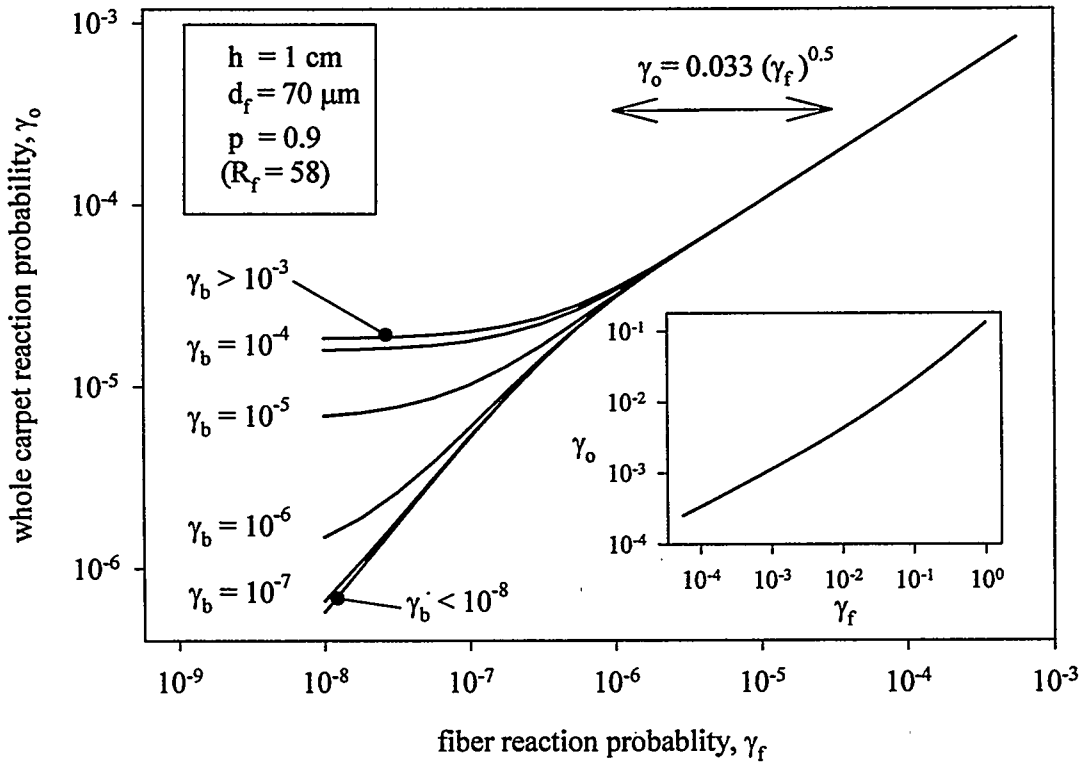

Figure 4.3. Whole carpet reaction probability (γ_o) vs. fiber reaction probability (γ_f) for specific cases of the backing reaction probability (γ_b) based on one-dimensional carpet diffusion model. In this case h = 1 cm, d_f = 70 μm, p = 0.9.

This figure demonstrates, for a specific carpet geometry, under what conditions

the fibers or the backing dominate in determining the whole carpet reaction probability. When the value of the fiber reaction probability, γ_f, is greater than 10^{-6}, the whole carpet reaction probability, γ_o, is not influenced by the reaction probability of the backing, γ_b. This compares well with Figure 4.2 which shows that between γ_f values of 10^{-6} and 10^{-5}, the ozone concentration, C′, just reaches the backing. Alternatively, for values of $\gamma_f < 10^{-7}$, the backing reaction probability, γ_b, becomes as or more important than γ_f in determining γ_o, provided $\gamma_b > 10^{-8}$. In the experiments described in Chapter 3, the backing reaction probability, γ_b, was found to be about 10^{-5}. The slope of the plot for $\gamma_b = 10^{-5}$ is fairly shallow in the region where $10^{-8} > \gamma_f > 10^{-6}$. For this 100-fold increase in γ_f, γ_o increases by only a factor of 4.6. The small increase in the whole carpet reaction probability indicates that as the fibers age, the whole carpet ozone reactivity will not change rapidly. However, for $\gamma_f > 10^{-5}$, γ_o increases in proportion with the square root of γ_f until flux to the tips of the fibers begins to become important. The inset plot in Figure 4.3 shows that there is an upward curvature to the whole-carpet reaction probability as flux to the fiber tips dominates.

4.3.4 Two-dimensional model of reactive gas uptake in carpet mat

The one-dimensional model has the limitation that it does not take into account concentration gradients in the horizontal direction. To remedy this, I developed a two-dimensional model of the carpet fiber system to investigate the influence of radial concentration gradients on the overall reaction probability of the carpet surface.

The structure of carpet can be loosely described as rows of cylinders aligned vertically and attached at their base to a horizontal backing. As seen from above, fibers

line up at somewhat regular intervals, with the average distance between fibers denoted w_f, and the porosity of the fiber mat denoted p. In this conceptual carpet model (see Figure 4.4), each fiber is centered in an identical square cell. Reactants diffusing into this cell are influenced entirely by the central fiber; it can be assumed, by symmetry, that there is no flux across the cell boundary.

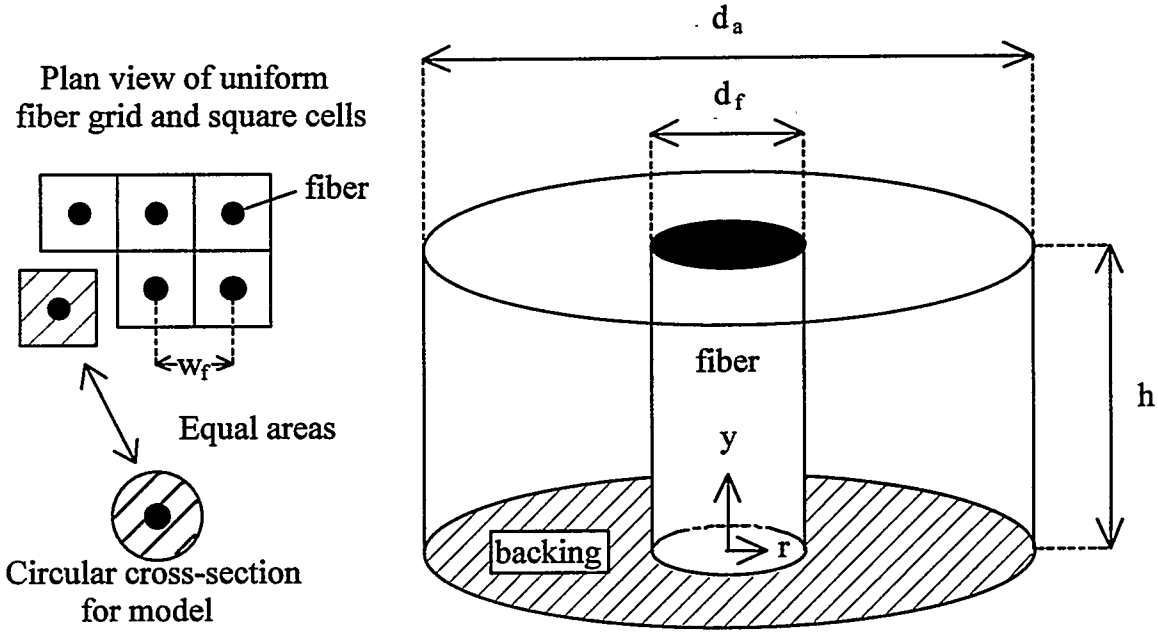

Figure 4.4. Geometric representation of carpet for two-dimensional (r,y) model of diffusion and reaction in fiber mat.

A mathematical model of diffusion and reaction using a square geometry requires three coordinate dimensions. To simplify the mathematics, but retain the most important spatial parameters (fiber diameter, length, and porosity), I allowed the square cell to relax to a circle with the same cross-sectional area. Thus, the model geometry, as shown in Figure 4.4, is a cylindrical fiber surrounded by an annular cylinder of air, with an annular disk at the bottom of the air cylinder representing carpet backing. The diameter, d_f, and length, L_f, of the fiber are taken directly from fiber measurements, while the diameter of

the annular air cylinder surrounding the fiber, d_a, can be determined by measuring the porosity of the fiber mat. The porosity is equal to the volume of the annular cylinder divided by the sum of the fiber and annular cylinder volumes. Thus,

$$d_a = d_f \frac{1}{\sqrt{1-p}}. \tag{4.42}$$

One complication of real carpets that must be addressed is the tortuosity of fibers. Carpet fibers generally take on two typical configurations: cut pile and closed-loop. Fibers are not entirely vertical or straight in either configuration in most carpets. To account for the "kinkiness" of real fibers, I can introduce a correction term. The amount of fiber surface area per volume of carpet mat increases as the height of the mat decreases (and the kinkiness of fibers increases). Fiber surface area is linearly dependent on fiber length and diameter. An appropriate correction term for this model is based on the actual fiber length (L_f) and actual mat height (h). The factor, L_f/h, can be used to modify d_f in the following analysis to capture this extra surface area. From measurements of carpet fibers tested in Chapters 2 and 3, the correction factor ranges between 1.1 and 1.5. Equation 4.42 is then modified to reflect this correction:

$$\tilde{d}_a = \tilde{d}_f \frac{1}{\sqrt{1-p}} \tag{4.43}$$

where,

$$\tilde{d}_f = \frac{L_f}{h} d_f \tag{4.44}$$

For the purposes of this analysis, I assumed the system was at steady-state, and that air movement above the fibers will not transfer momentum below the fiber tips. Thus, mass transfer to the carpet fibers and backing is due entirely to diffusion through

the annular air cylinder. Later in this chapter, I describe in more detail the analysis of advective transfer below the fibers tips, and the characteristic time to reach steady-state conditions. I also assume that the concentration of the reacting species at the tips of the fibers is constant in time and in the coordinate r. In the following analysis, the origin of the y-axis is shifted to the carpet backing and the concentration at the top of the fibers will be denoted C_o (this is identical to the wall concentration value, C_w, in the development of the reactive gas deposition model).

The concentration of ozone diffusing through the annular region under steady-state conditions is described by the following equation,

$$\frac{\partial^2 C}{\partial y^2} + \frac{1}{r}\frac{\partial}{\partial r}\left(r\frac{\partial C}{\partial r}\right) = 0 \qquad (4.45)$$

with four boundary conditions. The concentration at the top of the annular cylinder is uniform. At the fiber and backing, flux conditions are dependent on the reaction probability at those surfaces. At the outer wall of the annular cylinder, there is no net flux of the reacting species. These boundary conditions can be written mathematically as follows:

$$C = C_o \qquad y = h \qquad (4.46)$$

This represents constant pollutant concentration at top of the annular cylinder.

$$\frac{\partial C}{\partial r} = \frac{\gamma_f < v >}{4D} C \qquad r = \frac{\tilde{d}_f}{2} \qquad (4.47)$$

This represents flux at the fiber surface.

$$\frac{\partial C}{\partial y} = \frac{\gamma_b < v >}{4D} C \qquad y = 0 \qquad (4.48)$$

This represents flux at the carpet backing.

$$\frac{\partial C}{\partial r} = 0 \qquad r = \frac{\tilde{d}_a}{2} \tag{4.49}$$

This represents the no flux condition across outer boundary of annular cylinder.

Recall that the goal of this analysis is to determine the whole carpet reaction probability, γ_o, for a given set of geometric and reaction probability values of backing and fibers. The reaction probability of whole carpet, γ_o, is defined at the plane separating fibers from the fluid above. This parameter can be determined by calculating the flux of ozone into the top of the cylinder. The geometry and reactivity of independent parts of the carpet (fiber and backing) are, in this manner, related to the overall uptake phenomena. In words, the vertical mass flux to the top of the carpet fibers from above equals the mass flux into the annular cylinder plus the mass flux to the top of the fiber tips. Mathematically,

$$C_o \frac{\gamma_o \langle v \rangle}{4}\left(\frac{\pi \tilde{d}_a^2}{4}\right) = \int_{\tilde{d}_f/2}^{\tilde{d}_a/2} D \left.\frac{\partial C}{\partial y}\right|_{y=h} 2\pi r dr + C_o \frac{\gamma_f \langle v \rangle}{4}\left(\frac{\pi \tilde{d}_f^2}{4}\right) \tag{4.50}$$

Rearranging, the whole-carpet reaction probability, γ_o, is given by

$$\gamma_o = \frac{32D}{C_o \tilde{d}_a^2 < v > } \int_{\tilde{d}_f/2}^{\tilde{d}_a/2} \left.\frac{\partial C}{\partial y}\right|_{y=h} r dr + \gamma_f \left(\frac{\tilde{d}_f}{\tilde{d}_a}\right)^2 \tag{4.51}$$

calculated values of the concentration field are used to evaluate the concentration gradient at h.

For later analyses, it is useful to write the above expressions in dimensionless form. The governing equation (4.45) becomes,

$$\frac{\partial^2 C'}{\partial r'^2} + \frac{1}{r}\frac{\partial C'}{\partial r'} + \left(\frac{a}{b}\right)^2 \frac{\partial^2 C'}{\partial y'^2} = 0 \tag{4.52}$$

with boundary conditions,

$$C' = 1 \qquad y' = 1 \tag{4.53}$$

$$\frac{\partial C'}{\partial r'} = k_f C' \qquad r' = b \tag{4.54}$$

$$\frac{\partial C'}{\partial y'} = k_b C' \qquad y' = 0 \tag{4.55}$$

$$\frac{\partial C'}{\partial r'} = 0 \qquad r' = 1 \tag{4.56}$$

where,

$$C' = \frac{C}{C_o} \tag{4.57}$$

$$r' = \frac{2r}{\tilde{d}_a} \tag{4.58}$$

$$y' = \frac{y}{h} \tag{4.59}$$

$$a = \frac{\tilde{d}_f}{2h} \tag{4.60}$$

$$b = \frac{\tilde{d}_f}{\tilde{d}_a} \tag{4.61}$$

$$k_f = \frac{\gamma_f < v > \tilde{d}_a}{8D} \tag{4.62}$$

$$k_b = \frac{\gamma_b < v > h}{4D} \tag{4.63}$$

The parameters a, and b, are geometric parameters; k_f and k_b are parameters that quantify the reactivity of each surface. Note that, if the reaction probability is the same for both fiber and backing, k_f and k_b will only differ by a geometric factor, reducing the number of independent parameters to three. To find the whole carpet reaction probability, equation 4.51 can also be transformed into this dimensionless form,

$$\frac{\gamma_o}{\gamma_f} = \left(\frac{2a}{k_f b}\right)\int_b^1 \left.\frac{\partial C'}{\partial y'}\right|_{y'=1} r'dr' + b^2 \qquad (4.64)$$

I solved equation 4.52 numerically to determine the pollutant concentration field in the annular air cylinder. I compared the results from two different numerical methods to verify that the numerical solution was correct. In both cases, the MATLAB shell and language were used to write numerical solver routines.

Numerical integration of partial differential equations requires three main steps:

1. Definition of system geometry and placement of nodes.
2. Transformation of the PDE into a form allowing an estimate of individual node values based on adjacent node values.
3. Cyclic solution, point by point, or by a more advanced matrix method, until an acceptably converged solution is obtained.

Intermediate steps may be used to increase the efficiency of the method such as adaptive gridding.

One method I employed is a numerical solution written around the strengths of the Matlab programming language. The method uses the procedure outlined by Whitaker (1977) for solving partial differential equations with cylindrical geometry. The advantage of writing original code for solving the equation is that I can ensure that the code reflects

the procedure exactly. Using existing or commercially available code may raise questions about using a "black box" solution. The disadvantage of this procedure is that it does not allow for adaptive gridding. This becomes particularly problematic for solutions in which a steep concentration gradient exists. A complete description of this approach (Method 1) is provided in Appendix A.4.

The limitations of Method 1 can be overcome by introducing the concept of adaptive gridding (Method 2). By creating a non-uniform calculation grid, the process of finding a solution can become more efficient and accurate. Areas in the calculation space where there are shallow concentration gradients only need a few grid points to estimate the concentration field. In locations where the concentration gradient is steep, many more grid points can be used to accurately estimate local concentration values.

For example, in the case where the reaction probability is unity, the species concentration is zero at the fiber boundary ($r = d_f/2$), but equal to C_o at $y = h$. The concentration gradient may be very steep near the top of the annular cylinder, due to the discontinuity existing at $y = h$, $r = d_f/2$. In this region, many grid points may be necessary to accurately describe the concentration profile. Due to the high species loss rate at the fiber surface, the concentration below the fiber tip drops quickly to zero, and remains at zero throughout the rest of the cylinder volume. Few nodes are needed in the zero concentration zone. A method that calculates the concentration at closely spaced intervals near the discontinuity, and at widely spaced intervals in flat gradient regions will decrease calculation time and increase the accuracy and resolution of the concentration field.

Rather than add adaptive-gridding capability to the code of Method 1, I chose to use the Matlab "Partial Differential Equation Toolbox" (PDET) to analyze equation 4.45.

This toolbox has built in adaptive-gridding routines. By comparing the two methods on intermediate problems that either method handles adequately, the results of the Method 2 (black-box) calculation can be validated. This Toolbox was developed independently by COMSOL Europe AB and licensed to Mathworks, the supplier of Matlab. The PDE Toolbox uses the finite-element method described above with several modifications and improvements. Instead of a square grid, the Toolbox creates a non-uniform triangular mesh dependent on geometry, with calculations of function values taking place at the vertices of the triangles. By evaluating the function value at each node, the program can choose to increase node points in the areas of strong gradients. Program code used to access the Toolbox, and extract concentration fields and gradients can be found in Table A.4.2 in Appendix A.4.

4.4 Results of two-dimensional model compared to one-dimensional model

The results of three simulations are shown in Figures 4.5 – 4.7 for a specific set of geometric parameters (h = 1 cm, d_f = 70 μm, p = 0.9). The fiber reaction probability, γ_f, is set to 1, 0.01 and 0.001 in each figure respectively. Each figure contains three plots. The dashed line shows the results of the one-dimensional model. The two solid lines demonstrate the range of concentration profiles predicted by the two-dimensional model across the annular space. One plot shows the concentration profile at the outside of the annular cylinder (r′ = 1), the other shows the profile along at the fiber surface (r′ = b).

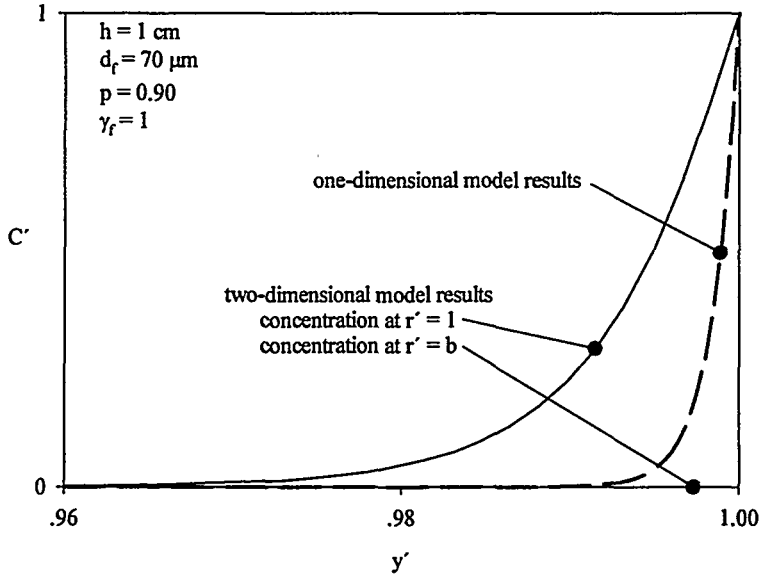

Figure 4.5. Concentration profile in annular space around fiber for $\gamma_f = 1$, $d_f = 70$ μm, p = 0.9. The figure contains three plots: the results of the one-dimensional model (dashed, heavy line) and two plots which demonstrate the range of concentration profiles (at r′ = 1, and r′ = b) predicted by the two-dimensional model. Note that the concentration profile for r′ = b is coincident with the y' axis because C′ = 0 at the fiber when $\gamma_f = 1$.

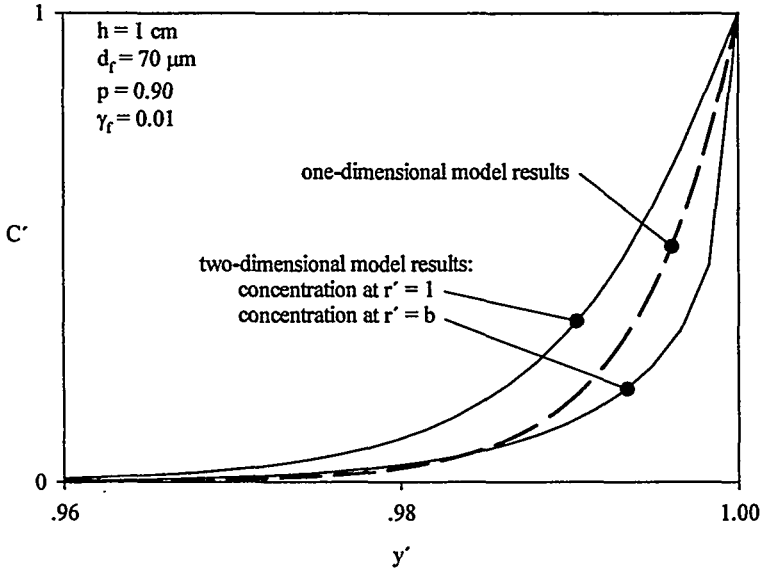

Figure 4.6. Concentration profile for $\gamma_f = 0.01$, $d_f = 70$ μm, p = 0.9. The figure contains three plots: the results of the one-dimensional model (dashed, heavy line) and two plots which demonstrate the range of concentration gradients (at r′ = 1, and r′ = b) predicted by the two-dimensional model.

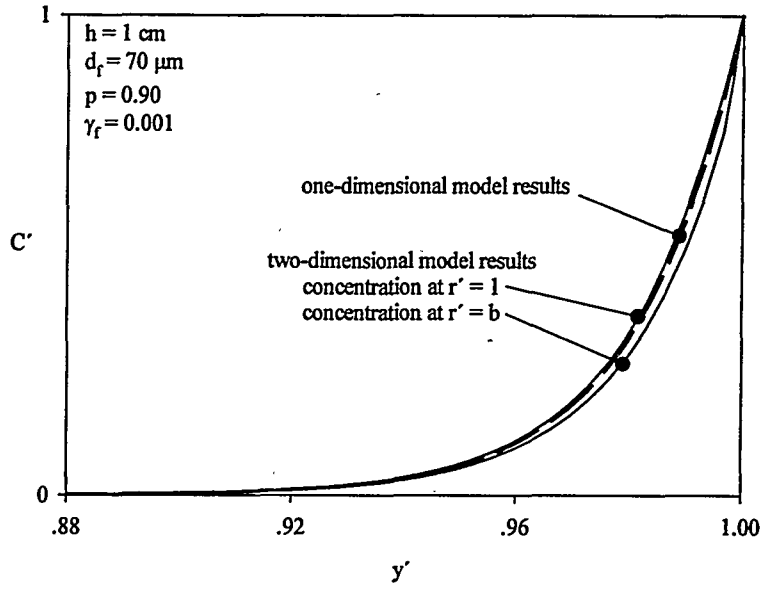

Figure 4.7. Concentration profile for $\gamma_f = 0.001$, $d_f = 70$ μm, $p = 0.9$. The figure contains three plots: the results of the one-dimensional model (dashed, heavy line) and two plots which demonstrate the range of concentration gradients (at $r' = 1$, and $r' = b$) predicted by the two-dimensional model.

In Figure 4.5, the reaction probability of the fiber, γ_f, is set equal to 1. There are sharp gradients in both the longitudinal and radial directions. The radial gradient can be inferred from the large difference in concentration profiles between $r' = 1$ and $r' = b$. The one-dimensional model cannot account for the resistance to diffusion in the radial direction as can the two-dimensional model. Thus, it over predicts the magnitude of the slope of the gradient along the y' axis. In this case, the two-dimensional model is likely to give a better estimate of the whole carpet reaction probability, γ_o, than the one-dimensional model. The two-dimensional model predicts that $\gamma_o = 0.108$, while the one-dimensional model predicts that $\gamma_o = 0.129$. Note that the value of γ_b does not influence the concentration profile because $C' = 0$ at $y' = 0$.

In Figure 4.6, the reaction probability of the fiber, γ_f, is set equal to 0.01. The concentration gradient in the radial direction is less sharp, but still noticeable. The one-

dimensional model does a better job of following the general contour of the concentration gradient along the y′ axis, but still slightly overpredicts γ_o. The two-dimensional model predicts that γ_o =0.0034, while the one-dimensional model predicts that γ_o = 0.0039.

In Figure 4.7, the fiber reaction probability is now reduced to 0.001. The radial concentration gradient is very small in this case; the longitudinal gradient dominates. The one-dimensional model results closely follow the concentration gradient of the two-dimensional model, suggesting that the one-dimensional model is adequate for predicting the whole-carpet reaction probability under these conditions. Indeed, both models predict that γ_o =0.0010.

The one-dimensional model appears to adequately predict γ_o for typical carpet geometries up to a fiber reaction probability of about 0.001. Even with γ_f = 1, the prediction is only in error by <20%. Ultimately, precise determination of the reaction probability where the uptake rate is very high may not be important. When the whole-carpet reaction probability is greater than 10^{-4}, the resistance to mass transfer through the turbulent boundary layer above the carpet dominates over surface uptake resistance. As shown in Figure 4.1, as the surface-reaction probability increases beyond 10^{-4}, the species deposition velocity remains constant. Therefore, the one-dimensional model is sufficiently accurate for indoor air modeling as a means of relating key carpet parameters (γ_f, γ_b, h, d_f, p) to the whole-carpet ozone uptake coefficient (γ_o).

4.5 Model comparisons to laboratory measurements

Experimental results show that ozone aging of the fibers can cause γ_f to decrease by 2 orders of magnitude or more, yet the whole carpet reaction probability diminishes

much more slowly. The models suggests that γ_o decreases (approximately) with the square-root of γ_f, and even more slowly when $\gamma_f < 10^{-6}$. Consider the curve in Figure 4.3 corresponding to $\gamma_b = 10^{-5}$. When γ_f decreases from 10^{-5} to 10^{-7} as is typical of the fibers in this study, γ_o decreases from 1.0×10^{-4} to 1.0×10^{-5}, i.e., only a factor of 10. The decrease in γ_o may be even smaller due to the fact that the backing ages more slowly than carpet fibers (i.e., the initial backing reaction probability is higher than 10^{-5}).

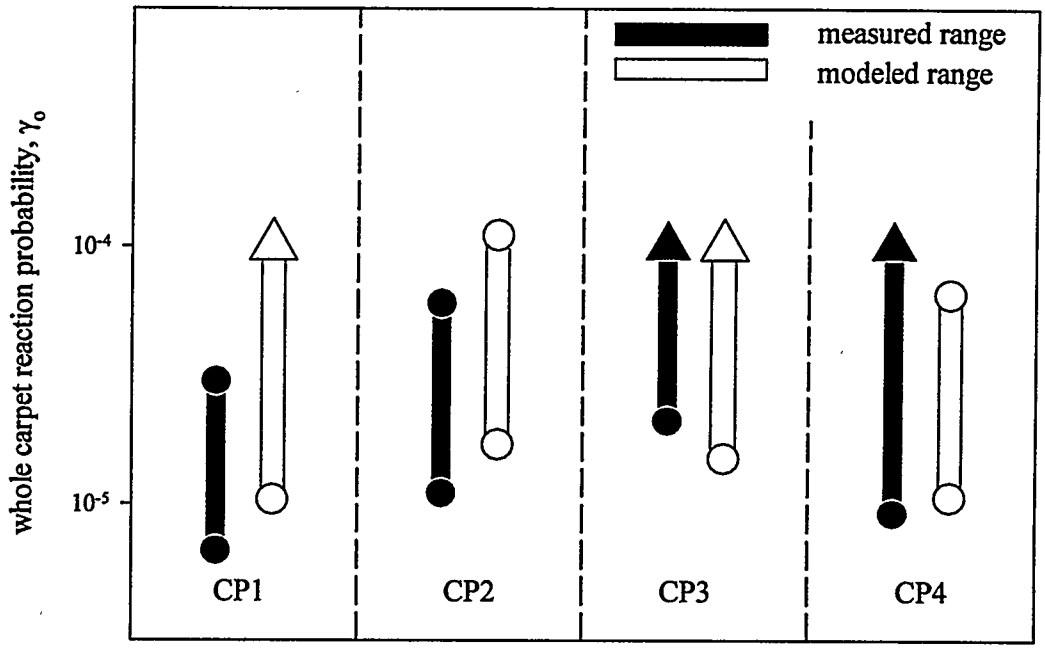

Figure 4.8. Range of whole carpet reaction probability, γ_o, values due to ozone aging of carpets CP1-CP4. Black bars represent the range of measured values, white bars represent the range of predicted values. Arrows indicate that the initial *measured* value was greater than 10^{-4} (black arrow), or initial fiber reaction probability, γ_f, used to derive the initial modeled γ_o, was greater than 10^{-5} (white arrow).

The whole carpet reaction probability, γ_o, obtained for CP3 (3.1×10^{-5}) at the end of 48 h (Table 3.2) is due to ozone reacting with fibers and backing whose reaction probability range has been measured. I applied these values to the one-dimensional fiber model to obtain a range over which I would expect γ_o to lie. For a fiber geometry given by

measurements of CP3 and allowing $\gamma_f = 10^{-5}$ and $\gamma_b = 5.0 \times 10^{-5}$ (the high range), the predicted whole carpet reaction probability is $\gamma_o = 9.1 \times 10^{-5}$. For $\gamma_f = 4.0 \times 10^{-7}$ and $\gamma_b = 2.7 \times 10^{-5}$ (the low range), the whole-carpet reaction probability result is $\gamma_o = 1.9 \times 10^{-5}$. This range of values includes the measured value of γ_o. A comparison of the measured and the predicted range of whole carpet reaction probabilities is shown in Figure 4.7. The black bars represent the range of values of γ_o measured experimentally, where the endpoints are given by the average value from those carpets tested twice or more. The white bars represent the range of values predicted using the model, where the input values of initial and final γ_f and γ_b are averages taken from Table 3.2.

The model captures the range of reaction probability values reasonably well. The aged whole-carpet reaction probability was about 10^{-5} for any given carpet. The model predicts this value as well. The initial value is more difficult to compare because it is often too high to measure or changes very rapidly at the beginning of an experiment. The model predicts that γ_o should be slightly higher than the value measured experimentally for carpets CP1, CP2 and CP4. This is surprising because the predicted value is based on a fiber reaction probability obtained in the fixed-bed reactor where cumulative uptake on fibers was potentially greater than that from the whole-carpet experiment. The average reaction probability of carpet fibers at the end of a fixed-bed experiment is likely to be lower than that of fibers at the end of a whole-carpet experiment, suggesting that the predicted whole-carpet value should be *lower* than the measured final value. The model also predicts that the initial value of CP4 is about 6×10^{-5}. However, the measured initial value was greater than 10^{-4}.

The fraction of ozone taken up by the fibers and backing was also obtained from

this model. For the geometric parameters used to obtain Figure 4.3, with $\gamma_f = 10^{-7}$, and $\gamma_b = 10^{-5}$, the fraction of ozone taken up by the fiber is 0.46 and by the backing is 0.54. For aged carpets, the fibers and backing consume ozone at approximately equal rates. For new carpets, the fibers take up most of the ozone.

4.6 Relative influence of carpet on indoor ozone removal

The large intrinsic surface area of carpet suggests that it may have the ability to take up much more ozone over the long run than flat surfaces. Painted or papered walls, carpeted, wood or vinyl flooring, and furniture all contribute to surface area in indoor spaces. However, few indoor furnishings contribute as much intrinsic surface area as carpet.

Much of the total superficial indoor surface area is due to walls, ceilings and floors. To evaluate the relative importance of painted walls to carpeted floor in reducing the ozone concentrations I looked to a published study of ozone interactions with latex paint. Under conditions (temperature and humidity) similar to those in this study, Reiss et al. (1994) showed that a painted surface in a tubular reactor aged such that the surface reaction probability dropped from 2×10^{-5} to 4×10^{-6}. I estimated the average cumulative uptake of ozone in their experiments to be about 0.5 $\mu g\ cm^{-2}$. The whole carpets in my studies were exposed to ozone such that the cumulative uptake was about 2 to 3 times higher than those in the Reiss et al. study. However, they further exposed paint samples to low levels of ozone in laboratory air for 9 months, reducing the reaction probability to 4×10^{-7}. The cumulative uptake of ozone could not be derived for this secondary exposure.

It is difficult to assign realistic values of reaction probability for comparison of

relative ozone uptake on painted and carpeted surfaces. This is because the reaction probability on either surface may decrease at different rates with exposure, and the installation of paint and carpet do not necessarily coincide. However, to facilitate the comparison, I evaluated three points in time, using the cumulative uptake of ozone as an independent variable to estimate the reaction probability on either surface. At time 1, the carpet and paint are installed concurrently and the reaction probability for paint and carpet are the measured initial values. At time 2, the cumulative uptake of ozone on each is about 0.5 $\mu g\ cm^{-2}$ (note that the time required to achieve this cumulative uptake value may be different for carpet and paint). At time 3, the final reaction probability measured for each material is used to represent a long period of exposure. Thus the latex paint reaction probability values for times 1, 2 and 3 are, respectively, 2×10^{-5}, 4×10^{-6}, and 4×10^{-7}. I averaged reaction probability values from all four carpets to obtain the respective carpet values at corresponding times of 5.1×10^{-5}, 1.7×10^{-5}, and 1.3×10^{-5}.

To determine the relative importance of carpet in reducing indoor concentrations of ozone, I compared the relative ozone removal rates on carpets and painted walls. The total rate of ozone deposition on all room surfaces is the sum of the individual rate terms. For example, in an unfurnished room, the total rate, r, of ozone removal would be represented by

$$r = C(v_{dc}S_c + v_{dw}S_w) \tag{4.65}$$

where v_{dc} is the carpet specific deposition velocity, v_{dw} is the wall specific deposition velocity, S_c is the horizontally-projected area of carpet (same area as defined for the determination of γ_o), and S_w is the total wall area. Thus the fractional rate of ozone removal by carpets, f, is

$$f = \frac{v_{dc} S_c}{v_{dc} S_c + v_{dw} S_w} \tag{4.66}$$

To calculate the individual deposition velocities in equation 4.66, I used the non-dimensional form of equation 4.14, with $u^* = 1$ cm s^{-1}. I assumed that the presence of carpet or wall roughness does not significantly enhance the deposition velocity by modifying fluid flow compared to flat surfaces. Thus equation 4.14 is valid for both surfaces.

I assumed that for an empty room, $(S_w/V)=1.6$ m^{-1}, and $(S_c/V)=0.4$ m^{-1}. Note that Mueller et al. (1973) estimated that the surface area to volume ratio of a furnished bedroom was 3.2 m^{-1} by evaluating each furnishing as a parallelpiped. In addition to the fractional uptake by carpet, I calculated the indoor/outdoor ozone concentration (C/C_o) in this room by using the steady-state version of equation 1.1 with no emission source and an air exchange rate, λ, of 1 h^{-1}. Figure 4.9 demonstrates predictions of "f" along with the indoor-outdoor ratio. I find that, at times 1, 2 and 3, respectively, $C/C_o = 0.20, 0.32, 0.54$ and $f = 0.23, 0.34, 0.77$. As these materials age, the carpet is transformed from a moderate ozone sink to the dominant ozone sink, and the ratio of indoor to outdoor ozone increases. Using a 24 h mean outdoor ozone value of 37 ppb, (the middle of a range of yearly average value for the Los Angeles area of 20-54 ppb; Cass et al., 1991), I estimate that it would require about 5 d to achieve 0.5 μg m^{-3} on carpet surfaces in this room. Thus while the large superficial area of walls is initially very important, after a relatively brief period of aging, the high intrinsic surface area of carpet causes it to dominate as a sink for ozone removal. The area weighted deposition velocity, $\overline{v}_d$, values for times 1, 2 and 3 are 0.056, 0.029, 0.012 cm s^{-1}.

Typical values of C/C_o range between 0.1 and 0.8 (Weschler et al., 1989). While these values surround my predicted range of C/C_o , Weschler reported that the range of values indoors is most strongly influenced by ventilation rate. Nazaroff et al. (1993) reported that the room averaged indoor deposition velocity for ozone clustered around 0.04 cm s^{-1} as inferred from field studies. Surfaces in buildings would typically have been exposed to more ozone than surfaces in my experiments, implying lower surface reactivity on surfaces in field sites. If the deposition velocity is about the same in all settings, then buildings characteristics may also be very similar, e.g. surface reactivity. This implies that aging of surfaces may not significantly influence ozone loss rates. Perhaps rapid aging results in a relatively stable value of the surface reaction probability, or other phenomena work to counteract aging (e.g. regeneration).

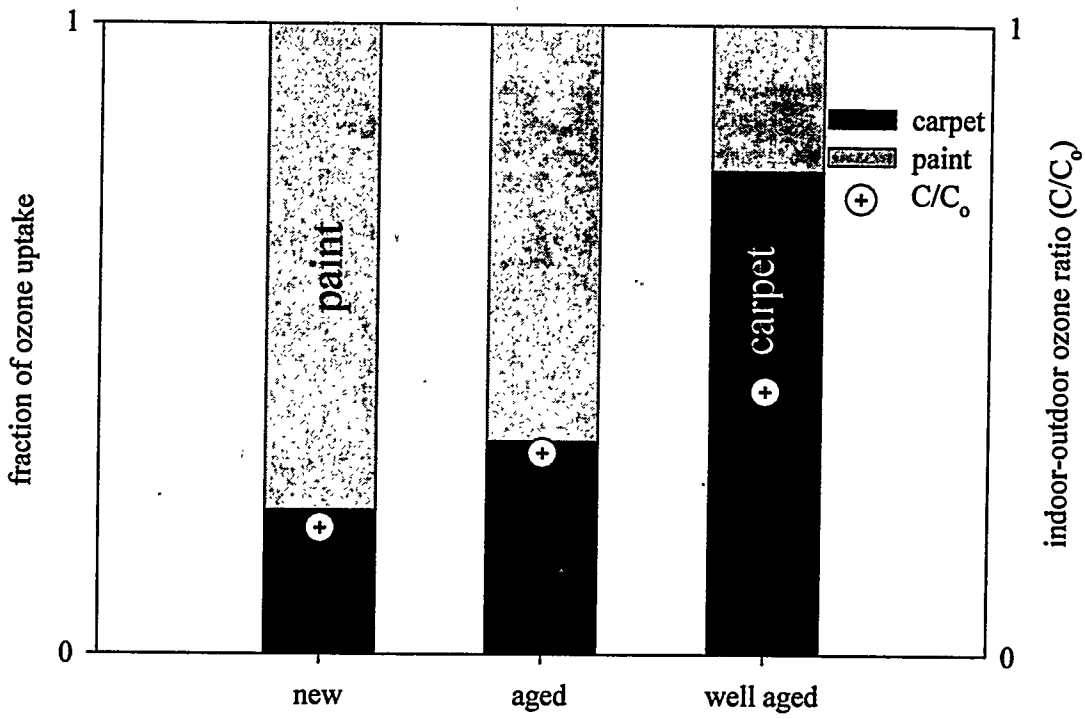

Figure 4.9. Relative influence of carpet and painted walls on ozone deposition when progressively aged. Black bars represent fraction of deposition due to carpet. Carpet becomes a dominant sink for ozone when both surfaces are well aged. The indoor-outdoor ratio of ozone (C/C_o) increases as both surfaces age, losing the ability to remove ozone from the indoor space.

4.7 Conclusions

In this chapter, I show that the internal surface area of carpet can be an important sink for ozone. The overall reaction probability of whole carpet is dependent on the geometry of carpet and on the specific reaction probability of the fiber and backing surface. Two transport models were developed to describe pollutant uptake in the carpet mat. I found that a one-dimensional model can satisfactorily describe ozone uptake on carpet with a typical fiber density, diameter and length. A two-dimensional model helps to describe radial concentration gradients that occur when the fiber reaction probability is very high, but the additional complexity is unnecessary for most circumstances. I show that the

model predicts the correct order of magnitude for the whole-carpet reaction probability when comparing model predictions with laboratory measurements. Model results also show that the ozone uptake is distributed approximately evenly between fiber surfaces and carpet backing for well aged carpet components.

I modified an existing model of turbulent mass transfer in enclosures to enable prediction of deposition velocity of reactive gases onto smooth surfaces. I combined this with the results of my experiments to show that, under typical indoor conditions, aged carpets may be a dominant ozone sink in a room with aged painted walls.

A limitation of this study is that a better model of mass transport of reactive gases to rough surfaces needs to be developed. The Lai-Nazaroff mass-transfer model is only valid for smooth surfaces and may not adequately predict deposition velocities due to roughness elements (carpet fiber tips) disturbing the turbulent boundary layer. I show that for roughness elements much smaller than 1 cm, the smooth surface model is probably sufficient. But for larger scale roughness features, a model which includes roughness should be coupled with a description of enhanced mass transfer in the advective zone below the fiber tips.

4.8 References

Bird, R.B.; Stewart, W.E.; Lightfoot, E.N. *Transport Phenomena*. John Wiley and Sons: New York. 1965.

Bejan, A. *Convection Heat Transfer*. 2nd ed. John Wiley and Sons: New York. 1995.

Brunn, H.H. *Hot-wire Anemometry: Principles and Signal Analysis*. Oxford University Press: Oxford, UK. 1995.

Cano-Ruiz, J.A.; Kong, D.; Balas, R.B.; Nazaroff W.W. *Atmospheric Environment*. **1993**, *27A*, 2039-2050.

Cass, G.R.; Nazaroff, W.W.; Tiller, C.; Whitmore, P.M. *Atmospheric Environment.* **1991**, *25A*, 441-451.

Corner, J.; Pendlebury, E.D. *Proceedings of the Physical Society.* **1951**, *B64*, 645-654.

Crump, J.G.; Seinfeld, J.H. *Journal of Aerosol Science.* **1981**, *12*, 405-415.

Einstein, A. *Ann. Physik.* **1905**, *17*, 549-560.

Hinds, W.C. *Aerosol Technology.* 2nd ed. John Wiley & Sons: New York. 1999.

Jerde, J. *Encyclopedia of Textiles.* Library of Congress-in-Publication Data. 1992.

Kim, J.; Moin, P.; Moser, R. *Journal of Fluid Mechanics.* **1987**, *177*,133-166.

Lai, A.C.K.; Nazaroff, W.W. *Journal of Aerosol Science.* **2000**, *31*, in press.

Massman, W.J. *Atmospheric Environment.* **1998**, *32*, 1111-1117.

Mueller, F.X.; Loeb, L.; Mapes, W.H. *Environmental Science and Technology.* **1973**, *7*, 342-346.

Nazaroff, W.W.; Ligocki, M.P.; Ma, T.; Cass, G.R. *Aerosol Science and Technology.* **1990**, *13*, 332-348.

Nazaroff, W.W.; Gadgil, A.J.; Weschler, C.J. in *Modeling of Indoor Air Quality and Exposure*, STP 1205, Nagda, N.L.; Ed. American Society for Testing and Materials: Philadelphia, PA, 1993.

Reiss, R.; Ryan, P.B.; Koutrakis, P. *Environmental Science and Technology.* **1994**, *28*, 504-513.

Welty, J.R.; Wicks, C.E; Wilson, R.E. *Fundamentals of Momentum, Heat and Mass Transfer.* John Wiley & Sons: New York, 1984.

Weschler, C.J.; Shields, H.C.; Naik, D.V. *Journal of the Air and Waste Management Association.* **1989**. *39*, 1562-1568.

Whitaker, S. *Fundamental Principles of Heat Transfer.* Pergamon Press: New York. 1977.

Zhang, J.S.; Shaw, C.Y.; Nguyen-Thi, L.C.; MacDonald, R.A.; Kerr, G. *ASHRAE Transactions.* **1995**, *101 part 2*, 116-124.

CHAPTER 5

Ozone Aging of Surfaces: Mechanisms and Models

5.1 Background

In this chapter, I explore possible causes of ozone "aging" of surfaces and compare them to experimental results. Aging is defined in this context as the progressive decrease in the ozone/surface reaction probability due to ozone exposure. This phenomena was initially reported by Altschuller and Wartburg (1961) and has been verified by several other researchers (Sabersky et al., 1973; Mueller et al., 1973; Reiss et al., 1994). In buildings, ozone aging of surfaces has the potential to reduce the effectiveness of surfaces in scavenging ozone. Surface aging can result in a higher indoor ozone concentration, relative to outdoor levels, effectively increasing exposure to building occupants.

In experiments described in Chapters 2, 3 and 6, all materials (specifically carpet, carpet components, and materials that line ducts) that I exposed to ozone exhibited aging. I found that the aging phenomena tends to follow this general form,

$$\gamma = A(U)^B \tag{5.1}$$

where γ is the surface reaction probability, U is the cumulative uptake of ozone and A and B are constants. The coefficient and exponent are unique for each carpet and component and are designated A_o and B_o for whole carpet, A_f and B_f for fibers, and A_b and B_b for backing. Several examples of this relationship are shown in Figure 5.1. This figure shows the results of three experiments, two measuring the reaction probability on carpet fibers (CP2 and CP3, length averaged reaction probability, $\bar{\gamma}_f$) and one whole

carpet experiment (CP2, whole carpet reaction probability, γ_o). As noted in Chapter 3, the length averaged reaction probability approximates the actual fiber surface reaction probability in the latter stages of the experiment. In this plot I have extended the rule stated in Section 3.3 to include more data points. This is to emphasize that the power-law nature of $\bar{\gamma}_f$ is persistent over most of the experimental range.

After a cumulative uptake of about 0.01 μg cm^{-2} of ozone on CP2 fibers, the data follow the power function of equation 5.1, with A= 4.2×10^{-8} [(μg cm^{-2})$^{0.91}$] and B = -0.91. The fibers from carpet CP4 behaved in a similar way, but the aging profile for fibers from carpets CP1 and CP3 was much steeper, with parameter B ranging from -2.2 to -5.3. Experiments with whole carpets, carpet backing and duct liners (see Chapter 6) generally resulted in more shallow aging curves, with parameter B ranging from -0.07 to -0.45. The purpose of this chapter is to explore mechanisms that may cause the observed behavior. I also show how the models used in the explorations can help to explain the phenomenon known as regeneration.

In Chapters 2 and 6, I show that volatile oxidized products are released from surfaces exposed to ozone. Ozone reactions that occur at or just below the surface can form products that may immediately leave the surface (or rapidly diffuse to the surface and volatilize). I suggest that the most likely ozone uptake mechanisms fall into two classes: (1) ozone may adsorb, then diffuse into the bulk of the material to react at internal reaction sites; (2) ozone may adsorb on a surface and react at or near the interface of the air and the surface. I explore both of these general mechanisms, including the influence of reaction rates, reaction orders, and material geometry. Mechanism (1) is analyzed by developing mathematical descriptions of ozone diffusion into, and reaction

with, internal sites present in an infinite slab and in a cylinder. Along with specific assumptions, the system of equations developed describes a Stefan problem (Crank, 1975) that can be solved analytically. A more general numerical solution to mechanism (1) is also discussed. Mechanism (2) is analyzed by developing a mathematical description of ozone sorption and reaction with sites present only at the solid surface of a material. Where the reaction is first order in both ozone and surface sites, the equations can be solved analytically.

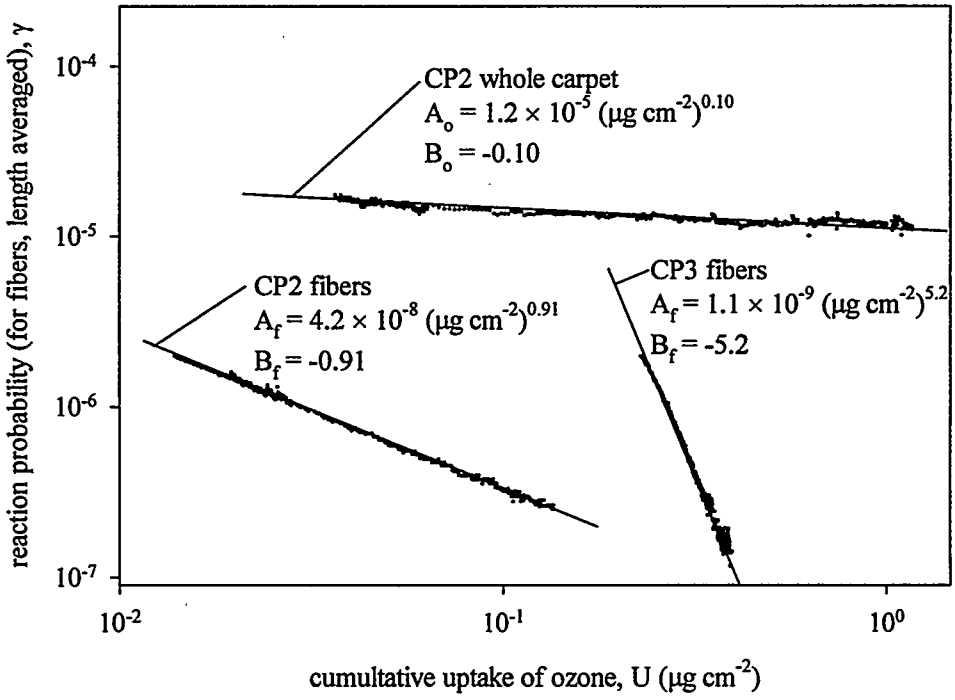

Figure 5.1. Selected data for comparison of regression results. Data from CP2 fibers and whole carpet experiments and CP3 fibers experiment.

Modeling pure surface kinetics does not seem to be able to adequately describe the observed behavior. A model of ozone diffusion into a slab with internal reaction sites does work well for a fixed value of B, but does not shed light on the experimentally observed variability in the coefficient B. Combining ozone diffusion/reaction in the bulk of carpet fibers with the carpet model described in Chapter 4, I find that the diffusion

model predicts that the power-law coefficient for whole carpet, B_o, will vary in response to the fiber-ozone kinetics. However, model calculations using independent measurements of the aging of fibers and backing to predict whole-carpet aging do not match well to the experimental results.

5.2 Surface aging due to diffusion of ozone into material with internal reaction sites

The first aging mechanism to consider is diffusion into the bulk material with reaction occurring at internal reaction sites. This analysis assumes that reactive surface sites have already been quenched. I discuss the kinetics of surface reactions in a later section. As sites are used up on the surface, ozone will have the opportunity to bypass the top surface of the material and migrate below the surface. Migration may occur by diffusion through macro or micro-pores into the material, or by diffusion into the bulk solid itself. In my experiments, the "bulk solid" is commonly a solid polymer or perhaps an oil coating.

It is generally accepted that ozone reacts in a first-order manner with building surfaces (Mueller et al., 1973; Sabersky et al., 1973). I will follow this rule in further analysis, but recognize that reaction sites may not always react with ozone in a first-order manner. The general form of the ozone (C) reaction with internal reaction sites (S) is

$$C + nS \rightarrow \text{products} \tag{5.2}$$

where n is the order of the reaction with respect to internal sites. The reaction rate (r) for fundamental kinetics is

$$r = -bS^n C \tag{5.3}$$

where b is a rate constant.

First, consider a system in which ozone diffuses into a flat slab of a solid material, and the reaction is first-order in both reactants (n=1). The governing one-dimensional equation describing the time dependent concentration of ozone within the solid material is

$$\frac{\partial C}{\partial t} = D_c \frac{\partial^2 C}{\partial z^2} - bSC \tag{5.4}$$

where, S and C are the volumetric concentrations of reaction sites and ozone in the solid material and D_c is the diffusion coefficient of ozone in the solid. The reaction sites may be stationary (as would be the case in which a large polymeric molecule has double bonds in its structure), or mobile (as in a reactive solvent). If mobile, the concentration of mobile sites is governed by

$$\frac{\partial S}{\partial t} = D_s \frac{\partial^2 S}{\partial z^2} - bSC \tag{5.5}$$

where D_s is the diffusion coefficient in the solid of mobile sites. The concentration of *stationary* sites is given by the above equation, without the diffusion term. This set of equations is nonlinear and cannot be solved explicitly without key simplifications.

Here, I discuss the dynamics of systems governed by these equations by examining specific cases. In general, however, some simplifications will apply to any case that includes ozone as the gaseous constituent diffusing into a solid polymeric slab. The diffusivity of ozone is likely to be much higher than that of the reactive compound (e.g., a reactive solvent molecule) or site S. Thus, in the short-term, the stationary form of equation 5.5 is appropriate. It is well known that the structural properties of polymers can change significantly as compounds diffuse into the polymer, stressing the matrix. The

concentration of ozone in the gas phase is very small compared to that of other gases (O_2, N_2) and is unlikely to significantly influence the structural properties of the solid as it displaces other gases. Thus, the diffusivity of ozone will be assumed to be both spatially and temporally constant.

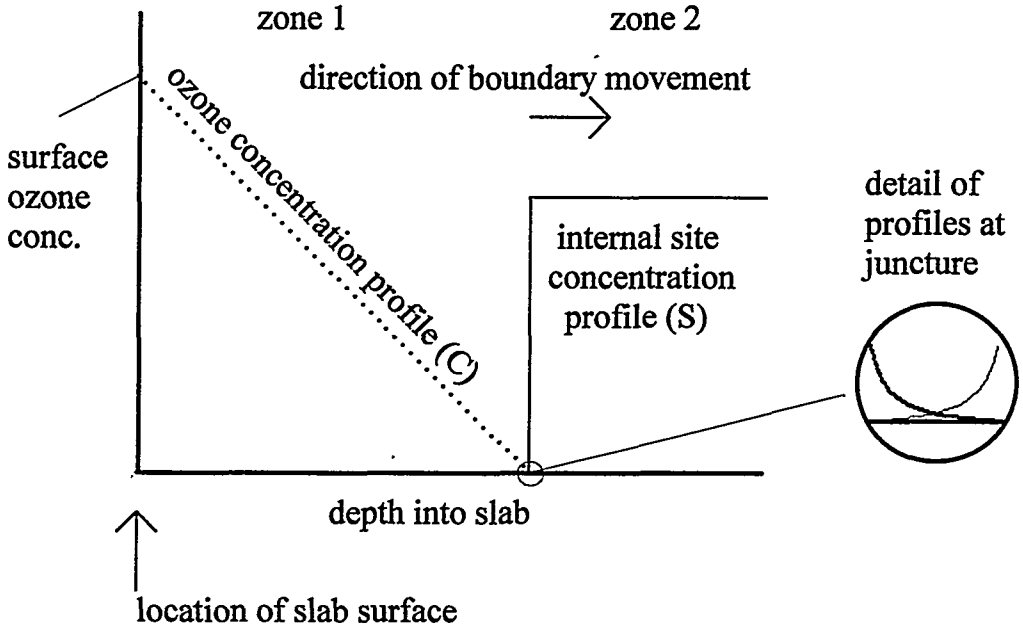

Figure 5.2. Diagram of moving boundary diffusion with reaction system (Stefan problem). Ozone (C) forms a linear concentration profile while oxidizing internal sites (S). The boundary between regions of high S concentration (zone 2) and low S concentration (zone 1) moves slowly to right of diagram.

5.2.1 Case 1: Stationary sites, flat, semi-infinite slab

Assume that the ozone-site reaction takes place very quickly, and there are not many sites available. These conditions can result in a system with a moving boundary, commonly referred to as a Stefan problem (Crank, 1975). Please refer to Figure 5.2 for a schematic representation. The flux of ozone into the slab is exactly equal to the rate at which sites are being consumed by ozone at the boundary per unit area. All reaction sites in the zone between the surface of the slab and the reaction front have been fully oxidized. There is a small zone in the region of the reaction front that does not adhere to

these assumptions (in the circular window), but its extent is small compared to the length of the zone that is fully oxidized.

Mathematically, this is treated as follows. The reaction rate is very fast, but in zone 1, the term bSC is zero because S=0 everywhere in zone 1. Equation 5.5 becomes inapplicable in zone I for the same reason. If the diffusivity is large enough, the time-dependent nature of the concentration profile can be neglected in a pseudo steady-state analysis. Thus, the following equation applies:

$$\frac{d^2C}{dz^2} = 0 \tag{5.6}$$

with these boundary conditions :

$$C = C_o \qquad \text{at } z = 0 \tag{5.7}$$

$$C \cong 0 \qquad \text{at } z = Z \tag{5.8}$$

In other words, the concentration at the surface is assumed to be constant and the second order rate constant is very large. The surface concentration was controlled at a nearly constant level for my experiments so the boundary condition in equation 5.7 would be applicable for model comparisons with experimental aging results.The pseudo steady-state concentration profile of ozone in this slab is linear and given by

$$C = C_o - \left(\frac{C_o}{Z}\right)z \tag{5.9}$$

We are interested in connecting the reaction probability, γ, of ozone at the surface to the cumulative uptake of ozone in the slab. The latter is simply the initial concentration of reaction sites times the length of zone 1

$$U = S_o Z \tag{5.10}$$

the reaction probability can be shown to be related to the flux at the surface by

$$\text{Flux} = \gamma\left(\frac{\langle v\rangle}{4}\right)C_o^g = -D_c\frac{dC}{dz} \tag{5.11}$$

where C_o^g is the gas phase concentration of ozone at the surface. The gas-phase concentration can be connected to the solid-phase ozone concentration at the surface by the solubility of ozone in the solid. Assuming that the partitioning between gas and solid phase at the interface (z=0) is at equilibrium

$$C_o = C_o^g\sigma \tag{5.12}$$

where σ is the solubility of ozone in the solid. Combining equations 5.9-5.12, I find that

$$\gamma = \frac{4D_c\sigma S_o}{\langle v\rangle U} \tag{5.13}$$

Equation 5.13 is of the form

$$\gamma = A(U)^B \tag{5.14}$$

where

$$A = \frac{4PS_o}{\langle v\rangle} \tag{5.15}$$

and B= -1. P is the permeability of ozone in the slab given by,

$$P=D_c\sigma \tag{5.16}$$

Equation 5.13 corresponds reasonably well with the dynamic behavior of systems such as that exhibited by ozone interactions with CP2 fibers (Figure 5.1) and CP4 fibers (B ranges from -0.8 to -0.91 with one outlier of -0.5). Equation 5.13 does not correspond to the empirical results of ozone aging of CP1 and CP3 fibers, which are presumably of similar geometry. Carpet fibers are not strictly flat slabs, so I discuss the influence of cylindrical geometry on these results in a later section.

The time-dependent nature of this system can also be determined. I find that the length of zone 1 will increase as a function of the square root of time when C_o is constant,

$$Z = \sqrt{\frac{D_c C_o t}{S_o}} \tag{5.17}$$

I assume that the cumulative uptake is zero at t=0. Combining equations 5.10, 5.13 and 5.17,

$$\gamma = \frac{4\sigma}{\langle v \rangle}\sqrt{\frac{D_c S_o}{C_o t}} \tag{5.18}$$

A plot of log(γ) vs. log(t) should yield a straight line with slope = -½.

5.2.2 Case 2: Stationary sites, cylindrical fibers

The fibers analyzed in my carpet work may be more amenable to diffusion analysis using cylindrical geometry. In cylindrical coordinates, the equations 5.4 and 5.5 are transformed to these forms:

$$\frac{\partial C}{\partial t} = D_c \frac{1}{r}\frac{\partial}{\partial r} r \frac{\partial C}{\partial r} - bSC \tag{5.19}$$

$$\frac{\partial S}{\partial t} = D_s \frac{1}{r}\frac{\partial}{\partial r} r \frac{\partial S}{\partial r} - bSC \tag{5.20}$$

A similar pseudo steady-state analysis can be applied to this system using the assumptions of Case 1. The results of this analysis in cylindrical coordinates are shown here

$$C = C_o\left(1 - \frac{\ln R - \ln r}{\ln R - \ln r'}\right) \tag{5.21}$$

$$\gamma = \frac{4P}{R\langle v \rangle}\left(\ln R - 0.5\ln\left(R^2 - \frac{U}{\pi S_o}\right)\right)^{-1} \tag{5.22}$$

where R is the radius of the cylinder and r′ is the location of the reaction front. The time dependent solution of the location of the reaction front, r′, is given by the transcendental equation,

$$r'^2 \ln r'^2 - r'^2 = \frac{4D_c C_o}{S_o} t - R^2 \tag{5.23}$$

which is valid where r′>0. Equation 5.22 does not, by itself, conform to equation 5.1. Surprisingly, however, plotting γ vs U using this equation results in a curve that mimics equation 5.1 very well, with B = -1.

Thus, in the case of diffusion of ozone into both a flat sheet and a cylindrical fiber, I find that the coefficient B is equal to –1. This may indicate that geometry is not so important, but that the process of diffusion is central to aging kinetics with a form as in equation 5.1. Still, only some of the experimental observations of aging are well described by this model.

5.2.3 Numerical analysis of governing equations of diffusion and reaction with internal sites

The mechanisms described in Sections 5.2.1 and 5.2.2 do not explain why some surfaces experience ozone aging such that they have values of the coefficient B other than –1 and ranging from –0.5 to -5. Several assumptions need to be relaxed to find situations where B ≠ -1. If no assumption is made about the relative magnitude of S_o, C_o, and b, then both governing equations (5.4, 5.5) may apply. The diffusion expression in equation 5.5 will still be ignored by retaining the assumption reaction sites, S, are stationary. Equations 5.4 and 5.5 will now be cast in non-dimensional form:

$$\frac{\partial C'}{\partial t'} = \alpha \frac{\partial^2 C'}{\partial z'^2} - \beta S' C' \tag{5.24}$$

$$\frac{\partial S'}{\partial t'} = -\delta S' C' \tag{5.25}$$

where

$$C' = \frac{C}{C_o} \tag{5.26}$$

$$S' = \frac{S}{S_o} \tag{5.27}$$

$$t' = \frac{t}{\tau} \tag{5.28}$$

$$\alpha = \frac{D_c \tau}{L^2} \tag{5.29}$$

$$\beta = bS_o\tau \tag{5.30}$$

$$\delta = bC_o\tau \tag{5.31}$$

where τ is a characteristic time scale and L is the thickness of the slab. There are three dimensionless coefficients, α, β and δ, that can be adjusted to determine under what conditions $B \neq -1$. Boundary and initial conditions for solving equations 5.24 and 5.25 are similar to those described in Section 5.2.1:

$$C'(t,0)=1 \tag{5.32}$$

$$S'(0,z)=1 \tag{5.33}$$

For this system, the equations are solved for a finite slab to investigate the influence that depletion of internal sites may have. I assume that the flux of ozone at the opposite end of the slab ($z = L$) is zero:

$$\frac{dC'}{dz'} = 0 \qquad \text{at } z' = 1 \tag{5.34}$$

This boundary condition defines a slab of thickness 2L that has a concentration $C' = 1$ at both sides, or a slab of thickness L that has an impermeable barrier at $z = L$. In the system where $C' \sim 0$ at $z = L$ for the entire time period over which the equations are solved, the system resembles an infinite slab. Therefore, this set of initial and boundary conditions covers most systems of interest.

The reaction probability, γ, and cumulative uptake, U, cannot be determined explicitly in this system without assumptions about the gaseous ozone concentration and the gas-solid partition coefficient (solubility), σ. Instead, I use the non-dimensional slope and its time integral as surrogates to determine B. As shown in equation 5.11, the reaction probability, γ, is proportional to the slope of the concentration profile at $z = 0$. The reaction probability is therefore also proportional to the non-dimensional slope at $z' = 0$:

$$\gamma \propto \left.\frac{dC'}{dz'}\right|_{z=0} \equiv \tilde{\gamma} \tag{5.35}$$

The symbol $\tilde{\gamma}$ is used to signify this dimensionless slope. By similar arguments, cumulative uptake, U, at time $t' = t_1'$ is proportional to the time integral of the slope at $z' = 0$:

$$U \propto \int_{t'=0}^{t_1} \left.\frac{dC'}{dz'}\right|_{z'=0} dt'' \equiv \tilde{U} \tag{5.36}$$

where t" is a dummy variable for integration and the symbol $\tilde{U}$ is used to signify this integral.

Just as the coefficient B is found to be the slope of the linearized form of equation 5.14,

$$\log_{10}(\gamma) = \log_{10}(A) + B \log_{10}(U) \tag{5.37}$$

the coefficient B is also the slope of equation 5.37 where γ and U are replaced by $\tilde{\gamma}$ and $\tilde{U}$ respectively.

The order of magnitude of the coefficient α can be found by using values relevant to ozone diffusing into carpet fibers. The diffusion coefficients for ozone in the nylon or poly-olefin fibers are not available. However the diffusion coefficient of H_2O (used as a surrogate for O_3) in nylon was shown to be about 10^{-10} to 10^{-8} cm^2 s^{-1}depending on the water concentration in nylon (Rouse, 1947). The characteristic time, τ, will be taken as 24 h, a typical experimental time period. The fiber diameter was of the order of 50 to 100 mm. The value of the coefficient, α, then ranges from about .08 to 35. A range of values for b, S_o, or C_o are unknown at this time. Instead, the coefficients β and δ were arbitrarily varied to determine under what conditions $B \neq -1$.

Numerical techniques described by Press, et al., were used to solve equations 5.24 and 5.25. The solution techniques are similar to those outlined in Appendix A.4. Based on the numerical analysis, a plot of $\tilde{\gamma}$ vs. $\tilde{U}$ was created to demonstrate the evolution of B (the slope) over the simulated time period. The plot appears nearly linear during time intervals where B is nearly constant. An example of concentration, C′, profiles at t′ = 0.02, 0.1, 0.5 and 1 are shown in Figure 5.3(a) for these coefficients: $\alpha = 0.5$, $\beta = 0.0005$, $\delta = 0.5$. A plot of log $\tilde{\gamma}$ vs. log $\tilde{U}$ is shown in Figure 5.3(b) and the slope, B, as a function of t′ is shown in Figure 5.3(c).

In this simulation, ozone, represented by C′, reaches z′ = 1 at about t′ = 0.1. The plot of $\log(\tilde{\gamma})$ vs. $\log(\tilde{U})$ appears nearly linear over the whole range, with the exception that it curves slightly downward between t′ = 0.5 and t′ = 1. In the region between t′ =

0.02 and $t' = 0.04$, B = -1. This suggests that in time intervals where the slab thickness is greater than the depth of ozone penetration, the predictions of Section 5.2.1 are robust, even where ozone concentration profiles are not linear.

The downward curvature between $t' = 0.5$ and $t' = 1$, is reflected in the plot of the slope in Figure 5.3(c). The value of the slope, B, starts to become smaller than -1 and eventually reaches B = -2.28 at $t' = 1$. This behavior is due to the fact that the ozone is beginning to deplete reaction sites in the center of the slab (with a thickness 2L). The assumption that the slope of the ozone concentration profile gets shallower as ozone reaches deeper into the slab is no longer valid because ozone has reached a barrier, changing the functional dependence of $\tilde{\gamma}$ vs. $\tilde{U}$. The value of B will continue to become smaller as $t' > 1$, As t' approaches infinity, B approaches $-\infty$.

Clearly, the plot of $\log(\tilde{\gamma})$ vs. is not linear in the region between $t' = 0.5$ and $t' = 1$ because the slope, B, varies from -1.13 to -2.28. However, a linear regression of $\log(\tilde{\gamma})$ vs. $\log(\tilde{U})$ in this region is fairly linear, with $r^2 = 0.991$, and B= -1.55. Depletion of sites in the center of the fiber may explain the appearance of a linear functionality in fiber experiments where B < -1. Alternatively, this behavior may be attributed to depletion of sites in a thin coating on the fiber. For example, fibers from carpet CP3 released a large amount of oxidized emission products that may have originated from a layer of oil on the surface. The diffusion coefficient in the oil layer may be much greater than that in the fiber itself. Thus the fiber surface may seem impermeable (simulating the zero flux boundary condition at $z' = 1$), relative to the permeability of the oil.

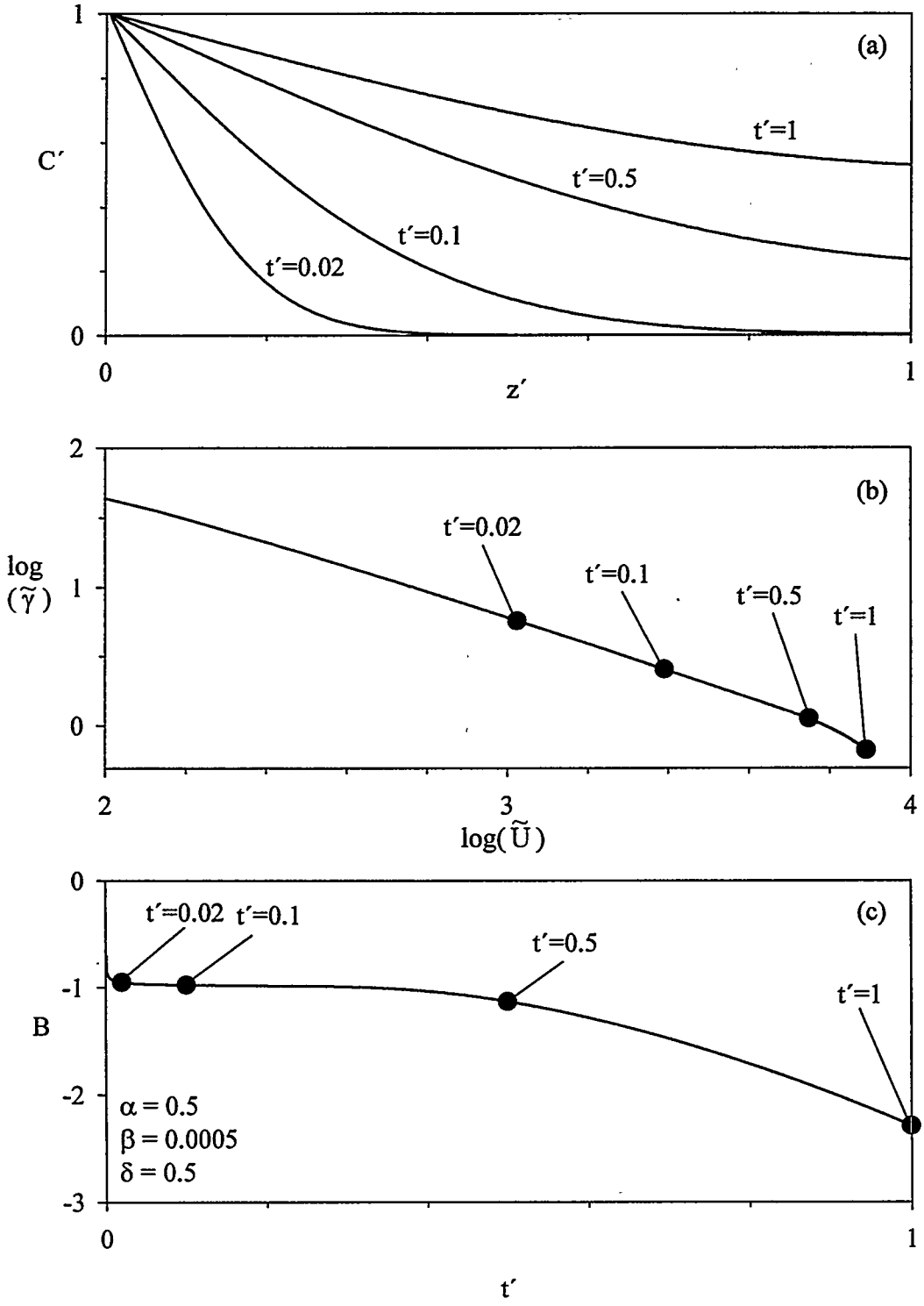

Figure 5.3. Numerical analysis of diffusion of ozone into slab with internal reaction: α = 0.5, β=0.0005, δ=0.5. a) plot of C′ vs. t′ with dimensionless concentration profiles at t′=0.02, 0.1, 0.5, and 1; b) plot of log($\tilde{\gamma}$) vs. log($\tilde{U}$); c) plot of B vs t′.

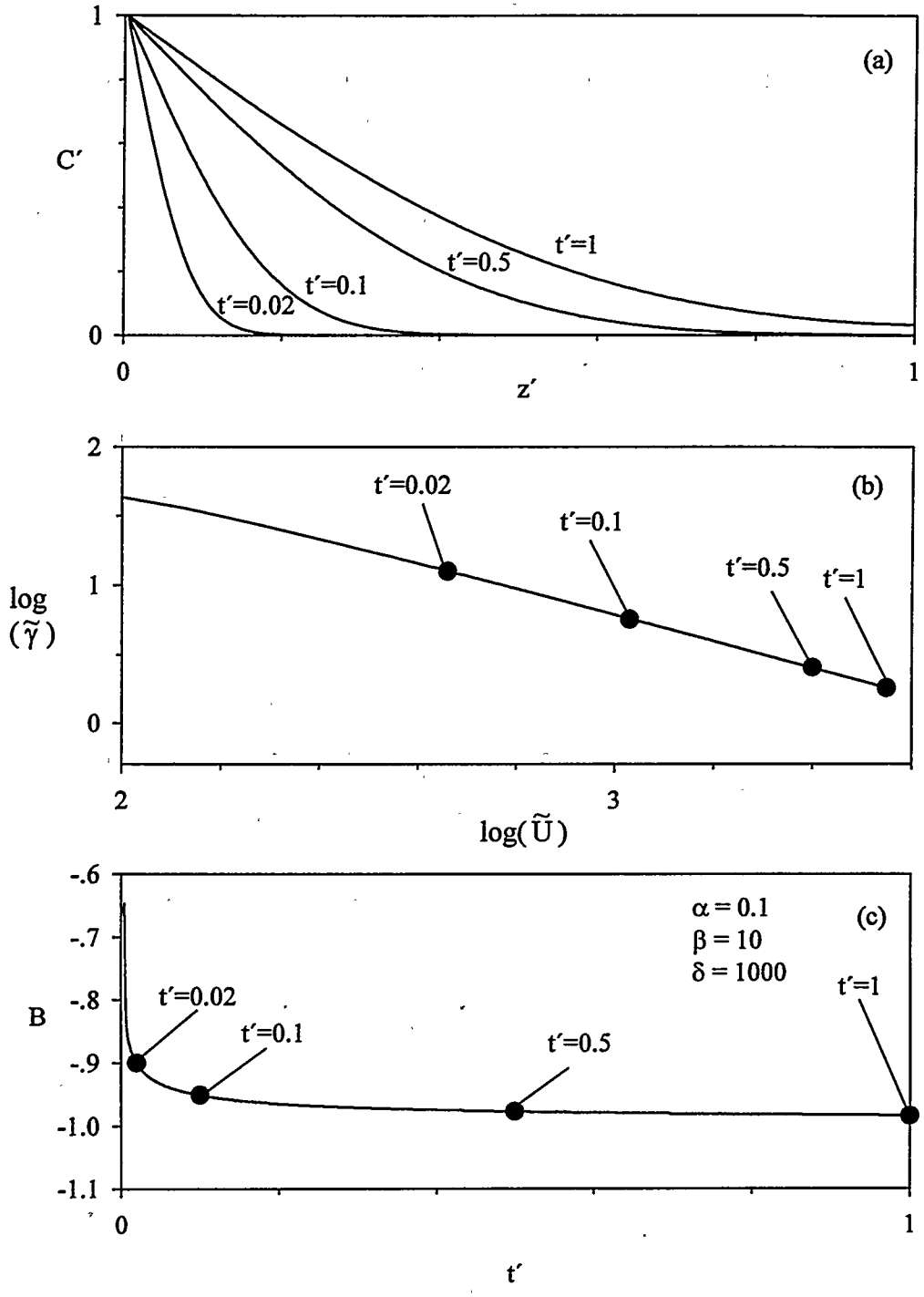

Figure 5.4. Numerical analysis of diffusion of ozone into slab with internal reaction: $\alpha = 0.1$, $\beta=10$, $\delta=1000$. a) plot of C′ vs. t′ with dimensionless concentration profiles at t′=0.02, 0.1, 0.5, and 1; b) plot of $\log(\tilde{\gamma})$ vs. $\log(\tilde{U})$; c) plot of B vs. t′.

A system in which ozone has not yet reached deeply into a slab may explain values of B greater than –1. The results of a simulation for a different set of coefficients (α=0.1, β=10 and δ=1000) are shown in Figure 5.4. In this simulation. the slope, B, is initially greater than –1 before the concentration profile reaches deeply into the slab. As the simulation progresses, B rapidly approaches -1. A linear regression of $\log(\tilde{\gamma})$ vs. $\log(\tilde{U})$ over the entire time interval shown results in B = -0.944 and $r^2 = 0.998$. Thus values of B greater than –1, such as those found for CP2 and CP4 fibers, may be explained by the dynamics of ozone diffusion and reaction, where ozone has not yet reached deeply into the fibers.

5.3 Surface aging due to surface reaction kinetics

In this section, I consider the possibility that ozone aging is due to irreversible ozone reactions with surface sites; the flux of ozone to the surface is a result of ozone loss at surface sites only. These sites become oxidized or otherwise inactive to further ozone reactions. If the flux is proportional to the remaining number of sites, then the flux will decrease with ozone exposure, perhaps resulting in the observed aging phenomena.

In this analysis, I find that the reaction probability response to cumulative uptake on a surface does not match that found for most materials studied in my research. However, for a clean, aluminum plate, a mechanism of surface site loss fits the observed ozone-aging profile will be shown in Section 5.5.

5.3.1 Case 3: Reaction 1st order in S and C, reaction sites identical

Consider a surface covered with a variety of reaction sites. These may be unsaturated compounds, reactive carbon sites, etc. Different sites may have different

reaction rates with ozone, due to species, location, or orientation. Initially, I assume that the surface is covered with a finite number of identical reaction sites, and that the reactions are first order with respect to both adsorbed ozone and the surface sites. Here is a description of the chemical mechanism:

$$C_o^g \leftrightarrow C \qquad \text{adsorption of ozone (C) to surface} \qquad (5.38)$$

$$C + S \rightarrow C - S \qquad \text{ozone reaction with surface sites (S)} \qquad (5.39)$$

The loss rate of surface sites is given by,

$$\frac{dS}{dt} = -b \cdot S \cdot C \qquad (5.40)$$

where S is the concentration of surface sites available for reaction (not yet reacted), C is the surface concentration of adsorbed ozone, and b is the reaction rate constant. The rate of change of the surface ozone concentration is given by,

$$\frac{dC}{dt} = \frac{\gamma < v >}{4} C_o^g - b \cdot S \cdot C \qquad (5.41)$$

where <v> is the Boltzmann velocity (3.6×10^4 cm/s) for ozone, and C_o^g is the concentration of ozone in the gas phase adjacent to the surface. The first term on the right-hand side describes the flux of ozone to the surface. The power-law functional dependence on cumulative uptake (equation 5.1) has been observed for reaction probabilities of about 10^{-5} and lower. This means that 99.99% of the ozone molecules that strike the surface bounce away, or are reversibly adsorbed. If a surface adsorption isotherm exists for ozone (equation 5.38), it is likely that an equilibrium state will exist, where surface reactions do not significantly change C over time. This means that the rate of change of C in equation 5.41 is zero. Further, since the ozone concentration used in these studies is very small, approximately one part in ten million, I will assume that the

adsorption isotherm is linear:

$$C_o^g = a \cdot C \tag{5.42}$$

where a is the proportionality constant for the linear isotherm. Combining equations 5.41 and 5.42, I find that

$$\gamma = \frac{4 \cdot b \cdot S}{a < v >} \tag{5.43}$$

For the duration of most of my experiments, the bulk ozone concentration was controlled at a constant value. The concentration of ozone near the surface, C_o^g, is also nearly constant for the duration of the experiment because the low reaction probability prevents a strong concentration gradient from forming (valid only where $\gamma << \gamma_{crit}$; see Section 4.2.2). Thus, equation 5.40 can be directly solved for S,

$$S = S_o e^{-b \cdot C \cdot t} \tag{5.44}$$

where S_o is the initial concentration of surface sites. Thus, combining equations 5.43 and 5.44, I obtain

$$\gamma = \left(\frac{4 \cdot b \cdot S_o}{a < v >} \right) e^{-\frac{b}{a} C_o^g \cdot t} \tag{5.45}$$

The term in parentheses represents the initial reaction probability subject to the limitation that this analysis may not be valid were the reaction probability is high in the initial moments of exposure.

The cumulative uptake of ozone on the surface can be found by taking the integral over time of the flux to the surface,

$$U = \int_0^t \frac{\gamma < v > C_o^g}{4} dt' \tag{5.46}$$

where U is the cumulative uptake of ozone by the surface, and t′ is a dummy variable for

purposes of integration. The reaction probability can be taken directly from equation 5.45, resulting in

$$U = \int_0^t \frac{b \cdot S_o \cdot C_o^g}{a} \cdot e^{-\frac{b \cdot C_o^g \cdot t'}{a}} dt' \qquad (5.47)$$

thus, the time dependent cumulative uptake is

$$U = S_o \left(1 - e^{\frac{-b \cdot C_o^g}{a} t} \right) \qquad (5.48)$$

A material balance can also relate the cumulative uptake to unreacted sites, on a molar basis, by

$$U = S_o - S \qquad (5.49)$$

Rearranging and combining with equation 5.43, I find that the reaction probability is linearly dependent on the cumulative uptake of ozone to the surface:

$$\gamma = \frac{4b}{a < v >} (S_o - U) = \gamma_o \left(1 - \frac{U}{S_o} \right) \qquad (5.50)$$

The experimental data do not support this form of the relationship (at least, not during the latter part of an exposure). The slope of log(g) vs log (U) for equation 5.50 decreases rapidly and may give instantaneous values of B that match those found experimentally for carpets CP1 and CP3. The rapid decrease in B is similar to that for the diffusion model in which sites at the center of a slab are being depleted. The large absolute values of B might be explained by a system in which a combination of surface interactions and diffusion mechanisms are taking place. In Section 5.5, I will present data from an experiment in which a cleaned aluminum plate was exposed to ozone in the reactor described in Chapter 2. In this case, the form of equation 5.40 fits the data well,

suggesting that this indeed is an appropriate model for a finite surface-site mechanism of aging.

5.3.2 Case 4: 1st order reaction, distribution of surface reaction rates

I provide the following analysis to eliminate the possibility that the observed effect is caused by a surface populated by a distribution of sites with different reaction rate constants. The rate of change in the concentration of an individual site type, S_i, with reaction rate constant b_i will be governed by an equation similar to equation 5.40,

$$\frac{dS_i}{dt} = -b_i \cdot S_i \cdot C \tag{5.51}$$

Similarly, equation 5.41 becomes

$$\frac{dC}{dt} = \frac{\gamma < v >}{4} C_o^g - \sum_{i=1}^{n} b_i \cdot S_i \cdot C \tag{5.52}$$

where n is the total number of different types of sites. The second term on the right hand side of equation 5.52 is the sum of the loss rate of ozone over all sites. Using the same arguments as before, equation 5.51 can be solved for S_i and equation 5.52 can be simplified to determine the reaction probability,

$$\gamma = \frac{4}{a < v >} \sum_{i=1}^{n} b_i S_i \tag{5.53}$$

or solving for the time dependent form,

$$\gamma = \frac{4}{a\langle v \rangle} \sum_{i=1}^{n} b_i S_{i,o} e^{\frac{b_i C_o^g t}{a}} \tag{5.54}$$

where $S_{i,o}$ is the initital concentration of i sites. The cumulative uptake can be found with a result similar to equation 5.49,

$$U = \sum_{i=1}^{n}\left(S_{i,o} - S_i\right) = S_{T,o} - \sum_{i=1}^{n} S_i \qquad (5.55)$$

where, $S_{T,o}$ is the total concentration of surface sites. Equations 5.53 and 5.55 cannot be solved explicitly. However, note that both γ and U are linearly dependent on each of S_1, S_2, S_3, ..., S_n. If the two n-dimensional vectors represented by γ and U are not orthogonal then each vector is linearly dependent on the other. Orthogonal vectors are independent of each other, but I assume that these two variables are connected and do influence each other and thus are not orthogonal. This means that γ is always linearly dependent on U for any combination of sites where the reaction order is one for each reactant.

These equations may be solved explicitly, if it is assumed that the concentration of sites, S, is a smooth function of the reaction rate constant b, or S(b). For example, S(b) could be a lognormal distribution of surface reaction rates. In the limiting case where $\Delta b \rightarrow 0$, equations 5.53 and 5.55 can be shown to be

$$\gamma = \frac{4}{a < v >} \int_0^{\infty} bS(b)db \qquad (5.56)$$

$$U = S_{T,o} - \int_0^{\infty} S(b)db \qquad (5.57)$$

Note that S(b) does not have the same dimensions as S_i (the units of S(b)db are identical to those of S_i). For functions, S(b), that are not defined or negative at either limit (0 or infinity), then the limits can be modified to reflect a proper integration over all sites. By the argument above, all functions, S(b), will result in γ being a linear function of the cumulative uptake, U.

5.3.3 Case 5: Reaction n^{th} order in S, identical reaction sites

While first-order reaction rate kinetics are common, it is possible that some reaction sites react under different apparent reaction orders. For a reaction which is nth order in the surface site,

$$\frac{dS}{dt} = -b \cdot S^n \cdot C \tag{5.58}$$

By the arguments used to derive equation 5.43,

$$\gamma = \frac{4 \cdot b \cdot S^n}{a < v >} \tag{5.59}$$

For every ozone molecule that is consumed, n sites are consumed:

$$nU = S_o - S \tag{5.60}$$

Combining equations 5.59 and 5.60,

$$\gamma = \frac{4b}{a < v >} (S_o - nU)^n \tag{5.61}$$

While this equation *is* a power function of the difference, (S_o-nU), this does not result in the functional dependence found in my experiments. The function may, however, appear similar to a power-law relationship (equation 5.1) in regions in which the relative change in nU is of the same order of magnitude as the relative change in the difference (S_o-U). As noted in Section 5.3.1, there may be intervals during which B matches experimentally derived values. However, the exponent B rapidly diminishes unless other ozone uptake mechanisms are involved.

5.4 Connecting experimental results with the interior diffusion model

I have established that a model of diffusion with reaction in a solid (or homogeneous) material can yield the functional dependence shown in equation 5.1,

where B= -1. Where ozone reactions deplete sites at the center of a homogeneous slab (with both sides of the slab exposed to ozone), the value of B can become less than -1, but is not constant. In the initial stages, B can be greater than -1, but tends to approach -1 as the ozone concentration profile reaches more deeply into the slab. Strictly speaking, the diffusion model may not apply to non-homogeneous materials, such as carpet. The value of B from carpet and duct liner experiments ranges from -0.07 to -0.47, but never approaches -1.

I suggest that an explanation for the low, porous material, absolute values of B may come from combining two models: the diffusion model of aging of homogeneous materials and the model of ozone penetration and deposition in a porous material. In the following analysis, I will develop a dynamic model of carpet aging that takes into account key information from these two models. From this analysis, I will show that, for a fleecy material undergoing diffusion aging, the effective power-law coefficient for whole carpet, B_o, is approximately -1/3. A more thorough numerical analysis will demonstrate this to be the case where the fiber power-law coefficient, B_f, is equal to -1.

5.4.1 Proportionality analysis to estimate value of the whole carpet power-law coefficient, B_o

In Chapter 4, a model of ozone diffusion into carpet was developed which resulted in an analytical expression for γ_o based on geometric factors, γ_b, γ_f, and diffusivity. In the present analysis, I relax the stipulation that γ_f is constant in time and direction, y. Indeed, where a carpet is exposed to ozone, the surfaces of the fiber tips will age more rapidly than surfaces deep within the fiber mat. Initially, most of the ozone is removed in the upper regions of the carpet mat with little reaching the backing. Since no

ozone reaches the carpet backing in this early period, the boundary condition at $y' = 0$ can be transformed to this expression:

$$\text{as } y \to -\infty \qquad C'=0 \tag{5.62}$$

The resulting system of equations represents diffusion with reaction into a semi-infinite slab where the backing has no effect on the outcome and $\gamma_f(y)$ is continuous down through the mat. Note that where γ_f (and thus A_1) is discontinuous in y, the analysis is invalidated. It is assumed that $\gamma_f(y)$ is continuous for this analysis. In a small region at the top of the fiber mat, the reaction probability, and thus the coefficient A_1 (see Section 4.3.3), is assumed to be constant in y over the thin slice dy. The result of solving equation 4.32 with the modified boundary condition, equation 5.62, and constant A_1, is,

$$C' = e^{-A_1(1-y')} \tag{5.63}$$

The reaction probability of a porous surface is given by equation 4.24 and shows that the reaction probability is proportional to $\frac{dC'}{dy'}$. In this case,

$$\left.\frac{dC'}{dy'}\right|_{y'=1} = A_{1,y'=1} \tag{5.64}$$

Thus,

$$\gamma_o \propto A_{1,y'=1} \tag{5.65}$$

By equation 4.33, A_1 is proportional to the square-root of γ_f:

$$A_1 \propto (\gamma_f)^{\frac{1}{2}} \tag{5.66}$$

Based on the analysis in Section 5.2.1, the reaction probability of the tips of the fibers is time dependent as shown in equation 5.18. This assumes that the model of internal diffusion and reaction outlined in Section 5.2.1 accurately describes fiber aging. For the

purposes of this discussion, the tips of the fibers will be exposed to a continuous concentration, C_o. Thus, the fiber reaction probability is proportional to the square-root of (1/t):

$$\gamma_f \propto t^{-\frac{1}{2}} \tag{5.67}$$

combining equations 5.66 - 5.68,

$$\gamma_o \propto t^{-\frac{1}{4}} \tag{5.68}$$

The cumulative uptake of ozone to the face of the carpet can be found by integrating the flux over time:

$$U_o \propto \int_0^t t^{-\frac{1}{4}} dt \propto t^{\frac{3}{4}} \tag{5.69}$$

Thus, combining equations 5.69 and 5.69 with equation 5.1,

$$t^{-\frac{1}{4}} \propto \left(t^{\frac{3}{4}} \right)^B \tag{5.70}$$

This analysis shows that the exponent for overall carpet aging is B_o=-1/3 for porous materials where the internal solid structures (fibers in the case of carpet) are subject to aging associated with internal reaction sites. The result, B_o = -1/3 lies in the middle of the range of experimentally determined values for carpet and duct liner.

It is interesting that this result was derived without the need to solve for the time and spatially dependent ozone concentration in the fiber mat. Also note that the coefficient B_o is dependent on none of the physical variables such as porosity, fiber diameter, etc. I will show in further analysis that B_o, however, is strongly dependent on the exponent for fiber aging, B_f (where $B_f \neq -1$) in a more rigorous numerical analysis.

5.4.2 Numerical analysis of the initial stage of porous material aging

In the previous section, I showed through a proportionality analysis that the power function coefficient, B_o, is approximately -1/3 when it is assumed that fibers age by the internal diffusion with reaction mechanism ($B_f = -1$). However, this analysis does not provide information about the concentration profile in the carpet mat as a function of time. In Section 4.6 I showed that ozone deposition would be distributed approximately equally between carpet fibers and backing if the carpet fibers were uniformly aged to a reaction probability, γ_f, of 10^{-7} and the backing reaction probability, γ_b, was 10^{-5}. In reality, the carpet fibers would age non-uniformly, with the most aged surfaces near the face of the carpet mat. Thus it is useful to develop a model which describes non-uniform aging of fibers, the concentration profile in the carpet mat, and the resulting whole carpet reaction probability with respect to time.

There is a second advantage to developing a more detailed model of carpet aging by ozone deposition. While the predictions of B_f match reasonably well with experimental results on nylon fibers, it makes sense to use the experimentally derived values of A_f and B_f to simulate whole carpet aging for comparison to whole carpet experiments. The proportionality analysis in Section 5.4.1 cannot be applied to a system where B_f is other than -1.

In the following analysis, only the initial stages of exposure will be considered. Analysis of the time-dependent concentration profile can take two forms. In the initial stages of exposure, as noted earlier, ozone is rapidly removed by the upper fiber surfaces. Thus, no ozone reaches the backing and the boundary conditions applied to equation 4.32 are

$$C' = 1 \qquad \text{at } y' = 1 \tag{5.71}$$

$$C' = 0 \qquad \text{at } y' = -\infty \tag{5.72}$$

However, because A_1 (a function of γ_f) is both a function of distance into the mat, y, and time, t, the governing equation cannot be solved explicitly. Instead, I make two key simplifications. First, pseudo steady-state analysis is applied since the characteristic time for ozone to diffuse through the fiber mat is significantly less than the time it takes for significant changes to occur in γ_f. Second, the concentration profile is described by splitting the domain into many vertical slices of thickness Δy. In each slice, $\gamma_f(y)$ is constant.

The concentration at the interface between slice n and slice n-1 is derived from equation 5.63, where $(1-y') = 1/n$,

$$C'(n-1,t) = C'(n,t)e^{\frac{A_1(n,t)}{n}} \tag{5.73}$$

where there are n slices of equal thickness. The concentration at the tips of the fibers, $C'(n,t) = 1$ at all times, and can be dropped from equation 5.73. The reaction rate coefficient, $A_1(n,t)$ is constant at time t in the slice between $y' = 1$ and $y' = 1-1/n$. By propagating this analysis down through the fiber mat, it becomes clear that

$$C(i,t) = e^{-\frac{1}{n}\sum_{j=i}^{n} A_1(j,t)} \tag{5.74}$$

Therefore, at any given time, provided the value of A_1 is known at every location through the fiber mat, a concentration profile can be found. For a sufficiently large number of slices, a continuous concentration profile can be predicted.

The coefficient A_1 must be determined using the functional dependence of the reaction probability on cumulative uptake. Recall that A_1 is proportional to the square-

root of γ_f. At a given time, γ_f is given by

$$\gamma_f(i,t) = A_f\left[U_f(i,t-\Delta t)+\gamma_f(i,t-\Delta t)C(i,t-\Delta t)\frac{\langle v\rangle}{4}\Delta t\right]^{B_f} \qquad (5.75)$$

where $U_f(i,t-\Delta t)$ is the cumulative uptake on the fiber up to time t-Δt and

$\gamma_f(i,t-\Delta t)C(i,t-\Delta t)\frac{\langle v\rangle}{4}\Delta t$ is the ozone uptake accumulated at location i over time interval Δt.

For equation 5.75 to be valid where t=0, an initial value of U must be measured or chosen. In my experiments, the initial value of the cumulative uptake was not known because the exposure history before the materials were tested was unknown. Instead, I chose to infer an initial cumulative uptake, $U_{initial}$, based on information about the initial value of the fiber reaction probability, $\gamma_{f\_initial}$,

$$U_{initial} = \left(\frac{\gamma_{f\_initial}}{A_f}\right)^{\frac{1}{B_f}} \qquad (5.76)$$

In some experiments, the $\gamma_{f\_initial}$, was not measurable because it was so large that all ozone was removed in the fixed bed apparatus. For these cases, I assume that $\gamma_{f\_initial} = 1$. I will discuss later the relative error in this approach.

By recursively evaluating equations 5.74 and 5.75, the concentration profile can be found as a function of time. Eventually, however, ozone begins to interact with the backing (in the case of carpet), invalidating the above analysis.

5.4.3 Numerical analysis of aging, including flux to backing

A second, more involved, numerical analysis is required to calculate the concentration profile where the presence of the backing influences ozone uptake.

Consider the general solution to equation 4.32 for a region in which the reaction rate coefficient A_1 is constant (the time parameter, t is dropped for clarity),

$$C' = k_1 e^{-A_1 y'} + k_2 e^{A_1 y'} \tag{5.77}$$

where k_1 and k_2 are coefficients that depend on boundary conditions. In the current model of this system, the carpet mat is split into n horizontal slices. In each slice, equation 5.77 describes the concentration profile. The coefficients k_1 and k_2 are unique to a given slice being dependent on the boundary conditions that apply in the given slice. The concentration at $y' = 1$ (coincident with the n^{th} slice) is given by

$$C'(n) = 1 = k_1(n) e^{-A_1(n)} + k_2(n) e^{A_1(n)} \tag{5.78}$$

The concentration at $y' = \frac{n-1}{n}$ is given by

$$C'(n-1) = k_1(n) e^{\frac{A_1(n)(n-1)}{n}} + k_2(n) e^{\frac{A_1(n)(n-1)}{n}} \tag{5.79}$$

The concentration between slice n and (n-1) is also given by an equation that corresponds to the parameters of slice (n-1),

$$C'(n-1) = k_1(n-1) e^{-A_1(n-1)\frac{(n-1)}{n}} + k_2(n-1) e^{A_1(n-1)\frac{(n-1)}{n}} \tag{5.80}$$

Equating equations 5.79 and 5.80 reduces the number of variables by dropping the concentration term,

$$k_1(n) e^{\frac{A_1(n)(n-1)}{n}} + k_2(n) e^{\frac{A_1(n)(n-1)}{n}} = k_1(n-1) e^{-A_1(n-1)\frac{(n-1)}{n}} + k_2(n-1) e^{A_1(n-1)\frac{(n-1)}{n}} \tag{5.81}$$

The two equations, 5.77 and 5.80 contain four unknown variables ($k_1(n)$, $k_2(n)$, $k_1(n-1)$, and $k_2(n-1)$). A solution necessitates two more equations, but the equation that describes the concentration at the interface between the next two slices adds two more variables,

$$k_1(n-1)e^{-A_1(n-1)\frac{(n-2)}{n}} + k_2(n-1)e^{A_1(n-1)\frac{(n-2)}{n}} = k_1(n-2)e^{-A_1(n-2)\frac{(n-2)}{n}} + k_2(n-2)e^{A_1(n-2)\frac{(n-2)}{n}} \quad (5.82)$$

This procedure of equating the concentration between slices must be repeated until the backing is reached ($y' = 0$). At this location, the boundary condition is given by a flux (in nondimensional format):

$$\frac{dC'}{dy'} = k_y C' \quad (5.83)$$

where

$$k_y = \left(\frac{\gamma_b \langle v \rangle h}{4D}\right) \quad (5.84)$$

An equation analogous to equation 5.82 can now be written for the backing surface:

$$-A_1(1)k_1(1) + A_1(1)k_2(1) = k_y\left(k_1(1) + k_2(1)\right) \quad (5.85)$$

The complete set of (n+1) equations creates 2n unknown variables. The remaining equations must come from a continuity condition between slices,

$$\left.\frac{dC'}{dy'}\right|_{y^+} = \left.\frac{dC'}{dy'}\right|_{y^-} \quad (5.86)$$

At the interface between slice (n) and (n-1), this continuity equation becomes

$$-A_1(n)k_1(n)e^{\frac{A_1(n)(n-1)}{n}} + A_1(n)k_2(n)e^{\frac{A_1(n)(n-1)}{n}} = -A_1(n-1)k_1(n-1)e^{\frac{A_1(n-1)(n-1)}{n}} + A_1(n-1)k_2(n-1)e^{\frac{A_1(n-1)(n-1)}{n}} \quad (5.87)$$

Along with the analogous equations between the subsequent slices, equation 5.87 provides (n-1) more independent equations that will allow a solution to be found. To solve this set of equations at a given time increment, I used the Matlab programming environment, selected for its powerful matrix manipulation routines. The set of equations

shown above allows a solution to be found at a moment in time. The general iterative procedure to determine the time-dependent nature of the concentration profile and reaction probability is the same as that used in Section 5.4.2. One additional equation is needed to take into account the time-dependent behavior of the backing reaction probability, γ_b, as described by equation 5.1. The program code for solving this set of equations, and predicting the aging rate of carpet is shown in Appendix A.5.

Figures 5.5 through 5.8 show the results of simulations of the time-dependent reaction probability due to carpet aging for carpets CP1 through CP4, along with laboratory measurements of aging for the same carpet. These independent parameters, as they applied to the specific carpet, were used for each simulation: functional dependence on cumulative uptake of γ_f and γ_b (parameters A and B), d_f, p, h. Common to each simulation were the diffusivity of ozone ($D = 0.167\ cm^2\ s^{-1}$) and concentration of ozone at fiber tips ($C=200\ \mu g\ m^{-3}$).

In frame (a) of each of the figures, the whole-carpet reaction probability, γ_o, is plotted with respect to the elapsed time. The general shape of the experimental data is tracked reasonably by the model prediction: rapid aging with flattening out of the reaction probability curve as exposure continues. For carpets CP1, CP2 and CP3, the model predicts that the carpet will age more rapidly than the experimental data suggests. The model predicts that the whole carpet reaction probability, γ_o, is much larger than the experimental value in the early periods of an exposure. During the 48 h simulation, the order of magnitude of the predicted reaction probability matches that of the experimental measurements, generally in the vicinity of 10^{-5}.

The slope of the log-log plot of γ_o vs. U is predicted to be much higher than that

determined experimentally for carpets CP1 and CP3. As suggested by the proportionality analysis in Section 5.4.1, the numerical model predicts that the whole carpet power function coefficient B_o equals -0.33 when that for the fibers, B_f is -1. As the power function coefficient B_f for fiber surfaces decreases below -1, B_o becomes smaller and the slope becomes steeper. However, even with B_f = -2.2 and -4.4, the experimentally derived values of B_o were -0.12 and -0.1 resulting in a much more shallow slope than predicted. The prediction of B_o for CP2 was somewhat better, but the slope is still predicted to be much more steep. The prediction for carpet CP4 is close to the experimentally derived value. For CP4, the absolute value of γ_o is over-predicted by only about 60% over the time period simulated, which I consider a good match.

The troublesome discrepancy between the slopes predicted by the model and those derived from experimental results may be due to the assumption that the carpet is a uniformly packed material. The structure of carpet used in the model development in Chapter 4 may not adequately describe the structure of real carpets. A cut pile carpet is typically comprised of fiber bundles, separated by uniformly spaced attachments to the carpet backing. In the model developed in Chapter 4, I assume that the fibers are not bundled, but are uniformly spaced.

As a thought experiment, consider a carpet made of uniformly spaced *bundles* of fibers. Think of the bundles as large fibers, as defined in the previous models. The power-function coefficient for the bundle, B_b, is dependent on the power function coefficient of individual fibers, B_f, inside the bundle. The bundle is a porous structure that adheres to the principles outlined in Sections 5.4.1 – 5.4.3, thus an estimate of B_b may be made with knowledge of individual fiber geometry and porosity of the bundle. As an example, B_f =

-2.2 for carpet CP1. The whole-carpet power-function coefficient for CP1 was predicted to be $B_o = -0.59$. From the whole-carpet aging model, I showed that as the absolute value of B_f decreases, so does B_o. The same might hold true of a model that uses fiber bundles in the place of fibers. In this case, the absolute value of B_b would be less than 1 and thus the absolute value of the predicted B_o would be < 0.33. The measurements of B_o for CP1, CP2 and CP3 are all around -0.1.

It is instructive to consider the bundle morphology from each of the tested carpets. Carpets CP1 and CP3 are cut-fiber, pile carpet. The bundles are formed from smaller twisted bundles, twisted around one another to form larger bundles. The "double-twisted" fibers form a tight bundle that is similar to that of some ropes. In contrast, the fiber bundles of carpets CP2 and CP4 are formed from loops of fibers that are much more independent. There appears to have been no intentional effort to twist the fibers around one another, although a small degree of twist is sometimes apparent. The differences between bundle morphology of the two types of carpet may explain some of the model results. There is a large discrepancy between the predicted and measured values of B_o for CP1 and CP3, less of a difference for CP2 and fairly close agreement for CP4. Carpets that contain tightly twisted bundles of fibers may not be adequately addressed by my model.

5.5 The negative experiment: aluminum plate

To this point, I have argued that the experimental aging profile fits the internal diffusion with reaction hypothesis, but not the pure, surface-reaction hypothesis. To test that the surface-reaction hypothesis is observable, I exposed an aluminum plate to ozone. A clean aluminum plate (with no surface coatings) will not allow ozone to diffuse below

the surface, and the aging profile should not match the power function.

In this experiment, I prepared a 232 cm^2 square sheet of aluminum by cleaning it with hexane and then methanol to remove any surface oils. The sheet was fitted with a Teflon frame and then placed in the 10.5 L electropolished chamber. The experimental procedure follows that described in Chapter 2 for whole-carpet experiments, with the exception that the chamber ozone mole fraction was controlled between 235 and 245 ppbv O_3. The humidity and temperature were maintained at 50% and 23 °C respectively.

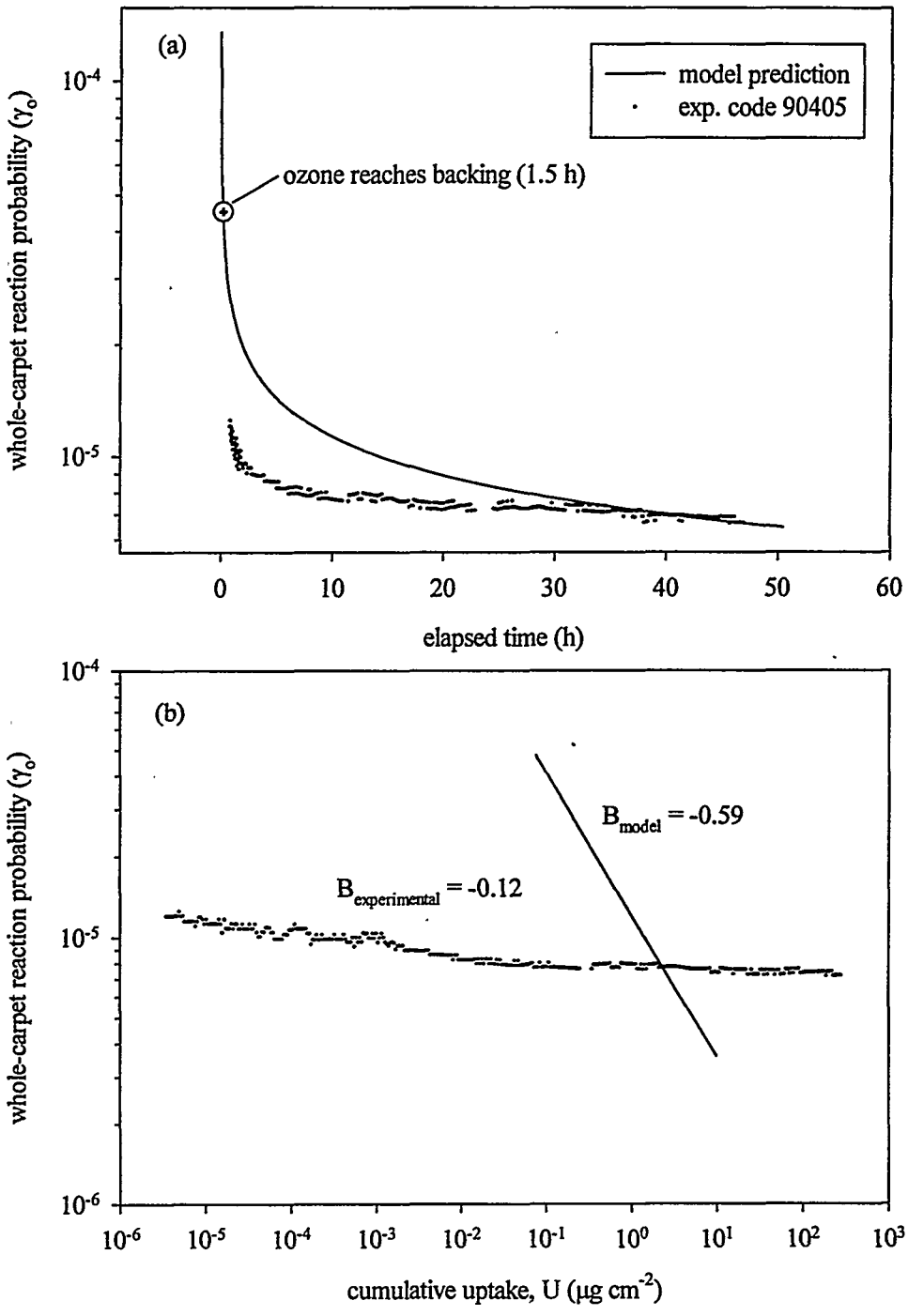

Figure 5.5. Model predictions and experimental measurements of aging of carpet CP1 with respect to ozone uptake: (a) whole-carpet reaction probability, γ_o, vs. elapsed time; (b) γ_o vs. cumulative uptake of ozone, U. Model parameters taken from experiment 80810 ($A = 2 \times 10^{-11}$ (μg cm^{-2})$^{2.2}$, B = -2.2) for fibers and 80408 ($A=10^{-5}$ (μg cm^{-2})$^{0.38}$, B=-0.38) for backing. Whole carpet data taken from experiment 90405. The time when the concentration of ozone at the backing is predicted to reach 1% that at the fiber tips is marked with a circled cross.

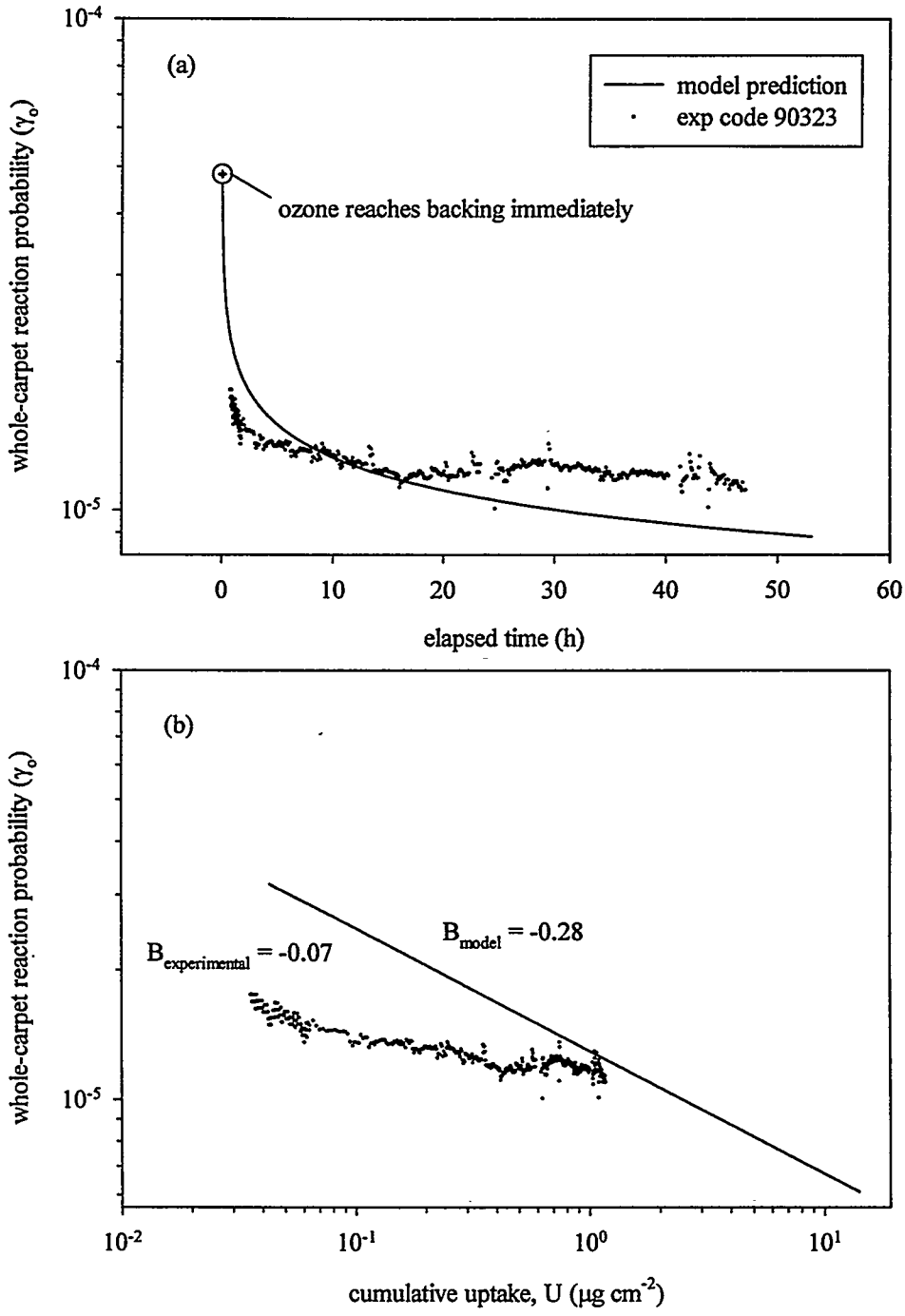

Figure 5.6. Model predictions and experimental measurements of aging of carpet CP2 with respect to ozone uptake: (a) whole-carpet reaction probability, γ_o, vs. elapsed time; (b) γ_o vs. cumulative uptake of ozone, U. Model parameters taken from experiment 80817 ($A = 4 \times 10^{-8}$ (μg cm^{-2})$^{0.9}$, B = -0.9) for fibers and 80602 (A=10^{-5} (μg cm^{-2})$^{0.28}$, B=-0.28) for backing. Whole carpet data taken from experiment 90323. The time when the concentration of ozone at the backing is predicted to reach 1% that at the fiber tips is marked with a circled cross.

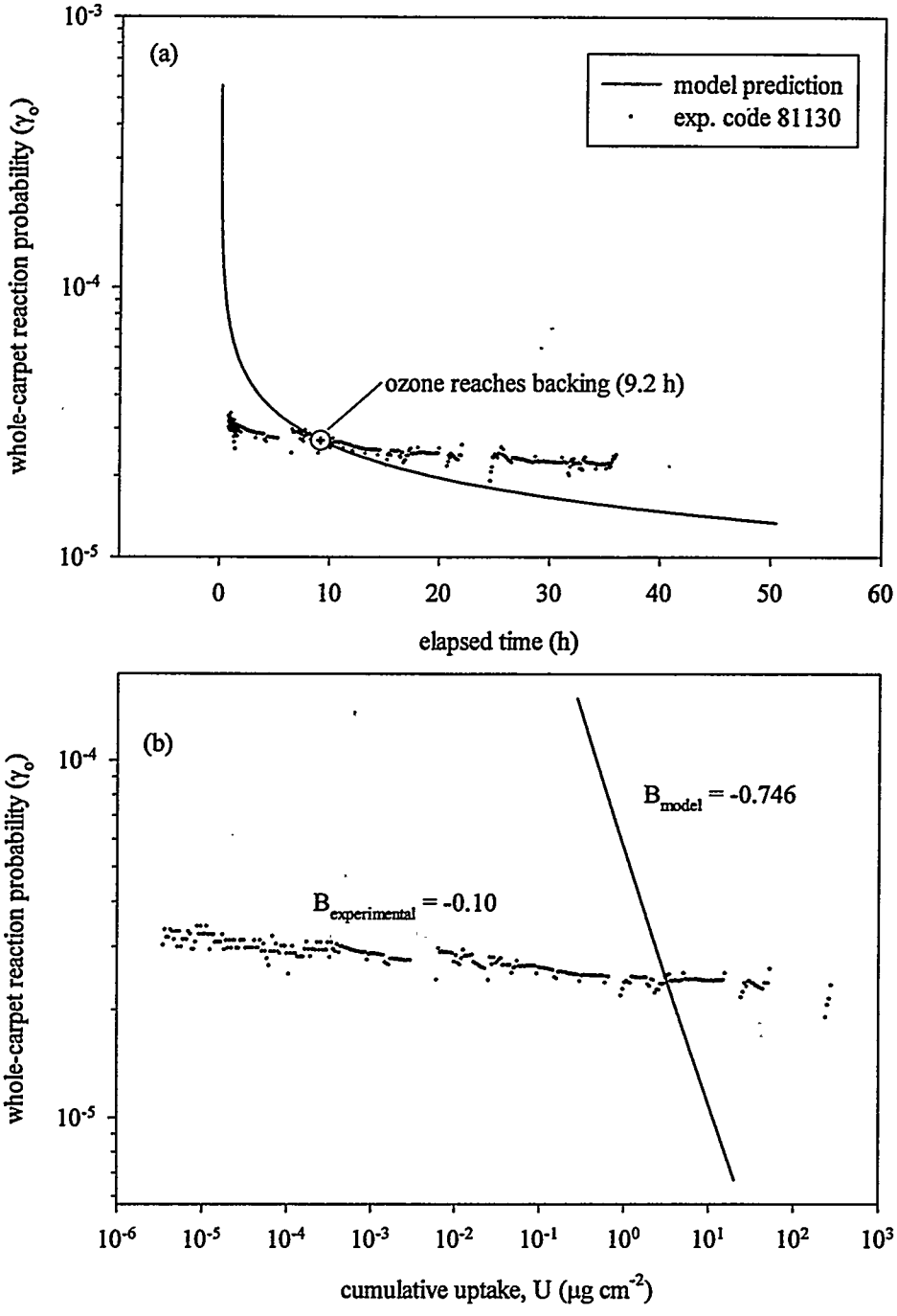

Figure 5.7. Model predictions and experimental measurements of aging of carpet CP3 with respect to ozone uptake: (a) whole-carpet reaction probability, γ_o, vs. elapsed time; (b) γ_o vs. cumulative uptake of ozone, U. Model parameters taken from experiment 80824 ($A = 3 \times 10^{-9}$ (μg cm^{-2})$^{4.4}$, B = -4.4) for fibers and 81215 ($A=4 \times 10^{-5}$ (μg cm^{-2})$^{0.47}$, B=-0.47) for backing. Whole carpet data taken from experiment 81130. The time when the concentration of ozone at the backing is predicted to reach 1% that at the fiber tips is marked with a circled cross.

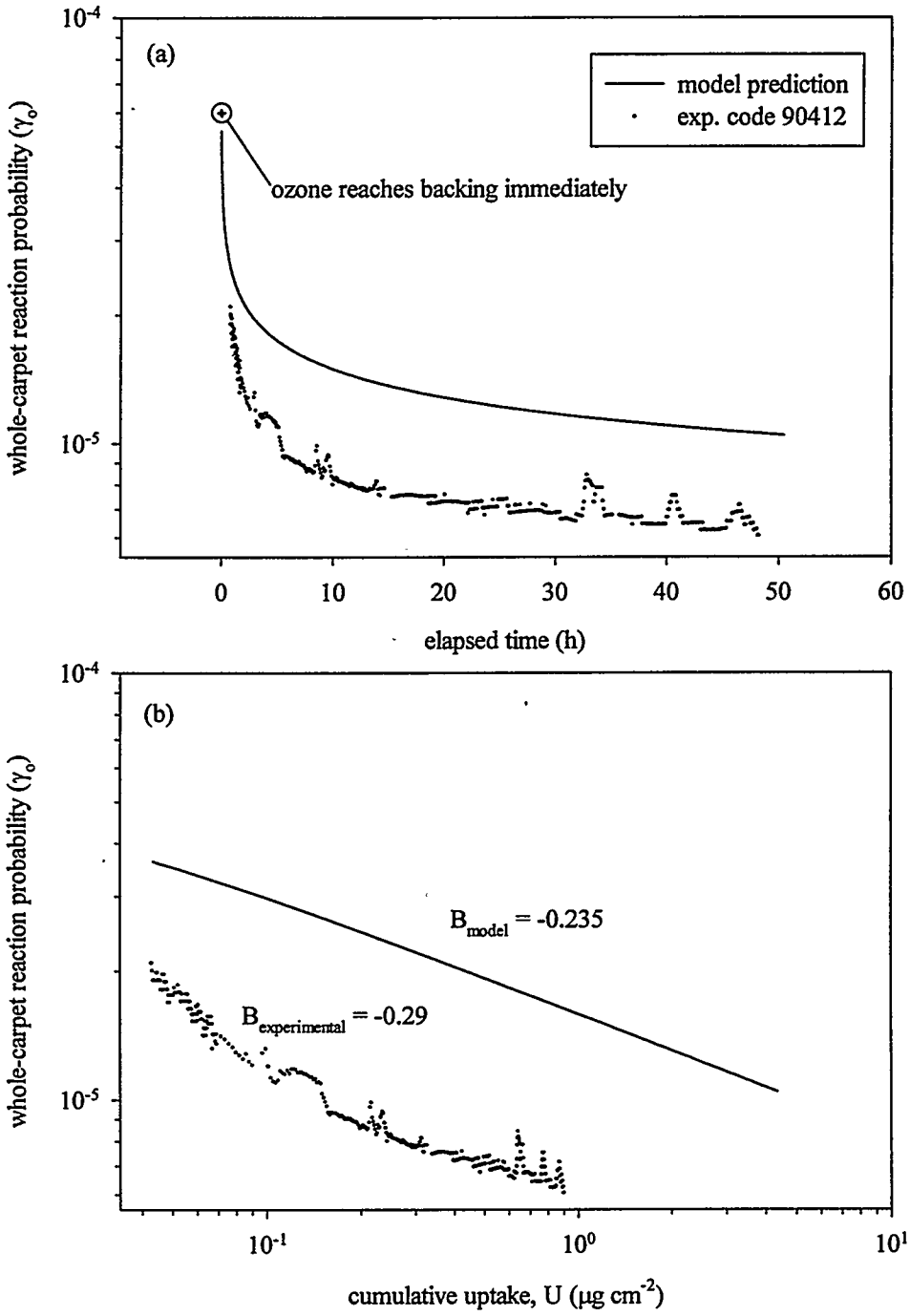

Figure 5.8. Model predictions and experimental measurements of aging of carpet CP4 with respect to ozone uptake: (a) whole-carpet reaction probability, γ_o, vs. elapsed time; (b) γ_o vs. cumulative uptake of ozone, U. Model parameters taken from experiment 80820 ($A = 6 \times 10^{-9}$ (μg cm^{-2})$^{0.8}$, B = -0.8) for fibers and 90419 ($A=1 \times 10^{-5}$ (μg cm^{-2})$^{0.28}$, B=-0.28) for backing. Whole carpet data taken from experiment 90412. The time when the concentration of ozone at the backing is predicted to reach 1% that at the fiber tips is marked with a circled cross.

The result of this experiment is shown as the reaction probability vs. cumulative uptake in Figure 5.9. The axes of Figure 5.9(a) are linear, while those of Figure 5.7b are logarithmic. Note that the functional dependence of the reaction probability on cumulative uptake appears approximately linear in Figure 5.9(a). There is a slight upward curvature early in the experiment, but the slope generally remains constant throughout. Recall that uncertainties in the calculation of the reaction probability become very large as γ drops below 10^{-7}. When these data are plotted using log-log axes, the reaction probability appears somewhat flat, but then drops off rapidly as shown in Figure 5.9(b). This behavior is indicative of a linear function plotted on a log-log scale. This is exactly what is expected if the functional dependence follows equation 5.50, or if the aging phenomena is due entirely to surface reactions.

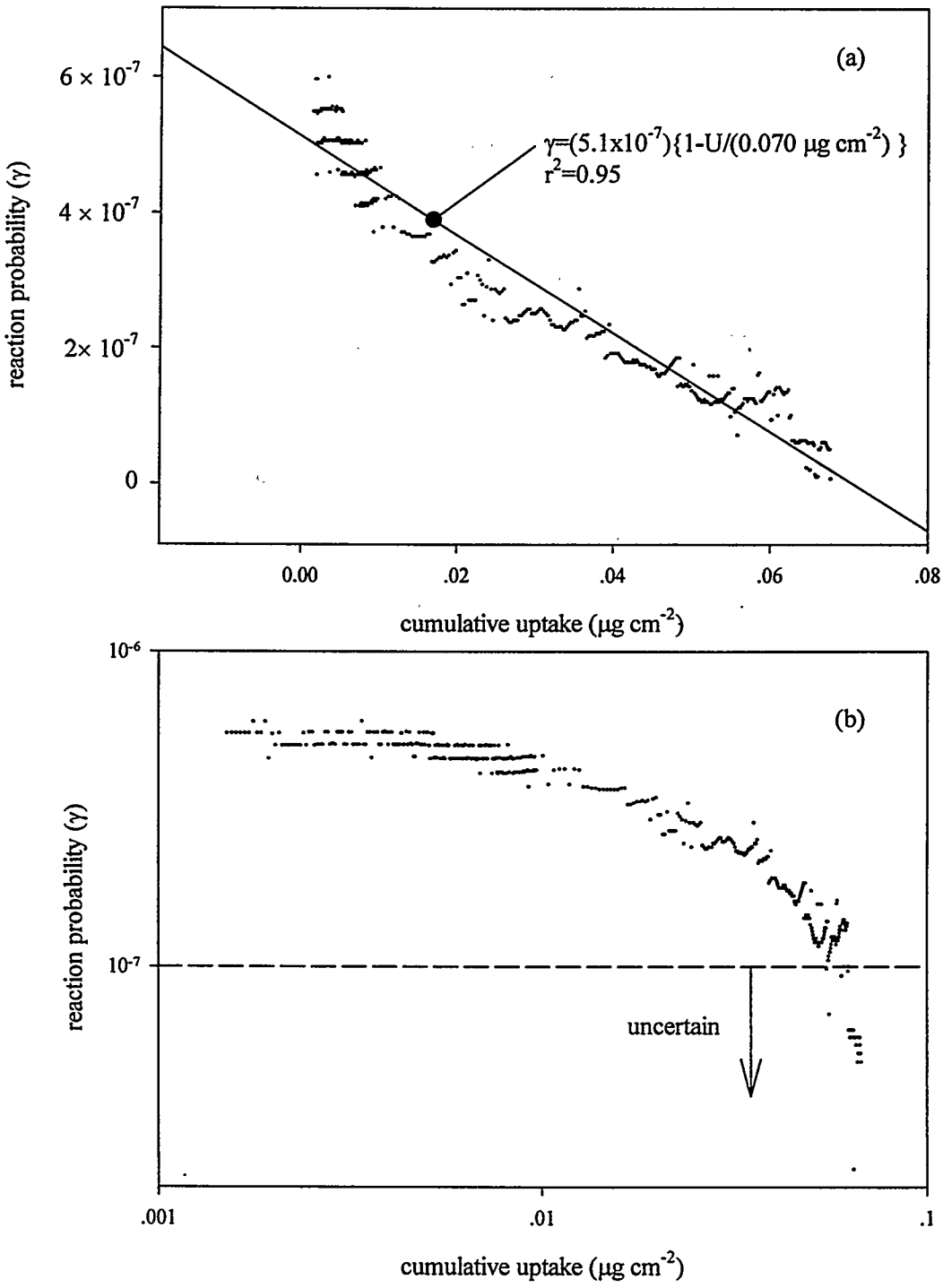

Figure 5.9. Aging of a clean aluminum plate: (a) reaction probability vs. cumulative uptake on linear axes; (b) reaction probability vs. cumulative uptake on logarithmic axes. The linear nature of the curve suggests that ozone oxidizes surface sites only.

A linear regression of this data set yields values of γ_o (5.1×10^{-7}) and S_o (0.070 μg O_3 cm^{-2}) in equation 5.50 ($r^2 = 0.95$). The units of S_o do not shed light on the potential number of sites available for reaction, so must be transformed by dividing S_o by (48 μg O_3 $\mu mole^{-1}$), yielding $S_o = 1.5 \times 10^{-3}$ μmoles cm^{-2}. This is equivalent to 8.8×10^{14} sites cm^{-2}, or about 11 $Å^2$ $site^{-1}$. An ozone molecule has an approximate molecular diameter of 2.3 Å, and a cross-sectional area of about 4 $Å^2$. Thus, the number of sites available is approximately equal to one third of a monolayer of ozone molecules on a smooth surface.

The aging phenomena on the clean aluminum plate does not follow a power function as observed for most other materials. This experiment lends more strength to the ozone diffusion/reaction hypothesis in carpet fibers and other materials by showing that it does not apply to an impermeable surface.

5.6 Regeneration of surfaces

The models of surface aging outlined in Sections 5.2 and 5.3 provide mechanisms that may explain how regeneration of surfaces occur. Sabersky et al. (1973) found that the deposition velocity of ozone to plywood increased if the plywood was exposed to clean air for a period, after an initial ozone exposure. In Chapter 6, I show that a duct liner briefly regenerated its ability to react with ozone when the material was stored in the absence of ozone for 1 week.

Consider the diffusive mechanism outlined in Section 5.2 for a material that has immobile reaction sites (S). After a period of exposure, there will be a zone (zone 1 in Figure 5.1) where the concentration of reaction sites is zero. A period that is free of ozone exposure will deplete this zone of ozone. When the material is once again exposed to ozone, there will be a brief period in which ozone will "refill" zone 1, eventually

recreating the linear concentration profile shown in Figure 5.1. The apparent initial reaction probability will be very high, but will rapidly decrease to approach the original reaction probability value.

Another possibility that will lead to more substantial regeneration is taken from equation 5.5. If the reaction sites, S, are *not* stationary, they may be mobile enough to influence the reaction probability after a "rest" period. In Section 5.2.1, I assume that the diffusivity of the reaction sites (D_s) is very small relative to the diffusivity of ozone. However, even if this is true, the diffusivity may be high enough to allow reactive molecules to diffuse up into zone 1 (effectively making zone 1 shorter, but now with a non-uniform concentration of S in zone 2) during rest periods. The resulting reaction probability at the onset of the next ozone exposure will be higher than at the end of the prior period because ozone does not have to travel so far to encounter a reactive site. The ability for the reacting molecule to diffuse towards the surface may also be important for predicting long-term emissions of secondary reaction products, such as aldehydes. If the material has large stores of reactive molecules, surface regions may get depleted during high ozone months in the summer, but become regenerated during the winter. This would lead to generally higher air concentrations of reaction products in early summer than in late summer.

One other aging mechanism is suggested by the assumption in Section 5.3.1 that the adsorption isotherm of ozone on a surface is established instantaneously. There may be a period upon initial exposure in which ozone must adsorb to the surface, leading to a brief period of high ozone flux.

5.7 Conclusions

Surface aging of materials due to continuous ozone exposure can strongly influence indoor concentrations of ozone. In this chapter, I suggested several mechanisms that may explain the observed pattern of aging on carpet and duct material surfaces. Where ozone diffuses below the surface of a non-fleecy material (such as fiber surfaces) and reacts with internal sites, a power function is predicted that relates the reaction probability to the cumulative ozone uptake. The functional *form* matches well with observations. The model predicts that the value of the coefficient of the power function, B, is initially greater than -1 as ozone begins to diffuse and react in the material. As the ozone concentration profile reaches more deeply into the material, the value of B approaches -1. As the concentration profile reaches the end of the slab and begins to deplete sites there, the value of B begins to drop below -1. These predictions may explain why values of B around –1 were found experimentally for two types of olefin carpet fiber. Other fibers were found to age with power-function coefficients that were much lower than -1 (~ -2 to -5). While the functional form of a surface reaction only mechanism of aging does not match a power-function, the instantaneous value of the slope of log(g) vs. log(U) can match that observed in experiments. A combination of the mechanisms of surface and internal reaction may explain the observed values of the coefficient B.

Aging of fleecy materials such as carpet was explored with a more complicated analysis. This analysis combines mass transport into the carpet mat with observed functional forms of fiber and carpet backing aging. The carpet analysis predicts that ozone aging will also follow the functional form of a power-law, where the whole carpet power-law coefficient, B_o, is about -1/3 when the fiber coefficient, B_f, is -1. Measured

values of the whole carpet power-law coefficient ranged from about -0.1 to -0.3. An experiment with a cleaned aluminum plate strengthens the diffusion-reaction hypothesis of ozone aging for carpet fibers by showing that aging is consistent with the surface-reaction model when an impermeable surface is exposed to ozone.

It is yet not clear why the absolute value of the power-function coefficients of some carpet fibers were so high. However, the relatively small absolute value of the coefficients for porous materials may be explained by combining the whole carpet model developed in Chapter 4 with the aging model of fiber and backing surfaces. Generally, the absolute value of the aging coefficient predicted by numerical analysis of aging of specific carpets was higher than that found experimentally, but the observed trend towards lower values in porous materials was the same as predicted. The predicted aging pattern of CP4 matched the experimentally derived pattern nicely. Carpets are manufactured in several different forms. Those carpets with the most uniform distribution of fibers may be better simulated by these aging models. A better model that considers more complex geometries of fibers and fiber bundles may better predict aging patterns of more complex carpets.

The mathematical form of the models allow them to be generalized to other reactions and other materials. The aging mechanisms explored in Sections 5.2 and 5.3 may be applicable to any reactive, gas-phase, species that reacts in a first-order manner with surface or internal sites. The materials described in these models can also be generalized. As long as the assumptions regarding the behavior of reactants and sites are met (e.g., stationary vs. mobile sites, constant diffusivity, etc.), the models should be applicable. The model describing diffusion with reaction in a porous fiber mat of carpet

may also be applicable to other porous materials, such as fabrics, ceiling tiles or even a thick layer of dust.

5.8 References

Altschuler, A.P.; Wartburg, A.F. *International Journal of Air and Water Pollution.* **1961**, *4*, 70-78.

Crank, J. *The Mathematics of Diffusion.* 2nd ed. Clarendon Press: Oxford. 1975.

Mueller, F.X.; Loeb, L.; Mapes, W.H. *Environmental Science and Technology.* **1973**, *7*, 342-346.

Reiss, R.; Ryan, P.B.; Koutrakis, P. *Environmental Science and Technology.* **1994**, *28*, 504-513.

Rouse, P.E. *Journal of the American Chemical Society.* **1947**, *69*, 1068.

Sabersky, R.H.; Sinema, D.A.; Shair, F.H. *Environmental Science and Technology.* **1973**, *7*, 347-353.

CHAPTER 6

Indoor Air Quality Impacts of Ventilation Ducts: Ozone Removal and Emissions of Volatile Organic Compounds[1]

6.1 Background

Air provided to mechanically ventilated buildings passes through heating, ventilation, and air conditioning (HVAC) systems that contain many materials. Ducts are typically fabricated of sheet metal and sealed with gaskets or duct sealant. Near vibrating machinery, ducts may be joined by sections made of flexible, polymer-coated fabric. Large amounts of fiberglass duct liners, with polymer resin coatings, are installed inside ducts to deaden sound and to increase thermal efficiency. Ventilation systems also contain particle filters made from materials such as glass fibers.

The quality of the air passing through these systems can be altered by four classes of processes: (1) primary emission of compounds, particularly volatile organic compounds (VOCs) from materials; (2) sorption and desorption processes between pollutants and surfaces; (3) pollutant removal by deposition or chemical reaction at surfaces; and (4) reaction between air pollutants and surface materials that lead to the release of chemically transformed compounds. Of particular interest for (3) and (4) are ozone-surface interactions, which tend to reduce the ozone concentration in the supply air, but may generate carbonyls or organic acids that can be released into the air.

---

[1] Chapter 6 published as Morrison, G.C.; Nazaroff, W.W.; Cano-Ruiz, J.A.; Hodgson, A.T.; Modera, M.P. *Journal of the Air and Waste Management Association.* **1998**, *48*, 941-952.

Some studies have reported a higher incidence of nonspecific health symptoms ("sick-building syndrome") among office workers in buildings with air conditioning, and possibly simple mechanical ventilation, than in buildings with natural ventilation (Burge, et al. 1987; Mendell and Smith, 1990). Attention in these cases has usually been focused on microbial contamination. However, another possible contributor to this observation is the emission of pollutants, such as VOCs, from HVAC systems. Ventilation systems have been identified as potentially significant sources of VOCs (Batterman and Burge, 1995; Mølhave and Thorsen, 1991) For example, Mølhave and Thorsen determined that the materials in the HVAC system of one building were responsible for 80% of all direct indoor emissions of VOCs.

Interactions of ozone with indoor surfaces has been quantified for rooms (Weschler et al., 1989; Nazaroff et al., 1993), but had not been studied for ducts. The rate at which ozone is removed at duct surfaces may be important since most of the outdoor air that enters mechanically ventilated buildings passes through ducts. In addition to ozone removal, compelling evidence from laboratory studies demonstrates the potential for ozone reactions at indoor surfaces to generate carbonyls and organic acids that are more irritating than their olefinic precursors. For example, exposure of carpet to ozone in a room-sized chamber reduced the gas-phase concentrations of some hydrocarbons while substantially increasing the concentrations of formaldehyde, acetaldehyde and C_5 -C_{10} aldehydes (See Chapter 2 and Weschler et al., 1992). Exposure of latex paint in a test system to ozone was observed to generate formaldehyde (Reiss et al., 1995a). Some evidence from field studies suggests that such reactions might increase concentrations of

aldehydes, ketones, and organic acids in houses (Reiss et al., 1995b; Zhang and Lioy, 1994).

This chapter addresses the impact on indoor air quality of duct liners and other materials found in the ducts of ventilation systems. I measured the emissions of VOCs and aldehydes, with and without exposure to ozone. In combination with mathematical models based on the principle of material balance, these measurements allow me to estimate the increase in indoor VOC concentrations caused by these ventilation system materials. I also measured the uptake of ozone by duct liners and galvanized sheet metal to predict the ozone removal efficiency for air flow through a typical ventilation duct section. The experiments were performed in a small, stainless steel chamber under conditions of controlled temperature, humidity and air-exchange rate.

6.2 Methods

6.2.1 Materials

The study materials, listed in Table 6.1, included new and used duct liners (NDL and UDL, respectively), a neoprene gasket, a flexible duct connector, duct sealant, galvanized sheet metal, a flexible spiral-wound duct, and air filters (AFs). Upon collection, the samples were packaged in multiple layers of aluminum foil and stored for periods up to several weeks prior to the experiments. (Used materials were stored for as much as a year in a freezer.) The new duct liners were either purchased from the supplier or obtained from a new roll at a sheet metal shop.

Duct liners are used primarily to reduce noise transmission from HVAC fans, but also for thermal insulation. Each duct liner was coated by the manufacturer on one side with a black resin material that is used to reduce fiber erosion into the airstream and also

to reduce airflow resistance. According to the manufacturers, NDL2 is coated with cured, cross-linked, phenol formaldehyde polymer hexamethylene tetramine, and NDL3 is coated with cured urea extended phenol-melamine-formaldehyde resin. The coatings for NDL1 and UDL are unknown but these duct liners appear similar to the others.

The study materials for ozone loss measurements, listed in Table 2, included galvanized sheet metal (GS), three new duct liners (NDL1, NDL2, and NDL3), and one used duct liner (UDL) that had been removed from a duct in 1989 and stored in a sealed container until measurement (in 1996).

6.2.2 Emissions of VOCs

All experiments were performed using the apparatus shown in Figure 2.3 and adhere to the experimental procedure discussed in Section 2.2 with exceptions noted here. The chamber was continuously ventilated at 1.0±0.05 L min^{-1} with nitrogen that was humidified to 50±5% relative humidity. The temperature and humidity inside the chamber were continuously measured using a Vaisala temperature and humidity probe.

Specimens of flat materials (typically 0.01 m^2) were cut from larger pieces and placed in stainless steel holders. The duct sealant was applied to a metal plate and weighed, and the exposed surface area was estimated from direct measurements of length, width, and height. The specimen was placed on a wire rack in a chamber, and the chamber was then sealed and ventilated. Gas samples for the analyses of total VOCs (TVOC), individual VOCs, formaldehyde, and acetaldehyde were collected from the chamber exhaust stream for elapsed times centered at 3, 6, and 24 h after the chamber was first sealed.

Samples for TVOC and VOC analyses were collected at 0.1 L min^{-1} for 20 min on multisorbent tubes and were analyzed by thermal desorption gas chromatography/mass spectrometry. TVOC was calculated from the total ion-current response. An average response factor was calculated based on the individual relative response of characteristic compounds on a mass basis versus an internal standard (bromofluorobenzene). These compounds were n-hexane, n-octane, n-nonane, n-undecane, n-dodecane, 1,2,4-trimethylpentane, benzene, toluene, ethyl benzene, and m-xylene. The lower limit of quantification for the TVOC analysis was about 25 μg m^{-3}. Individual VOCs were quantified using pure standards. Formaldehyde, acetaldehyde, and acetone samples were collected for 60 min at 0.5 L min^{-1} on treated dinitrophenylhydrazine (DNPH) cartridges and analyzed by high-performance liquid chromatography. The lower limit of quantification for these compounds was approximately 1 μg m^{-3}. The lower limit of quantification for the TVOC emission rate from a material with an exposed surface area of 0.01 m^2 was ~300 μg m^{-2} h^{-1}. For combined C_5 -C_{10} aldehydes, the lower limit of quantification was ~150 μg m^{-2} h^{-1}, largely because of variability in the background concentrations of nonanal and decanal. For total measurable carbonyl compounds, the lower limit of quantification for emissions was ~200 μg m^{-2} h^{-1}. The lower quantification limit for formaldehyde, acetaldehyde, and acetone emissions was ~20 μg m^{-2} h^{-1}.

For selected materials, emissions were measured in the presence of ozone (Table 6.3). In these experiments, the inlet ozone mole fraction was set to ~120 ppb. The average outlet ozone levels ±1 standard deviation (variability) are reported in Table 6.3. Exposure was initiated immediately after the 24-h unexposed emissions period, without

removing the specimen from the chamber, and was maintained for an additional 24-h period.

The emission rate of an analyte was calculated by means of the following equation, derived from material balance:

$$E = \frac{Q(C - C_o)}{A} \tag{6.1}$$

where E is the emission rate of the analyte per unit area of material ($\mu g\ m^{-2}\ h^{-1}$), Q is the volumetric flow rate of the gas stream ($m^3\ h^{-1}$), C is the concentration of the analyte in the chamber exhaust ($\mu g\ m^{-3}$), C_o is the chamber background concentration ($\mu g\ m^{-3}$), and A is the exposed surface area of the material (m^2).

To put the emission results in perspective, I conducted simple model calculations of the impact of a duct system on indoor air contaminant concentrations. The model assumes that indoor air is well-mixed, including the air in the ducts. This assumption is supported by the high recirculation rate typical of conventional HVAC system design. Species are assumed to be nonreactive and emitted at a steady rate. The increment in contaminant concentration caused by the duct system, C_d, is then given by a steady-state material balance:

$$C_d = \frac{E_d}{Q} \tag{6.2}$$

where the emission rate from the duct system, E_d, is assumed to be entirely due to duct liner and duct sealant, found to be the dominant emission sources

$$E_d = A_{dl}E_{dl} + A_{ds}E_{ds} \tag{6.3}$$

Here, A_{dl} is the area of duct liner, A_{ds} is the area of exposed sealant, E_{dl} is the species emission factor for duct liner, and E_{ds} is the species emission factor for duct sealant. Estimates for A_{dl} and A_{ds} are discussed in a later section.

6.2.3 Ozone deposition

The ozone uptake rate at duct surfaces was parameterized by the deposition velocity, v_d (Nazaroff et al., 1993),

$$F = v_d C \qquad (6.4)$$

where F is the deposition flux (mass or mol per area per time) and C is the airborne ozone concentration near the surface. In determining deposition velocity from chamber experiments and in predicting ozone loss in model duct systems, I consistently used the superficial surface area, given by a plane of the same dimensions as the exposed surface. Please refer to Chapter 3 for a description of deposition velocity and its relationship to the reaction probability.

I measured the reaction probability for several duct liners and for galvanized sheet metal. I also measured the rate at which the surface of the material ages, thus reducing its ability to scavenge ozone. This information allows me to predict ozone removal for air flow through a ventilation duct as a function of time.

The ozone uptake experiments were conducted in the same apparatus as described above with the following exceptions. The stainless steel chamber lid was replaced with a Teflon lid. The sample material was placed in a Teflon frame so that only the upper surface was exposed and the sample itself was placed on a Teflon shelf. The compressed gas for these experiments was air (instead of N_2), which was passed through an activated carbon trap to remove trace organic contaminants. Ozone was generated by exposing a

fraction of the airflow to ultraviolet light. A portion of the vented exhaust was sampled by the ozone analyzer. An electromechanical three-way valve was used to control the air-stream feeding the ozone analyzer so that either supply air or chamber air ozone concentrations could be measured.

Each of the test materials was cut to a square 0.15 m on a side and was placed in a Teflon frame so that only the upper surface was exposed. (For duct liners, some excess fiberglass was removed from the bottom so that it would fit in the Teflon frame.) This assemblage was then placed in the chamber on a Teflon shelf and the chamber was sealed. One 24-h experiment was performed on galvanized sheet metal, two of the three new duct liners, and the one used duct liner at 100 ppb. For one sample of new duct liner, NDL2, two 100-ppb experiments and one 200-ppb experiment were performed using three different samples. Also, the sample from the first 100-ppb NDL2 experiment was sealed in aluminum foil for a week after the end of the experiment, then subjected to a second 24-h, 100-ppb experiment. This experiment was performed to measure any regeneration of the duct liner's ability to remove ozone.

Prior to each experiment, the chamber, Teflon frame, and shelf were washed in methanol and dried in an oven at 65 °C. The Teflon parts were then sealed in the reactor. Subsequently, the chamber was ventilated for 4 h with air containing a high ozone level, >4000 ppb. This procedure quenched the reactor walls so that the baseline removal of ozone in the reactor was less than 1% under standard experimental conditions. The material was exposed to a constant ozone concentration throughout an experiment by way of a feedback control system as described in Chapter 2 and Appendix A.1.

In separate experiments, I measured the mass-transport-limited deposition velocity for two material geometries. The experiments were analogous to those used for measurement of the mass-transport limited deposition velocity on carpet, as described in Section 3.2.2. A copper plate was coated with a concentrated solution of potassium iodide and allowed to dry. This plate was placed in the reactor to measure v_t for the galvanized sheet metal. A piece of NDL1 was soaked in a concentrated solution of potassium iodide and allowed to dry. It was placed in the reactor to measure v_t for duct liners.

Deposition velocity was determined from the experiments by modeling the chamber as an ideal continuously mixed flow reactor (CMFR). The governing equation for ozone concentration in the chamber, derived from material balance, is

$$V\frac{dC}{dt} = QC_{in} - C(Q + A_s v_d) \qquad (6.5)$$

where V is the chamber volume (10.5 L), t is time, C is the ozone concentration in the chamber air, C_{in} is the inlet ozone concentration, Q is the airflow rate through the chamber (1.2 L min^{-1}), A_s is the superficial area of test material (232 cm^2), and v_d is the deposition velocity. Since C is measured continuously, the slope dC/dt is known. The parameters Q, V, A_s, and C_{in} are also known. Thus, v_d can be evaluated as a function of time from equation 6.5. Steady-state analysis that includes ozone deposition to chamber surfaces as an additional loss mechanism can be found in Chapter 3, Section 3.2.2. For steady-state conditions, the reaction probability can be calculated using equation 3.1.

The experimental uncertainty in measuring γ is estimated to be ±40%, ±10%, ±30%, respectively, for reaction probabilities 10^{-4}, 10^{-5}, and 10^{-6}. The uncertainty is larger for $\gamma > 10^{-4}$ because, for our experimental configuration, ozone removal for $\gamma >$ ~10^{-4} occurs at approximately the mass-transport-limited rate. Uncertainty is larger for γ

$< 10^{-6}$ because, at this low level of reactivity, little ozone is lost as air passes through the test chamber, and the difference between the inlet and outlet concentration of ozone is small.

Experimentally, I observed an aging effect in which the uptake coefficient for some materials changed by more than an order of magnitude over time. To model this phenomenon, I assume that the uptake coefficient is a function solely of the cumulative ozone removed by the surface. Empirically, I found that a power function provided a good fit to data:

$$\gamma = A(U)^B \tag{6.6}$$

where U is the cumulative ozone uptake (i.e., the integrated flux to surface) in mol cm^{-2},

$$\int_0^t v_d C dt \tag{6.7}$$

Given the uptake coefficient, γ, the ozone removal efficiency in a ventilation duct can be predicted. As described in the appendix of Morrison et al. (1998), an analogy with heat transfer was used to estimate ozone removal efficiency for ducts in which γ is constant. A numerical approach was applied to incorporate experimental information on aging.

6.3 Results and discussion

6.3.1 VOC emissions

Measured VOC emission rates at an elapsed time of 24 h are reported in Table 6.1. The neoprene gasket and the duct sealant had the highest TVOC emission rates of 7,200 and 8,800 $\mu g\ m^{-2}\ h^{-1}$, respectively. Two of the used duct liners (UDL2 and UDL3) also had relatively high TVOC emission rates, ~1,000 $\mu g\ m^{-2}\ h^{-1}$. The highest emissions

of C_5 -C_{10} aldehydes came from UDL2, UDL3, and the duct sealant. The fact that the used duct liners were significantly stronger emitters than new liners suggests the possibility that contamination, in the form of dust deposition and/or VOC sorption, may have an important influence on VOC dynamics in ventilation systems.

Many of the materials exhibited low emission rates. For example, the two new duct liners (NDL2 and NDL3), two used duct liners (UDL4 and UDL5), the spiral-wound duct, the galvanized sheet metal, and two air filters (AF1 and AF2) all had TVOC and combined C_5 -C_{10} aldehyde emission rates that were below the lower limits of quantification at 24 h. For all of the materials, the concentrations of the analytes in the chambers generally declined with time during the 24-h test period.

The specific compound most strongly emitted from UDL3 was 2,2,4-trimethyl-1,3-pentanediol diisobutyrate, or TXIB, a commonly used plasticizer. The used fan-box insulation emitted mainly chlorinated compounds, likely from the manufacture of the stiff foam. The neoprene gasket emitted many compounds that were tentatively identified as branched alkanes and alkenes, and alkyl substituted aromatics. The aldehyde emissions from the duct sealant were dominated by a single compound, hexanal. The used duct liners produced a number of n-aldehydes above the quantification threshold. Quantifiable emissions of formaldehyde were observed for NDL3, UDL3, UDL4, and AF4. Quantifiable emissions of acetaldehyde were found for UDL4, the duct sealant, and AF3. Few specific compounds, other than aldehydes, were resolvable in the VOC emission spectra from UDL2, or from the duct sealant.

Because of their elevated rates of TVOC emission, the neoprene gasket and the duct sealant were selected for investigating the effects of ozone exposure on emissions.

Two new duct liners, NDL2 and NDL3, were also selected because the exposed surface area of duct liner in HVAC systems is typically large. The emission rates of TVOC and aldehydes from these four materials at the end of a 24-h period during which they were exposed to ozone, and the average downstream ozone concentration, are shown in Table 6.3. The emissions of both TVOC and C_5 -C_{10} aldehydes from NDL2 increased with exposure; the increase in the TVOC value is largely explained by the increase in the production of aldehydes. For both the neoprene gasket and the duct sealant, there was a decline in the emission rate of TVOC. This decline may, in part, be attributed to a natural decay in the emission rate over time. The emissions of C_5 -C_{10} aldehydes from the neoprene gasket increased with exposure to ozone. For the duct sealant, there was a small decrease in the emission rate of C_5 -C_{10} aldehydes and a substantial increase in the emission rate of acetaldehyde. The emissions from NDL3 were relatively unaffected by exposure to ozone. The relatively large standard deviation in outlet ozone concentration for these materials reflects the steady increase in outlet concentrations due to material aging.

Because of their relatively low emissions or the low exposed surface area in ducts, the study materials are not expected to be dominant contributors to the indoor TVOC concentrations, in the absence of ozone exposure. The increase in TVOC concentration associated with duct material use was estimated for a relatively new building (Soda Hall; volume = 1.4×10^4 m^3) on the campus of the University of California at Berkeley. Based on discussions with the building manager and examination of building plans, I assumed that the supply duct was lined with 34 m^2 of UDL2 and that the area of exposed duct sealant was 0.7 m^2. From equation 6.3 and the emissions data in Table 6.1, the TVOC

emission rate from duct materials was estimated to be $E_d = 38$ mg h^{-1}. Assuming a ventilation rate of 1×10^4 m^3 h^{-1} (corresponding to an air-exchange rate of 0.7 h^{-1}) for this building, the estimated increase in indoor TVOC concentration caused by emissions from duct materials would be approximately 4 μg m^{-3}. This increment is small compared with the reported weighted-average geometric mean in established office buildings (60 buildings, 384 measurements) of 180 μg m^{-3} (Brown et al., 1994).

The study results suggest that exposures of some HVAC system materials to atmospheric ozone may result in increases in the concentrations of C_5 -C_{10} aldehydes, a group of odorous chemical irritants. For example, the exposure of NDL2 to ozone produced a combined C_5 -C_{10} aldehyde emission rate of ~400 μg m^{-2} h^{-1} (Table 6.3). For the scenario outlined above, this emission rate from 34 m^2 of material would contribute ~1.4 μg m^{-3} to the combined C_5 -C_{10} aldehyde concentration of the building. This contribution represents a nonnegligible fraction of the odor thresholds for some of these compounds (e.g., compare with the odor thresholds of 13 μg m^{-3} for nonanal and 6 μg m^{-3} for decanal (Devos et al., 1990)).

Table 6.1. Emission rates of total volatile organic compounds (TVOC) and aldehydes from duct components.[a]

material	emission rate μg m^{-2} h^{-1} TVOC	formaldehyde	acetaldehyde	acetone	C_5-C_{10} aldehydes	most common VOCs	most common aldehydes
new duct liners							
NDL2	b	b	b	29	b		
NDL3	b	40	b	b	b		
used duct liners							
UDL2	950	b	b	87	220	unresolvable	C_6, C_9, C_{10}
UDL3	1280	37	b	38	260	TXIB[c]	C_8, C_9, C_{10}
UDL4	b	29	25	b	b		
UDL5	b	b	b	b	b		
used fan box insulation	1140	d	d	b	b	CCl_3F, chlorobenzene	
neoprene gasket	7200	b	b	b	b	branched alkanes & alkenes, alkyl substituted aromatics	
duct connector	670	b	b	b	b		
duct sealant	8800	b	67	b	760	unresolvable hydrocarbons	C_6
sprial wound duct	b	b	b	b	b		
galvanized sheet metal	b	b	b	b	b		
air filters							
AF1	b	b	b	b	b		
AF2	b	b	b	b	b		
AF3	550	b	20	57	b		
AF4	430	38	b	b	b		

[a] measured at the end of 24 h test period, in the absence of ozone exposure

[b] b = below quantification limit: 300 μg m^{-2} h^{-1} for TVOC; 20 μg m^{-2} h^{-1} for formaldehyde, acetaldehyde, and acetone; 150 μg m^{-2} h^{-1} for C_5-C_{10} aldehydes.

[c] TXIB = 2,2,4-trimethyl-1,3-pentanediol, diisobutyrate.

[d] sample lost or invalid.

Table 6.2. Ozone uptake coefficient parameters.[a]

material	$A[(cm^2\ mol^{-1})^{-B}]$	B	r^2	γ (24 h)	sample mass (g)
galvanized sheet steel[b]	2.5×10^{-24}	-1.99	0.94	1.1×10^{-6}	na
NDL1[b]	7.3×10^{-11}	-0.66	0.97	7.9×10^{-6}	na
NDL2[c]	5.2×10^{-10}	-0.64	0.79	3.2×10^{-5}	9.25
NDL2[d]	1.9×10^{-8}	-0.39	0.85	1.5×10^{-5}	8.7
NDL2[e]	1.0×10^{-8}	-0.45	0.93	1.5×10^{-5}	7.72
NDL3	2.8×10^{-8}	-0.36	0.80	1.5×10^{-5}	na
UDL	1.8×10^{-8}	-0.46	0.81	4.8×10^{-5}	na

[a] The parameters A and B quantify the aging effect (see equation 6.6); r^2 indicates the correlation between log (γ) and log (U); γ (24 h) is the measured uptake coefficient following 24 h of exposure to ozone at 100 ppb.
[b] exposure level of ozone strayed up to 130 ppb because of low overall ozone removal.
[c] parameter values based on initial 24-h, 100 ppb exposure experiment; data from second experiment shown in Figure 6.4.
[d] second sample of NDL2, exposed to 100 ppb for 24 h.
[e] third sample of NDL2, exposed to 200 ppb for 24 h.

Table 6.3. Emission rates of total volatile organic compounds (TVOC) and aldehydes from duct components after exposure to ozone for 24 h.

material	emission rate ($\mu g\ m^{-2}\ h^{-1}$)[a]					ozone (ppb)	
	TVOC	HCHO	CH_3CHO	acetone	C_5-C_{10} aldehydes	inlet	chamber /outlet
NDL2	550	b	20	166	380	110	72 ± 12
NDL3	b	60	b	b	b	140	31 ± 8
neoprene gasket	6400	b	b	120	330	140	65 ± 9
duct sealant	4000	24	290	b	660	100	27 ± 15

[a] b = below quantification limit: 300 $\mu g\ m^{-2}\ h^{-1}$ for TVOC; 20 $\mu g\ m^{-2}\ h^{-1}$ for formaldehyde, acetaldehyde, and acetone; 150 $\mu g\ m^{-2}\ h^{-1}$ for C_5-C_{10} aldehydes.

6.3.2 Ozone deposition

For duct liners NDL2 and UDL, the initial uptake coefficient was so high as to be indistinguishable from unity. The initial value of the uptake coefficient for NDL1 and NDL3 was ~10^{-4}. The final, 24-h, values of γ for duct liners cluster around 10^{-5} (Table 6.2). Interestingly, the final uptake coefficient for the used duct liner, UDL, was about four times higher than for NDL1 and NDL3. However, since I lack information about the

history of ozone exposure, particle deposition, or manufacturing details for UDL, I cannot draw conclusions about the source or significance of this difference. The 24-h value of γ for galvanized sheet metal was ~10^{-6}, about 10 times less than those for the duct liners.

All of the materials exhibited aging when continuously exposed to ozone, as illustrated by Figure 6.1. To maintain 100 ppb in the chamber air, the inlet ozone level begins above 300 ppb, then, as ozone reacts less rapidly, is reduced over the period of the experiment to less than 250 ppb.

The mass-transport-limited deposition velocity, v_t, was measured to be 0.19 cm s^{-1} for galvanized sheet metal (represented by a copper plate) and 0.16 cm s^{-1} for the coated duct liner. It is surprising that v_t for the flat plate is higher than that for the duct liner, since the duct liner appears to have a higher intrinsic surface area and the increased roughness would be expected to enhance mass transfer. This unexpected result could occur if the fluid dynamics between the two systems were significantly different. The only apparent difference in conducting the experiments was that the top surface of the copper plate (as well as the galvanized sheet metal) was approximately 1.5 cm lower than the top surface of the duct liner.

The evolution of the measured deposition velocity, v_d, is illustrated in Figure 6.2 for sample NDL2. Note that the initial deposition velocity value is 0.23 cm s^{-1}, which is higher than the measured transport-limited deposition velocity, v_t. One possible explanation for this discrepancy is that the fluid dynamics were somewhat different between the two experiments. For example, the surface of the duct liner that was not coated with KI might have been rougher or had more intrinsic surface area. There are

some differences in the pattern of fibers and the roughness of the surface of the duct liner, but the roughness "scale" appears to be similar. A second possibility is that some ozone loss occurs by homogeneous gas-phase reactions, not accounted for in this calculation. Since the mechanism causing the discrepancy is unknown, I used the measured value of 0.16 cm s^{-1} for v_t and, in determining the uptake coefficient, discarded measurements for which $v_d > v_t$.

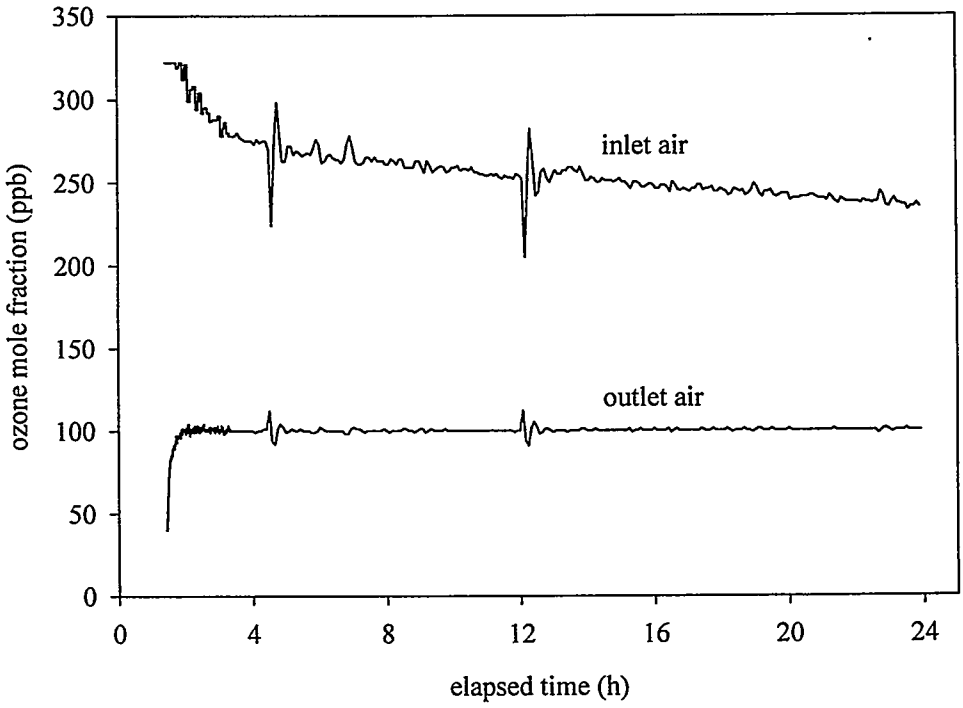

Figure 6.1. Inlet and outlet ozone levels as functions of time for ozone uptake experiment on a sample of new duct liner, NDL2. During the first 1.5 h, the ozone generator was calibrated and the sample was not exposed to ozone (data not shown).

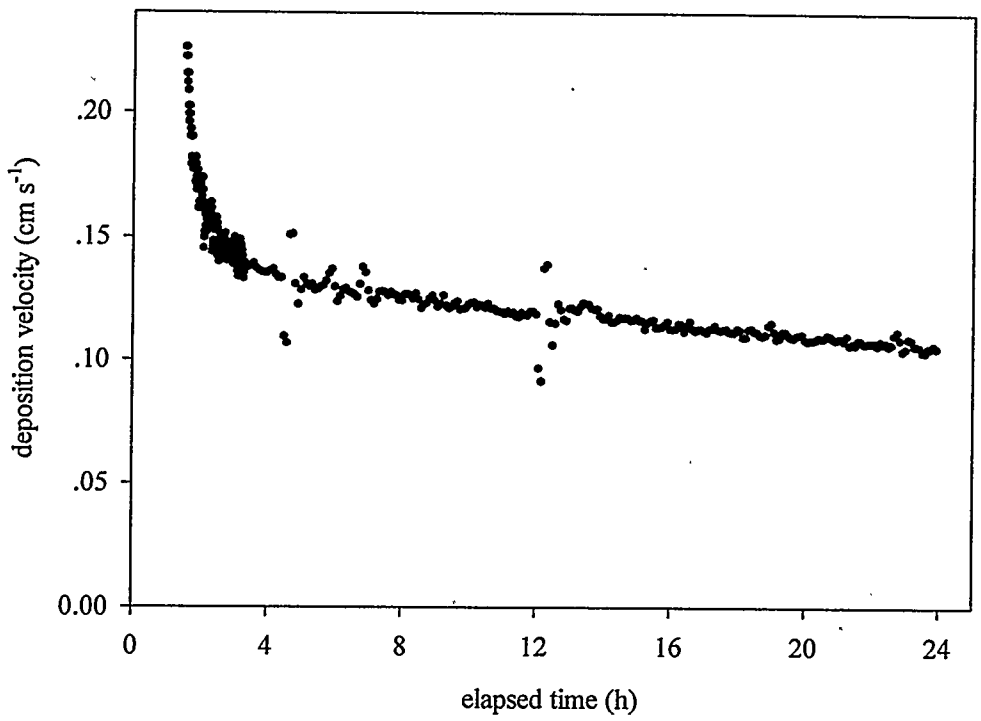

Figure 6.2. Deposition velocity (v_d) for a sample of new duct liner, NDL2, as a function of time. These results represent the interpretation of data from Figure 6.1.

I also discarded values from the first 20 min of exposure because the rapidly changing ozone concentrations produce large errors in estimating γ. The parameters A and B, used to describe aging according to equation 6.6, were obtained by linear regression of $\log(\gamma)$ versus log(U) using all other measurements (Table 6.2). This relationship is illustrated for one sample in Figure 6.3; similar curves were obtained for the other materials. The result of the repeated 24-h experiment on the same sample of NDL2 is shown in Figure 6.4 which shows that following a brief increase in uptake coefficient associated with regeneration, the ozone scavenging rate returns to a profile consistent with predictions from the first 24-h exposure.

The assumption that the uptake coefficient is purely a function of cumulative ozone uptake suggests that the results of three NDL2 experiments should yield identical

estimates of the parameters A and B in equation 6.6. The predicted uptake coefficient based on the 200-ppb NDL2 experiment is, on average, about 35% lower than that predicted by the first 100 ppb experiment. However, the initial deposition velocity varied among experiments: 0.23±0.02 cm s^{-1} for the first 100-ppb experiment, 0.15±0.02 cm s^{-1} for the second, and 0.17±0.02 cm s^{-1} for the 200-ppb experiment. Such a large difference in the initial deposition velocity, and in the estimates of A and B, may be due to intrinsic differences in the three samples themselves. Note that the mass of the first sample exposed to 100 ppb is 20% greater than that of the sample exposed to 200 ppb. I also observed that the apparent bulk density of the fiberglass mat varied. On the assumption that the initial deposition velocity was a better measure of the mass-transport-limited deposition velocity, I recalculated A and B for these experiments and found that the curves for the first 100-ppb experiment and the 200-ppb experiment largely overlapped. This result substantiates the assumption that the cumulative uptake of ozone is a key controlling variable influencing aging. However, the repeated 100-ppb experiment does not match well the first experiment using this same approach.

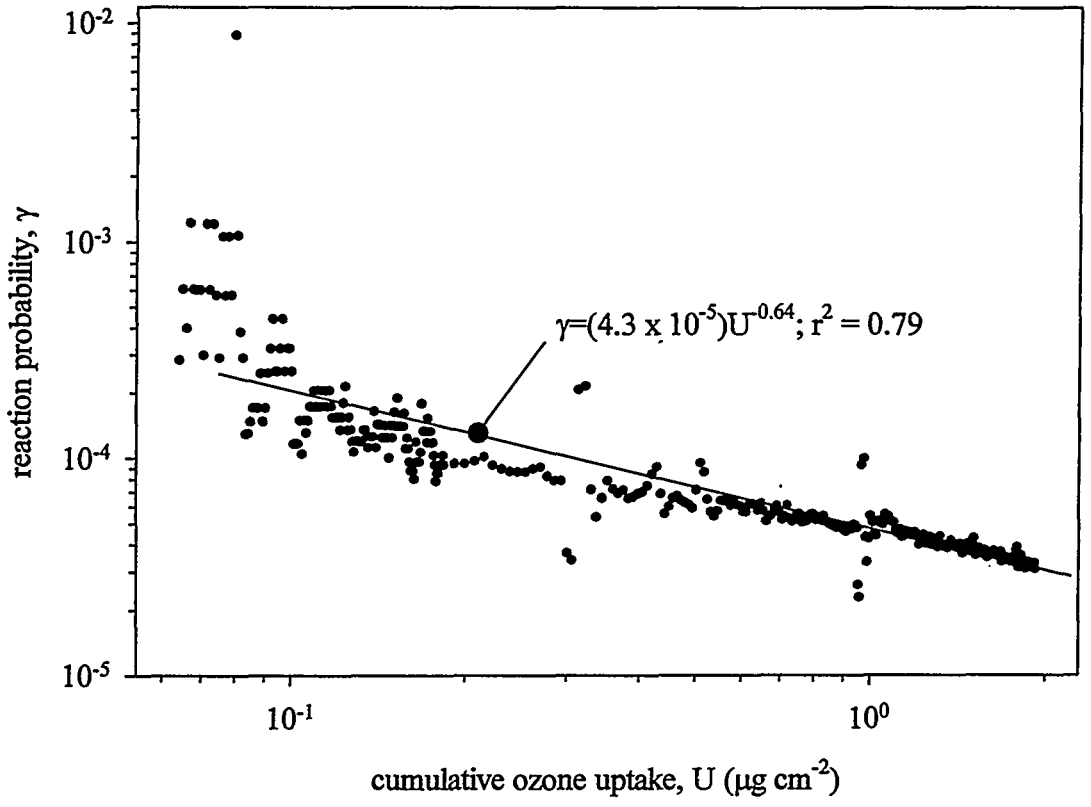

Figure 6.3. Reaction probability, γ, as a function of the cumulative ozone uptake, U, for a sample of new duct liner, NDL2. The results correspond to data in Figure 6.1. The line represents a linear regression of log(γ) vs. log(U).

The test results for ozone scavenging were used to predict the ozone removal efficiency for an air-supply duct. Input parameters were based on the same building, Soda Hall, used for the assessment of VOC impact. A rectangular duct with cross-sectional dimensions of 1.2 × 1.5 m was considered. The volumetric airflow rate through the duct was 8.25 $m^3 s^{-1}$. Calculations were conducted for 30-m lengths of lined duct and for 30-m and 150-m lengths of galvanized sheet metal. For each simulation, a period of 240 h was considered with the inlet ozone level fixed at 37 ppb, corresponding to the middle of the reported range of annual average values for Los Angeles, 20–54 ppb (Cass et al., 1991).

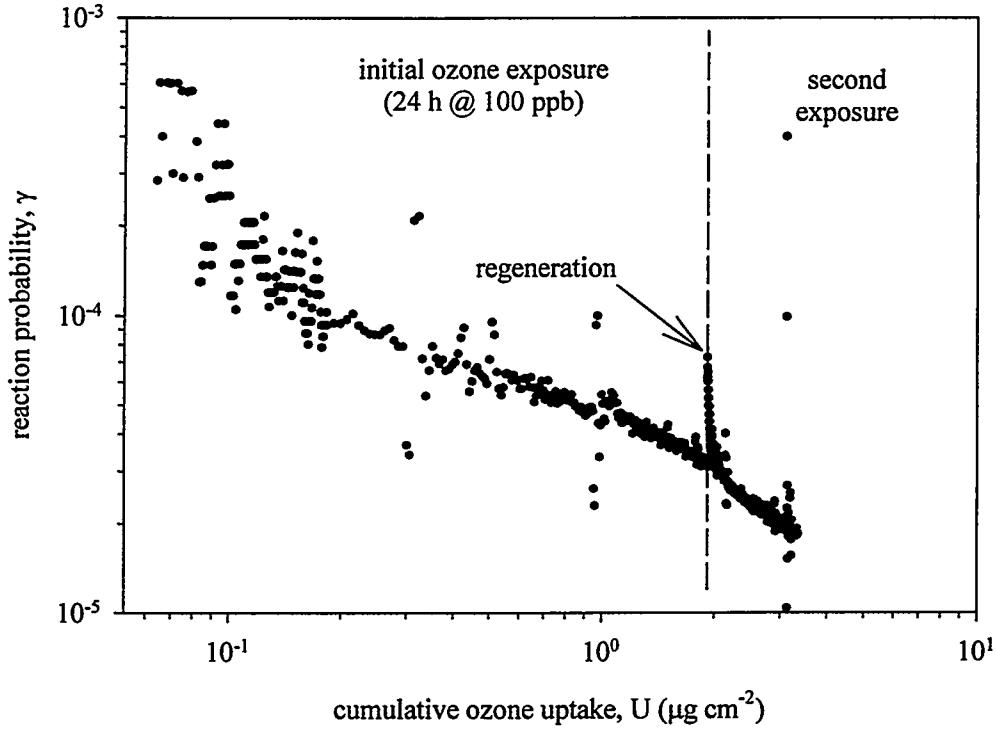

Figure 6.4. Reaction probability, γ, as a function of the cumulative ozone uptake, U, for a sample of new duct liner, NDL2. The sample was exposed to 100 ppb ozone for 24 h, stored for one week without exposure, then subjected to a second exposure for 24 h at 100 ppb.

The predicted ozone removal efficiency, η, is plotted as a function of time in the presence of aging for all lining materials in Figure 6.5. The curve for NDL2 is based on values of A and B determined from the first 100-ppb experiment. The ozone removal efficiency in this simulated duct is small. Note that NDL2 was the most "active" duct liner, in that η changed the most over the simulated exposure period. According to predictions, NDL2 initially removes as much ozone as UDL, but quickly loses the ability to remove ozone. After an extended exposure, the used duct liner is the most efficient ozone scavenger, with a long-term removal efficiency of about 3%. Figure 6.5 also shows that ducts lined only with galvanized sheet metal are unlikely to remove significant amounts of ozone, even where the length-to-hydraulic diameter (L/D_h) ratio is large.

Note that these predictions are only valid for the duct portion of an HVAC system, and do not account for ozone loss on fans and filters. There is some indication that soiling may increase the ozone uptake coefficient. However, I cannot do a meaningful analysis of this phenomenon with the results from only one used duct liner. It is unknown how much of an effect soiling of the inner surfaces of the duct, or differences in humidity, might have on the overall ozone removal efficiency and reaction byproduct emissions.

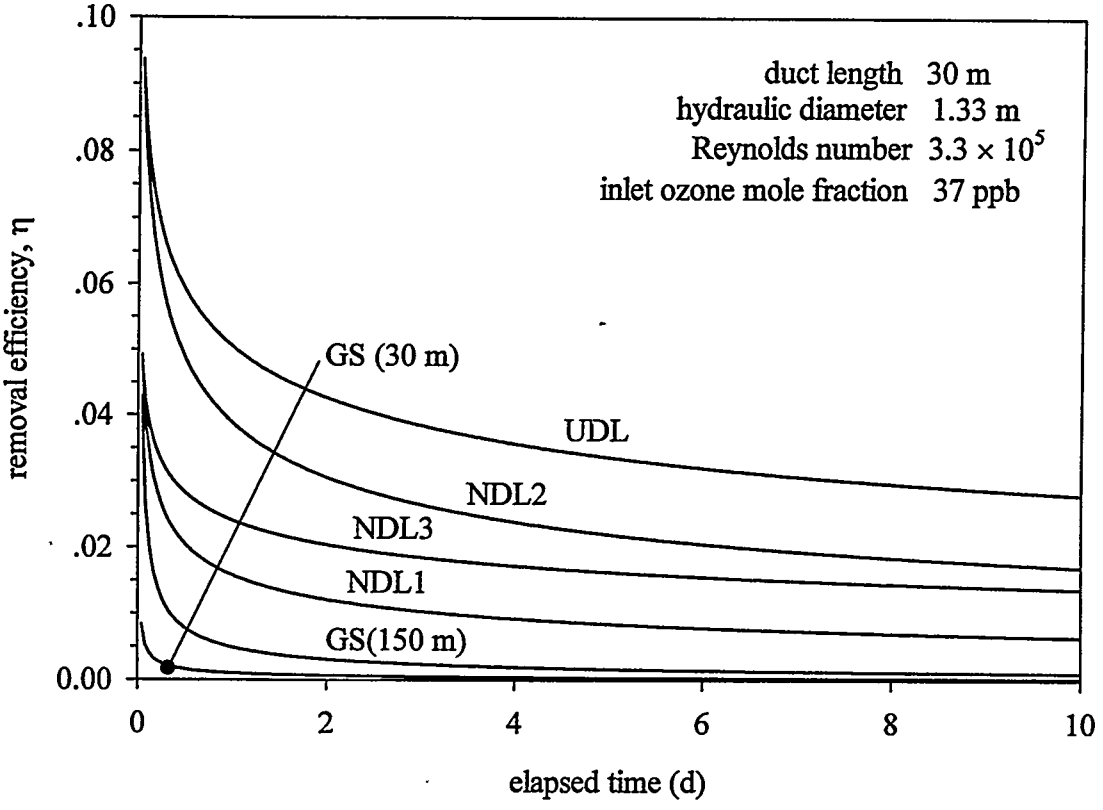

Figure 6.5. Ozone removal efficiency for tested materials as a function of time in a simulated duct. All duct lengths are assumed to be 30 m except for one GS case at 150 m, as noted. NDL = new duct liner; UDL = used duct liner; and GS = galvanized sheet steel. Calculations assume that the duct surface is hydrodynamically smooth.

6.4 Conclusions

The results of this study indicate that materials used for ventilation system ducts can have a small but discernible influence on the concentrations of ozone and VOCs in indoor air. Among the materials studied, duct liners appear most important as they are used in large quantity in duct systems, exhibit substantial reactivity with ozone, and, in some cases, emit VOCs at substantial rates. Oxidation reactions between ozone and duct materials can produce aldehydes at sufficiently high rates that predicted indoor concentration increments may be a significant fraction of the odor threshold. Additional work would be needed to understand how the presence of dust that accumulates in ducts over the long term influences indoor air pollutant levels.

6.5 References

Batterman, S.A.; Burge, H. *HVAC&R Research.* **1995**, *1*, 61-80.

Burge, S.; Hedge, A.; Wilson, S.; Bass, J.H.; Robertson, A. *Annals of Occupational Hygiene.* **1987**, *31*, 493-504.

Brown, S.K.; Sim, M.R.; Abramson, M.J.; Gray, C.N. *Indoor Air.* **1994**, *4*, 123-134.

Cass G.R.; Nazaroff W.W.; Tiller C.; Whitmore P.M. *Atmospheric Environment*, **1991**, *25A*, 441-451.

Devos, M.; Patte, F.; Rouault, J.; Laffort, P.; Van Gemert, L.J.; Eds. *Standardized Human Olfactory Thresholds*. Oxford University Press: Oxford, 1990.

Nazaroff, W.W.; Gadgil, A.J.; Weschler, C.J. In *Modeling of Indoor Air Quality and Exposure*; Nagda, N.L., Ed.; ASTM STP 1205; American Society for Testing and Materials: Philadelphia, PA, 1993; pp 81-104.

Mendell, M.J.; Smith, A.H. *American Journal of Public Health.* **1990**, *80*, 1193-1199.

Mølhave, L.; Thorsen, M. *Atmospheric Environvironment* **1991**, *25A*, 241-249.

Morrison, G.C.; Nazaroff, W.W.; Cano-Ruiz, J.A.; Hodgson, A.T.; Modera, M.P. *Journal of the Air and Waste Management Association.* **1998**, *48*, 941-952.

Reiss, R.; Ryan, P.B.; Koutrakis, P.; Tibbetts, S.J. *Environmental Science and Technology.* **1995a**, *29*, 1906-1912.

Reiss, R.; Ryan, P.B.; Tibbetts, S.J.; Koutrakis, P. *Journal of the Air & Waste Management Association.* **1995b**, *45*, 811-822.

Weschler, C.J.; Shields, H.C.; Naik, D.V. *Journal of the Air Pollution Control Association.* **1989**, *39*, 1562-1568.

Weschler, C.J.; Hodgson, A.T.; Wooley, J.D. *Environmental Science Technology.* **1992**, *26*, 2371-2377.

Zhang, J.; Lioy, P.J. *Indoor Air.* **1994**, *28*, 95-105.

CHAPTER 7

Summary and Recommendations for Future Research

7.1 Summary of results

One of the primary goals in the study of air pollution is to gain a deeper understanding of the underlying processes that control pollutant concentrations. Ambient (outdoor) air quality has been vigorously studied for many years, with great resulting advances in our knowledge of the chemistry and physical dynamics of pollutants. However, the study of pollutants in indoor air may be just as important when we consider two well established facts: 1) people spend most of their time indoors and 2) indoor concentrations of pollutants usually do not match outdoor concentrations even when the pollutants originate outdoors. Reactive species concentrations are reduced through interactions with the large amount of indoor surface area. At the same time, direct indoor emissions cause the concentrations of many species, including numerous volatile organic compounds, to be considerably higher indoors. Outdoor measurements and models may not be directly applicable to the indoor setting. Much more research must be directed to understanding the underlying chemistry and physical dynamics of pollutants in indoor spaces.

To that end, I studied the interactions of ozone with indoor surfaces. In these investigations, I measured specific parameters, such as the ozone reaction probability of carpet and duct materials, and the emission rates of primary and secondary organic compounds. I developed models of mass transport and deposition of reactive gases to carpet. I used dynamic surface aging data to reduce the range of physical models

describing ozone uptake and surface quenching. I then combined models and measurements to make predictions of pollutant concentrations in typical indoor settings.

An important finding was that for every mole of ozone reacting with carpet roughly 0.5 moles of aldehydes are released into the air, during the initial stages of exposure. The evidence of a (nearly) direct trade-off between ozone and aldehydes leads to several public health questions. Would we be better off with high ozone deposition, resulting in lower indoor ozone concentrations but higher levels of odorous aldehydes? Or is the health of the public better served by eliminating reactive precursors on carpets, reducing indoor concentrations of aldehydes but increasing indoor exposures to ozone? Or, is it possible to modify surface coatings such that ozone scavenging is maintained but aldehyde release is suppressed? The results of this dissertation cannot directly address these questions, but nevertheless shed some light on the public health implications of the presence of carpet in occupied spaces. More importantly, these studies can help illuminate issues pertaining to the general class of indoor air pollutant-surface interactions. Mathematical models developed here might also be used to predict indoor concentrations of pollutants that are subsequently combined with human exposure models.

7.1.1 Ozone reactive chemistry and indoor surfaces

When Weschler et al. (1992) found that ozone induced emissions of odorous oxidized compounds from carpet, they showed that even moderate concentrations of reactive pollutants could significantly degrade indoor air in unexpected ways. I expanded on that original carpet study and found that some carpets can release large amounts of very odorous unsaturated aldehydes. Models of building spaces suggest that the

emissions would result in concentrations that exceed odor thresholds even when ambient ozone levels are low. Long term airing of carpets reduces these secondary emissions in all cases, but the reductions are moderate compared to the drop in primary emissions. The modest reduction in secondary emissions suggests that long-term airing of carpets is not a practical control strategy.

I used the relative emissions of oxidized reaction products to better identify precursors of aldehyde emissions. The pattern of emissions, specifically high nonanal emissions, suggests that the surface is coated with vegetable oil or derivatives. The formation of other compounds, such as 2-nonenal, indicates that steps used to process the vegetable oil may have isomerized existing double bonds to form conjugations in the carbon backbone of the precursor. I suggest that 9,11-octadecadienoic acid (or an ester derivative) is a probable precursor for the strong emissions of 2-nonenal. According to my modeling interpretation of the experimental data, secondary emissions due to ozone deposition could result in odorous levels of 2-nonenal for several years after installation of carpet in a home.

Several interesting physical and chemical mechanisms were deduced by investigating the dynamic emission rate of ozone reaction products with carpet surfaces. Strong adsorption of aldehydes to carpet surfaces may partially account for the slow decay of chamber aldehyde concentrations in the absence of ozone. Strong sorption of aldehydes to carpet would result in lower daily peak concentrations indoors. However, the carpet in this case would act as a reservoir for these compounds, releasing them into rooms even when ozone concentrations are low enough to result in negligible formation of aldehydes.

I also observed that the 2-nonenal emissions were significantly delayed with respect to other aldehyde species. This may indicate that a stable intermediate is formed in advance of 2-nonenal. The intermediate's stability kept 2-nonenal from being emitted immediately. I suggest that the intermediate is an ozonide, stabilized by an adjacent double bond. The formation of the stable ozonide, along with delayed decomposition to the aldehyde can further reduce concentrations of 2-nonenal during peak ozone periods. But, once again, this acts as a storage mechanism, releasing 2-nonenal during low ozone periods.

Duct materials also released aldehydes when exposed to ozone. I combined the experimentally measured aldehyde emission rates with a indoor air quality model to show that secondary emissions from the materials that line ducts may result in aldehyde concentrations that approach odor thresholds.

7.1.2 Ozone deposition to surfaces

I measured the rate of ozone uptake on carpets and the materials that line ducts. Ozone uptake was parameterized by the reaction probability. I found that the ozone reaction probability of whole carpet, carpet backing and duct liners was approximately 10^{-5}. This value is similar to that measured for painted surfaces (Reiss et al. 1995a). The reaction probability on galvanized sheet steel was about 10^{-6}. On carpet fibers and a cleaned aluminum sheet, the value was about 10^{-7} or less. The low value for the reaction probability on carpet fibers and aluminum is comparable to that found for glass (Sabersky et al., 1973).

Models were developed to describe reactive gas (using ozone as an archetype) deposition to surfaces. A model of turbulent mass transport was combined with the

surface uptake resistance to create a general model of reactive gas deposition indoors. This model predicts that the area-averaged deposition velocity in a typical room would range from 0.02 cm s^{-1} to 0.06 cm s^{-1} for an area-averaged ozone reaction probability of 10^{-5}, a value typical of carpet or painted surfaces. This deposition velocity range nicely brackets the reported typical indoor value of 0.04 cm s^{-1} (Nazaroff et al., 1993). A separate model was developed to predict the reaction probability of carpet based on the reaction probability of the components of carpet (fibers and backing). This model accurately predicted that the reaction probability of whole carpet should be about 10^{-5}, based on independent measurements of the reaction probability of fibers and backing.

The mathematical models of mass transport and deposition of ozone were used along with measurements of the reaction probability of carpet and its components to show that carpet can be an important sink for ozone compared to painted walls. The carpet fiber model also showed that carpet backing could be as important as carpet fibers in reducing ozone concentrations indoors.

7.1.3 Ozone aging of surfaces

In experiments with carpets and duct materials, I found that the surface reaction probability, γ, is reduced by continued exposure to ozone, but typically stabilized to about 10^{-5} for carpet and duct liner. I recognized that the measured dynamics of ozone surface aging might be used to test models of surface quenching. The aging of surfaces appears to follow a power function relationship where the reaction probability is proportional to the cumulative uptake of ozone, raised to a negative power. I developed two general models of ozone aging of surfaces: a diffusion with internal reaction model and an external surface reaction model. The model of diffusion with internal reaction resulted in a

relationship that followed the general form of observed surface aging. To adequately model all observations, a combination of surface reaction and internal reaction mechanisms may be required.

Whole carpet was found to age more slowly than carpet fibers. This is because ozone initially reacts to age the fiber tips only, while more reactive surfaces remain unexposed deep in the carpet mat. As ozone progressively ages surfaces deeper in the carpet mat, the whole carpet reaction probability slowly decreases. Both carpet aging models and measurements show this effect, but at present there is only a qualitative agreement between the two.

7.2 Future research directions

In the course of my research, I have identified several areas that merit more attention. In general, there is much more to be accomplished in the area of pollutant-surface interactions. Indeed, indoor surfaces themselves are not well characterized both with respect to morphology and chemical properties. In the following sections, I identify areas where further research can strengthen, broaden or refute my findings and suggest specific methods to carry out this research.

7.2.1 Reactive chemistry and indoor surfaces

The kinetics and mechanisms of ozone reactions at air/solid interfaces are not well established. Much research has focused on homogeneous chemistry of ozone in the gas phase or in solution. My results suggest that mechanisms similar to those that occur in solution are at work when ozone attacks double bonded compounds at or below the surface. This should be verified spectroscopically, if possible. The difficulty in measuring

compounds involved in these reactions lies in the nature of interfaces themselves. The total mass of target species may be very small, making measurement by any method difficult. It is also difficult to measure these compounds *in situ* due to limitations in existing analytical techniques used for surface measurements.

I suggest the following method for determining the relative surface concentrations of precursors and products. First, I believe that a model surface should be coated with a model compound to simplify analysis of kinetics and mechanisms. To investigate how compounds behave on carpet fibers, the model surface could be a polyolefin or nylon, and the model precursor might be 9,11-octadecadienoic acid. This surface must then be exposed to ozone and the surface species collected at specific time intervals. Many species can simply be extracted from the surface using appropriate solvents. In practice, these extracts are typically reduced in volume using cold-distillation techniques so that the target compounds are concentrated for analysis using gas chromatography with a mass-selective detector (GC/MS). Some compounds must be derivitized to increase the sensitivity of analytical methods, such as GC/MS, to identify the compounds. Some compounds, such as organic acids, may also be amenable to ion chromatography. I identified a stabilized ozonide as a possible reservoir for aldehydes. Detection of the stable ozonide in solution may be better accomplished using infrared absorption spectroscopic techniques. Ozonides are very sensitive to temperature and moisture. Thus, a well thought-out sample handling procedure must be developed. The technique can be used to investigate variables such as humidity and contamination (soiling) on reaction products and kinetics. Ultimately, real surfaces and real contaminants must be

investigated using the same techniques to verify that model systems simulate real surfaces.

A less direct way to investigate the kinetics of ozonide formation and decomposition on real surfaces may simply rely on experimental methods used in my carpet studies. I suggested that the slow decay of aldehydes in the carpet chamber without ozone was due to a combination of strong sorption and delayed ozonide decomposition. The sorption kinetics on carpet of aldehydes should be measured in the absence of ozone. Thus the relative magnitude of the two mechanisms can be quantified. Techniques such as those developed by Won et. al. (1999) should be adequate to measure sorption kinetics of aldehydes on carpets.

Field studies would be useful in verifying the predicted concentrations of aldehydes in buildings furnished with carpet. I estimated that concentrations of several aldehydes would exceed odor thresholds in a typical residence fitted with carpet CP3. Researchers have found some evidence that the concentrations of specific aldehydes correlated with the concentration of ozone in field houses (Reiss et al., 1995b; Zhang et al., 1994). They did not measure aldehydes heavier than hexanal. However, my experiments show that nonanal (and maybe 2-nonenal) are the most important secondary emissions from carpets. To verify that odorous levels of aldehydes can be attained in a field site, carpet CP3 or its equivalent could be installed in a residence. The air-exchange rate and concentrations of ozone and aldehydes should be measured. I am especially intrigued by the possibility that independent measurements of ozonide decay kinetics might be used to predict dynamic indoor concentrations of aldehydes, where carpets are exposed to diurnal variations in ozone concentrations. Field studies could also be used to

test the prediction that the concentration of 2-nonenal rises slowly over a period of several weeks, rather than following the rise and fall of ozone concentrations.

Accepted mechanisms for ozone attack on double bonds indicate that organic acids are formed as well as aldehydes. Organic acids can have odor and pungency thresholds that are an order of magnitude lower than aldehydes. The available analytical techniques did not allow me to quantify these compounds. However, I did qualitatively identify some acids emitted from all carpets. Better estimates of the odor potential of carpets can come from quantification of acid emissions due to oxygen or ozone oxidation. Organic acids may be quantified using ion chromatography or derivitized and quantified using a GC/MS.

While carpet and painted walls make up a significant fraction of indoor surface area, other surfaces may be important as well. Other textiles, such as clothing and upholstery, may be manufactured with reactive surfaces similar to that of carpet. Many homes use wood, vinyl, linoleum and other materials as floor coverings. Testing these materials for ozone reactivity and secondary emissions would help to build a more complete picture of indoor ozone dynamics.

7.2.2 Reactive gas deposition to surfaces

The mass-transport model of ozone deposition developed in this dissertation is a general model that may apply to any gas that can react with surfaces. Field studies directed to testing the performance of the model should be performed. Field tests should include methods to measure the friction velocity, u*, as well as a direct measure of the deposition of the reactive gas. For example, a room could be outfitted with fans to vary the level of turbulent mixing. The parameter u* could be measured using laser-doppler

velocimetry (Lai and Nazaroff, 2000). Filter paper impregnated with $NaNO_2$ could be installed on a wall to measure ozone uptake. The compound, $NaNO_2$ reacts rapidly with ozone to form $NaNO_3$. Thus, the formation rate of the nitrate ion is a measure of ozone deposition which can be compared to model predictions using the turbulent mass-transfer model of reactive gases.

The performance of the mass-transfer model could also be tested by using other reactive gases, such as NO_2 or SO_2. Similarly, the reaction probability of reactive gases other than ozone on carpet components can be incorporated into the model of reactive gas diffusion into the carpet mat and uptake on carpet surfaces.

The ozone reaction probability on all whole carpet samples, at the end of an exposure experiment, was about 10^{-5}. However, the emission rate of summed aldehydes, at the end of the an aired carpet experiment, ranged from about 80 $\mu g\ m^{-2}\ h^{-1}$ (CP1) to 600 $\mu g\ m^{-2}\ h^{-1}$ (CP3). This finding suggests that there may be ways to reduce the emissions of aldehydes while retaining the intrinsic ability of carpet to react with and remove ozone from living spaces. If materials can be manufactured that effectively consume ozone, but release no volatile byproducts, the public health quandary posed by the trade-off between ozone and volatile secondary products might be avoided. A broader survey of new carpets and other materials may indicate if some existing furnishings meet the requirements necessary to be a good ozone sink and a low emitter of secondary reaction products.

7.2.3 Aging of surfaces

The internal reaction model of ozone aging of surfaces helps to explain the functional form of surface aging. Under certain circumstances, the model may even

provide an explanation for the steep nature of aging for fibers from carpets CP1 and CP3. More work is needed here to understand the differences among surfaces. The integrated model of aging and ozone diffusion through the carpet mat succeeds in describing the general tendency of whole carpet to age with a small power function coefficient relative to that measured on fibers. These model predictions tend to over predict the absolute magnitude of the power function coefficient. Thus the models must be improved. For example, a description that includes a variable density mat with discrete fiber tufts may predict shallower aging curves.

Mathematical models of physical processes must be integrated with data, which feed into and support the modeling efforts. At this point, more data are required to verify that a diffusion model of ozone surface aging is appropriate. Direct measurement of the diffusivity of ozone through a polymer matrix would be very difficult due to ozone reactivity. I suggest that model surfaces, such as those discussed earlier, be exposed to ozone and the depth of oxidation be measured. Infrared spectroscopy is often used to detect the carbon-oxygen bond present in solutions. For a surface, an alternative would be to use diffuse reflectance spectroscopy. In this method, infrared light penetrates the surface of a solid sample, and is absorbed or reflected as diffuse light. The diffuse light is measured and wavelength absorption is used to identify and quantify bond types.

Successful models of surface aging may provide tools for evaluating the effectiveness of potential control strategies. For example, the formulation of paint for walls could be modified to include a reducing agent that reacts irreversibly with ozone (and hopefully does not form a secondary, volatile product). Important questions regarding the effectiveness and longevity of an ozone control method such as this could

be addressed using the models described in this dissertation. The toxic species NO_2 is reduced on rush mats to NO, resulting in lower indoor concentrations of this species (Nishimura et al., 1986). The effectiveness of these mats or other indoor surfaces (Spicer et al., 1989) in reducing concentrations of NO_2 could be addressed by combining models of mass transport, diffusion into the material, and NO_2 aging of surfaces if applicable. The reactive gas deposition model shows that increasing air turbulence may increase pollutant deposition rates. The model could be used to determine if the increased turbulence induced by fans, for example, could effectively reduce reactive gas concentrations indoors.

There is a general need to better characterize indoor surfaces. Several studies have showed that humidity can increase ozone deposition to surfaces. Characterization of water distribution on real surfaces may help explain these findings. Contamination as the result of soiling may also influence pollutant deposition, kinetics and reaction mechanisms. Modeling studies of compound diffusion to and from the surface would be strengthened by measurements of surface area, pore structure and pore-size distribution. I believe that well characterized surfaces will allow us to confidently accept or reject present theories of pollutant-surface interactions.

7.3 References

Lai, A.C.K.; Nazaroff, W.W. *Journal of Aerosol Science*. **2000**, *31*, in press.

Nazaroff, W.W.; Gadgil, A.J.; Weschler, C.J. in *Modeling of Indoor Air Quality and Exposure*, STP 1205, Nagda, N.L.; Ed. American Society for Testing and Materials, Philadelphia, PA, 1993.

Nishimura, H.; Hayamizu, T.; Yanagisawa, Y. *Environmental Science and Technology*. **1986**, *20*, 413-416.

Reiss R.; Ryan, P.B.; Koutrakis, P.; Tibbetts, S.J. *Environmental Science and Technology*. **1995a**, *29*, 1906-1912.

Reiss R.; Ryan, P.B.; Tibbetts, S.J.; Koutrakis, P. *Journal of the Air and Waste Management Association*. **1995b**, *45*, 811-822.

Sabersky, R.H.; Sinema, D.A.; Shair, F.H. *Environmental Science and Technology*. **1973**, *7*, 347-353.

Spicer, C.W.; Coutant, R.W.; Ward, G.F.; Joseph, D.W.; Gaynor, A.J.; Billick I.H. *Environment International*. **1989**, *15*, 643-654.

Weschler, C.J.; Hodgson, A.T.; Wooley, J.D. *Environmental Science and Technology*. **1992**, *26*, 2371-2377.

Won, D.; Corsi, R.L.; Rynes, M. *Proceedings of the 92nd Annual Meeting of the Air and Waste Management Association*. **1999**, Paper number 99-105.

Zhang, J.; Lioy, P.J. *Indoor Air*. **1994**, *28*, 95-105.

APPENDICES

A.1 Computer Algorithm for Control of Reaction Chamber Ozone Concentrations and Data Collection

The reaction probability of ozone with a surface tends to diminish with continued exposure. In a reactor experiment, as described in Section 2.2.2, the difference between the inlet and exhaust concentration of ozone will change with time because of this effect. The exhaust concentration, for a CMFR with a constant inlet ozone concentration, will slowly rise during an experiment. The exhaust concentration corresponds with the internal chamber concentration (sample exposure concentration). This introduces a slowly changing variable which may make analysis of aging phenomena more difficult. In general, it is desirable to keep most environmental variables constant during an experiment.

This program was designed to maintain the internal chamber ozone concentration at a constant level (nominally 100 ppb). As the reactivity of the material sample diminishes, the program responds by decreasing the inlet ozone concentration. The result is a constant exhaust (and exposure) ozone concentration during the entire experiment. The program consults an input file, shown in Figure A.1.1 every 5 minutes. This file contains the instructions for control setting (calibration mode, control mode on, control mode off, program end), valve settings, and data write frequency to an output file.

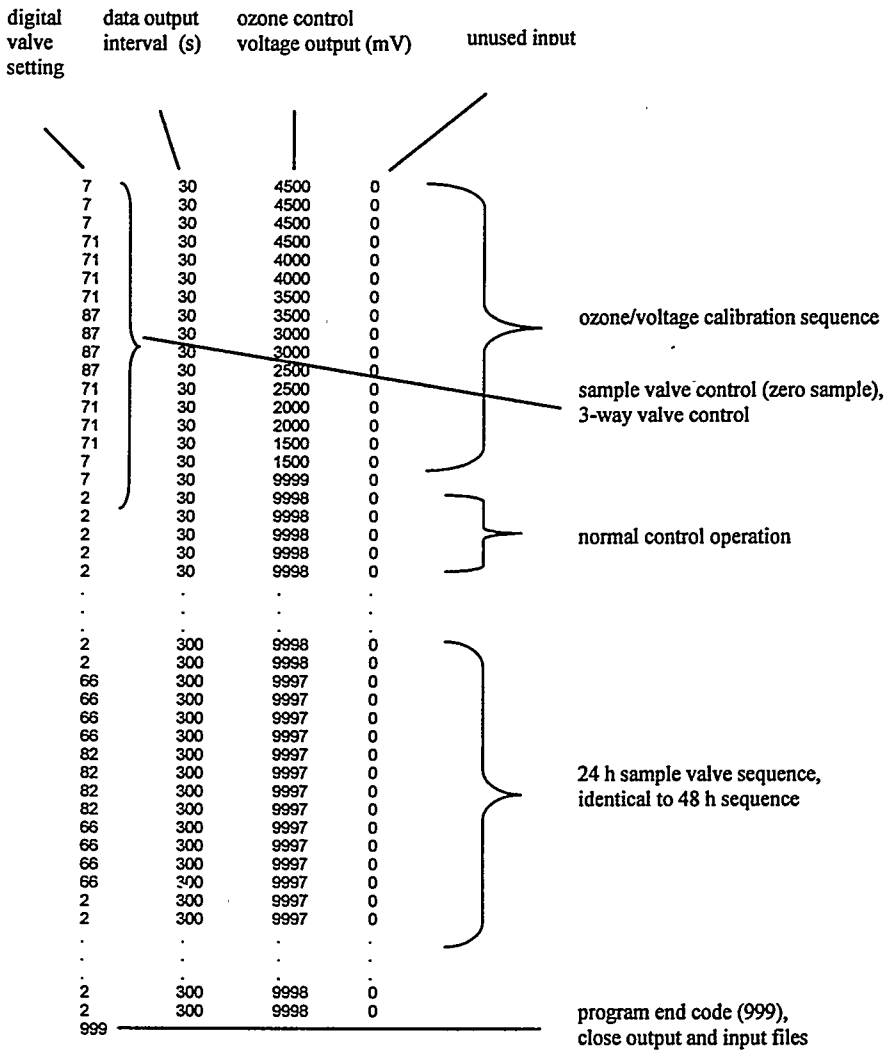

Figure A.1.1. Input file for control algorithm.

Because of physical limitations on the reactor apparatus, only one gas stream can be sampled for ozone concentration at a given time. I placed a Teflon 3-way valve upstream of the reactor so that either (valve on) the inlet gas stream or (valve off) the exhaust gas stream is directed to the ozone analyzer. Initially, the inlet gas stream is sampled while the program (through the D/A board) outputs a voltage sequence (4.5 V, 4.0 V, ...1.5 V; 10 minutes each) to the power control system of the ozone generator. The average resulting ozone concentration at each voltage level is recorded and at the end of the sequence, subjected to a least-squares linearization to obtain slope and intercept

parameters. During the rest of the experiment, the output voltage of the D/A board is assumed to correspond to the inlet ozone concentration, with an adjustment to take into account any small changes in the inlet feed stream flowrate.

The circuit used to amplify the D/A signal for use by the UV lamp ballast is shown in Figure A.1.2. The lamp will operate when the voltage to the ballast is between 12 V and 24 V. The UV output of the lamp is linearly proportional to ballast voltage in this range. To operate the lamp with computer control, the circuit amplifies the 0-5 V signal to 0-12 V, then adds 12 V to this value.

The lamp and flow-tube assembly shown in Figure A.1.2 is used to create ozone in a flowing air stream. The UV lamp is shielded by an aluminum sleeve that can be manually adjusted to control the flux of UV energy entering the quartz tube. This mechanism can be used to crudely control the resultant ozone concentration in the air stream.

After calibration, the program switches off the 3-way valve so that the inlet stream starts to feed the reactor and the exhaust stream is directed toward the ozone analyzer. The D/A voltage is set to maximum (4.5 V) to maximize the rate of rise to the setpoint. When the ozone concentration at the exhaust reaches 90% of the setpoint, the control routine is allowed to begin adjusting the inlet ozone concentration.

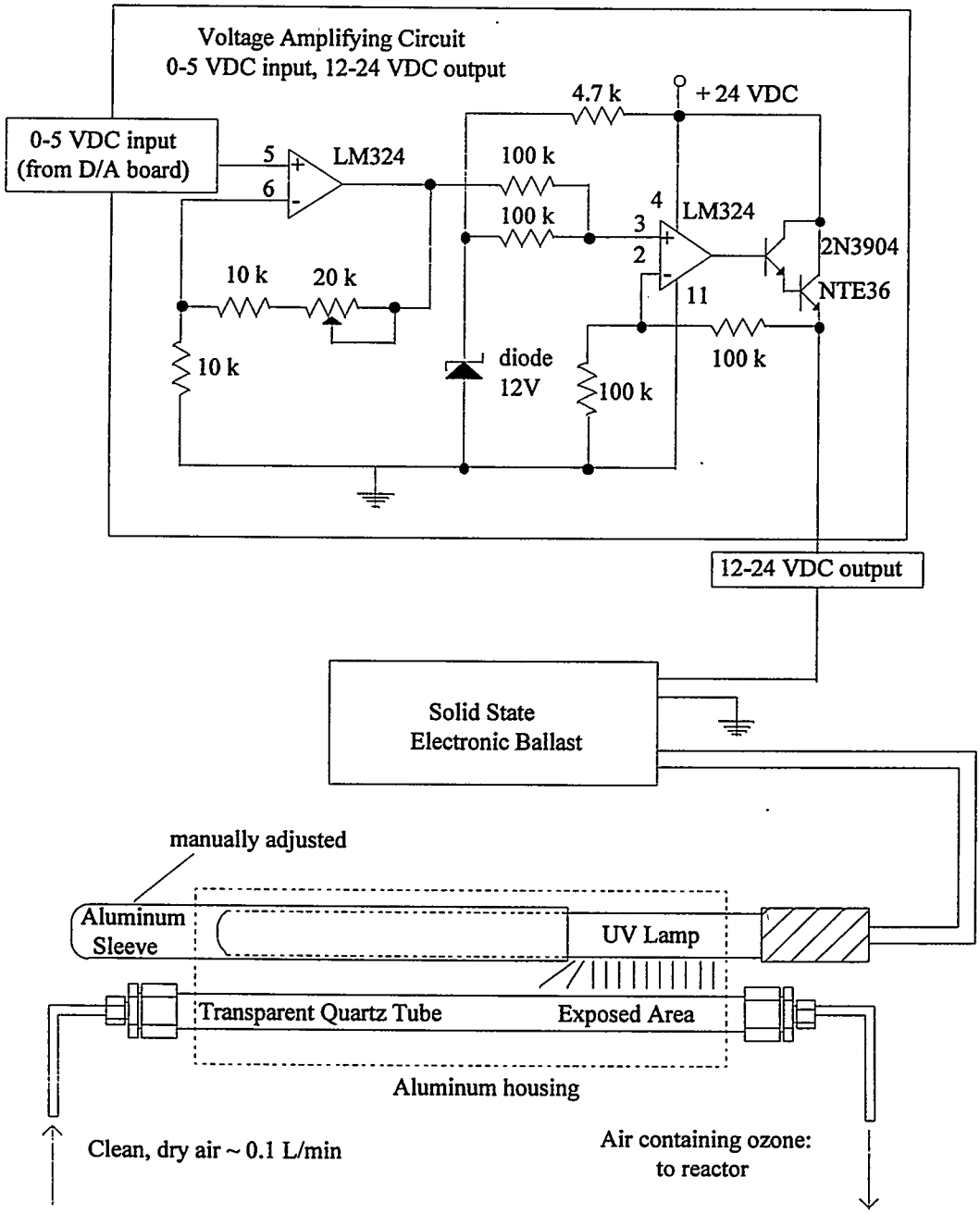

Figure A.1.2. Ozone generator voltage control circuit diagram and ozone generator.

The control routine is based on knowledge of the probable dynamic characteristics of CMFR reactors. For a CMFR containing reactive media, the dynamic ozone concentration is given by

$$\frac{dC}{dt} = \frac{Q}{V}(C_{in} - C) - \frac{A_s v_d C}{V} \qquad (A.1.1)$$

where C is the exhaust ozone concentration, C_{in} is the inlet ozone concentration, V is the reactor volume, A_s is the area of the reactive surface, v_d is the ozone deposition velocity, and Q is the volumetric flowrate through the reactor. The control program proceeds by assuming that the deposition velocity remains steady during a designated time interval (30 sec to 5 min depending on the input file) and that the rate of change of the concentration during that time interval can be approximated by

$$\frac{dC}{dt} = \frac{(C(t_1) - C(t_o))}{\Delta t} \qquad (A.1.2)$$

where $C(t_o)$ is the concentration at the beginning of the time interval, $C(t_1)$ is the concentration at the end of the time interval, and Δt is the length of the time interval. Substituting for dC/dt, equation A.1.1 can be rearranged such that the only unknown parameter, v_d, is isolated,

$$v_d = \frac{Q}{A_s}\frac{(C_{in} - C(t_1))}{C(t_1)} - \frac{(C(t_1) - C(t_o))}{C(t_1)}\frac{V}{A_s \Delta t} \qquad (A.1.3)$$

Now a new value of C_{in} can be calculated which will correspond to a steady state value of C. Rearranging equation. A.1.1, and assuming steady state conditions,

$$C_{in} = C_{sp}\left(\frac{A_s v_d}{Q} + 1\right) \qquad (A.1.4)$$

where C_{sp} is the setpoint chamber ozone concentration.

This method tends to approach the setpoint concentration slowly. The program has two features that speed up the approach to setpoint. As mentioned earlier, the control voltage is maximized until the chamber ozone concentration is near the setpoint. The program then invokes an integral parameter that forces the ozone concentration to rise more rapidly than it would with just the main control routine. It also helps minimize the

influence of step changes in voltage due to unforseen problems (voltage spike, misread voltage, etc.).

The program records temperature, flowrate, humidity and ozone concentration (through the A/D board). This information is output in a data file, a portion of which is shown here, as Figure A.1.3. Each channel corresponds to the voltage input from a specific device. These are converted to engineering units in post-processing for analysis.

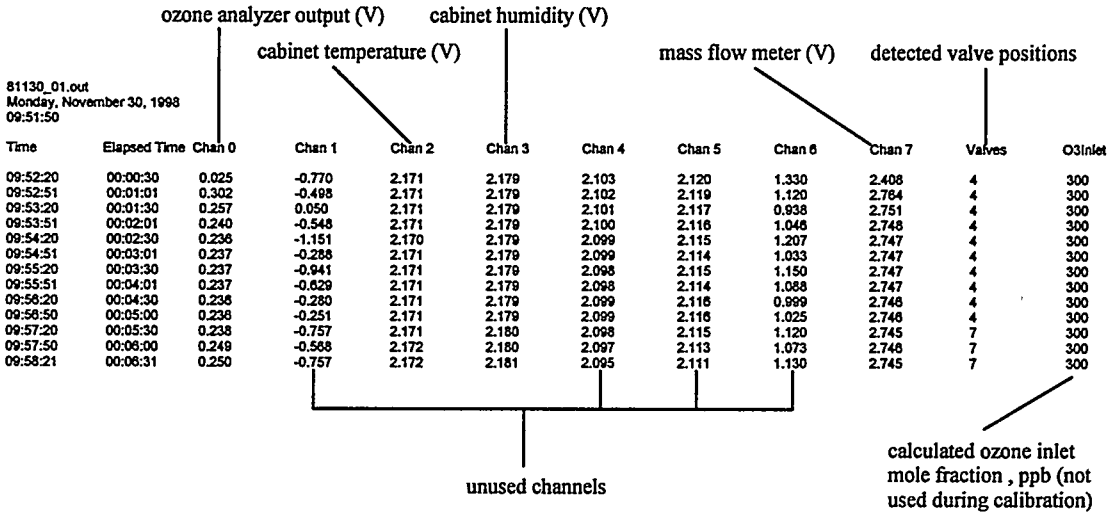

Figure A.1.3. Output file from control and measurement algorithm.

Table A.1.1. Computer algorithm for control of reaction chamber ozone concentrations and data collection: program code.

```
'
'   Ozone control, and data acquisition program
'
' This program is used to control ozone in a CMFR chamber
' as well as operate valves and collect data (temp, humidity,
' flowrate)
'


'
' The following section is used to initialize the
' "Computer Boards Inc." A/D board
'
Const BoardNum% = 0
Const Direction% = DIGITALOUT
Dim aiarraytmp(8)
Dim aiarray(8), avgaiarray(8, 1250)
Dim avgaiarraytmp1(8, 1250)
Dim avgaiarraytmp2(8)
Dim bintemp%(8)
Dim linearray(50, 2)

'
' The following subroutine, analogout, initializes the analog output
' to the board, and continuously watches a two grids on the GUI
' (equivalent to a memory location) to set the analog output from the
' A/D board. Several other subroutines place values in the grid locations
' for ozone control output.
'
Sub analogout (ao%())
  'Convert these to bit values then output
  Static ao_bit%(2)
  grid2.Col = 2
  For i = 0 To 1
  aotmp! = ao%(i) / 500
  Chan% = i: Rang% = 1
  ULStat% = cbFromEngUnits%(BoardNum%, Rang%, aotmp!, ao_bit%(i))
  ULStat% = cbAout%(BoardNum%, Chan%, Rang%, ao_bit%(i))
  grid2.Row = i + 1
  grid2.Text = Format(ao%(i), "0000")
  Next i
End Sub

'
' The following subroutine draws a plot of ozone vs time. It refreshes the
' screen at intervals designated by an input file.
'
Sub BoxPlot (O31, pcolor)
   xratio = deltatoto& / (upx)
   xratiot = xratio - Int(xratio)
   yratio = O31 / YO3
   xlen = lrx - ulx
   ylen = lry - uly
   If Int(xratio) > plotchk Then
      paintx = Int(ulx + xlen / 2)
      painty = Int(uly + ylen / 2)
      Line (ulx + 1, uly + 1)-(lrx - 1, lry - 1), QBColor(7), BF
      plotchk = Int(xratio)
      oldscreenx = ulx
      Call drawbox
   End If

   screenx = CInt(xratiot * xlen) + ulx
   screeny = lry - CInt(yratio * ylen)
   Line (oldscreenx, oldscreeny)-(screenx, screeny), QBColor(pcolor)
   oldscreenx = screenx
   oldscreeny = screeny
```

```
End Sub

'
' This is a timer program, used to ensure that data collection takes
' place at the right times.
'
Sub checktime (logicpass, c2, delta, deltatot&)

   tnow = Now ': deltatime = second(tnow) - seconds(tstart)
   deltaday& = Val(Format$(tnow, "y")) - Val(Format(tstart, "y"))
   deltahour& = Hour(tnow) - Hour(tstart)
   deltamin% = Minute(tnow) - Minute(tstart)
   deltasec% = Second(tnow) - Second(tstart)
   ' This doesn't take leap years into account



   If deltasec% < 0 Then
      deltasec% = 60 + deltasec%
      deltamin% = deltamin% - 1
   End If
   If deltamin% < 0 Then
      deltamin% = 60 + deltamin%
      deltahour& = deltahour& - 1
   End If
      If deltahour& < 0 Then
      deltahour& = 24 + deltahour&
      deltaday& = deltaday& - 1
   End If
   If deltaday& < 0 Then deltaday& = 365 + deltaday&

   deltatot& = 86400 * deltaday& + 3600 * deltahour& + 60 * deltamin% + deltasec%

   c = deltatot& / delta
   e = Int(c)
   c1 = c - e
   If c1 >= c2 Then logicpass = False Else logicpass = True
   c2 = c1
End Sub

'
' This subroutine talks to the digital I/O board, setting output
' based on GUI binary input value
'
Sub chkSetBit_Click (Index As Integer)
   BitNum% = Index
   BitValue% = chkSetBit(BitNum%).Value

   ULStat% = cbDBitOut%(BoardNum, PortType%, BitNum%, BitValue%)
   If ULStat% = 68 Then
   MsgBox "Boards only supports bit numbers less than " + Format$(BitNum%, "0"), 0, "Bit value too high"
   'ElseIf ULStat% <> 0 Then
      'Stop
   End If
End Sub

'
' This subroutine, Command1_Click, is realized on the GUI as a button that,
' when "clicked", starts the program going. The user is required to input
' a file name for data output in the GUI window before starting the program.
' Once the button is clicked, all digital outputs are set to zero (typically,
' closing a valve), a timer is enabled, the GUI used for the rest of program
' operation is drawn. Subroutine getgoing is called to initialize various
' features.
'
Sub Command1_Click ()
   Open ("c:\vb\lbl\" + outfilename) For Output As #1
   Open "c:\Vb\lbl\pfr_168h.txt" For Input As #2
   counter = 0:
```

```
    For i = 0 To 7
       bintemp%(i) = 0
    Next i
    Timer1.Enabled = True
    'Call drawbox
    'Text1.Text = Str$(Grid1.Width)

    ' set valve 0 to initially on!!'
    bintemp%(0) = 1
    ' set valve 1 to on initially
    bintemp%(1) = 1
    ' !!!!!!!!

    Call valveset(bintemp%())
    Call getgoing
    Call analogout(ao%())

End Sub

'
' This subroutine is used to shut down the program. Digital outputs are all
' set to zero.

Sub Command2_Click ()
    For i = 0 To 7
     chkSetBit(i).Value = 0
    Next i

    Close #1
    Close #2

End
End Sub
'
'
' The following subroutine draws the rectangle (on the GUI used for
' continous plotting of ozone concentrations. Subroutine getgoing calls
' this subroutine with location and aspect ratio.
'
Sub drawbox ()
'ulx = 300: uly = 2000: lrx = 3300: lry = 5000

Line (ulx, uly)-(lrx, lry), QBColor(4), B
'Form1.BackColor = QBColor(2)
End Sub
'
' Subroutine engunit changes input voltages to engineering units
'
Sub engunit (tmpvolt, ii, tmpengunit)
    tmpengunit = engunitmandb(ii, 0) * tmpvolt + engunitmandb(ii, 1)
End Sub

'
' This subroutine reads a file
' that tells the program how quickly to sample for data points, to control
' ozone or not, how to set digital output values, when to stop.
'
Sub Fileread ()
    Static bin%(8)
'
' input 999 designates the end of the program run. Files are closed,
' program is stopped
'
Line Input #2, linestring$
   If linestring$ = "999" Then
    Close #1
    Close #2
    End
   End If
```

```
i = 0
ii = 0
firstnum$ = ""
secondnum$ = ""
thirdnum$ = ""
char$ = ""
linelen = Len(linestring$)
Do While Not (char$ = Chr$(9))
   i = i + 1
   firstnum$ = firstnum$ + char$
   char$ = Mid$(linestring$, i, 1)
Loop
i = i + 1
char$ = Mid(linestring$, i, 1)
Do While Not (char$ = Chr$(9))
    secondnum$ = secondnum$ + char$
    i = i + 1
    char$ = Mid$(linestring$, i, 1)
Loop
i = i + 1
char$ = Mid(linestring$, i, 1)
Do While Not (char$ = Chr$(9))
    thirdnum$ = thirdnum$ + char$
    i = i + 1
    char$ = Mid$(linestring$, i, 1)
Loop

For iii = (i + 1) To linelen.
   char$ = Mid$(linestring$, iii, 1)
   fourthnum$ = fourthnum$ + char$
Next iii

vbin = Val(firstnum$): outputdelta = Val(secondnum$)
ao%(0) = Val(thirdnum$): ao%(1) = Val(fourthnum$)
End Sub

'
' Subroutine Form_Load loads the GUI for program output and control
'

Sub Form_Load ()

'These lines are here in order to catch errors.
'They refer to Computer Boards Universal Library functions

   ULStat% = cbDeclareRevision(CURRENTREVNUM)
   ULStat% = cbErrHandling%(DONTPRINT, DONTSTOP)
   If ULStat% = 27 Then
   GoTo 10
   Print #1, "Error 27  "; Format$(Now, "dd/mm/yy hh:mm:ss")
   form1.CurrentX = 100: form1.CurrentY = 1800

   form1.Print "Error 27  "; Format$(Now, "dd/mm/yy hh:mm:ss")
   Else If ULStat% <> 0 Then Stop
   End If
10  'jump over stop statement
   ULStat% = cbDConfigPort%(BoardNum%, PortNum%, Direction%)
   'If ULStat% = 27 Then
   'GoTo 10
   'Print #1, "Error 27  "; Format$(Now, "dd/mm/yy hh:mm:ss")
   'form1.CurrentX = 100: form1.CurrentY = 1800

   'form1.Print "Error 27  "; Format$(Now, "dd/mm/yy hh:mm:ss")
   'Else
   'If ULSTAT% <> 0 Then Stop
   'End If
```

```
    For i = 0 To 7
    grid1.ColWidth(i) = grid1.Width / 8 - 25
    Next i
    For i = 0 To 2
    grid1.RowHeight(i) = grid1.Height / 3.3
    Next i
    grid1.Row = 0
       grid1.FixedAlignment(0) = 2
       grid1.Col = 0: grid1.Text = "Time"
       grid1.FixedAlignment(1) = 2
       grid1.Col = 1: grid1.Text = "O3_#1"
       grid1.FixedAlignment(2) = 2
       grid1.Col = 2: grid1.Text = "NA"
       grid1.FixedAlignment(3) = 2
       grid1.Col = 3: grid1.Text = "T3"
       grid1.FixedAlignment(4) = 2
       grid1.Col = 4: grid1.Text = "T4"
       grid1.FixedAlignment(5) = 2
       grid1.Col = 5: grid1.Text = "H3"
       grid1.FixedAlignment(6) = 2
       grid1.Col = 6: grid1.Text = "H4"

    For i = 0 To 2
    grid2.ColWidth(i) = grid2.Width / 3.2
    Next i
    grid2.RowHeight(0) = grid2.Height / 7.5
    For i = 1 To 8
    grid2.RowHeight(i) = grid2.Height / 10
    Next i
    grid2.Col = 0
       grid2.FixedAlignment(0) = 2
       For i = 0 To 7
       grid2.Row = i + 1: grid2.Text = Str$(i)
       Next i
    grid2.Row = 0
       grid2.FixedAlignment(0) = 2
       grid2.Col = 0: grid2.Text = "Channel"
       grid2.FixedAlignment(1) = 2
       grid2.Col = 1: grid2.Text = "Input (V)"
       grid2.FixedAlignment(2) = 2
       grid2.Col = 2: grid2.Text = "AnOut (mV)"
       outfilename = InputBox("Enter output file name:", "Output Log File")
    Autoredraw = True
End Sub

'
' Subroutine getgoing initializes pretty much everything.
'

Sub getgoing ()
   tstart = Now
   ' time between writes to file and screen, outputdelta
   ' time between reads and sets of the valves, valvedelta
   ' both [=] seconds
   outputdelta = 30: valvedelta = 300
   ' Size and location of Box
   ulx = 300: uly = 2000: lrx = 3300: lry = 5000
   ' Lower and upper limit on Y scale in ppb ozone
   loy = 0: upy = 200: YO3 = 150
   ' upper limit on X scale in seconds
   upx = 7200
   ' Initial valve setting
   vbin = 4
   ' Initial analog output values
   ao%(0) = 4500: ao%(1) = 0
   linecount = 0
   ' This need to be removed: simulates O3in
   O3in = 300: O3max = 300: O3min = 160: m = 100: b = 50
```

```
    oldscreenx = ulx: oldscreeny = lry
    ' Set O3 setpoint and chamber air exchange rate(lambda)
    O3setpoint = 100: lambda = .114
    ' Set engineering units for output
    engunitmandb(0, 0) = 1000: engunitmandb(0, 1) = 6
    engunitmandb(1, 0) = 1000: engunitmandb(1, 1) = 16
    engunitmandb(2, 0) = 20: engunitmandb(2, 1) = -20
    engunitmandb(3, 0) = 20: engunitmandb(3, 1) = -20
    engunitmandb(4, 0) = 20: engunitmandb(4, 1) = 0
    engunitmandb(5, 0) = 20: engunitmandb(5, 1) = 0
    engunitmandb(6, 0) = 1: engunitmandb(6, 1) = 0
    engunitmandb(7, 0) = 1: engunitmandb(7, 1) = 0
       form1.CurrentX = 200
       form1.CurrentY = 0

       form1.Print outfilename
       form1.CurrentX = 200
       form1.Print "Start time:  "; Format$(tstart, "hh:mm:ss")
       form1.CurrentX = 200
       form1.Print Format$(tstart, "dddd, mmmm dd, yyyy")

       Print #1, outfilename
       Print #1, Format$(tstart, "dddd, mmmm dd, yyyy")
       Print #1, Format$(tstart, "hh:mm:ss")
       Print #1,
       Print #1, "Time"; Chr$(9); "Elapsed Time"; Chr$(9); "Chan 0"; Chr$(9); "Chan 1"; Chr$(9); "Chan 2"; Chr$(9); "Chan
3"; Chr$(9); "Chan 4"; Chr$(9); "Chan 5"; Chr$(9); "Chan 6"; Chr$(9); "Chan 7"; Chr$(9); "Valves"; Chr$(9); "O3Inlet"
       Print #1,
       Call drawbox
End Sub

'
' This Function subroutine takes input from subroutine "readchannels". Data collected from
' a calibration of the ozone analyzer (vs input voltage to power controller)
' is subjected to a linear least-squares analysis to determine the functional
' relationship between input voltage and inlet ozone concentration
'
Function linearize (linearray(), linecount, m, b)

For i = 0 To (linecount - 1)
   xsum = xsum + linearray(i, 0)
   ysum = ysum + linearray(i, 1)
Next i
xavg = xsum / (linecount): yavg = ysum / (linecount)
For i = 1 To (linecount - 1)
   sxsqrsum = (linearray(i, 0) - xavg) ^ 2 + sxsqrsum
   sysqrsum = (linearray(i, 1) - yavg) ^ 2 + sysqrsum
   sxysum = (linearray(i, 0) - xavg) * (linearray(i, 1) - yavg) + sxysum
Next i
sxsqr = sxsqrsum / (linecount)
sysqr = sysqrsum / (linecount)
sxy = sxysum / (linecount)
'r = sxy / (sx * sy)
sx = Sqr(sxsqr)
sy = Sqr(sysqr)


r = sxy / (sx * sy)
m = r * sy / sx: b = yavg - r * xavg * sy / sx
Print #1, "m= "; Chr$(9); m; "b= "; Chr$(9); b

End Function
'
' This function subroutine converts calculated inlet
' concentration to analog output to the power controller
' using linear parameters calculated in "linearize" funcition subroutine
'
Function o3_to_ao% (O3in, m, b)
o3_to_ao% = (O3in - b) / m
'
```

```
End Function
'
' This Function subroutine is the heart of the ozone control routine
' It uses two main functions
' (1) determine inverse decay time constant lambdal and use this
' in conjunction with a dynamic CMFR equation to set the inlet ozone
' concentration
' (2) integral control to smooth out some rapid changes that occur due
' to misread voltage, voltage spikes, etc. It also reduces control oscillation.
'

Function O3Inlet (O3engunit_temp, O3engunit_previous, deltat)
    ' Integral control parameter aint
    aint = .5
    O3Int_new = O3engunit_previous * (1 - aint) + O3engunit_temp * aint


    ' deltat is in seconds, need lambdal in inverse minutes
    deltatmin = deltat / 60
    O3slope = (O3Int_new - O3engunit_previous) / deltatmin
    lambdal = (lambda * (O3in + O3in_old) / 2 - O3slope) / ((O3engunit_temp + O3engunit_previous) / 2)

    form2.Text1.Text = O3slope
    form2.Text2.Text = lambdal
    form2.Text3.Text = O3engunit_temp
    O3in_old = O3in
  If O3engunit_temp / O3setpoint > .7 Then
    O3in = lambdal * O3setpoint / lambda

  Else
    O3in = O3max
  End If
  If O3in < O3min Then
    O3in = O3min
  End If
  If O3in > O3max Then
    O3in = O3max
  End If
  O3Inlet = O3in
  O3engunit_previous = O3Int_new
End Function
'
' This subroutine is used to output a line of data to the output file
' every time interval, where the time interval is set by the input file.
'

Sub outputtofile (avgaiarraytmp1(), vbin, counter)
  Print #1, Format$(tnow, "hh:mm:ss"); Chr$(9);
  Print #1, Format$(tnow - tstart, "hh:mm:ss"); Chr$(9);
  grid1.Col = 0: grid1.Row = 1
  grid1.Text = Format$(tnow - tstart, "hh:mm:ss")
  For i = 0 To 7
  avgaiarraytmp2(i) = 0
  Next i

  For i = 0 To 7
    atmp = 0
    For j = 0 To (counter - 1)
      avgaiarraytmp2(i) = avgaiarraytmp2(i) + avgaiarraytmp1(i, j)
      atmp = atmp + 1
    Next j
    If i = 0 Then
    ch1tmp = avgaiarraytmp2(0)
    End If

    avgaiarraytmp2(i) = avgaiarraytmp2(i) / (atmp)
    Print #1, Format(avgaiarraytmp2(i), "0.000"); Chr$(9);
    Call engunit(avgaiarraytmp2(i), i, iengunit)
    If i < 7 Then
      grid1.Col = i + 1
```

```
        grid1.Text = Format(iengunit, "###.0")
        If i = 0 Then o3engunit = iengunit
      End If
    Next i
    Call BoxPlot(o3engunit, 1)
  ' grid2.Col = 2: grid2.Row = 1: grid2.Text = Format(ch1tmp, "0.000")
  ' grid2.Row = 2: grid2.Text = Format(atmp, "0000")
  ' grid2.Row = 3: grid2.Text = Format(avgaiarraytmp1(0, 0), "00.000")
  ' grid2.Row = 4: grid2.Text = Format(avgaiarraytmp1(0, counter - 1), "00.000")
    Print #1, vbin; Chr$(9); O3in; Chr$(9); lambdal
    counter = 0

End Sub

'
' Displays elapsed time on GUI
'

Sub outputtoscreen ()
    grid1.Col = 0: grid1.Row = 1
    grid1.Text = Format$(tnow - tstart, "hh:mm:ss")

End Sub

Sub readchannels (aiarraytmp())
Gain% = BIP5VOLTS

For i = 0 To 7
    Chan% = i
    ULStat% = cbAin%(BoardNum%, Chan%, Gain%, DataValue%)
'   aiarraytmp(i) = (10 * Datavalue%) / 65536 + 5

    ULStat% = cbToEngUnits(BoardNum%, Gain%, DataValue%, engunits!)
    aiarraytmp(i) = engunits!
Next i
' This is a temporary section for program testing
' Simulates the ozone concentration in the chamber
' **   A = .3: b = 20
' **   lambdal_temp = A * Exp(-b * (elapsedtime)) + lambda
    'form2.Text1.Text = lambdal_temp
' **   deltat_temp = elapsedtime - (el_t_old)
    'form2.Text3.Text = deltat_temp
' **   o3concout = o3old * Exp(-lambdal_temp * 1440 * deltat_temp) + O3in * (lambda / lambdal_temp) * (1 - Exp(-
lambdal_temp * 1440 * deltat_temp))
    form2.Text4.Text = O3in
    form2.Text5.Text = o3concout
' **   o3old = o3concout: el_t_old = elapsedtime
' **   aiarraytmp(0) = o3concout / 1000 - .006
End Sub

Sub Timer1_Timer ()

    Call readchannels(aiarray())
      Text1.Text = "Time:  " + Format$(Now, "hh:mm:ss")
      Text2.Text = "Elapsed Time:  " + Format$((Now - tstart), " hh:mm:ss")
      elapsedtime = Now - tstart


    '   grid1.Col = 0: grid1.Row = 1: grid1.Text = Format$(Now, "hh:mm:ss")

      grid2.Col = 1
      For i = 0 To 7
        avgaiarray(i, counter) = aiarray(i)
        grid2.Row = (i + 1)
        grid2.Text = Format$(aiarray(i), "0.000")
      Next i
      counter = counter + 1
    Call checktime(outputFT, outputTemp, outputdelta, deltatoto&)
    Call checktime(valveft, valveTemp, valvedelta, deltatotv&)
    'text5.Text = outputTemp
```

```
    'text6.Text = valveTemp

    If outputFT Then
     Call outputtofile(avgaiarray(), vbin, counter)
    End If

    If valveft Then
     Fileread
     x = ToBinary(vbin, bintemp%())
     ' analogout ao%()
     Call valveset(bintemp%())
     If ao%(0) <= 5000 Then
        analogout ao%()
        If ao%(0) = aotemp% Then
           linearray(linecount, 0) = ao%(0)
           linearray(linecount, 1) = o3engunit
           linecount = linecount + 1
        End If
        aotemp% = ao%(0)
     ElseIf ao%(0) = 9999 Then
        x = linearize(linearray(), linecount, m, b)
        O3max = b + m * 4500
        O3min = b + m * 1500
     ElseIf ao%(0) = 9998 Then
        'O3max = b + m * 4500
        'O3min = b + m * 1500

        O3in = O3Inlet(o3engunit, O3engunit_previous, valvedelta)
        ao%(0) = o3_to_ao%(O3in, m, b)
        analogout ao%()
        o3inold = ao%(0)
     ElseIf ao%(0) = 9997 Then

     End If
    End If


End Sub

Function ToBinary (vbin, bin%())
   vbintemp = vbin
   For i = 7 To 0 Step -1
      vpos = 2 ^ i

      If (vbintemp / vpos > 1) Or (vbintemp / vpos = 1) Then
         bin%(i) = 1
         vbintemp = vbintemp - vpos
      Else
         bin%(i) = 0
      End If
      ToBinary = 1
   Next i
End Function
Sub valveset (bin%())
   'Static bin%(8)
   For i = 0 To 7
      chkSetBit(i).Value = bin%(i)
      ULStat% = cbDBitOut(BoardNum%, AUXPORT, i, bin%(i))
   Next i
End Sub
```

A.2 Average Emission Rates Of Identified Compounds

Tables A.2.2 – A.2.9 contain time averaged emission rate data for compounds emitted from carpets CP1-CP4. They are arranged by columns into experiment type with headings described in Table A.2.1. The emission rates are averaged over the time period shown in the "emissions averaging time (h)" row beginning at 0 h for a specific experiment. A sampling time line is provided in Figure A.2.1.

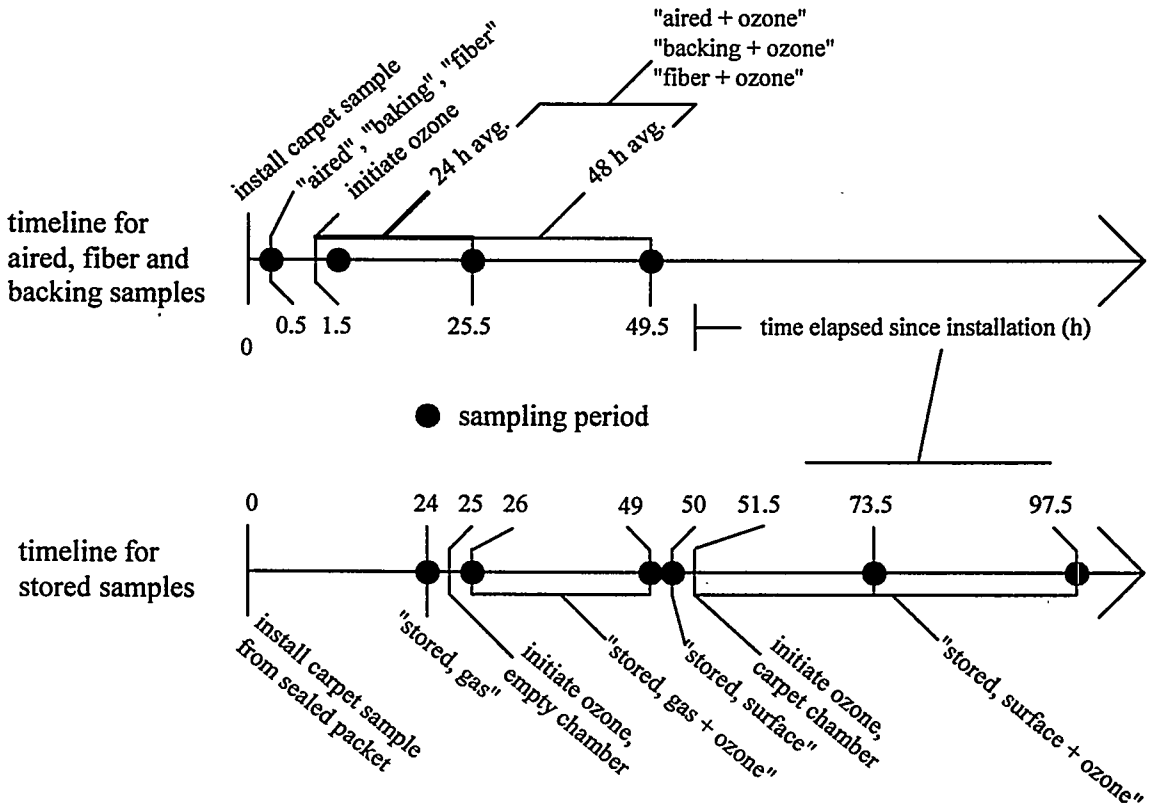

Figure A.2.1. Sampling time line for aired, backing, fiber and stored samples. Black circles denote sampling periods.

Table A.2.1 Description of table headings for Tables A.2.2 – A.2.9

heading	explanation
stored, gas	Stored carpet sample emission rate without ozone. Sample taken 24 h after installing carpet in ventilated 10.5 L chamber.
stored, gas + O_3	VOC samples taken from exhaust of "empty" chamber shown in Figure 2.4. Samples represent ozone reactions with gas phase species only; O_3 = 100 ppb
stored, surface	Stored carpet sample emission rate without ozone. Sample taken ~48 h after installing carpet in ventilated 10.5 L chamber.
stored, surface + O_3	Stored sample exposed to ozone at 100 ppb in ventilated 10.5 L chamber. Reaction products due to both gas-phase and surface-phase reactions.
aired	Aired carpet sample emission rate without ozone in ventilated 10.5 L chamber.
aired + O_3	Aired carpet sample exposed to ozone at 100 ppb in ventilated 10.5 L chamber
backing	Carpet backing sample emission rate without ozone in ventilated 10.5 L chamber.
backing + O_3	Carpet backing sample exposed to ozone at 100 ppb in ventilated 10.5 L chamber.
fiber	Fiber sample emission rate without ozone in ventilated tubular reactor. Emission rate normalized by *fiber* area.
fiber + O_3	Fiber sample exposed to ozone at 100 ppb in ventilated tubular reactor. Emission rate normalized by *fiber* area.

Table A.2.2. Average emission rates of identified compounds: carpet sample CP1, stored and aired carpets.[a]

		average emission rate ($\mu g\ m^{-2}\ h^{-1}$)					
compound	**ID**	**stored, gas**	**stored, gas+O_3**	**stored, surface**	**stored, surface +O_3**	**aired**	**aired + O_3**
emissions averaging time (h)		b	24	b	48	b	48
aldehydes							
formaldehyde	Q	nm	23	9.3	2.4	0.3	3.9
acetaldehyde	Q	nm	2.8	0.3	2.6	0.9	12.2
propanal	Q	nm	8.7		1.8		3.3
butanal	Q		2.5		2.3		1.3
pentanal	Q		3.1		3.9		1.6
hexanal	Q	1	7.6	0.8	24.4	2	3.0
heptanal	Q	2.5	3.0	0.4	19.1	0.9	3.4
octanal	Q		15.6	4.6	19.5	2.7	4.7
nonanal	Q	10.3	24.7	3.3	111	6.8	11.3
decanal	Q	8.6	28.1	0.8	43.3	10.1	8.7
undecanal	Q	1	2.3		4.1	0.9	0.8
dodecanal	Q	4.7	5.6	2.2	6.5	2.8	1.7
tridecanal	Q						0.5
3-methylbutanal	Q		1.4		1.2		
unsaturated aldehydes							
2-octenal	Q				5.1		
2-nonenal	Q				26.1		tr
ketones							
2-butanone	Q		4.5	0.3	2.5		
2-pentanone	Q		1.5		0.7		
2-hexanone	Q		1.0		0.4		
2-heptanone	Q		1.1		0.4		
2-octanone	Q						
2-nonanone	Q		0.35				
2-decanone	Q				0.2		
hydrocarbons							
branched alkanes	T	>>tr	>>tr	>>tr	>>tr		
branched C11-C12 alkenes	T	>>tr	>>tr	>>tr	>>tr		
4-phenylcyclohexene (4-PCH)	I	11.7	1.3	5.1	0.7		
organic acids							
octanoic acid	T						
nonanoic acid	I						
decanoic acid	I						
misc compounds							
dodecanol	Q	113.8	30.3	32	34.9	9.1	2.5
4-PCH ox. isomer 1	NI		tr		tr		
4-PCH ox. isomer 2	NI		tr		tr		
TVOC		905	425	227	363	100	107
TAAER		206	128	20.9	273	26.5	56.3
TME ($mg\ m^{-2}$)			3.1		13.1		
other compounds detected							
stored, gas phase + O_3	methylisobutylketone(I), 3-methyl-2-pentanone (I), 3-methyl-2-hexanone (T), 4-methyl-2-hexanone (T), cyclopentenone (I), 3,5 dimethyloctanone (T), branched pentanone and octanone (T), 2-ethylhexanol (I)						
stored, surface+gas+O_3	gas phase + O_3 compounds, branched nonanal, decanal and undecanal (T), 3-methyl-2-heptanone (T)						
aired, O_3	3-methyl-2-heptanone (T), branched nonanal and decanal (T)						

[a] Key to symbols and abbreviations: I, identified with primary standard; Q, identified with primary standard and quantified; T, tentative identification based on retention times and ion fragmentation pattern; NI, not identified; tr, trace levels by operator estimation; >>tr much larger than trace but not quantified; nm, not measured; blank cell, below level of detection. TVOC , total volatile organic compounds based on total ion current; TAAER, total average aldehyde emission rate; TME, total aldehyde mass emitted.

[b] No averaging period for single sample.

Table A.2.3. Average emission rates of identified compounds: carpet sample CP1, carpet backing and fibers.[a]

		average emission rate ($\mu g\ m^{-2}\ h^{-1}$)			
compound	**ID**	**backing**	**backing+O_3**	**fibers**	**fibers +O_3**
emissions averaging time (h)		b	24	b	24
aldehydes					
formaldehyde	Q	5.6	1.9		
acetaldehyde	Q	6.5	5.0		
propanal	Q		1.7		
butanal	Q		1.5		0.4
pentanal	Q	1.2	2.6		0.30
hexanal	Q	2.3	6.5		0.35
heptanal	Q	1.5	8.6		0.67
octanal	Q	7.2	15.6	0.4	2.0
nonanal	Q	18	54.7	1.2	2.4
decanal	Q	29.5	43.8	2	0.19
undecanal	Q	3.1	3.4	0.2	0.1
dodecanal	Q	4.4	4.3	0.2	
tridecanal	Q	2.3	2.1		
3-methylbutanal	Q				
unsaturated aldehydes					
2-octenal	Q				
2-nonenal	Q		8.5		0.38
ketones					
2-butanone	Q		1.5		
2-pentanone	Q		0.5		
2-hexanone	Q				
2-heptanone	Q				
2-octanone	Q				
2-nonanone	Q				
2-decanone	Q				
hydrocarbons					
branched alkanes	T				
branched C_{11}-C_{12} alkenes	T				
4-phenylcyclohexene (4-PCH)	I				
organic acids					
octanoic acid	T	tr	tr		
nonanoic acid	I	tr	tr		
decanoic acid	I	tr	tr		
misc compounds					
dodecanol	Q	25.1	25.1	2.7	.05
4-PCH ox. isomer 1	NI				
4-PCH ox. isomer 2	NI				
TVOC		232	253	14.9	17.7
TAAER		81.6	160	4.0	3.32
TME ($mg\ m^{-2}$)			3.8		0.16
other compounds detected					
carpet backing + O_3	3-methyl-2-hexanone (T), 6-methyl-5-heptenone (T), cyclopentenone (I), nonenol (T), branched nonanal (T)				
carpet fibers + O_3	3-methyl-2-heptanone (T), 6-methyl-5-heptenone (T), branched nonanal (T), dimethylundecadienone (T),				

[a] Key to symbols and abbreviations: I, identified with primary standard; Q, identified with primary standard and quantified; T, tentative identification based on retention times and ion fragmentation pattern; NI, not identified; tr, trace levels by operator estimation; nm, not measured; blank cell, below level of detection. TVOC , total volatile organic compounds based on total ion current; TAAER, total average aldehyde emission rate; TME, total aldehyde mass emitted.
[b] No averaging period for single sample.

Table A.2.4. Average emission rates of identified compounds: carpet sample CP2, stored and aired carpets.[a]

		average emission rate ($\mu g\ m^{-2}\ h^{-1}$)					
compound	**ID**	**stored, gas**	**stored, gas+O_3**	**stored, surface**	**stored, surface +O_3**	**aired**	**aired + O_3**
emissions averaging time (h)		b	24	b	48	b	48
aldehydes							
formaldehyde	Q		0.9		28.6	14.9	21.8
acetaldehyde	Q	0.3	2.0		18.3	1.6	7.1
propanal	Q		2.5		9.9	9.0	9.1
butanal	Q		2.1		9.8		7.8
pentanal	Q		1.8		11.8		10.4
hexanal	Q		1.5		17.1	1.8	15.1
heptanal	Q	3.9	0.9		18.8	1.8	17.8
octanal	Q				42.1	5.5	29.8
nonanal	Q	11.9	4.3	1.1	81.5	9.0	77.0
decanal	Q	12.8	3.5		26.9	17.5	31.2
undecanal	Q		0.7	4.8	4.5	1.5	5.0
dodecanal	Q	5.7	6.0		15.2	2.6	4.0
tridecanal	Q					1.5	1.7
3-methylbutanal	Q		1.2		2.2		
ketones							
2-butanone	Q		3.7		5.1	1.1	2.6
2-pentanone	Q		1.4		2.8		1.8
2-hexanone	Q		0.9		2.7		1.9
2-heptanone	Q		1.0		2.6		1.7
2-octanone	Q						1.6
2-nonanone	Q				1.7		1.4
2-decanone	Q				0.4		0.8
2-undecanone	Q						0.4
3-methyl-2-butanone	Q		1.2		1.1		
3-methyl-2-pentanone	Q		2.0		2.0		
hydrocarbons							
branched alkanes	T	>>tr	>>tr	>>tr	>>tr		
branched C_{11}-C_{12} alkenes	T	>>tr	>>tr	>>tr	>>tr		
4-phenylcyclohexene (4-PCH)	I	37.8	2.3	11.1	11.8		
organic acids							
octanoic acid	T					tr	tr
nonanoic acid	I					tr	tr
decanoic acid	I					tr	tr
misc compounds							
dodecanol	Q	291	109	122	186	9.4	10.2
4-PCH ox. isomer 1	NI		tr		tr		
4-PCH ox. isomer 2	NI		tr		tr		
TVOC		1603	623	637	918	171	253
TAAER		30.2	26.5	1.4	287	66	238
TME ($mg\ m^{-2}$)			1.3		13.7		12.1
Other compounds detected							
stored, gas phase + O_3	methylisobutylketone(I), 3-methyl-2-pentanone (I), 2-methyl-3-pentanone(T),2-methyl-3-heptanone(T), 3-methyl-2-hexanone (T), 4-methyl-2-hexanone (T), cyclopentenone (I), 3,5 dimethyloctanone (T), branched octanone (T), 3-methylpentanal,						
stored, surface+gas+O_3	gas phase + O_3 compounds						
aired, O_3	octane (Q), nonane (Q), branched nonanal (T)						

[a] Key to symbols and abbreviations: I, identified with primary standard; Q, identified with primary standard and quantified; T, tentative identification based on retention times and ion fragmentation pattern; NI, not identified; tr, trace levels by operator estimation; >>tr much larger than trace but not quantified; nm, not measured; blank cell, below level of detection. TVOC , total volatile organic compounds based on total ion current; TAAER, total average aldehyde emission rate; TME, total mass aldehyde emitted.

[b] No averaging period for single sample.

Table A.2.5. Average emission rates of identified compounds: carpet sample CP2, carpet backing and fibers.[a]

		average emission rate ($\mu g\ m^{-2}\ h^{-1}$)			
compound	**ID**	**backing**	**backing+O_3**	**fibers**	**fibers +O_3**
emissions averaging time (h)		b	48	b	24
aldehydes					
formaldehyde	Q	2.5	3.3		
acetaldehyde	Q		8.9		0.1
propanal	Q		4.6		
butanal	Q	1.5	7		tr
pentanal	Q	2.3	8.3		0.25
hexanal	Q	10.7	12.8		0.25
heptanal	Q	3.3	11.4		0.38
octanal	Q	11	18.2		0.47
nonanal	Q	26.5	41.1		1.4
decanal	Q	32.6	29.9		0.81
undecanal	Q	3.7	5.1		0.19
dodecanal	Q	3.6	4.5		tr
tridecanal	Q	2.6	2.1		tr
ketones					
2-butanone	Q	1.7	2.2		tr
2-pentanone	Q		1.5		tr
2-hexanone	Q		1.8		
2-heptanone	Q	0.8	1.8		
2-octanone	Q		1.7		
2-nonanone	Q		1.6		
2-decanone	Q		1.0		
2-undecanone	Q		tr		
organic acids					
octanoic acid	T	tr	tr	tr	tr
nonanoic acid	I	tr	tr	tr	tr
decanoic acid	I	tr	tr	tr	tr
misc compounds					
dodecanol	Q	6.1		9.3	6.4
4-PCH ox. isomer 1	NI				
4-PCH ox. isomer 2	NI				
TVOC		259	204	137	110
TAAER		100	157	0	3.9
TME ($mg\ m^{-2}$)			7.5		.092
other compounds detected					
carpet backing + O_3	3-methyl-2-heptenone (T), nonenol (T), branched nonanal (T)				
carpet fibers + O_3	3-methyl-2-heptanone (T), 6-methyl-5-heptenone (T), branched nonanal (T), dimethylundecadienone (T)				

[a] Key to symbols and abbreviations: I, identified with primary standard; Q, identified with primary standard and quantified; T, tentative identification based on retention times and ion fragmentation pattern; NI, not identified; tr, trace levels by operator estimation; nm, not measured; blank cell, below level of detection. TVOC , total volatile organic compounds based on total ion current; TAAER, total average aldehyde emission rate; TME, total mass aldehyde emitted.
[b] No averaging period for single sample.

Table A.2.6. Average emission rates of identified compounds: carpet sample CP3, stored and aired carpets.[a]

		average emission rate ($\mu g\ m^{-2}\ h^{-1}$)					
compound	**ID**	**stored, gas**	**stored, gas+O_3**	**stored, surface**	**stored, surface +O_3**	**aired**	**aired + O_3**
emissions averaging time (h)		b	24	b	48	b	72
aldehydes							
formaldehyde	Q	7.4			1.2	3.7	3.7
acetaldehyde	Q	1.0			4.7	8.3	5.9
propanal	Q	5.9			2.8	4.0	5.0
butanal	Q		1		10.4		6.1
pentanal	Q		1.3		15.8	1	15.0
hexanal	Q		1.2		34.2	0.7	23.2
heptanal	Q		0.9		69.6	1.5	61
octanal	Q		2.9		41.2	0.5	30
nonanal	Q	3.0	4.0	1.3	314	4.7	240
decanal	Q	0.8	2.8	0.6	36.4	1	16.2
undecanal	Q	1.9	1.1	2.1	8.3	1.6	6.8
dodecanal	Q	1.8	1.0	1.8	6.6		tr
tridecanal	Q				5.6		tr
unsaturated aldehydes							
2-octenal					14.9	0.3	3.1
2-nonenal					230	2.0	176
t,t-2,4-nonadienal					18.7		tr
ketones							
2-butanone	Q		1.9		3.5	0.3	1.5
2-pentanone	Q		0.7		2.4	0.6	2.1
2-hexanone	Q		0.4		2.0		
2-heptanone	Q				2.3		
2-octanone	Q				2.7		
2-nonanone	Q		0.5		2.0		
2-decanone	Q		0.6		1.8		
2-undecanone	Q				1.0		
3-methyl-2-butanone	Q		0.6		0.1		
3-methyl-2-pentanone	Q		0.9		0.2		
2-cyclopenten-1-one	Q				2.6		
hydrocarbons							
branched alkanes	T	>>tr	>>tr	>>tr	>>tr		
branched C_{11}-C_{12} alkenes	T	>>tr	>>tr	>>tr	>>tr		
4-phenylcyclohexene (4-PCH)	I	23.2	1.6	17.6	4.8		
organic acids							
octanoic acid	T					tr	tr
nonanoic acid	I					tr	tr
decanoic acid	I					tr	tr
misc compounds							
dodecanol	Q	0	2.5	2.1	2.4	tr	tr
4-PCH ox. isomer 1	NI		tr		tr		
4-PCH ox. isomer 2	NI		tr		tr		
TVOC		401	146	342	581	334	1364
TAAER		17.6	16.7	1.6	813	29	591
TME ($mg\ m^{-2}$)			0.4		98		30
other compounds detected							
stored, gas phase + O_3	methylisobutylketone(I), 2-methyl-3-pentanone(T),3-methyl-2-heptanone(T), 3-methyl-2-heptanone (T), 4-methyl-2-heptanone (T), 3,5 dimethyloctanone (T), 3-methylpentanal						
stored, surface+gas+O_3	gas phase + O_3 compounds, 6-methyl-5-hepten-2-one (T), branched C_9-C_{11} aldehydes (T), octane(Q), nonane(Q)						
aired, O_3	octane (Q), branched C_9-C_{11} aldehydes (T), 2-heptenal(Q)						

[a] Key to symbols and abbreviations: I, identified with primary standard; Q, identified with primary standard and quantified; T, tentative identification based on retention times and ion fragmentation pattern; NI, not identified; tr, trace levels by operator estimation; >>tr much larger than trace but not quantified; nm, not measured; blank cell, below level of detection. TVOC , total volatile organic compounds based on total ion current; TAAER, total average aldehyde emission rate; TME, total aldehyde mass emitted. [b] No averaging period for single samples.

Table A.2.7. Average emission rates of identified compounds: carpet sample CP3, carpet backing and fibers.[a]

		average emission rate ($\mu g\ m^{-2}\ h^{-1}$)			
compound	**ID**	**backing**	**backing+O_3**	**fibers**	**fibers +O_3**
emissions averaging time (h)		b	120	b	120
aldehydes					
formaldehyde	Q		0.7		
acetaldehyde	Q	3.4	3.0		
propanal	Q		2.6		
butanal	Q	tr	5.7		0.4
pentanal	Q	2.1	12.4		0.9
hexanal	Q	2.6	18.8		1.4
heptanal	Q	4.2	44.2		5.4
octanal	Q	7.8	24.3		1.9
nonanal	Q	16.3	186		15.0
decanal	Q	12.5	24.6		1.8
undecanal	Q	2.1	8.1		0.7
dodecanal	Q				
tridecanal	Q				
unsaturated aldehydes					
2-octenal	Q	0.8	3.5		0.4
2-nonenal	Q	11.2	125		10.6
t,t-2,4-nonadienal	Q		tr		tr
ketones					
2-butanone	Q	tr	1.4		tr
2-pentanone	Q		1.5		tr
2-hexanone	Q				
2-heptanone	Q				
2-octanone	Q				
2-nonanone	Q				
2-decanone	Q				
2-undecanone	Q				
organic acids					
octanoic acid	T	tr	tr	tr	tr
nonanoic acid	I	tr	tr	tr	tr
decanoic acid	I	tr	tr	tr	tr
misc compounds					
dodecanol	Q	tr	tr		
4-PCH ox. isomer 1	NI				
4-PCH ox. isomer 2	NI				
TVOC		526	800	98	142
TAAER		66	459	39	38.6
TME ($mg\ m^{-2}$)			55		4.6
other compounds detected					
carpet backing + O_3	octane (Q), branched C_9-C_{11} aldehydes (T), 2-heptenal(Q)				
carpet fibers + O_3	octane (Q), branched C_9-C_{11} aldehydes (T)				

[a] Key to symbols and abbreviations: I, identified with primary standard; Q, identified with primary standard and quantified; T, tentative identification based on retention times and ion fragmentation pattern; NI, not identified; tr, trace levels by operator estimation; nm, not measured; blank cell, below level of detection. TVOC , total volatile organic compounds based on total ion current; TAAER, total average aldehyde emission rate; TME, total aldehyde mass emitted.

[b] No averaging period for single samples.

Table A.2.8. Average emission rates of identified compounds: carpet sample CP4, stored and aired carpets.[a]

		average emission rate ($\mu g\ m^{-2}\ h^{-1}$)					
compound	**ID**	**stored, gas**	**stored, gas+O_3**	**stored, surface**	**stored, surface +O_3**	**aired**	**aired + O_3**
emissions averaging time (h)		c	24	b	48	b	48
aldehydes							
formaldehyde	Q		nm		7.0	13.3	8.1
acetaldehyde	Q		nm		7.8	9.3	10.6
propanal	Q		nm		4.2	13.7	7.0
butanal	Q		3.3		3.6		0.9
pentanal	Q		3.7		6.4		2.2
hexanal	Q		2.5		27.4		5.6
heptanal	Q		2.4		47.7		6.6
octanal	Q				34.2	3.4	8.8
nonanal	Q		8.3		152	6.3	57.9
decanal	Q		7.5		41.8	10.4	22.0
undecanal	Q		1.9		4.4	0.7	1.2
dodecanal	Q		5.5	3.0	5.3	1.3	0.5
tridecanal	Q					0.7	
3-methylbutanal	Q		2.3		1.9		
unsaturated aldehydes							
2-octenal	Q				22.5		
2-nonenal	Q				20.6		
t,t-2,4-nonadienal	Q				tr		
ketones							
2-butanone	Q		5.5		4.3		1.4
2-pentanone	Q		1.9		1.5		
2-hexanone	Q		0.7		1.0		
2-heptanone	Q		1.9		1.0		
2-octanone	Q						
2-nonanone	Q						
2-decanone	Q				tr		
2-undecanone	Q						
3-methyl-2-butanone	Q		1.7		0.8		
3-methyl-2-pentanone	Q		2.8		2.0		
2-cyclopenten-1-one	Q		0		0.4		
hydrocarbons							
branched alkanes	T		>>tr	>>tr	>>tr		
branched C_{11}-C_{12} alkenes	T		>>tr	>>tr	>>tr		
4-phenylcyclohexene (4-PCH)	I		1.4	4.1	0.7		
organic acids							
octanoic acid	T					tr	tr
nonanoic acid	I					tr	tr
decanoic acid	I					tr	tr
misc compounds							
dodecanol	Q		42.5	37.3	28.3	4.7	1.2
4-PCH ox. isomer 1	NI						
4-PCH ox. isomer 2	NI						
TVOC			818	765	595	81.4	181
TAAER			33.2		386	57.8	132
TME ($mg\ m^{-2}$)			0.8		18.5		6.4
other compounds detected							
stored, gas phase + O_3	methylisobutylketone(I), 3-hexanone(T),3-methyl-2-hexanone(T), 4-methyl-2-hexanone(T), 3-methyl-2-heptanone (T)						
stored, surface+gas+O_3	gas phase + O_3 compounds, branched C_9-C_{11} aldehydes (T), octane(Q), nonane(Q)						
aired, O_3	octane (Q), branched C_9-C_{11} aldehydes (T), 2-heptenal(Q)						

[a] Key to symbols and abbreviations: I, identified with primary standard; Q, identified with primary standard and quantified; T, tentative identification based on retention times and ion fragmentation pattern; NI, not identified; tr, trace levels by operator estimation; >>tr much larger than trace but not quantified; nm, not measured; blank cell, below level of detection; TVOC , total volatile organic compounds based on total ion current; TAAER, total average aldehyde emission rate; TME, total aldehyde mass emitted.

[b] No averaging period for single samples. [c] sample considered unacceptable and removed from data set.

Table A.2.9. Average emission rates of identified compounds: carpet sample CP4, carpet backing and fibers.[a]

		average emission rate ($\mu g\ m^{-2}\ h^{-1}$)			
compound	**ID**	**backing**	**backing+O_3**	**fibers**	**fibers +O_3**
emissions averaging time (h)		b	48	b	24
aldehydes					
formaldehyde	Q	7	4.6		
acetaldehyde	Q	14	11.8		
propanal	Q	5	2.5		
butanal	Q		1.9		0.09
pentanal	Q		2.7		0.13
hexanal	Q	4.6	10.1		0.08
heptanal	Q	2.3	11.6		0.11
octanal	Q	13	14.2		0.22
nonanal	Q	23.4	109		0.8
decanal	Q	23.5	27.4		1.10
undecanal	Q	2.5	2.4		
dodecanal	Q	3.1	2.4		
tridecanal	Q	1.9	1.0		
ketones					
2-butanone	Q		1.4		0.09
2-pentanone	Q				
2-hexanone	Q				
2-heptanone	Q				
2-octanone	Q				
2-nonanone	Q				
2-decanone	Q				
2-undecanone	Q				
organic acids					
octanoic acid	T	tr	tr	tr	tr
nonanoic acid	I	tr	tr	tr	tr
decanoic acid	I	tr	tr	tr	tr
misc compounds					
dodecanol	Q	2.3	0.8		
4-PCH ox. isomer 1	NI				
4-PCH ox. isomer 2	NI				
TVOC		227	160	53	127
TAAER		100	202	0	2.6
TME ($mg\ m^{-2}$)			9.7		0.06
other compounds detected					
carpet backing + O_3	1-butoxypropanal(T), branched C_9-C_{10} aldehydes(T), 3-methyl-2-heptanone (T), octane (Q), nonane (Q)				
carpet fibers + O_3	octane (Q), nonane (Q)				

[a] Key to symbols and abbreviations: I, identified with primary standard; Q, identified with primary standard and quantified; T, tentative identification based on retention times and ion fragmentation pattern; NI, not identified; tr, trace levels by operator estimation; nm, not measured; blank cell, below level of detection. TVOC , total volatile organic compounds based on total ion current; TAAER, total average aldehyde emission rate; TME, total aldehyde mass emitted.
[b] No averaging period for single sample.

A.3 Gas-Phase Ozonation of 4-Phenylcyclohexene

A.3.1 Experimental

A diffusion vial containing pure 4-phenylcyclohexene (4-PCH) was placed in a 10.5 L stainless steel chamber. The diffusion vial had a neck length of 2.0 cm and opening diameter of 0.4 cm. A measured stream of air at 1.1 L/min was allowed to ventilate the chamber and the system was allowed to equilibrate for 24 hours at 23 °C in a temperature controlled cabinet. The exhaust from this chamber was introduced into a second 10.5 L chamber along with 0.1 L/min air containing ozone (for an initial sample, the ozone generator was shut off). The concentration of ozone in the combined streams (1.2 L/min) was 100 ppb. Samples for the analysis of VOCs on GCMS were taken at the exhaust of the second chamber. See Section 2.2 for more detail on the experimental apparatus.

A.3.2 Results

The concentration of ozone at the outlet averaged 95 ppb. The concentration of 4-phenylcyclohexene before the introduction of ozone was 66.6 $\mu g\ m^{-3}$. Upon introduction of ozone, the 4-PCH concentration dropped to 23.6 $\mu g\ m^{-3}$ (see Figure A.3.1 (b)). Two products of the reaction were recognized in the GC/MS trace. Neither of these compounds could be identified using pure standards. However, enough information was obtained from analysis of the mass fragment spectra to allow suggest molecular formula and structure.

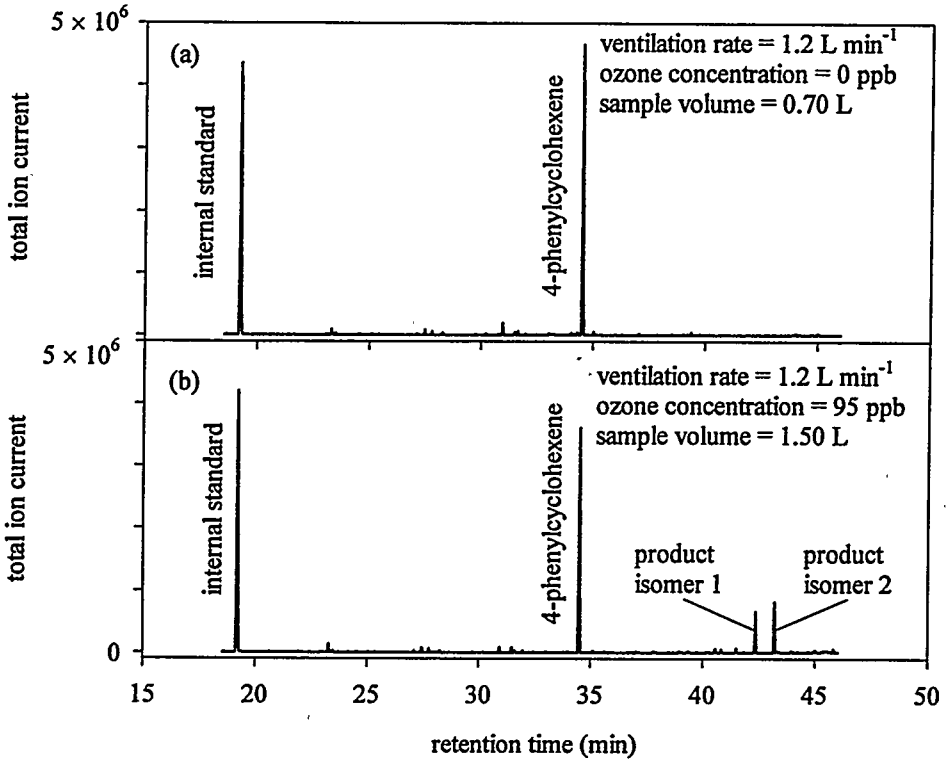

Figure A.3.1. Total ion current for samples taken from gas phase ozonation of 4-phenylcylcohexene: (a) sample taken before addition of ozone; (b) sample taken 1.5 h after ozone stabilized at 95 ppb.

These two compounds eluted within one minute of each other (42.25, 43.20), and about 8 minutes after 4-PCH (34.5 min). The fragmentation pattern of both compounds, shown in Figure A.3.2, were characterized by strong signals at m/z 91, m/z 115, m/z 128-129, m/z 143, m/z 157, and very strong molecular ion at m/z 172. The patterns are similar enough to suggest that the compounds are isomers with a very similar structure. Based on this evidence and analysis of "loss" ions, I suggest that both isomers have a molecular weight of 172, and a molecular formula of $C_{12}H_{12}O$. The fragmentation pattern suggests that the phenyl group of the precursor compound, 4-PCH, is retained and attached to an unknown structure. The oxygen in the unknown structure is likely to be in the form of a carbonyl or oxirene (see example Figure A.3.3 (b)), as part of either a doubly-unsaturated acyclic structure (see example in Figure A.3.3 (c)), a singly unsaturated ring, or bicyclic

structure. Several compounds that fit these criteria have known fragmentation patterns, but do not match those found in this study. The best match from the NIST/EPA/NIH database is a bicyclic oxirene, 1a,2,7,7a-tetrahydro-, (1a.alpha., 2.alpha., 7.alpha, 7a.alpha.)-(M)2,7-ethanonaphth[2,3-b]oxirene shown in Figure A.3.4 (a). Other structures with near matches (but which can probably be ruled out as candidates) are also shown in Figure A.3.4.

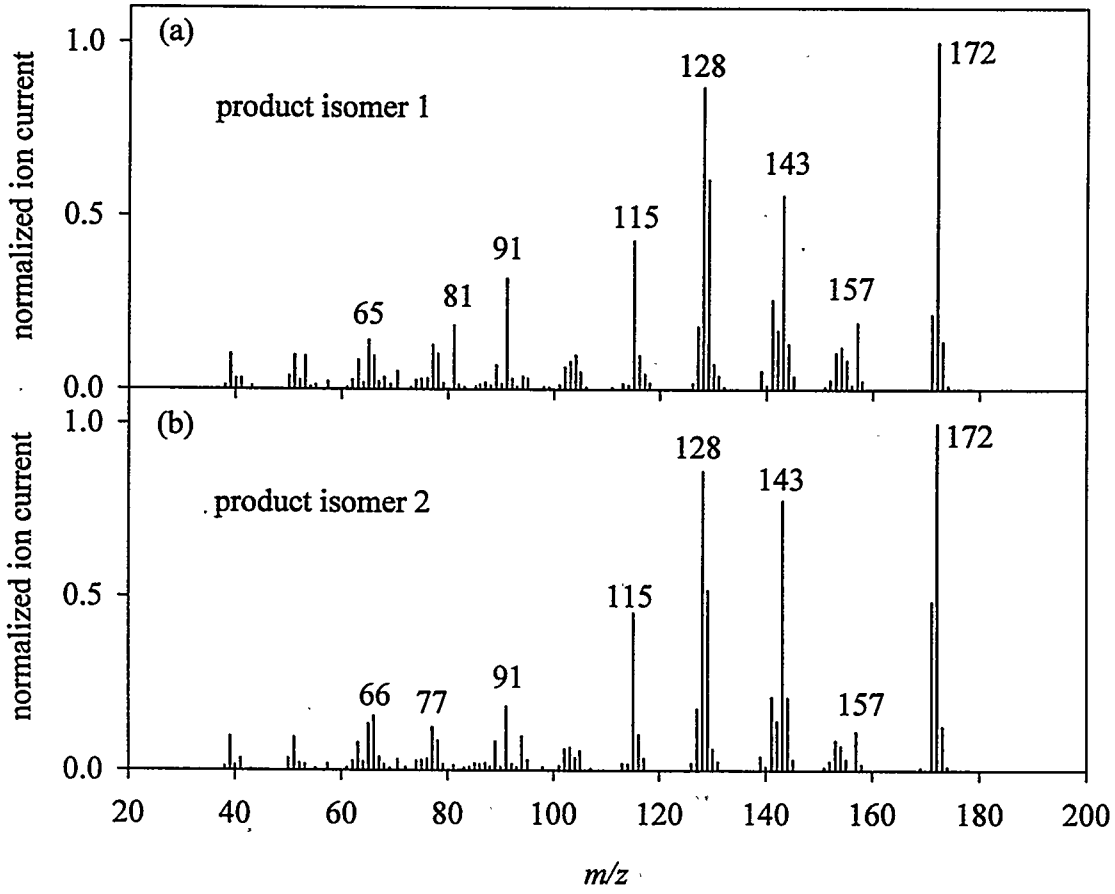

Figure A.3.2. Fragmentation patterns for 4-PCH product isomers.

An approximate value of the yield for these two compounds can be found. To obtain a molar concentration of a given isomer, I assumed that the GC/MS total ion response factor for these two compounds is similar to 4-PCH and quantified their mass

based on an integration of their total ion signal. I then define the yield of isomer 1 to be the molar concentration of isomer 1 divided by the difference between the 4-PCH molar concentration with and without ozone. Using this method, the isomer 1 yield was about 10% and isomer 2 about 13%, with a total product yield of 23%.

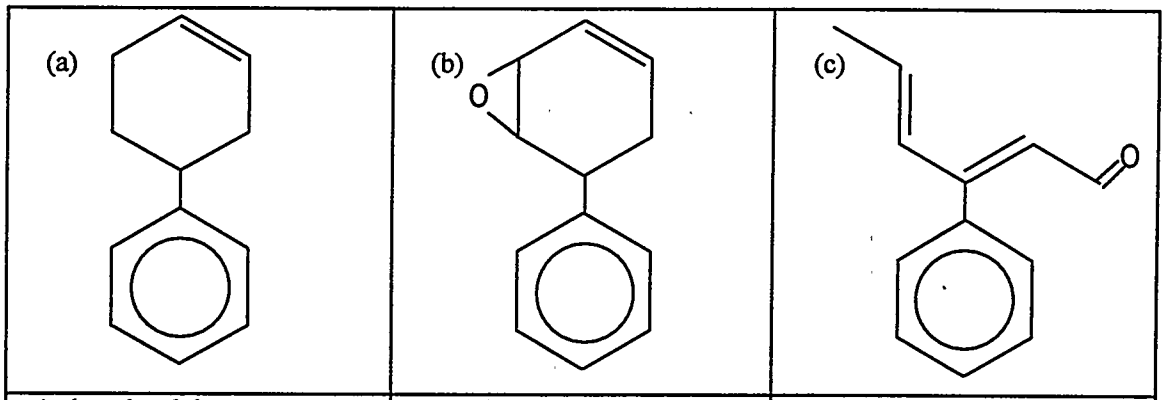

Figure A.3.3. 4-Phenylcyclohexene and two possible product structures based on ion fragmentation pattern of isomers 1 and 2.

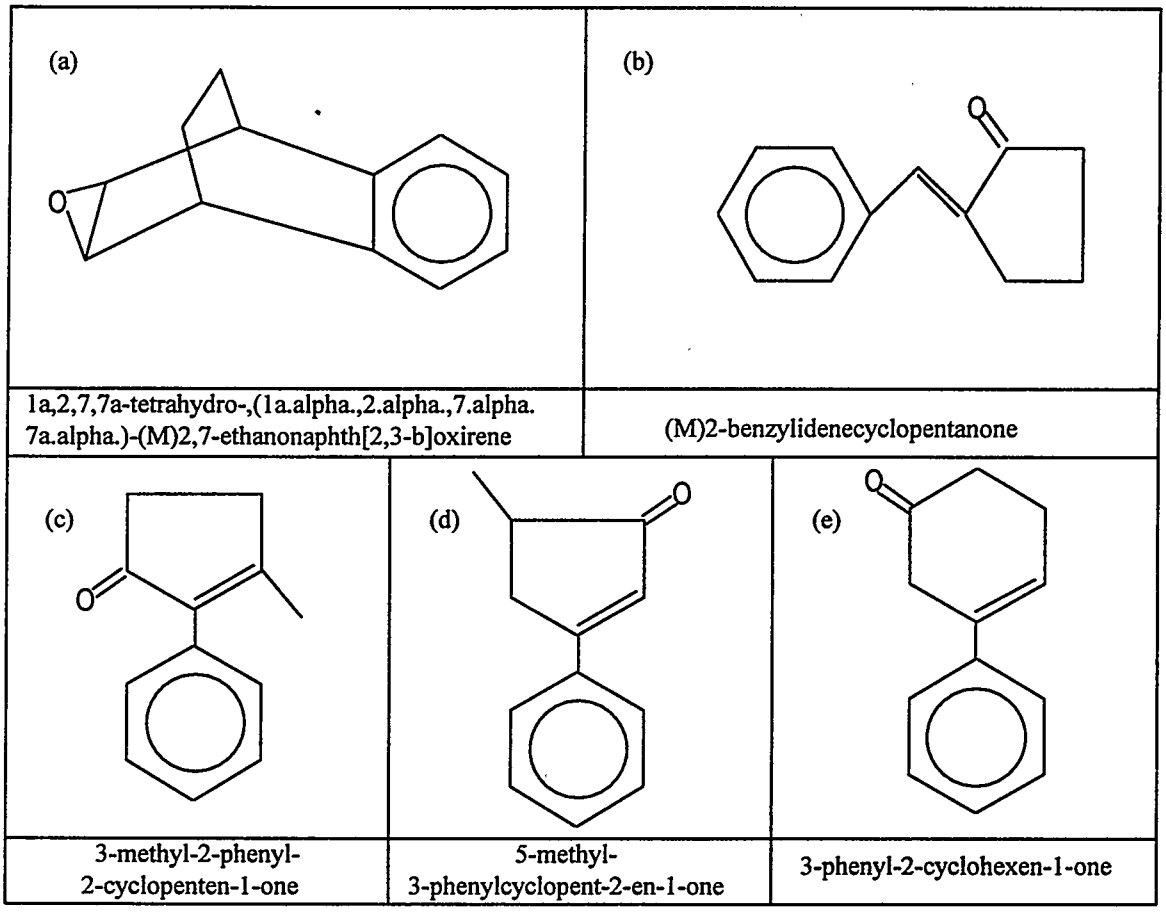

Figure A.3.4. Possible isomers that match the structural criteria based on the ion fragmentation pattern. The ion fragmentation patterns for these compounds are known (NIST database), but do not positively match those of the unknown compounds.

For each ozone molecule reacted, somewhat more than one molecule of 4-PCH reacted. The difference in inlet and outlet molar concentration for ozone was about 5 ppb. The difference in molar concentration for 4-PCH was 6.6 ppb.

A.3.3 Discussion

The molecular formula of the products of the reaction of ozone with 4-PCH is a puzzle. Typically, ozone reacts with unsaturated (but not aromatic) ring structures to open the ring, leaving a carbonyl group at the end of each "arm" (Grosjean et al., 1992). A hypothetical reaction mechanism is shown in Figure A.3.5 and is based on mechanistic

studies of terpenes (Grosjean, op cit.). This product does not match the profile described in Section A.3.2. It is possible that this compound is heavy enough or polar enough to be "missed" by GCMS analysis.

Direct oxidation by ozone may not explain the product isomers. However, ozone oxidation of double bonds typically produces OH radicals as shown in the mechanism in Figure 2.2. Atkinson showed that the oxidation of 1-methylcyclohexene (a methyl analog to 4-PCH) reacts to yield 90% OH radicals (Atkinson et al., 1995). These radicals may react with double bonds to form compounds quite different from those of direct ozone oxidation. Attack by OH radicals on a double bond offers the possibility of different pathways to the formation of oxidized products. Steric or electronic effects caused by the presence of the benzene ring may also influence the outcome of this reaction. At this time, I can offer no specific mechanism for the production of these two isomers.

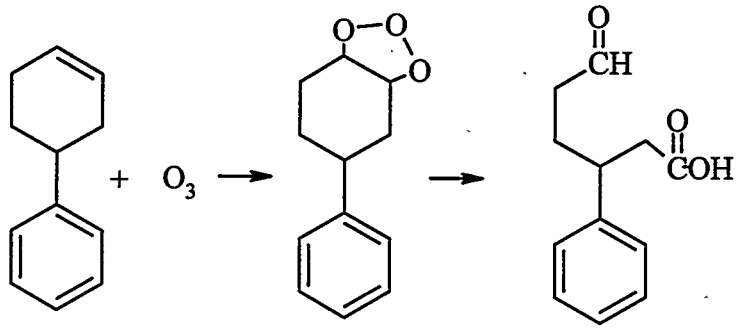

Figure A.3.5. Hypothetical mechanism for the oxidation of 4-PCH with ozone.

Weschler et al., (1992) calculated that the second-order rate constant for the reaction of ozone with 4-PCH was about 5×10^{-16} cm^3 $molecule^{-1}$ s^{-1}. My reactor was designed to simulate steady state conditions, with the emission rate from the diffusion vial remaining constant throughout the experiment. I can calculate the second-order rate constant, $k_{O3/4PCH}$, for this reaction, assuming that my reactor simulates a CMFR,

$$k_{O3/4PCH} = \frac{Q\left(C^{i}_{4PCH} - C^{o}_{4PCH}\right)}{V\left(C^{o}_{4PCH}C^{o}_{O3}\right)} \qquad (A.3.1)$$

where Q is the flowrate, V is the reactor volume, and C^i and C^o are the inlet and outlet concentrations of the subscripted compounds. I find that $k=1.5 \times 10^{-15}$ cm^3 $molecule^{-1}$ s^{-1}, which is about 3 times the value measured by Weschler et al. Note that Weschler et al. performed their experiment in a 20 m^3 chamber containing carpet; the environment and conditions were different from those in my experiment. The high surface area to volume ratio of my reactor may enhance reaction rates at the stainless steel surfaces (acting catalytically), augmenting the rate constant.

A.3.4 References

Atkinson, R.; Tuazon, E.C.; Aschmann, S.M. *Environmental Science and Technology.* **1995**, *29*, 1860-1866.

Grosjean, D.; Williams, E.L. II; Seinfeld, J.H. *Environmental Science and Technology.* **1992**, *26*, 1526-1533.

Weschler, C.J.; Hodgson, A.T.; Wooley, J.D. *Environmental Science and Technology*, **1992**, *26*, 2371-2377.

A.4 Computer Algorithm to Calculate Concentration Gradient in Carpet Mat: Description of Numerical Method for Solving Two-Dimensional Model, Static Nodal Grid.

A.4.1 Method for numerically solving partial differential equation in cylindrical coordinates

In Chapter 4, I introduce a model of ozone diffusion into and deposition onto the fiber and backing of carpet. The geometry of this model is built around the assumption that fibers are cylindrical, with ozone diffusing through an annular space around the fibers. The governing equation to be solved is cast (equation 4.53) in cylindrical coordinates. The following is a description of the numerical method used for solving equation 4.52 with boundary conditions given in equations 4.53 – 4.56

The system geometry over which equation 4.52 is defined is a unit square. Nodal points define the location where the concentration is evaluated. More nodal points provide a more detailed description of the concentration field in the unit square. On a given axis, each node is equidistant from other nodes, and is laid out in a rectangular grid pattern as shown in Figure A.4.1 This makes the program code simpler and easier to de-bug than code including adaptive gridding techniques.

The selection of the number of nodes is dependent on the largest gradient in the concentration field. For solutions that have only shallow gradients in the concentration field, few node points need to be specified to obtain an accurate description of the concentration field and, ultimately, the species flux into the carpet system. Where sharp gradients occur (e.g. where the species removal rate at the fiber surface is high), the number of node points must increase substantially to capture details of the gradient. As

the number of nodes increase, so does the time required to obtain a convergent solution. Method 2 (see text Chapter 4, Section 4.3.4). addresses the issue of steep gradients by applying adaptive gridding techniques. Method 1, described here, is used to validate solutions where both methods work well (shallow gradient).

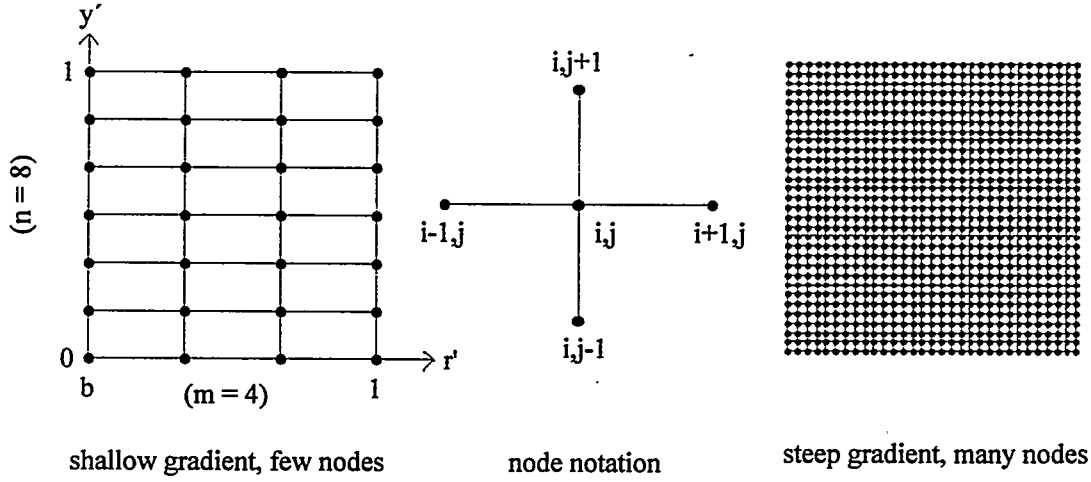

Figure A.4.1 Numerical method 1 calculation node layout.

The partial differential equation shown in equation 4.52 must be transformed into a form that utilizes the finite-difference technique. The finite-difference technique used in this analysis is based on the Taylor series expansion. To outline the derivation of numerical integration methods, consider a one-dimensional function C(y). In a Taylor expansion, a small incremental increase, Δy, in function C(y) can be approximated by a series expansion,

$$C(y+\Delta y) = C(y) + \Delta y \frac{dC(y)}{dy} + \frac{\Delta y^2}{2} \frac{d^2C(y)}{dy^2} + \cdots \qquad \text{(A.4.1)}$$

Likewise, a small incremental decrease can be approximated thus,

$$C(y-\Delta y) = C(y) - \Delta y \frac{dC(y)}{dy} + \frac{\Delta y^2}{2} \frac{d^2C(y)}{dy^2} - \cdots \qquad \text{(A.4.2)}$$

Accuracy of the estimate increases by evaluating increasing numbers of terms, but each

subsequent term of the expansion is progressively smaller. A first-order estimate of the slope (first derivative term) can be made by dropping the second-order and higher terms and rearranging equation A.4.1. However, a better method, which results in higher order accuracy is to subtract equation A.4.2 from A.4.1 and rearrange to obtain,

$$C(y+\Delta y)-C(y-\Delta y)=2\Delta y\frac{dC(y)}{dy}+2\frac{\Delta y^3}{6}\frac{d^3C(y)}{dy^3}+\cdots \qquad (A.4.3)$$

In dropping all third order and higher terms from equation A.4.3, second order accuracy is retained. Thus, to evaluate the first derivative, at location y,

$$\frac{dC(y)}{dy}\cong\frac{C(y+\Delta y)-C(y-\Delta y)}{2\Delta y} \qquad (A.4.4)$$

In a one-dimensional coordinate system, y represents the location of a node, with (y + Δy) and (y-Δy) locations of the two adjacent nodes. In a two-dimensional problem, such as that posed by equation 4.52, the difference equations are somewhat more complex.

In this analysis, I followed the numerical methods outlined by Whitaker (1977) for cylindrical coordinates. On a square grid, where there are m nodes along the r′ coordinate and n nodes along the y′ coordinate,

$$r_i' = b+i\Delta r' \qquad i=0,1,2,\cdots,m \qquad (A.6.5)$$

$$y_j' = j\Delta y' \qquad j=0,1,2,\cdots,n \qquad (A.4.6)$$

where, recall, b is the lower limit of r′, representing the fiber surface. At node (i,j), the three terms of equation 4.52 can be approximated by these finite difference forms,

$$(b+i\Delta r')\frac{C'_{i+1,j}+2C'_{i,j}+C'_{i-1,j}}{\Delta r'^2}+\frac{C'_{i+1,j}-C'_{i-1,j}}{2\Delta r'}+\left(\frac{a}{b}\right)^2(b+i\Delta r')\frac{C'_{i;j+1}+2C'_{i,j}+C'_{i,j-1}}{\Delta y'^2}=0 \qquad (A.4.7)$$

By rearranging equation A.4.7, the term $C'_{i,j}$ can be isolated and evaluated using previously calculated values (or an initial estimate) at the surrounding nodes. Each node is evaluated in this manner until the entire nodal field has been updated. This procedure can be repeated until the difference between the previous and present set of concentration field values is sufficiently small.

Equation A.4.7 can also be modified to fit a form that is amenable to solution through matrix manipulation. Rearranging the equation,

$$\left[(b+i\Delta r')-\left(\frac{\Delta r'}{2}\right)\right]C'_{i-1,j}-2\left[(b+i\Delta r')\left(1+\left(\frac{a}{b}\right)^2\left(\frac{\Delta r'}{\Delta y'}\right)^2\right)\right]C'_{i,j} + \left[(b+i\Delta r')+\left(\frac{\Delta r'}{2}\right)\right]C'_{i+1,j}=\left[(b+i\Delta r')\left(\frac{a}{b}\right)^2\left(\frac{\Delta r'}{\Delta y'}\right)^2\right]\left[C'_{i,j+1}+C'_{i,j-1}\right] \tag{A.4.8}$$

This equation can be expressed in the more compact form,

$$A_i C'_{i-1,j}+B_i C'_{i,j}+D_i C'_{i+1,j}=E_{i,j} \qquad i=1,2,3,\ldots,m-1 \tag{A.4.9}$$

This represents m-1 equations that can be written in matrix form:

$$\begin{bmatrix} B_1 & D_1 & & & & & \\ A_2 & B_2 & D_2 & & & & \\ & A_3 & B_3 & D_3 & & & \\ & & & \ddots & & & \\ & & & A_{m-2} & B_{m-2} & D_{m-2} & \\ & & & & A_{m-1} & B_{m-1} & \end{bmatrix}\begin{bmatrix} C'_{1,j} \\ C'_{2,j} \\ C'_{3,j} \\ \vdots \\ C'_{m-2,j} \\ C'_{m-1,j} \end{bmatrix}=\begin{bmatrix} \tilde{E}_{1,j}-A_1C'_{0,j} \\ \tilde{E}_{2,j} \\ \tilde{E}_{3,j} \\ \vdots \\ \tilde{E}_{m-2,j} \\ \tilde{E}_{m-1,j}-D_{m-1}C'_{m,j} \end{bmatrix} \tag{A.4.10}$$

where, $j=1,2,3,\ldots,n-1$ and

$$\tilde{E}_{i,j}=\left[(b+i\Delta r')\left(\frac{a}{b}\right)^2\left(\frac{\Delta r'}{\Delta y'}\right)^2\right]\left[\tilde{C}'_{i,j+1}+\tilde{C}'_{i,j-1}\right] \tag{A.4.11}$$

The previously calculated values (or initial estimate) of the concentration field, $\tilde{C}'_{i,j}$. are

used to evaluate $\tilde{E}_{i,j}$. Once again, equation A.4.10 can be represented in a more compact form,

$$[B]_j[C']_j = [\tilde{E}]_j \tag{A.4.12}$$

Matrix $[B]_j$ is made up of known constants, $[C']_j$ is the desired concentration field along the j^{th} row of nodes, and $[\tilde{E}]_j$ made up of pre-calculated (or an initial estimate of) adjacent row values and boundary node values. If matrix $[B]_j$ can be inverted, then $[C']_j$ can be directly calculated,

$$[C']_j = [B]_j^{-1}[\tilde{E}]_j \tag{A.4.13}$$

By progressively evaluating $[C']_j$ for each j with equation A.4.13, then evaluating $[\tilde{E}]_j$ from the previous calculation cycle, the values that represent the concentration field will converge to a solution. Note that only the "inner" node values are calculated using this method. The edge node values can be found by examining the boundary conditions.

Along the top of the annular cylinder, the concentration is set to a constant value. Thus, each node in the top row of concentration values is simply,

$$C'_{i,n} = 1 \tag{A.4.14}$$

Along the inner cylinder wall where $r' = b$, the gradient boundary condition given by equation 4.54 can be transformed to,

$$\frac{\tilde{C}'_{n-1,j} - C'_{n,j}}{\Delta r'} = k_r C'_{n,j} \tag{A.4.15}$$

or, rearranging,

$$C'_{n,j} = \frac{\tilde{C}'_{n-1,j}}{\left(k_r + \frac{1}{\Delta r'}\right)} \tag{A.4.16}$$

Similarly, along the bottom of the annular cylinder, the concentration can be calculated,

$$C'_{i,m} = \frac{\tilde{C}'_{i,m-1}}{\left(k_y + \frac{1}{\Delta y'}\right)} \tag{A.4.17}$$

Along the outer boundary of the cylinder, $r' = 1$, the flux is zero. This forces the concentration gradient along the r' coordinate to zero. The mathematical consequence of this is that the boundary value, and the adjacent node in the next column must be identically equal,

$$C'_{1,j} = \tilde{C}'_{2,j} \tag{A.4.18}$$

At this point, all values in the nodal grid have been accounted for.

I chose the Matlab programming environment because it is built around solving matrix problems such as this. The program code for solving equation 4.52 can be found in Table A.4.1. The program is arranged into 3 "m-files". In the Matlab environment, m-files can represent primary programs, functions, subroutines, etc. I arranged the code in the following way. File "carpet4.m" is used to set up the variables, such as h_r, h_y, a, and b and create output files for later analysis. Once the variables are defined, function m-file "findflux4.m" is called. This function takes the raw data from function "findconc3.m" to evaluate the flux at the surface of the carpet ($y' = 1$). The heart of the analysis takes place in "findconc3.m" where the concentration field is determined and returned to "findflux4.m" for further analysis. Once the flux has been determined it is returned to

"carpet4.m", and reinterpreted into a form matching the reaction probability at the surface (whole-carpet reaction probability).

The code for solving the *dimensional* form of equation 4.52 (equation 4.45) with adaptive gridding is shown in Table A.4.2.

A.4.2 Reference

Whitaker, S. *Fundamental Principles of Heat Transfer*. Pergamon Press: New York. 1977.

Table A.4.1. Program code for algorithm to calculate concentration gradient in carpet mat: computer code for two-dimensional model, static nodal grid.

Main program "carpet4.m"

```
clear
% This program runs with assumption that gamma(r)=gamma(z)
%
% This program finds the surface reaction ratio
%
r2overL=1
omega=1
begintime=datestr(now)
toler=0.00000001;maxiter=20000;i=0;k=0;span=2;
flux=ones(span,1);
xhr=zeros(1,span);yhz=zeros(1,span);

for r1overr2=0.1:0.1:0.2
A_ratio=1/((1-r1overr2*r1overr2)+2*r1overr2/r2overL+r1overr2*r1overr2)
for hr=logspace(-7,-6,span);
  i=i+1
  xhr(i)=log10(hr);
  hz=hr/r2overL;
  yhz(i)=log10(hz);
  flux(i)=findflux3(r2overL,r1overr2,hr,hz,omega,toler,maxiter);
  gamma_ftip_ratio(i)=2*flux(i);
  surf_reac_ratio(i)=A_ratio*gamma_ftip_ratio(i);
end
fluxformat=blanks(span*6+1);
for i=1:span
  aa=(i-1)*6+1;
  bb=aa+5;
  fluxformat(aa:bb)='%5.6f ';
end
cc=(span)*6;
fluxformat(cc:cc+1)='\n';
dimstring=['_'num2str(r2overL) '_' num2str(r1overr2) '_'];
i=0;
log10(flux);
gamma_ftip_ratio
surf_reac_ratio
file=['carflux' dimstring 'equal.out'];
fileid=fopen(file,'w');
fprintf(fileid,fluxformat,log10(gamma_ftip_ratio));
fprintf(fileid,fluxformat,surf_reac_ratio);
fclose(fileid);
begintime
endtime=datestr(now)
end
```

Function "findflux3.m"

```
function y=findflux3(r2overL,r1overr2,hr,hz,omega,toler,maxiter)
global conctemp3
n=12;m=12;Concprime=0.0*ones(n,m);Concprime(1:n,m)=ones(n,1);
maxiter=100000;
conctemp1=findconc3(n,m,Concprime,r2overL,r1overr2,hr,hz,omega,toler,maxiter);
r2overLtemp=r2overL;

maxiter=500;
nn=60;mm=60;jj=0;mmtemp=mm;
conctemp2=interp2(conctemp1,1:((n-1)/(nn-1)):n,(1:((m-1)/(mm-1)):m)');
conctemp3=findconc3(nn,mm,conctemp2,r2overL,r1overr2,hr,hz,omega,toler,maxiter);
```

```
mesh(conctemp3);pause(.1);
datestr(now)

mmtemp=round(0.9*mm);
conctest=conctemp3(2,mmtemp);
conctemp6=conctemp3;
while conctest<0.1 ;
  conctemp3=conctemp6;
  r2overLnew=(mm-1)*r2overLtemp/(mm-mmtemp);
  conctemp4(1:nn,1:(mm-mmtemp+1))=conctemp3(1:nn,mmtemp:mm);
  conctemp5=(interp1(1:1:(mm-mmtemp+1),conctemp4',(1:((mm-mmtemp)/(mm-1)):(mm-mmtemp+1))))';
conctemp5(1:nn,mmtemp);
conctemp6=findconc4(nn,mm,conctemp5,r2overLnew,r1overr2,hr,hz,omega,toler,maxiter);
  conctemp6(2,1:mm);
  conctest=conctemp6(2,mmtemp);
  r2overLtemp=r2overLnew;
  conctemp5=conctemp4;
  jj=jj+1;
end
rintervals=(0:1/(nn-1):1);
if jj<1;
  tempvariable=2*((1-r1overr2)*rintervals+r1overr2)*(mm-1)/(nn-1)/(1+r1overr2);
  for jjj=1:(nn-1)
    cavgback(jjj)=(conctemp3(jjj,1)+conctemp3(jjj+1,1))/2;
    dcavgtop(jjj)=(conctemp3(jjj,mm)-conctemp3(jjj,mm-1)+conctemp3(jjj+1,mm)-conctemp3(jjj+1,mm-1))/2;
    ravg(jjj)=(r1overr2+(jjj)*(1-r1overr2)/(nn));
  end
  for jjj=1:(mm-1);
    cavgfiber(jjj)=(conctemp3(1,jjj)+conctemp3(1,jjj+1))/2;
  end
  fluxtobacking=dot(cavgback(1:nn-1),ravg)*(1-r1overr2)/(nn-1)
  dot(cavgfiber(1:mm-1),ones(1,mm-1))/(mm-1)
  (r1overr2/r2overL)
  fluxtofiber=(r1overr2/r2overL)*dot(cavgfiber(1:mm-1),ones(1,mm-1))/(mm-1)
  r1overr2*r1overr2/2
  flux=fluxtofiber+fluxtobacking+r1overr2*r1overr2/2
  fluxtop=dot(dcavgtop(1:nn-1),ravg)/(nn-1)*(mm-1)
else
  for jjj=1:(mmtemp-1);
    cavgfiber1(jjj)=(conctemp3(1,jjj)+conctemp3(1,jjj+1))/2;
  end
  for jjj=1:(mm-1);
    cavgfiber2(jjj)=(conctemp6(1,jjj)+conctemp6(1,jjj+1))/2;
  end
  for jjj=1:(nn-1);
    dcavgtop(jjj)=(conctemp6(jjj,mm)-conctemp6(jjj,mm-1)+conctemp6(jjj+1,mm)-conctemp6(jjj+1,mm-1))/2;
    ravg(jjj)=(r1overr2+(jjj-0.5)*(1-r1overr2)/(nn-1));
  end
  fluxtop=(mm-1)*dot(dcavgtop,ravg)/(nn-1)/((0.1)^(jj-1));


  fluxtofiber1=(0.1^(jj-1))*(r1overr2/r2overL)*dot(cavgfiber1(1:mmtemp-1),ones(1,mmtemp-1))/(mmtemp-1);
  fluxtofiber2=(0.1^(jj))*(r1overr2/r2overL)*dot(cavgfiber2(1:mm-1),ones(1,mm-1))/(mm-1);



  flux=fluxtofiber1+fluxtofiber2+r1overr2*r1overr2/2;
end
y=flux;
```

Function "findconc3.m"

```
function y=findconc3(n,m,Concprime,r2overL,r1overr2,hr,hz,omega,toler,maxiter)

iter=0
conc=Concprime;

dr=(1-r1overr2)/(n-1);
```

```
dz=1/(m-1);
bdrsub=(r1over2/dr);
sqrdrdz=(r2overL*dr/dz)*(r2overL*dr/dz);
B = -2*(1+sqrdrdz);
for i=2:n-1
  A(i)=(1-1/2/(bdrsub+i-1));
  C(i)=(1+1/2/(bdrsub+i-1));
  coeftemp(i,i:i+2)=[A(i) B C(i)];

end
coef=coeftemp(2:n-1,3:n);
coefinv=inv(coef);
D=zeros(n-1,m);
error=100;
while (error>toler*n*m&iter<maxiter)
for jj=2:m-1;

      D(2:n-1,jj)=-sqrdrdz*(Concprime(2:n-1,jj+1)+Concprime(2:n-1,jj-1));

    end
Dprime=D;
Dprime(2,1:m)=D(2,1:m)-(1-1/2/(bdrsub+1))*Concprime(1,1:m);
Dprime(n-1,1:m)=D(n-1,1:m)-(1+1/2/(bdrsub+(n-2)))*Concprime(n,1:m);

for i=2:m-1
  conc(2:n-1,i)=coefinv*Dprime(2:n-1,i);%\coef)';
end
conc(2:n-1,1)=conc(2:n-1,2)/(1+dz*hz);
conc(1,1:m-1)=conc(2,1:m-1)/(1+dr*hr);
conc(n,1:m-1)=conc(n-1,1:m-1);%/(1+dr*hr);
error1=(conc-Concprime);
error=sum(sum(abs(error1)));
Concprime=Concprime+omega*error1;
iter=iter+1;
if (iter/100==round(iter/100))
  iter
  error
  pause(.01)
end

end
fileid=fopen('iter.out','a');
fprintf(fileid,'%3.6f %3.6f %5.0f\n',hr,hz,iter);
fclose(fileid);
iter
mesh(conc);
pause(1)
y=conc;
```

Table A.4.2. Program code for algorithm to calculate concentration gradient in carpet mat: two-dimensional model, adaptive nodal grid.

Main program "carpet_setup5.m"

```
%Mfile for determining carpet reaction probability
%global hr_bound hz_bound;
clear;
figure(1)
iter=1;iter2=5
while iter2<6;
  iter2=iter2+1
  switch iter2
  case 1, b_dimless=0.125
  case 2, b_dimless=0.205
  case 3, b_dimless=0.293
  case 4, b_dimless=0.416
  case 5, b_dimless=0.59
  case 6, b_dimless=0.316
  end
  ii=0;

while ii<iter
 close('all','hidden');
  ii=ii+1;

%gammar=10^(-(10-(ii+9)/2));
%gammaz=10^(-(10-(ii+9)/2));
gammar=.0000001;gammaz=1e-5;
Diff=0.167;
Boltz_vel=3.6e4;
L=1;
a_dimless=0.007/2;
%b_dimless=0.9;
%r1=a_dimless*L;
r1=a_dimless;
r2=r1/b_dimless;
hr_bound=gammar*Boltz_vel/4/Diff;
hz_bound=gammaz*Boltz_vel/4/Diff;


carpet5b(r1,r2,hr_bound,hz_bound);
    % First, export the solution.
    % Next, convert to gradient (triangle mid point data)
    pde_fig=findobj(allchild(0),'flat','Tag','PDETool')
    u = get(findobj(pde_fig,'Tag','PDEPlotMenu'),'UserData');
    h=findobj(get(pde_fig,'Children'),'flat','Tag','PDEMeshMenu');
    hp=findobj(get(h,'Children'),'flat','Tag','PDEInitMesh');
    he=findobj(get(h,'Children'),'flat','Tag','PDERefine');
    ht=findobj(get(h,'Children'),'flat','Tag','PDEMeshParam');
    p=get(hp,'UserData');
    e=get(he,'UserData');
    t=get(ht,'UserData');

    params=get(findobj(get(pde_fig,'Children'),'flat','Tag','PDEPDEMenu'),...
        'UserData');
    ns=getuprop(pde_fig,'ncafd');
    nc=ns(1); na=ns(2); nf=ns(3); nd=ns(4);
    c=params(1:nc,:);
    [ux,uy]=pdegrad(p,t,u);

    % Then convert to node point data
    un=pdeprtni(p,t,ux);

    % then use tri2grid
    x=0:L/200:L;
    y=r1:((r2-r1)/200):r2;
    unxy=tri2grid(p,t,un,x,y);
```

```
    uxy=tri2grid(p,t,u,x,y);
    gamma_overall(ii)=y*unxy(1:201,201)*((r2-r1)/200)*8*Diff/Boltz_vel/r2/r2+gammar*(r1/r2)^2
     %gamma_overall=y*unxy(1:51,51)*((r2-r1)/50)*8*Diff/Boltz_vel/r2/r2+gammar*(r1/r2)^2
     gamma_overall_2(ii)=gammar*(uxy(1,1:201)*ones(201,1)*(2*r1/r2/r2/200)+(r1/r2)^2)+gammaz*2*(r2-
r1)/200/r2/r2*(r1:(r2-r1)/200:r2)*(uxy(1:201,1))
     fiberfrac=gammar*(uxy(1,1:201)*ones(201,1)*(2*r1/r2/r2/200)+(r1/r2)^2)/gamma_overall_2(ii)
     backingfrac=gammaz*2*(r2-r1)/200/r2/r2*(r1:(r2-r1)/200:r2)*(uxy(1:201,1))/gamma_overall_2(ii)
   end
  area_ratio=1+2*r1*L/r2/r2
  gamma_compare=[logspace(-8,5,iter);gamma_overall;gamma_overall_2]
  tempstring=[num2str(a_dimless) '_' num2str(b_dimless) '_' num2str(-log10(gammar)) '_' num2str(-log10(gammaz)) '.out']
  fid=fopen(tempstring,'w');
  tempformat='%1.2e %1.4e %1.4e\n';
  fprintf(fid,tempformat,gamma_compare);
  fclose(fid);
end
nn=30;mm=30;
concTBtemp=interp2(uxy,1:((201-1)/(nn-1)):201,(1:((201-1)/(mm-1)):201)');
d3z=[0:L/(nn-1):L];
d3r=[r1:(r2-r1)*1/(mm-1):r2]/r2;
concTB=cat(1,d3z,d3r,concTBtemp);
fid=fopen('d:\MATLAB\bin\concTB.txt','w')
tempformat=('');ia=0;
while(ia<(nn+1))
  ia=ia+1;
  tempformat=([tempformat,'%1.4f ']);
end
tempformat=([tempformat,'%1.4f\n']);


fprintf(fid,tempformat,concTB);
status=fclose(fid)
```

Function "carpet5b.m"

```
function temp=carpet5b(r1,r2,hr_bound,hz_bound)
%pdemodel
%global hr_bound hz_bound;
r1
r2
hr_bound
hz_bound
hz_bound
L=1
[pde_fig,ax]=pdeinit;
pdetool('appl_cb',1);
pdetool('snapon','on');
set(ax,'DataAspectRatio',[1 1 1]);
set(ax,'PlotBoxAspectRatio',[1 1 1]);
set(ax,'XLim',[0 L]);
set(ax,'YLim',[0 2*r2]);
set(ax,'XTickMode','auto');
set(ax,'YTickMode','auto');
pdetool('gridon','on');

% Geometry description:
pderect([0 L r1 r2],'R1');
set(findobj(get(pde_fig,'Children'),'Tag','PDEEval'),'String','R1')

% Boundary conditions:
pdetool('changemode',0)
pdesetbd(4,...
'neu',...
1,...
[num2str(hz_bound,4) '*y'],...
```

```
'0')
pdesetbd(3,...
'neu',...
1,...
'0',...
'0')
pdesetbd(2,...
'dir',...
1,...
'1',...
'1')
pdesetbd(1,...
'neu',...
1,...
[num2str(hr_bound,4) '*y'],...
'0')

% Mesh generation:
setuprop(pde_fig,'Hgrad',1.3);
setuprop(pde_fig,'refinemethod','regular');
pdetool('initmesh')

% PDE coefficients:
pdeseteq(1,...
'y',...
'0.0',...
'0',...
'1.0',...
'0:10',...
'0.0',...
'0.0',...
'[0 100]')
setuprop(pde_fig,'currparam',...
['y  ';...
'0.0';...
'0  ';...
'1.0'])

% Solve parameters:
setuprop(pde_fig,'solveparam',...
str2mat('1','4641','25','pdeadworst',...
'0.5','longest','0','1e-4','','fixed','inf'))

% Plotflags and user data strings:
setuprop(pde_fig,'plotflags',[1 1 1 1 1 1 1 1 0 0 0 1 1 0 1 0 0 1]);
setuprop(pde_fig,'colstring','');
setuprop(pde_fig,'arrowstring','');
setuprop(pde_fig,'deformstring','');
setuprop(pde_fig,'heightstring','');

% Solve PDE:
pdetool('solve')
temp=0;
```

A.5 Computer algorithm to predict carpet aging and time dependent concentration gradients

A.5.1 Introduction to the algorithm

Carpet fibers age nonuniformly in a system where ozone must diffuse into the carpet mat from the carpet tips to the backing. The algorithm shown in Table A.5.1 accounts for the reaction probability and cumulative ozone uptake for "n" horizontal slices of carpet mat (fibers surfaces) to predict the whole-carpet ozone uptake rate (and whole carpet reaction probability, γ_o) dynamically.

Table A.5.1. Program code for algorithm to predict carpet aging and time dependent concentration gradients.

```
clear
%
% program for determining concentration profile and ozone flux
% in carpet mat. Time dependent reaction probabilities on fibers.
%
n=30;% number of increments carpet mat is split into
%
Co=0.0002% concentration of ozone at fiber tips (ug/cu cm)
% Input variables: backing gamma, height(h), boltzman velocity,
% diffusivity, porosity, fiber diameter
%
gammaib=.0001;h=.55;boltz_vel=3.6e4;Diff=0.167;p=0.898;df=0.007;
gammaif=6e-6;
%
% Initial fiber reaction probability
%
gammaf=gammaif*ones(n,1);
gammab=gammaib;
%
% carpet backing flux factor E
%
E=gammaib*boltz_vel*h/4/Diff;
%
% Setup initial fiber flux variable, A
%
tempvariable_A=h*h*boltz_vel*(1-p)/df/Diff
A_initial=sqrt(tempvariable_A*gammaf);
A=A_initial;
%
%
%
A1=zeros(n); AA1=zeros(n); A2=zeros(n); AA2=zeros(n);
k1=ones(n,1);k2=k1;
C=zeros(n,1);C(n)=1;Conc=zeros(n+1,1);Conc(n+1,1)=1;
nvector=[0:1:n-1]';
```

```
cumulative_uptake=0;
%
% Initial time increments
%
t=0;time_increment=1.05;time_increment2=1.1;initial_time_increment=1;
%
% factors A and B which describe fiber aging
%
Agamma=6e-9;Bgamma=-0.8;Agammab=1e-5;Bgammab=-0.47;

%
% Initial cumulative uptake on fiber UCo
%
UCo=(gammaif/Agamma)^(1/Bgamma)*ones(n,1);UCb=(gammaib/Agammab)^(1/Bgammab);
%
t_iter=0;
%
% The next section iteratively calculate concentration
% based on the assumption that, initially, the backing has little influence
% on the concentration profile. This speeds the overall calculation.
%
while gammaf(1)>0.0001

  t_iter=t_iter+1;
  for i=n:-1:1
    tempvariable=A(i:n)/n;%.*[(n-i+1)/n:-1/n:1/n]';
    Conc(i)=exp(-sum(tempvariable));% concentration at vertices between segments
    Conc_mid(i)=mean([Conc(i+1) Conc(i)]);% segment midpoint concentration
    clear tempvariable;
  end

  Conc_dim_mid=Co*Conc_mid;% convert from dimensionless to dimensional concentration
  %
  % Initialize time incrementing
  %
  if t==0
    t2=t+0.0001
  else if t<1e6
      t2=t*time_increment;
    else
      t2=t*time_increment2;
    end

  end
  deltat=t2-t;% time increment from previous iteration
  %
  % Cumulative uptake on fiber
  %
  UCo=UCo+deltat*boltz_vel*Conc_dim_mid'.*gammaf/4;
  UCb=UCb+deltat*boltz_vel*Conc(1)*gammab*Co/4;
  %
  % Recalculation of fiber reaction probability based on
  % previous time interval exposure
  %
  gammaf=Agamma*(UCo).^Bgamma;
  gammab=Agammab*(UCb)^Bgammab
  A=sqrt(tempvariable_A*gammaf);
  t=t2
  %
  % animated graphical display of concentration gradient in carpet mat
  %
  plot(Conc);
  pause(.4);
  %
  % calculation of whole carpet reaction probability (gamma naught)
  %
  gamma_o=4*Diff*A(n)/h/boltz_vel;
  %
  % cumulative uptake on whole carpet
  %
```

```
  cumulative_uptake=cumulative_uptake+Co*gamma_o*boltz_vel*deltat/4
  output(t_iter,1:5)=[cumulative_uptake gamma_o t gammaf(1) Conc(1)];
end
%semilogy(output(1:t_iter,3),output(1:t_iter,2));
%pause
 if t==0
   t=0.0001
 end
%
% The following section uses the full solution to the concentration
% differential equation, including flux at the backing
%
while t<1e6
  t2=t*time_increment;
  t_iter=t_iter+1;
  E=gammab*boltz_vel*h/4/Diff;
    %
    % The following code sets up the appropriate matrices for
    % calculation of k1 and k2 in the solution to the full equation
    %
  A1(n,n)=exp(-A(n));A2(n,n)=-exp(A(n));
  AA1(1,1)=A(1)+E;AA2(1,1)=A(1)-E;

for i=1:n-1
  A1(i,i)=-exp(-A(i)*i/n);
  A1(i,i+1)=exp(-A(i+1)*i/n);
  A2(i,i)=exp(A(i)*i/n);
  A2(i,i+1)=-exp(A(i+1)*i/n);
  AA1(i+1,i)=A(i)*exp(-A(i)*i/n);
  AA1(i+1,i+1)=-A(i+1)*exp(-A(i+1)*i/n);
  AA2(i+1,i)=A(i)*exp(A(i)*i/n);
  AA2(i+1,i+1)=-A(i+1)*exp(A(i+1)*i/n);
end
%
% calculation of coeffients k1 and k2
%

k2=inv(eye(n)-(inv(AA2)*AA1*inv(A1)*A2))*inv(AA2)*AA1*inv(A1)*C;
k1=inv(A1)*(A2*k2+C);
%
% calculation of the concentration gradient
%
Conc(1:n,1)=k1.*exp(-(times(A,nvector/n)))+k2.*exp(times(A,nvector/n));
  Conc_mid=mean([Conc(1:n)';Conc(2:n+1)']);
  Conc_dim_mid=Co*Conc_mid;
  deltat=t2-t;
  %
  % cumulative uptake on fiber
  %
  UCo=UCo+deltat*boltz_vel*Conc_dim_mid'.*gammaf/4;
    UCb=UCb+deltat*boltz_vel*Conc(1)*gammab*Co/4;

  %
  % recalcultion of fiber reaction probability
  %
  gammaf=Agamma*(UCo).^Bgamma;
    gammab=Agammab*(UCb)^Bgammab;
  A=sqrt(tempvariable_A*gammaf);
  t=t2
  plot(Conc);
  pause(.4);
  %
  %  whole carpet reaction probability and cumulative uptake
  %
  gamma_o=4*Diff*A(n)/h/boltz_vel;
  cumulative_uptake=cumulative_uptake+Co*gamma_o*boltz_vel*deltat/4
  output(t_iter,1:5)=[cumulative_uptake gamma_o t gammaf(1) Conc(1)];
end
figure(2);
loglog(output(1:t_iter,1),output(1:t_iter,2));
```

```
figure(3);
plot(output(1:t_iter,3),output(1:t_iter,2));

ABfactors=polyfit(log(output(250:470,1)),log(output(250:470,2)),1)
```